Advanced laboratory testing of smart grid applications with power hardware-in-the-loop approach

Von der
Fakultät für Elektrotechnik und Informationstechnik
der
Technischen Universität Dortmund
genehmigte

Dissertation

zur Erlangung des akademischen Grades
Doktor der Ingenieurwissenschaften

von

Alfio Spina, M.Sc.

Dortmund, 2021

Referent:	Prof. Dr.-Ing. habil. Christian Rehtanz
Korreferent:	Prof. Dr.-Ing. Gianfranco Chicco

Tag der mündlichen Prüfung: 09.09.2021

Acknowledgements

I would like to express my sincere gratitude to Prof. Dr.-Ing. Christian Rehtanz for supervising this thesis and kindly supporting me during the overall Ph.D. experience at TU Dortmund University. Especial acknowledgements to Prof. Dr.-Ing. Gianfranco Chicco for co-supervising this thesis and for providing precious suggestions.

My research was supported by several people without whom this thesis would not be complete. I would like to thank Dr.-Ing. Christoph Aldejohann for his fundamental contribution and support during my practical work at the Smart Grid Technology Lab. Especial acknowledgements to Dr.-Ing Kalle Rauma for his collaboration and for providing precious ideas during my research work. Particular thanks to Mara Holt and to everybody at the Smart Grid Technology Lab for providing technical and non-technical support and creating a friendly and collaborative environment. I would like to extend my thanks to all the further members of the ie^3 Institute who directly and indirectly supported my work.

Finally, I would like to express my special thank and my extremely gratitude to my family for supporting and encouraging me during the overall period of my study.

Dortmund, July 2021

Abstract

This work addresses practical issues in the design and operation of advanced smart grid test infrastructures. Both aspects are analyzed with particular emphasis on test facilities including Power hardware-in-the-loop (PHIL) systems. The minimal requirements along with an architectural classification of the elemental laboratory equipment are suggested for the suitable facility design and effective operation. A set of fundamental operational use-cases are formulated for the straightforward applicability of advanced testing approaches especially based on the PHIL technique. The assessed design and operational aspects are evaluated on an existing smart grid laboratory equipped with a PHIL system together with typical full-scale smart grid components. Particularly, a number of representative test-cases are selected and performed by operating the existing PHIL system according to the suggested operational use-cases. Results show the potential together with the actual implementation issues arising when performing advanced PHIL tests for practical research applications.

Kurzfassung

Diese Arbeit adressiert praktische Fragen beim Design und Betrieb von erweiterten Smart-Grid-Testinfrastrukturen. Beide Aspekte werden mit besonderem Schwerpunkt auf erweiterten Testeinrichtungen einschließlich Power Hardware-in-the-Loop (PHIL)-Systemen analysiert. Die minimalen Anforderungen zusammen mit einer Architekturklassifizierung der elementaren Laborgeräte werden für das geeignete Design der Einrichtung und den effektiven Betrieb vorgeschlagen. Eine Reihe grundlegender betrieblicher Anwendungsfälle wird für die praktische Anwendbarkeit fortschrittlicher Testansätze formuliert, die insbesondere auf der PHIL-Technik basieren. Die bewerteten Design- und Betriebsaspekte werden in einem bestehenden Smart-Grid-Labor evaluiert, das mit einem PHIL -System zusammen mit typischen Smart-Grid-Komponenten in vollem Maßstab ausgestattet ist. Insbesondere wird eine Reihe von repräsentativen Prüffällen ausgewählt

und durch den Betrieb des bestehenden PHIL-Systems entsprechend den vorgeschlagenen betrieblichen Anwendungsfällen durchgeführt. Die Ergebnisse zeigen das Potenzial sowie die tatsächlichen Implementierungsprobleme, die bei der Durchführung erweiterter PHIL-Tests für praktische Forschungsanwendungen auftreten.

Contents

List of Figures

List of Tables

Abbreviations

ADC	Analog-to-Digital Converter
API	Application Programming Interface
BESS	Battery Energy Storage System
BJT	Bipolar Junction Transistor
BMS	Battery Management System
CHIL	Controller hardware-in-the-loop
CHP	Combined Heat and Power
CPU	Central Processing Unit
DAC	Digital-to-Analog Converter
DER	Distributed Energy Resources
DFT	Discrete Fourier Transform
DIM	Damping Impedance Method
DSO	Distribution System Operator
DSR	Distributed Series Reactor
EMC	Electromagnetic Compatibility
EMI	Electromagnetic Interferences
EMT	Electromagnetic Transient
EV	Electric Vehicle
FACTS	Flexible AC Transmission System
FPGA	Field-Programmable Gate Array
HIL	Hardware-in-the-loop
HuT	Hardware under Test
HV	High-Voltage
HVDC	High-Voltage Direct Current
IA	Interface Approach

ICT	Information and Communications Technology
IGBT	Insulated Gate Bipolar Transistor
I/O	Inputs and Outputs
ITM	Ideal Transformer Method
LPF	Low-Pass Filter
LV	Low-Voltage
MOSFET	Metal Oxide Semiconductor Field Effect Transistor
MPP	Maximum Power Point
MPPT	Maximum Power Point Tracking
MV	Medium-Voltage
NCS	Naturally Coupled System
OLTC	On-Load Tap Changer
PA	Power Amplifier
PCC	Point of Common Coupling
PCIe	Peripheral Component Interconnect Express
PHIL	Power hardware-in-the-loop
PLC	Programmable Logic Controller
PLL	Phase Locked Loop
PMU	Phasor Measurement Unit
PV	Photovoltaics
PWM	Pulse-Width Modulation
RCD	Residual Current Device
RES	Renewable Energy Sources
RMS	Root Mean Square
ROS	Rest of the System
RTS	Real-Time Simulator
SCADA	Supervisory Control and Data Acquisition
SFP	Small Form-factor Pluggable
SGTL	Smart Grid Technology Lab
SIL	Safety Integrity Level
SIS	Safety Instrumented System
SoC	State of Charge

SSN	State-Space-Nodal
TCP/IP	Transmission Control Protocol/Internet Protocol
THD	Total Harmonic Distortion
TNA	Transient Network Analyzer
VEP	Venios Energy Platform
VPN	Virtual Private Network

Chapter 1

Introduction

A transformation of the energy system is taking place in many countries around the world. This includes structural changes as well as the deployment of innovative solutions for the development of a sustainable, reliable and economically affordable energy supply infrastructure. Environmental policy together with technological progress represent the principal driving factors leading to such transformation. In November 2016, the German government deliberated the Climate Action Plan 2050 [1]. This establishes the development strategy for the long-term reduction of greenhouse gas emission in compliance with the Paris Agreement [2]. According to [1], the German target includes a reduction of greenhouse gas emissions of 55 % by 2030 and 80 % to 95 % by 2050 (compared with 1990). Electricity sector plays a relevant role for the achievement of such decarbonization targets. Energy production from conventional power plants, mainly based on fossil fuels, is going to be replaced by Renewable Energy Sources (RES) such as Photovoltaics (PV) or wind generation. This energy can be used to cover typical electricity demand but also to serve different fields. In fact, electricity from RES can directly be used in other forms by the electrification of strategical sectors such as transportation and heating. This leads to the deployment of innovative assets in power systems. For instance, due to the technological advance on Electric Vehicles (EVs), a relevant growth

in electrification of road transportation is expected within the next few years [3]. This leads to the development of a suitable charging infrastructure as additional power system technology. The use of renewable energy via the electrification of heating systems also leads to new components such as heat pumps while further technologies known as Power-to-X make use of electricity to supply sectors which cannot be electrified directly: shipping, aviation, heavy industry, just to mention a few. Technology advancement on co-generation systems such as Combined Heat and Power (CHP) plants enhances their application for both heating and electricity supply of buildings or urban districts. Among others, these technologies enable more effective storage of renewable energy in different forms within a comprehensive multi-energy system [4].

1.1 Background

The high penetration of RES together with the increasing share of innovative technologies result in structural consequences as well as management issues for a secure and reliable power system infrastructure. Conventionally, electricity was produced from large power plants connected to the transmission system and delivered to the final costumers through the distribution grid. However, RES such as PV or smaller wind plants are typically of a smaller power size and installed at different locations on the distribution grid. This leads to structural changes of power systems as electricity production takes place at distribution level by various Distributed Energy Resources (DER), thus altering the conventional unidirectional power flow. Moreover, electricity production from RES (as PV and wind) depends on variable factors such as actual weather conditions. Therefore, the large penetration of RES contributes to higher power flow volatility. Electrification of the energy and transportation sectors increases the overall electricity demand, thus challenging the actual power system infrastructure. Moreover, these innovative loads result in a different behaviour with respect to the well established patterns for conventional electricity demand. On the one

hand, these new characteristics of generation and demand can challenge the secure power system operation. Extreme behaviors such as generation or load peaks are more likely to happen. Therefore, more efforts are required to keep the global balance between electricity production and consumption. Moreover, grid violations such as voltage deviation or power congestion can also challenge power system operation at local level. On the other hand, such innovative components also provide additional opportunities for grid operators to improve power system management. In fact, various innovative assets have the potential to adapt their generation or consumption behavior in a controllable manner compared to their natural power profile. This flexibility can be used by network operators to adjust power profiles, thus avoiding grid violations. Moreover, advanced components such as inverter–based DER can be properly controlled to provide additional ancillary services for supporting grid operation. Innovation in typical assets for Distribution System Operators (DSOs) such as On-Load Tap Changer (OLTC) transformers can mitigate the impact of RES [5], [6]. Further components such as line voltage regulators [7–10] or power flow controllers [11], also provide additional control for grid operation, thus potentially reducing the need for additional grid extensions.

Over the past few years, the concept of smart grids has been introduced by the research community to define a suitable grid infrastructure to accommodate and accelerate the roll-out of such innovative technology. Even though a single and comprehensive community–accepted definition is not yet achieved, smart grids are generally intended as intelligent distribution grids where information is exchanged among grid users and assets. This information is used for automatic coordination or control actions such as balancing active power, coordinating generation and storage, providing active power flexibility to the electricity market, keeping voltages and currents of the distribution grids within given limits or providing active and reactive power flexibility to the transmission grid. The introduction of the smart grid concept increases the complexity of the power system.

The effective implementation of aforementioned smart grid functionalities requires the deployment of innovative solutions and technologies from different domains. Particularly, the application at distribution grid level of coordination and automation systems, advanced metering infrastructure, reliable and secure ICT become fundamental elements within the smart grid framework.

1.2 Motivation

Suitable testing approaches are required to ensure reliability, safety and proper system integration of innovative smart grid solutions and technologies before deployment. On the one hand, there is a need for testing methods to be capable to reproduce system complexity that reflects the actual smart grid architecture. This includes test activities with complex setups that involve multiple components also from different domains within a comprehensive system-level perspective. On the other hand, accurate outcomes must be provided to ensure results fidelity with respect to the actual real-world behaviors.

Conventional testing approaches such as full simulation, full hardware and field tests might result not longer suitable if considered individually. Software simulations and hardware setups represent the main approaches for testing complex systems in a controlled environment. Simulations can be practically scaled and can cover a wide range of scenarios, thus improving test coverage. Furthermore, worst-case conditions such as system failures can be assessed in a secure manner and without additional costs in the development phase. However, results of software simulation are strictly related to the accuracy of the simulated model. Especially for complex models, the simulation outcomes might require further measures to be validated. In contrast to simulation, the outcomes from hardware setups result in a close to real-world behavior, thus enhancing system validation. However, the development of complex hardware setups that are capable

to serve for multiple targets often results cost expansive and impractical. As a consequence, full hardware tests usually consist of small-scale setups that are limited to specific applications. Field tests permit to detect possible unexpected events and behaviors otherwise not considered within software simulation or hardware tests. However, testing on an uncontrolled environment (as the actual field), generally reduces the possibility to test under worst-case scenarios. Moreover, a field test is the most risky approach due to possible critical consequences (in terms of security and costs) in case of system failure. Therefore, a field test is usually the last step on the validation process.

Beside conventional methods, advanced laboratory testing procedures such as hardware-in-the-loop and co-simulation can be applied to enhance testing and validation at the component and at the system level. The former aims to overcome the limitations of full simulation tests and full hardware setups by merging these two approaches. Thanks to modern real-time simulators, physical components can be virtually interconnected with a simulated environment. Moreover, by means of dedicated supply systems, also power components can be interfaced within a software simulation, thus enabling the so called Power hardware-in-the-loop simulation. Within the co-simulation approach, multiple simulators can be coordinated to perform an overall simulation, thus reducing the computational effort of the single simulator. Moreover, multi-domain system models such as power system, heating system, information and communication technology can be implemented within the overall simulation without further simplifications or abstractions otherwise needed for a single simulation platform. The application of the hardware-in-the-loop technique within a co-simulation setup is also a possible procedure to further enhance the validation of the outcomes.

1.3 Scientific and technical objectives

This thesis aims to assess practical issues in the design and operation of advanced smart grid test infrastructures. These practical aspects are considered with particular emphasis on smart grid test facilities based on power hardware-in-the-loop technique. Particularly, the following three main aspects are considered:

1) **Design:** identification of the key design and quality attributes that advanced smart grid test facilities should provide. Particular emphasis is given to assess what is the minimal equipment and how it can be allocated within a proper architectural configuration especially for hosting PHIL systems.

2) **Operation:** analysis of the fundamental operational use-cases in order to identify the potential applications for advanced laboratory testing especially by means of PHIL systems. The goal is to determine how flexibly such systems can be operated to extend their applicability and the related criticisms to be considered.

3) **Application:** an existing laboratory infrastructure is considered as case-study in order to evaluate the applicability of the assessed design and operational aspects in a real-world facility. Exemplary test-cases are selected and performed in order to evaluate test capability and challenges in case of realistic research applications.

1.4 Thesis outline

This work is structured in seven main chapters. Chapter 2 and Chapter 3 are mainly based on scientific literature and technical reports.

Chapter 2 provides a summary of the state-of-the-art in the area of testing and validation with main focus on power system applications.

Chapter 3 includes a more detailed overview of the PHIL approach for advanced power system testing. This includes a description of the major components of a PHIL setup along with the principal hardware interfacing methods.

Chapter 4 assesses the major design and operational aspects for advanced laboratory infrastructures based on PHIL systems. The principal requirements along with the essential equipment and architectural concerns are analyzed. Furthermore, a formulation of the fundamental operational use-cases including PHIL systems is proposed.

Chapter 5 describes an existing smart grid laboratory that provides a study-case for the assessed design and operational concerns. Particularly, the design and system integration of a PHIL system are discussed in detail as a fundamental part of the test facility and principal element within this work.

Chapter 6 provides some practical implementations and laboratory tests on the deployed PHIL system in order to validate its fundamental test functionalities.

Chapter 7 collects the results of a selected set of laboratory test-cases based on realistic research applications for smart grids. These representative test-cases include testing at the component and at the system level which involve the application of the PHIL system.

Chapter 8 gives a final and critical evaluation of the overall outcomes of this thesis together with recommendations for further work.

Chapter 2

State-of-the-art

This chapter summarizes the state-of-the-art in testing, verification and validation approaches with main focus on power system applications. First, the major concerns about a system development process are introduced in a more general form. Later, the principal testing methods applied to power systems are discussed with a distinction between conventional and advanced testing approaches. Major concerns about strengths and weaknesses of these approaches are considered with particular emphasis on validation perspective within the smart grid paradigm. Lastly, a brief review of the present work related to smart grid laboratories along with considerations about relevant gaps in the available literature is given.

2.1 System development

The development of complex systems such as the smart grid one, requires appropriate approaches that ensure safety and reliability and enhance system integration before the deployment. System engineering approach is widely adopted in different application fields to define the development process of such complex systems. In contrast to traditional disciplines, within the system engineering approach a whole system is defined as a set of interrelated smaller systems or components working together toward

a common objective [12]. Many different models that specify a series of steps for system development within the systems engineering approach have been developed over the years. These methodologies vary in terms of the progression that is followed through the phases of the development process [13]. A largely adopted model is the so called V-model. The V-model exists under several variants that are developed according to the given application field [14]. Fig. 2.1 shows a minimal and more general representation of the V-model diagram. The development stages are articulated in four different

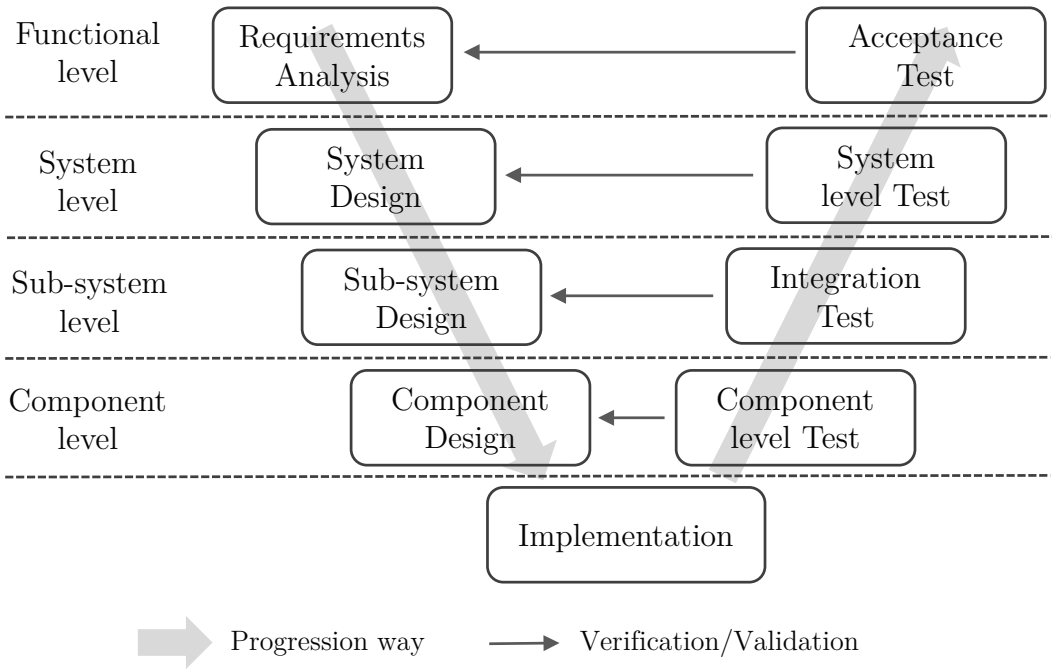

Fig. 2.1: The V-model for Systems Engineering Process

abstraction levels: component, sub-system, system and functional level. Particularly, the left-hand part refers to the design process while the right-hand part considers the testing process. As main features of this approach, verification and validation are performed at each abstraction level, thus ensuring that all the implemented parts meet both functional specifications and user requirements. The description of the development stages suggested by the the V-Model are discussed in the following sections.

2.1.1 Requirements, design and implementation

In accordance with the considered V-model, the principal preliminary stages that lead to complex system implementation can be summarized as:

Requirements analysis: consists of the examination of the properties that the overall system must provide for its final deployment. Requirements can be classified as functional and non-functional requirements. The former ones refer to the specific functions that the system must perform. The latter ones, define the principal quality attributes that the system must fulfill to perform a given function.

Design: consists of the translation of the defined requirements into the specifications for the correct system development. According to the V-model, design starts with the definition of the specifications for the overall system followed by the more detailed design at the sub-system and at the component level.

Implementation: refers to the practical realization of the designed system. According to the specific case, the implemented element can be a software or a hardware part or a combination of both.

2.1.2 Testing

Testing is applied to software and hardware parts of the developed system. Depending on the given abstraction level, testing includes:

Component-level test: also known as unit test, refers to test activities at the component level in order to prove that each individual element fulfills the design specifications.

Integration test: aims to prove the correct integration of the multiple components which are assembled to construct larger sub-systems. This is particularly important for complex systems where the individual components and sub-systems are created from multiple developers

from different fields. The correct interface of those heterogeneous parts is essential for the correct operation of the final system.

System-level test: consists of a set of trials that aims to prove the correct operation of the overall system functionalities.

Acceptance test: is typically performed by the customer itself to prove that the overall system meets the user-defined requirements.

2.1.3 Verification and validation

System testing can be intended as the activity conducted to perform verification and validation. These two terms refer to a different set of activities. As mentioned in [15], diverse definitions for verification and validation are given in the scientific and engineering literature. Among others, the following definitions are considered as reference for the context of this work.

According to the modelling and simulation community [15]:

> *Verification* is the process of determining that a model implementation accurately represents the developer's conceptual description and specification.
>
> *Validation* is the process of determining the degree to which a model is an accurate representation of the real world from the perspective of intended uses of the model.

According to the IEEE Community [16]:

> *Verification* is the process of evaluating a system or component to determine whether the system of a given development phase satisfies the conditions imposed at the start of that phase.
>
> *Validation* is the process of evaluating a system or component during or at the end of the development process to determine whether a system or component satisfies specified requirements.

The first definition fits with most of development processes related to power system applications. In fact, the use of mathematical models for describing power systems is a largely adopted method. Therefore, verification and validation with respect to the evaluation of model's effectiveness is an essential aspect. However, such models are supposed to be converted into practical systems for the final deployment. Therefore, according to the second definition, verification and validation referred to the satisfaction of the specified functional conditions is also appropriate.

2.2 Testing approaches for power systems

In the perspective of validation, testing approaches for power systems are distinguished between conventional and advanced approaches. To the former ones belong traditional methods and tools typically adopted for power system analysis, testing and validation. Among others, full simulation, full hardware and field tests represent the principal conventional approaches. The latter ones refer to innovative techniques that aim to overcome limitations of conventional approaches. In this regard, Hardware-in-the-loop (HIL) and co-simulation are the most promising advanced methods. HIL aims to improve test capability by combining simulation and physical parts within a common setup. Within a co-simulation, multiple simulators can be coordinated to perform a joint simulation. This reduces the computational effort of a single simulator and enhance parallel multi-domain simulation.

Advanced approaches are not intended to be the substitute of conventional approaches. According to the specific application, conventional testing approaches can still be suitable. However, the additional features provided by advanced approaches make those methods a promising option to meet the innovative test requirements needed for enhancing the smart grids development. The state-of-the-art in both the main conventional and advanced approaches is summarized in the following section.

2.2.1 Conventional simulation

The use of software tools for power system simulation is a common and largely adopted practice. A simulation consists of mathematical models of physical systems running on a generic computer that allow studies in both steady-state and dynamic conditions. Conventional simulation is also called offline simulation to distinguish from the real-time simulation approach (later introduced). Depending on the analysis or testing purpose, a suitable simulation model can be selected. The selection criterion for a suitable simulation model is generally based on the dynamics of the phenomena to be analyzed. The most used simulation methods applied to power system studies are as follows.

Root Mean Square (RMS) simulation (also known as Phasor-type simulation) consists of frequency-domain models where alternating quantities are approximated as sinusoidal waveforms at the network fundamental frequency. Typically, RMS models are implemented within the Phasor (here the name Phasor-type) or Laplace domain. The former is typically used for modelling power system components while the latter is often used for modelling component's controllers. In both cases, the power system is described by algebraic equations rather than differential equations, thus reducing the computation time and allowing for large scale simulations. Applying the Discrete Fourier Transform (DFT) within a discrete time-step ($T_\mathbf{s}$) to a periodic signal $x(\tau)$, $\tau \in [t - T_\mathbf{s}, t]$, the related phasor expression is obtained, as shown in (2.1) [17].

$$x(\tau) = A_0 cos(2\pi f_0 t + \varphi_0) \overset{DFT}{\Longleftrightarrow} X = A_0 e^{j\varphi_0} \tag{2.1}$$

where:

- A_0 Amplitude at the fundamental frequency
- f_0 fundamental frequency
- φ_0 phase at the fundamental frequency
- X phasor representing $x(\tau)$

As drawback, the assumption of RMS simulation neglects the representation of subcycle phenomena. This limitation can be observed when phenomena of interest have a dominant frequency deviation greater than ± 5 Hz with respect to the network fundamental frequency [18]. Moreover, most RMS simulations are based on symmetrical models, thus neglecting unbalance conditions. For this reason, RMS simulation is mainly used to assess classical power system issues such as planning, operation and stability analysis of large interconnected power systems where a detailed representation of transients can be neglected [19].

Electromagnetic Transient (EMT) simulation consists of time-domain models to reproduce the instantaneous voltage and current waveforms. EMT simulation adopts equivalent models deduced from the differential equations that govern power systems and is capable of representing not only electromagnetic phenomena but also the frequency dependence of network components, harmonics, unbalanced networks, power electronic devices, including the switching transients as well as the detailed controls and protection systems [20]. However, large scale simulations of such detailed models require higher computational efforts with respect to RMS simulations. EMT simulation consists of three main steps:

1. Discretization
2. Numerical integration
3. Network solution

Discretization is needed for the digital representation of the continuous waveforms quantity within a defined time-step (T_s). Then, a numerical integration method is used to solve differential equations that describe power system elements such as inductors or capacitors. The trapezoidal integration rule is one of the most applied approaches [21]. After numerical integration, all power system elements are modelled by the relationship between branch currents and nodal voltages.

The resulting system of algebraic equations that describes the state of the system at time t can be expressed in the following form:

$$\big[Y(T_\mathrm{s})\big]\big[v(t)\big] = \big[i(t)\big] - \big[I(t - T_\mathrm{s})\big] \tag{2.2}$$

where:

$\big[Y(T_\mathrm{s})\big]$	admittance matrix
$\big[v(t)\big]$	vector of nodal voltages
$\big[i(t)\big]$	vector of injected node currents of external sources
$\big[I(t-T_\mathrm{s})\big]$	vector of current sources from past history terms

The solution of (2.2) depends on the vector of current sources representing past history terms. This data storing might lead to memory issues especially for large simulations. The integration time-step can be fixed or variable during the simulation and determines both the accuracy and the complexity of the computation process. With the fixed approach the admittance matrix is not varying, thus reducing computation efforts. However, if the network includes switching elements (such as power electronics–based components) the admittance matrix varies and a recalculation is needed. Within the variable approach, time-step is reduced to increase accuracy when fast dynamics occur and increased during slow dynamics. The time-step variability will affect the buffer sizes continuously, thus challenging the computation [22]. A viable method to speed up computation is known as Bergeron's method [23]. In case of transmission system models, the natural delay due to the propagation of the electromagnetic waveforms on long transmission lines can be used to split the network into subsystems that can be solved independently. Each subsystem consists of a smaller admittance matrix that can be solved in much shorter time. If computational time for one of these subsystems is still too large, the common practice is to add artificial delays to enable parallel processing. An artificial delay is usually implemented by

adding a line with a given length adjusted to obtain a propagation time of one time-step. However, adding artificial delays implies additional parasitic inductances and capacitances that might affect the simulation outcomes [22].

Dynamic Phasor approach was proposed in [24] and applied for large power system simulations [25] as well as for power electronics–based components simulation [26]. Dynamic Phasor simulation can be intended as an extension of RMS where the periodical system quantities are described by a set of time varying Fourier coefficients that provide a suitable approximation of the original waveform. The Dynamic Phasor representation for a periodic waveform $x(\tau)$ on the time interval $\tau \in [t - T_{\mathbf{s}}, t]$ is expressed in (2.3). This approach provides more accurate models than the RMS ones along with less computation duty with respect to detailed EMT models.

$$x(\tau) \approx \sum_{n \in N} X_{\mathbf{n}}(t) e^{jn2\pi f_0 \tau} \tag{2.3}$$

where:

N	set of Fourier coefficients approximating $x(\tau)$
$X_{\mathbf{n}}(t)$	n^{th} time-variant Fourier coefficients (dynamic phasor)
f_0	fundamental frequency

Hybrid simulation techniques can also be used to combine EMT and RMS or Dynamic Phasor models into the same simulation [27], [28]. According to the object of the test, some of the simulated elements are approximated with RMS or Dynamic Phasor approach while EMT models are used for detailed system representation.

Many simulation tools are nowadays available for power system modeling and simulation. A detailed review of power system simulation tools is provided in [29] and [30]. A review of simulation tools particularly focusing on EMT simulation is given in [31]. Most simulation tools provide a

graphical environment together with model libraries that allow power system modelling as block-diagram. These tools speed up the modelling and implementation process. In fact, common power system parts such as transmission lines or classical power sources do not need to be modelled from scratch, thus allowing users to focus on theoretical concepts rather than programming issues. On the other hand, most commercial tools do not permit or limit the modification of default models and generally require costly licenses. Beside commercial products, open source software packages mainly based on Java and Python can be viable alternative for power system analysis and simulation. Most of these tools perform RMS simulation for power system calculation. In [32] the use of Python is particularly encouraged due to its flexibility and competitive performance. In [33], [34] a distribution grid planning tool based on Java Agent Development Framework (JADE) is introduced. The agent–based modelling approach is implemented to convert non-electric data (e.g., weather and economic information) into power feed-in and consumption while system state is obtained by time series load flow calculation. In [35], [36] a similar tool is also deployed to simulate agent–based control strategies for the flexible power system operation.

Validation of software simulation remains one of the most important issue. EMT modeling provides accurate simulation outcomes. However, EMT models might also need to be validated. Typically, simulation outcomes require to be compared with measurements from the field to be validated [22]. A comparison between the different models running on different simulation programs is also widely used in model validation. For example, a simplified RMS model can be checked against a well- proven EMT simulation [20].

2.2.2 Conventional laboratory–based testing

Conventional laboratory–based tests are performed on a physical environment that includes hardware elements connected together to implement a testbed. Testing with hardware aims to overcome the limitations of full simulation especially with respect to modelling issues. Full hardware setups are suitable for specific components or small systems testing. However, for wide and distributed systems as the power system infrastructure, it is obviously required to confine hardware setups within small representations. Therefore, hardware testing facilities aim to prove and validate power system applications on a reduced-scale setup in order to scale up the results to the real-world equivalent afterwards. One of the first applications was to use the analog Transient Network Analyzer (TNA) to emulate a power network by means of reduced-rate physical resistors, inductors and capacitors. In particular, the TNA was used for testing software and hardware controllers of Flexible AC Transmission System (FACTS) and High-Voltage Direct Current (HVDC) transmission. In [37] a small-scale analog TNA was used to validate the operation of reduced-scale hardware model of a Dynamic Power Flow Controller. However, the use of lumped parameters to represent transmission lines, unrealistic modelling of losses, ground mode of transmission lines and magnetic non-linearities represent the main limitations for TNAs [21]. Moreover, due to their cost and maintenance requirements TNAs were gradually replaced by real-time digital simulators or used for educational purposes [38].

Testing with full-rate hardware equipment is also an option. The HVDC Test Center [39] recently developed at TU Dortmund University is an example of such large-scale facilities. As main advantage, these infrastructures reproduce test conditions very close to field applications, thus enhancing validation purposes. As drawbacks, conventional full-scale facilities require high investment and maintenance costs and often personnel with special qualifications are essential to safely operate with specific components. Furthermore, the reconfiguration of those setups for different test purposes

often results in cost expensive investments. Therefore, full-scale laboratories are usually designed for limited and specific test purposes.

Along with the traditional laboratory setting, there is a rising tendency of living laboratories. Many times that is done by harnessing the power network in a university campus area, for example, by monitoring and automation equipment so that it can be used to implement new control strategies or test devices [40–43]. Such an approach can be cost-efficient due to the fact that the main infrastructure (cabling, transformers, possible generators, etc.) exists already and there is no lack of reality. On the other hand, the use is more restricted in order not to affect the normal network operation.

2.2.3 Field tests

Field tests are performed after the component installation at its final place of utilization. These are usually supplementary to factory tests (either simulations or laboratory tests) and therefore may not provide a complete investigation of the deployed component or system capabilities [16]. Tests under specific conditions such as worst-case scenarios or failure operations are not feasible directly within the field. However, field trials are still of importance for the validation of innovative components, system architectures and concepts. Particularly, aspects related to the integration and interface of those innovations within the existing power system can be properly assessed. Furthermore, unpredictable behaviors otherwise neglected due to the simplifications needed within simulations or laboratory tests can be analysed for further improvements. However, setting up a field test require much efforts and resources. Typically, special agreements between different involved parts such as research centers, manufacturers and grid operators are essential.

2.2.4 Real-time simulation

Real-time simulation refers to fixed-step solver methods where the simulator's clock is synchronized to the universal time. Therefore, a given period of actual time represents the same period of time in the system being modeled; simulated time advances at the same rate as actual time [16]. Although real-time simulation can also be performed as RMS simulation, EMT simulation type is the most of interest. In real-time simulation, the execution time (T_e), namely the time interval to process inputs, model calculation and outputs, should be shorter or equal to the defined time-step (T_s). If not, the simulation is not considered as real-time one, so that is called not-real-time simulation. A graphical representation of this concept is shown in Fig. 2.2. In the event that T_e is shorter than T_s, an idle time occurs before the following sample. This available time can be used to compute more calculations. Diversely, when T_e is greater than T_s overruns occur. In this case, the execution process is truncated before being completed, thus providing incorrect outcomes. In practice, overruns create distortion of the waveforms thereby producing an erroneous behavior of the system.

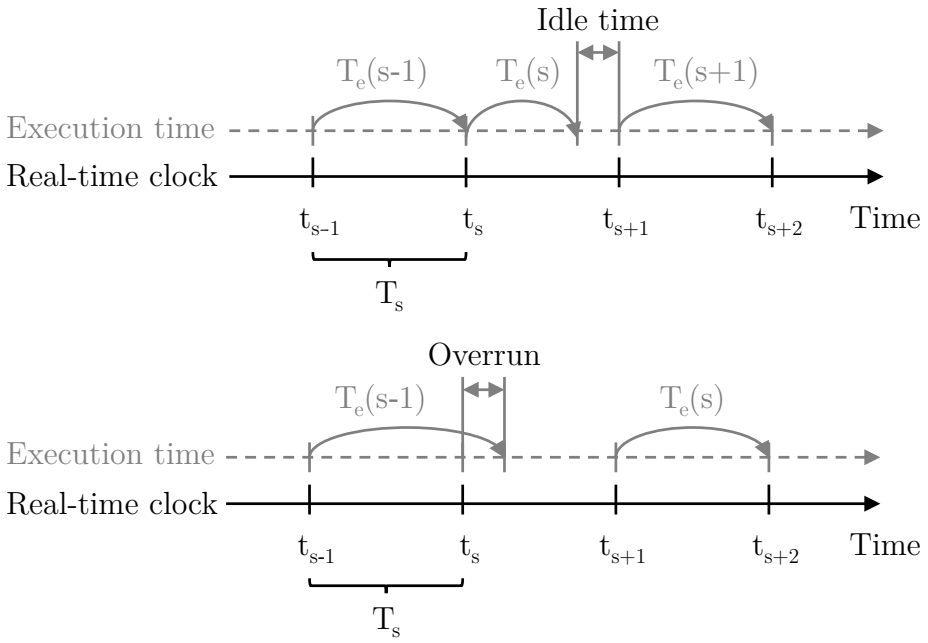

Fig. 2.2: Relationship between execution time and real-time clock in case of real-time simulation (top) and not-real-time simulation (bottom) [44]

Several approaches can be applied to avoid overruns. In case of transmission system models, the Bergeron's method (prior introduced for offline EMT simulations) can be applied. By the way, this decoupling method is not suitable for distribution grids where line and cable connections are much shorter and usually modelled with lumped elements. Also adding artificial delays can be problematic because the introduced parasitic inductances and capacitances will be larger compared to the actual component values. Therefore, the standard decoupling methods should be carefully used in distribution systems [22]. In [45] the State-Space-Nodal (SSN) method is introduced as more general approach to compute the time-domain solution of EMT real-time simulation. In contrast to offline EMT simulation where all the nodal voltages must be solved simultaneously, within the SSN approach the user arbitrarily selects the unknown nodal voltage points thereby splitting the overall network in subgroups (SSN groups). This approach reduces the time to compute the admittance matrix, thus allowing for faster simulations. Fig. 2.3 shows a comparison of nodes, branches and partitions between classical EMT nodal admittance method and SSN approach for an exemplary three-phase grid with π-model lines. Within the classical

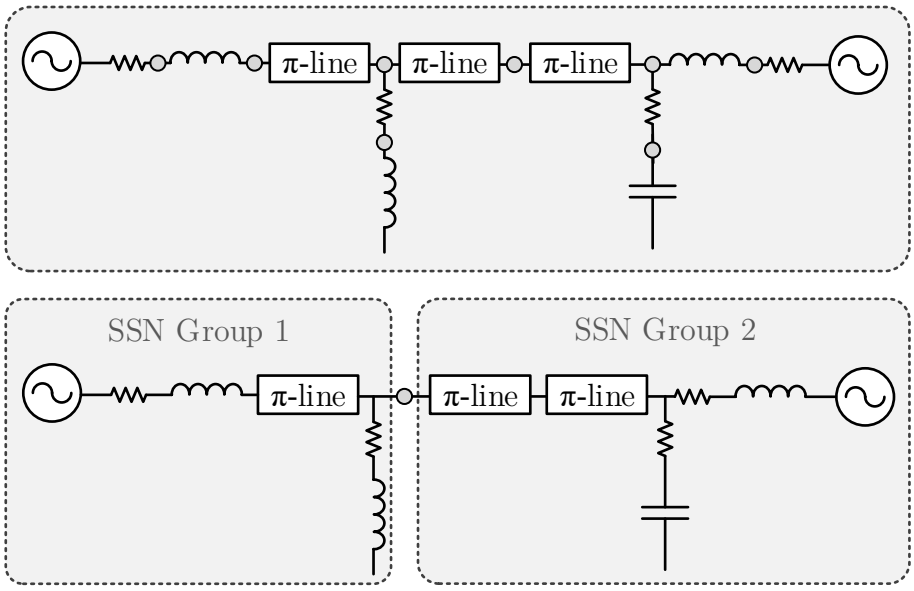

Fig. 2.3: Exemplary comparison of nodes, branches and partitions for classical EMTP nodal admittance method (top) and SSN approach (bottom), deduced from [22]

EMT approach (upper part), the grid consists of 18 nodes and 9 branches. Applying the SSN approach, the number of nodes can be reduced to 3 and the grid is split into two partitions (SSN groups). Therefore, the concept of branches from the classical approach is replaced with the more general multi-terminal partition element of the SSN method.

In the event that the SSN group's equations are too large, they can also be computed in parallel on different processor cores but without delays, thus accelerating the simulation even more. The SSN method is successfully applied to improve the simulation performance of large distribution networks in [46], [47]. It should be mentioned that even applying the SSN approach, the limited computation capability of the simulation platform might still lead to overruns. In those worst-cases, it might be needed either to increase the time-step of the simulation or to reduce the model complexity.

In contrast to offline EMT simulation, real-time simulation is usually performed on a dedicated hardware architecture: the Real-Time Simulator (RTS). The hardware design of a RTS differs depending on the manufacturer, in case of commercial products, or according to user requirements in case of custom-made configurations. However, most RTSs consist of two main physical platforms called target and host.

The target platform represents the core of a RTS and accommodates the required hardware for the simulation computation, the internal buses and the Inputs and Outputs (I/O) board for interfacing external physical devices (HIL purpose). Multi-parallel Central Processing Units (CPUs) and Field-Programmable Gate Arrays (FPGAs) are the state-of-the-art in hardware components for real-time computation. A comparison between these two technologies with respect to RTSs is given in [48] and [49]. CPU–based RTSs are more suitable for large-scale power system simulations involving complex solver methods. However, their limited sampling frequency allows low-bandwidth simulations. Moreover, additional delays due to the limited data transfer rate of the Peripheral Component Interconnect Express (PCIe) should be considered when performing HIL. Typically,

CPU–based simulations can achieve a minimal time-step in the 10–50 µs range [50]. FPGA–based RTSs, require more efforts for the model implementation and, therefore, they are less effective for complex computations. On the other hand, FPGA is more suitable for high-bandwidth applications (0.1–1 µs range [50]). Indeed, FPGA models can run at very high sampling rates and the I/O systems are directly connected to the model without the PCIe bus. This makes FPGA technology more suitable for HIL tests that require high dynamics. Hybrid architectures can include both CPUs and FPGA on the same target. In this case, FPGAs can be used for faster I/O processing.

The host is usually a generic computer where a defined software is used to manage all the implementation stages of a real-time simulation. Within CPU–based RTSs, the host computer permits model implementation and debugging also in offline mode. Then, the model is compiled into the target platform for the real-time simulation. In case of FPGA–based RTSs, the host can also be used to program the FPGAs. Furthermore, the host computer allows for managing and monitoring the simulation during real-time executions. Usually, commercial solutions also provide Application Programming Interfaces (APIs) based on common scripting tools for online model parameters update, thus enhancing automatic tests execution. Typically, the communication between the target platform and the host computer consists of an Ethernet link. Further features for commercial RTSs are later discussed in Section 5.3.2 with respect to a practical implementation.

Two main improvements of real-time simulation with regard to testing and validation can be deducted. On the one hand, RTSs provide a higher computation capability than classical offline EMT simulators, thus extending simulation and testing to larger power systems or more complex components. In fact, small benchmark models that are typically used as representative networks can be replaced with larger power systems models based on real-world network data. On the other hand, the possibility to incorporate

physical components within HIL approach allows for more close to real-world results. In fact, replacing model parts with the respective physical components reduces propagation of errors due to model approximations, thus improving the overall outcomes.

2.2.5 Hardware-in-the-loop

One of the main features of real-time simulation is the capability to interact with a physical component by exchanging digital or analog signals in real-time. The HIL simulation is realized when one or more parts are physical components that are connected to the rest of a simulated system. In this case, the scope of the simulation is the hardware device testing. A basic HIL setup requires three main components: the Hardware under Test (HuT), a simulator, and the interface between them. The HuT represents the object of the test and can be generally intended as a physical device that includes various units such as control, measurements, communication and power elements. Typically, a RTS is used to perform HIL simulations. However, for slow dynamic applications, HIL based on offline simulation can also be possible. In this case, the time period of the interaction between the simulator and the HuT must be larger than the maximum time for computation [51]. In [52], an optimal charging control for Electric Vehicles (EVs) is investigated with a HIL setup based on Python simulation. In this case, grid loads as well as the charging controller are simulated in Python with one second time-step while further physical components are looped within the simulation. Apart from specific applications, HIL approach based on real-time simulation remains the most common method. Therefore, in the rest of this work the HIL approach is referred as the real-time one. The interface is defined as the shared boundary between the simulation and the physical environment [16]. The interface consists of different components according to the nature of the HuT to be interfaced. Fig. 2.4 shows a schematics of the principal HIL techniques.

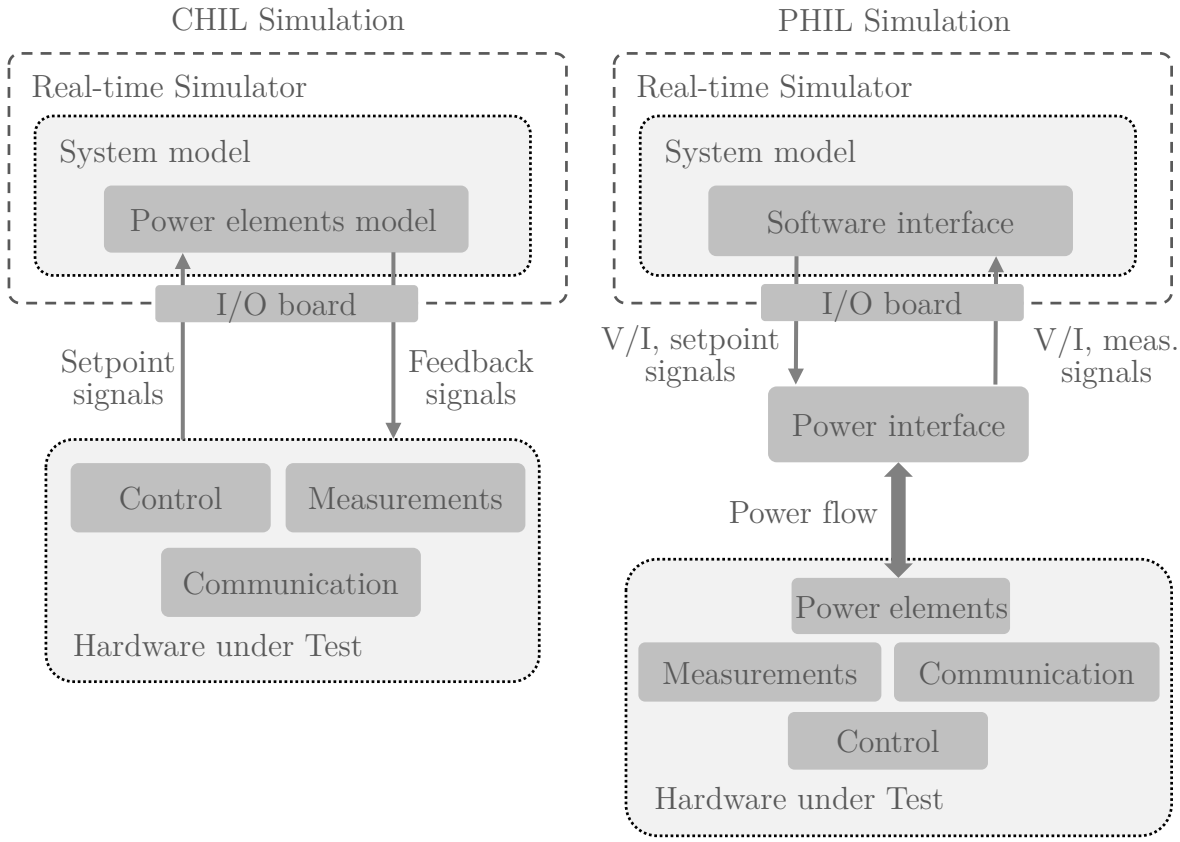

Fig. 2.4: Block diagram of the majors HIL simulation techniques: CHIL simulation (left-hand), PHIL simulation (right-hand)

When the HuT is a controller and its power elements are modelled within the RTS, the simulation is called Controller hardware-in-the-loop (CHIL). In this case, the HuT exchanges analog or digital signals (setpoints and feedbacks) with the RTS. Therefore, the interface consists of the I/O board of the RTS. The I/O board is equipped with Digital-to-Analog Converters (DACs) and Analog-to-Digital Converters (ADCs) for analog signals exchange. Digital I/O are also included to permits communication message exchange (e.g., based on Transmission Control Protocol/Internet Protocol (TCP/IP)). Indeed, within a CHIL simulation the HuT can include not only the controller unit but also the measurements and communication units. Diversely, the power apparatus of the HuT is entirely modelled within the simulation. Therefore, CHIL simulation is a reasonable option for those applications in which otherwise testing including power elements would require a complex hardware setup. Concerning power system simula-

tion, the CHIL approach is largely adopted for testing protection devices [53], [54]. In this case, power system failures can be reproduced within the simulation, thus reducing the risk of damaging expensive equipment while the physical protection device can still be safely tested. Previous works demonstrate that CHIL simulation also enhances the automation in application oriented testing of physical devices [55]. Another classical application is the validation of FACTS [56], [57] or controllers for wind plants [58], [59]. In fact, due to the power rating and complexity of these components a full hardware setup would require a dedicated test infrastructure. Further typical CHIL applications include testing of measurement devices such as Phasor Measurement Units (PMUs) for grid monitoring [60], [61]. Due to the upcoming smart grid concept, CHIL simulation is nowadays applied for research on distribution grids [62]. In recent work, CHIL is applied for testing innovative grid management concepts [63] or combined measurement, protection and control devices [64] as well as controllers for specific technologies such as storage systems [65], [66] or EV charging stations [67]. However, the precision of the simulation outcomes are strictly related to the accuracy of the power part's model. Moreover, possible interface non-idealities such as delays might also compromise the correctness of the results.

When the HuT includes its power apparatus, a power flow emulation between the device and the simulated system is required and the simulation is called Power hardware-in-the-loop (PHIL). In addition to the I/O board, a power interface is needed to scale up the signals coming from the RTS, thus supplying the HuT. The measurements from the physical environment are fed back to the simulator thereby closing the loop. Typically, the measurement system is embedded to the power interface. The software interface reproduces the measurements from the physical HuT within the simulated system. In contrast to the power elements model for the CHIL setup, the software interface is an elemental model (typically a controlled source) that transfers the electrical measurements from the HuT to the

simulated system. This represents the main advantage of PHIL simulation; complex and detailed models are no longer needed because the model of the power apparatus is replaced by the physical component. However, the design of the software interface must be properly coordinated with the power interface configuration in order to guarantee the stability and the adequate accuracy of the overall PHIL setup (see Chapter 3). The most common PHIL application is the testing of power converters. This also includes components from various fields such as aerospace [68], naval applications [69], rail transportation [70], [71] or automotive [72]. Concerning power system applications, conventional PHIL simulation includes grid emulation for testing grid connected inverters [73–76] or further electrical components such as motors and drives [77], [78]. Special setups as in [79] consider multi-physics PHIL, thus combining mechanical and electrical parts emulation. Least popular is the application of PHIL for components emulation such as loads [80], cables [81], [82] or electrical machines [83], [84].

2.2.6 Co-simulation

Co-simulation refers to a test approach where multiple and independent simulation tools are coordinated together to perform an overall joint simulation. The involved tools, exchange a defined amount of data as output, in order to share their own outcomes with the rest of the simulators, and as input for internal model updating. Therefore, the overall simulation computation is distributed into multiple simulators, thus enhancing large-scale and more complex simulations. Furthermore, specialized tools for different domains such as heating systems or Information and Communications Technology (ICT) systems can be included in addition to power system tools which is an essential aspect within smart grids applications. Recent work on power system co-simulation includes efforts to integrate communication, automation and control [51], [85].

Co-simulation is particularly of interest not only for conventional simulation but also with respect to real-time simulation and HIL testing. Indeed, one of

the limitations of HIL is the limited scale of the hardware test environment. Typically, the available equipment of a laboratory facility belong to a specific domain and technology. Therefore, co-simulation would be a viable option to merge the test capabilities from different test infrastructures. The share of heterogeneous components might benefit the single facility by avoiding extra costs due to additional facility extensions. Moreover, merging the expertise from different fields contributes to achieving higher quality results. In recent work, experimental co-simulation tests are performed involving test facilities form different geographical location also including remote PHIL [86], [87]. The main challenge of such co-simulations remain the synchronisation and coordination of such distributed setups taking into account the required data transfer architectures and the non-idealities of live data streaming. Further barriers related to data sharing policy or cyber security might also be a limitation when linking different facilities.

2.3 Related work and relevant gaps

Over the past few years, the number of test facilities in the area of smart grids in Europe and worldwide has significantly increased. Research laboratories focused on smart grids exist in several forms and for different research targets. Within this review, mainly research laboratories with a public or semi-public character are considered, this means universities and public or partly public research institutions. A recent survey based on numerous smart grid laboratories worldwide [88], shows that most facilities are active on diverse areas such as Distributed Energy Resources (DER), Distribution Automation, Grid Management, Electromobility, Energy Storage, just to mention a few. Typically, laboratories cover multiple topics in combination rather than a specific one. For instance, a quite common research target includes combined studies on DER and Grid Automation. The survey also shows a common trend on interactions between different facilities within collaborative activities. This include a two-way exchange of data and expertise as well as sharing of test capability by joint setups.

In addition to the scientific focus, laboratories largely vary in size and testing approach. According to the laboratories gathered in [89], the major test facilities in Europe operate at Low-Voltage (LV) level. Such facilities are characterized by AC power rating between 100 and 500 kVA with a voltage level up to 400 V, as typical European LV distribution networks. Just a few facilities operate at Medium-Voltage (MV) level with voltage rating over 10 kV. DC testing is also a common practice. DC power rating between 10 and 50 kW with voltage level up to 400 V, and in many cases also between 400 and 2000 V, are the most common. Many facilities also include a number of physical busbars that typically varies between 3 to 5 to connect multiple components within a desired grid topology.

Further reports confirm the rising tendency of most test facilities to perform HIL simulation in the form of both CHIL and PHIL [89–91]. This endorses the fact that HIL has become a largely accepted testing approach for smart grid applications within the recent years. Smart grid laboratories based on HIL should be designed properly in order to enhance the capability of this testing approach. However, most of the publicly available resources seem to underestimate the design and development aspects for HIL facilities. Aspects such as functional and non-functional requirements or minimal type and amount of necessary components are usually not assessed in the current literature. Major effort is particularly given for describing a holistic approach for smart grid testing also including HIL techniques, as in [92], [93]. Similar smart grid testing methodologies are investigated in [94]. However, minor concerns are given with respect to the design concepts and suitable architectural options for such smart grid laboratories. Moreover, while most studies deal with the application of HIL for a specific test purpose, less resources assess the issue of defining the practical use-cases and recommended procedures for applying this technique in a more extensive manner. Many works focus on the assessment of PHIL and its implementation [50], [95]. However, most of those works mainly focus on a single and more general understood use-case where a physical component

can be tested as if connected to an actual electric grid. Therefore, for a clearer understanding of the test capabilities within the HIL approach, a more detailed and generalized classification of the use-cases for the effective utilization of this testing method is needed. Other works focus on the theoretical assessment of PHIL especially concerning stability and accuracy issues with different interface approaches (see Chapter 3). However, less emphasis is given on the definition of configuration schemes for more general use-cases.

As part of this thesis, the aforementioned considerations are taken into account and further analyzed to provide a valuable contribution on these lacking aspects.

Chapter 3

Fundamentals of PHIL simulation

Concerning power system applications, a typical PHIL setup can be simplified with an equivalent circuit. The overall simulated network as well as the physical HuT to be interfaced are modeled with a Thévenin equivalent circuit, as shown in Fig. 3.1. The grid model from the software side is represented by the voltage source V_{SW} and the equivalent impedance Z_{SW}. The equivalent model of the simulated grid is also called Rest of the System (ROS). Similarly, the HuT can be generalised as voltage source V_{HuT} along with its impedance Z_{HuT}. The interface apparatus implements the interconnection between the hardware and the software side and consists

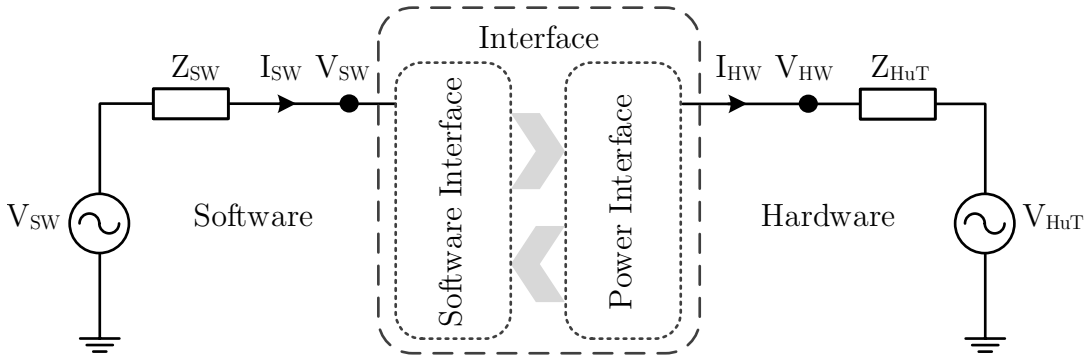

Fig. 3.1: Equivalent circuit of a PHIL setup

of two elements: a power interface and a software interface. The former is the hardware component in charge to emulate the electrical connection point of the simulated network into the physical environment. The latter is the software model that reproduces the electrical behavior of the HuT within the simulated network. The Interface Approach (IA) defines the configuration and the specifications of both the power interface and the software interface within a PHIL setup. These specifications include the type, quantity and function of the interconnection circuits and the type and form of signals to be interchanged between those circuits [16].

3.1 Power interface

Although some applications might require a conventional generator [96], [97], the most common power interface for PHIL simulations consists of Power Amplifiers (PAs). The PA is a power electronics–based device able to amplify an input signal by modulating an external power source. The PA is the output stage of an overall power conversion system that typically includes a main grid converter (to provide the DC supply to the PA) along with the required additional components such as filters, control unit, measurements and communication systems. A simplified schematics of a PA system is shown in Fig. 3.2 where the PA is depicted with a triangle. The input and output quantities can be either voltages or currents. Power can also be used as an input or output quantity but usually is considered as

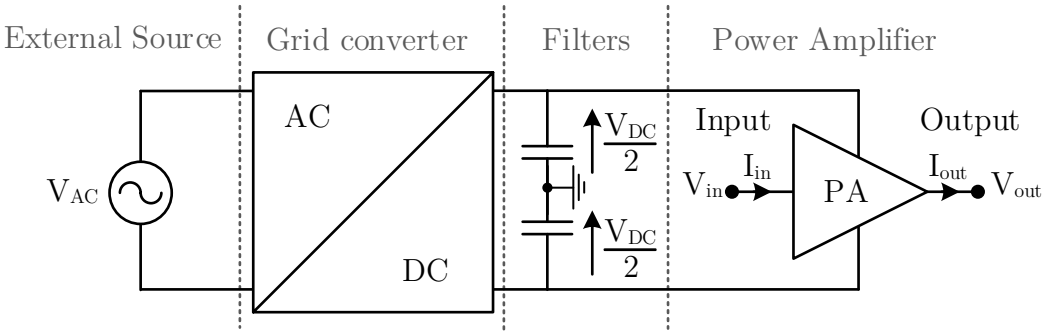

Fig. 3.2: Simplified schematics of a power amplifier system

a dependent quantity. Ideally, a PA should have unity gain with an infinite bandwidth and no time delay, but this is neither achievable nor affordable [50]. In reality, undesired effects such as time delays, sensor noise, gain- and phase-error and offset are present. Some of those non-ideal effects also depend on the PA's technology.

3.1.1 Technology of power amplifiers

Power transistors such as Bipolar Junction Transistors (BJTs), Insulated Gate Bipolar Transistors (IGBTs) or Metal Oxide Semiconductor Field Effect Transistors (MOSFETs) are the most common controllable devices that implement a specific PA stage. Depending on the way of driving the power transistors, PAs are grouped into two main categories: linear or switched-mode. In linear PAs the power transistors are driven as variable resistors. Each transistor operates in conduction mode ("on" state) along the linear zone of its I/V characteristics. In switched-mode PAs the power transistors are driven as controlled switches, thus commuting between conduction and interdiction mode ("off" state) with a defined frequency.

Linear PAs are further divided into different operation classes. Operation classes A, B, AB, and C are the most popular [98–100]. Fig. 3.3 shows the operating principle of those amplifier classes for a BJT with ideal I/V characteristics. The instantaneous base-emitter voltage $v_{\mathrm{be}}(t)$ represents the input signal while the instantaneous base current $i_{\mathrm{b}}(t)$ is the current conducted by the transistor. The biasing point (q) determines the conduction angle of the transistor. In Class A operation, the transistor conducts over the whole period (2π) of the input signal. Class B operation is defined for π conduction angle. In this case, only half cycle of the alternating input signal is converted into current. Therefore, an additional transistor is needed to reproduce the whole input waveform. Class AB is introduced to overcome the phenomenon of crossover distortion typical for Class B operation (not shown here but detailed described in [99]). In Class AB operation, each transistor conducts between π and 2π . Lastly, Class C operation is defined

for conduction angles greater than 2π. Fig. 3.4 shows an exemplary class

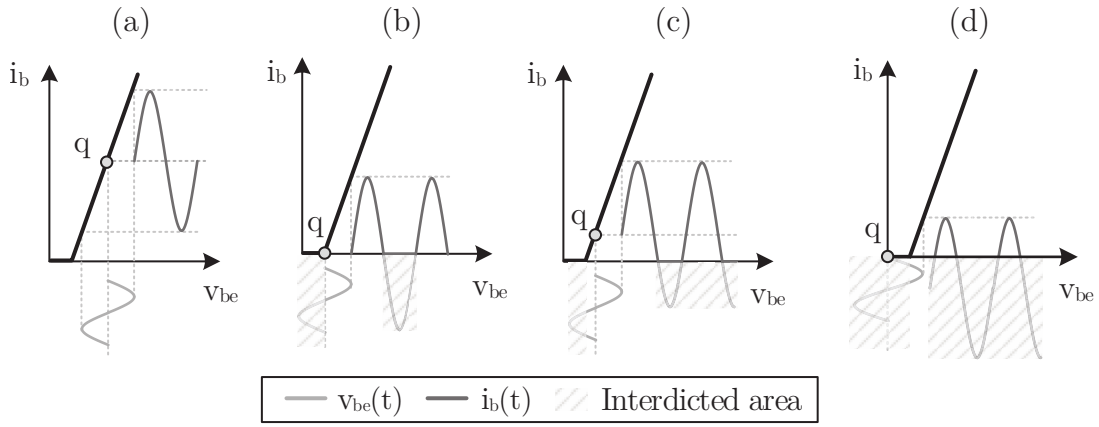

Fig. 3.3: Operation classes for linear power amplifiers in case of ideal transistor: (a) Class A, (b) Class B (c) Class AB, (d) Class C

AB linear PA and the respective input and output voltage waveforms. Two transistors are need in order to amplify both positive and negative half cycles of the input signal. The input voltage is directly sent to the power transistors and the output voltage is linearly amplified according to the transistor characteristics.

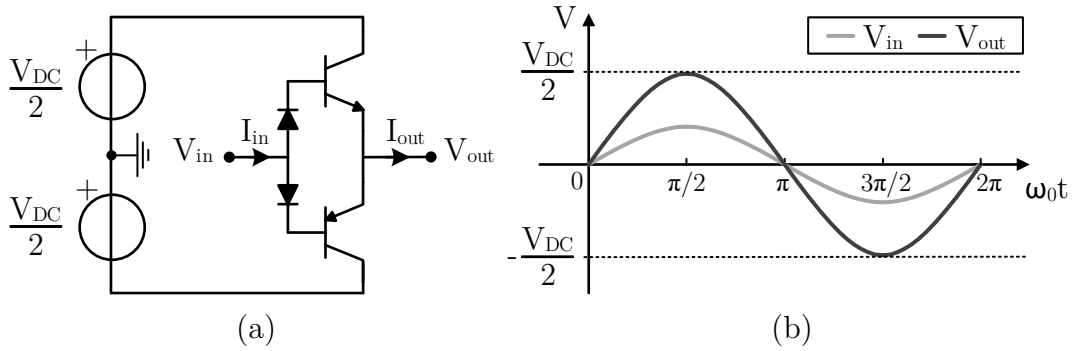

Fig. 3.4: Exemplary Class AB linear power amplifier: (a) Push-pull configuration, (b) Voltage waveforms

Switched-mode power amplifiers (also known as Class D amplifiers) generate the output quantity by switching between two or more voltage or current levels. A modulator processes the input signal and provides a two-level switching signal that determines the state of the transistor (on or off). The typical modulation technique is the Pulse-Width Modulation (PWM).

The input signal is compared with a triangular waveform with a frequency greater than the highest frequency in the input waveform. The frequency of the PWM determines the switching frequency of the power transistor. The output waveform is filtered by using inductive and capacitive reactors. The reactors supply the PA output within the time intervals in which the transistor is in the interdiction state. Fig. 3.5 shows an exemplary topology of a switched-mode PA known as half-bridge configuration together with its typical waveforms.

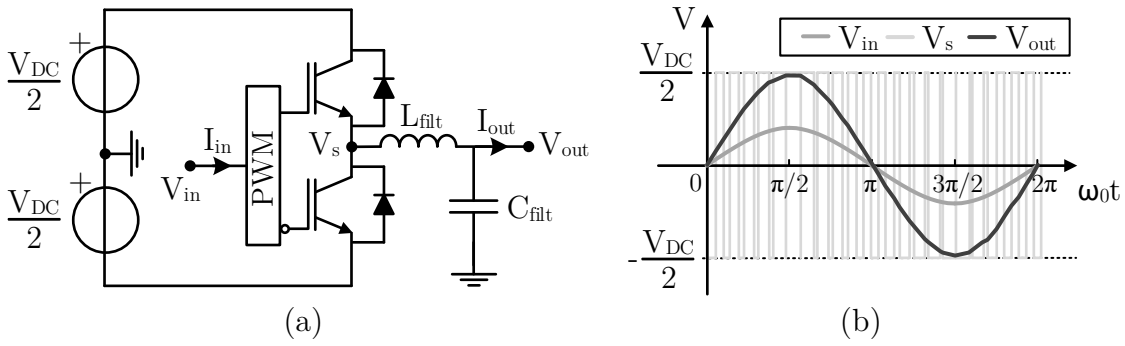

Fig. 3.5: Exemplary switched-mode power amplifier: (a) Half-bridge IGBT configuration, (b) Voltage waveforms

3.1.2 Technology comparison for PHIL

The selection between linear and switched-mode technology determines not only the performance but also the weight, size and cost of the overall PA system. As underlined in [101], there is no technology better than another one but the appropriate solution is the one that meets the specific application requirements. Previous work examined the performance of linear and switched-mode PAs with main focus on PHIL applications [102], [103]. Linear PAs provide more effective dynamic characteristics such as high bandwidth (up to 20 kHz [50]) and fast response time. However, the conduction losses of the power transistors drastically reduce the overall efficiency. The theoretical maximum efficiency is 50 % for Class A, 78.5 % for Class B and even less than 78.5 % for Class AB operation [98]. Therefore, linear PAs are suitable for low power PHIL applications. Switched-mode

PAs provide a higher efficiency due to the lower conduction losses of the power transistors. Although additional components such as filters contribute to system losses, the overall efficiency is typically greater than 80 % [101]. Moreover, switched-mode PAs are characterized by additional sources of distortion inherent their operating principle. Distortion due to dead-time, output ripple, non-idealities and external factors such as Electromagnetic Interferences (EMI) typically limit the bandwidth of switched-mode PAs. The switching frequency can be selected, in order to optimize the dynamic behavior and have an effective bandwidth of up to 2–10 kHz [50]. Therefore, switched-mode PAs are preferred for PHIL simulation ranging from small-scale power applications up to the megawatt range where efficiency is predominant rather than system dynamics.

3.2 Interface Approaches

The selection of the appropriate IA is usually based on a trade-off between its performance in terms of stability and accuracy and the complexity of its practical implementation. Both depend on the configuration requirements of the software interface and the power interface (depending on the selected IA additional hardware components could be required). Several alternative IAs are proposed and analyzed in [50, 104–106]. As result of these studies, the so called Ideal Transformer Method (ITM) and Damping Impedance Method (DIM) are suggested as the most effective IAs for PHIL simulations not only in terms of stability and accuracy but also due to their practical implementation [107], [108]. Moreover, ITM and DIM provide good performance also in case of non-linear HuT as power converters [105]. According to the nature of the HuT to be interfaced, each IA can be configured as voltage-type or current-type. Fig. 3.6 shows the equivalent circuit of the ITM for both voltage-type (V-ITM) and current-type (I-ITM) configurations. According to its simple implementation, the ITM can be considered as the most natural interface scheme for a PHIL simulation. Both software and power interfaces have minimal requirements. The software interface

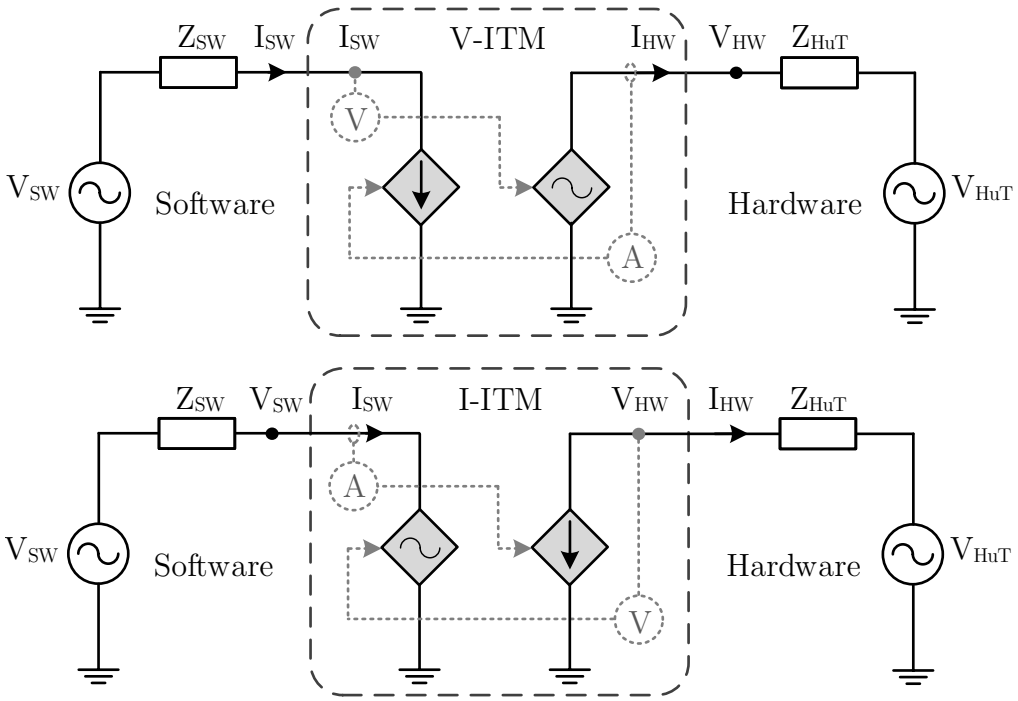

Fig. 3.6: Equivalent circuit for the ITM IA: voltage type (top), current type (bottom)

is implemented as a controlled generator. Additional resistors are usually needed to improve the convergence of the solution. However, the contribution of those components on the performance of the overall simulation can be usually neglected. The power interface (here ideally represented as controlled generator) does not require particular settings or additional hardware components to be included. From both software and hardware sides only one measurement is required to perform the virtual connection between the two circuits.

The DIM can be implemented with a minimal configuration [104], [107], as shown in Fig. 3.7. Compared to the ITM, the software interface for the DIM requires one additional controlled generator and a virtual damping impedance (Z_{D}). In contrast to the ITM, two measurements are needed from the hardware side in order to virtually connect the two circuits. As discussed in the following section, the damping impedance must be properly designed to meet the stability and accuracy requirements for the overall PHIL setup.

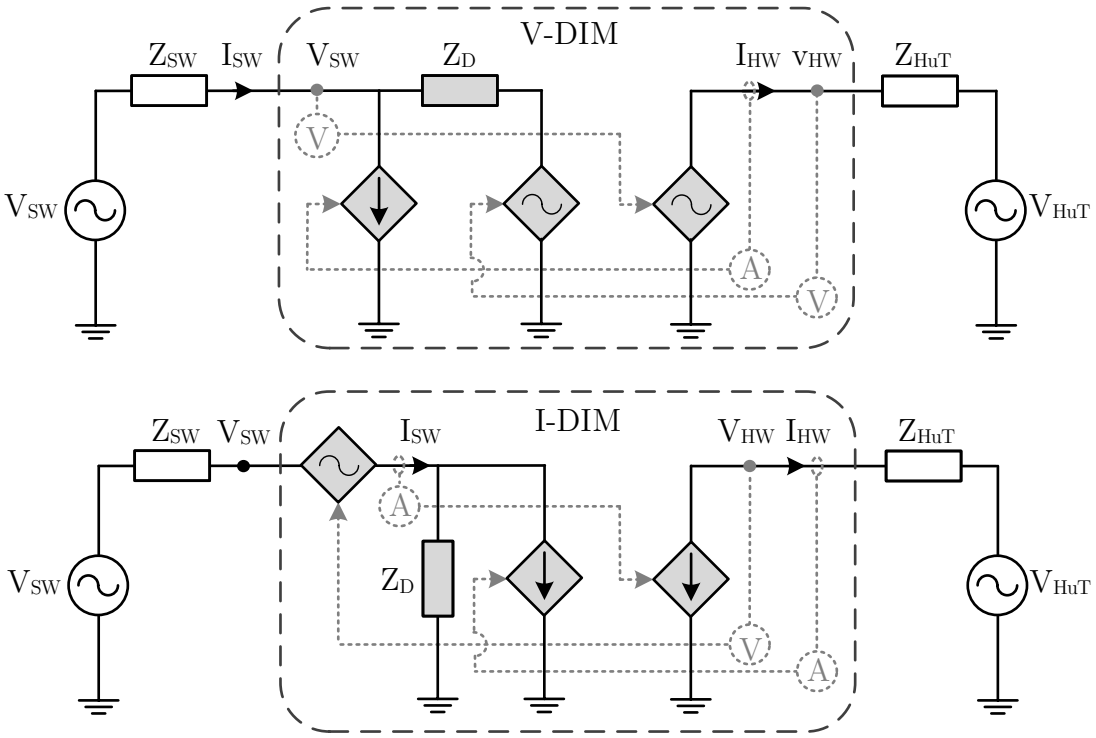

Fig. 3.7: Equivalent circuit for the DIM IA: voltage type (top), current type (bottom)

3.3 Stability and accuracy

Stability and accuracy issues represent the main challenges in developing and operating PHIL testbeds. Within a PHIL setup a number of non-idealities such as PA bandwidth, sensor noise and time delay may affect both system stability and accuracy. In case of unstable PHIL simulation voltage and current waveforms result extremely distorted and diverge to amplitudes that might highly exceed the normal operating range. Therefore, stability of a PHIL must be properly evaluated before the implementation in order to prevent test failures and preserve the integrity of the overall looped physical components. Accuracy is an index of performance and precision of the results for a PHIL test. Therefore, accuracy is of importance to validate the overall PHIL experiment. Several approaches can be applied to quantify accuracy of PHIL simulations. However, the definition of a community accepted approach still remains an open research issue. Previous work

suggests two principal approaches for stability evaluation [109]. The two approaches are discussed hereunder.

Time-domain approach

The time-domain approach consists of preliminary offline simulations where the whole PHIL setup (including the HuT) is implemented within a simulation model. The non-idealities of the looped components are also included within the simulation. Then, the simulation outcomes are analysed in order to define the stability limits of the specific setup. The main drawback of this method is that accurate models of the looped component are required.

Frequency-domain approach

The frequency-domain approach is largely applied for preliminary stability and accuracy evaluation. The non-ideal behavior of a PHIL setup can be modelled considering the transfer function of the looped parts. In [110] a detailed characterization of PHIL setups is suggested. An exhaustive analysis of the delay contribution is also given in [111]. However, a simplified approach is typically preferred for preliminary analysis. Fig. 3.8 shows the block diagram in the Laplace domain for a general PHIL setup. The signal from the simulation (S_{SW}) and the signal from the hardware (S_{HW}) can be either voltages or currents according to the adopted IA. The equivalent impedance from the software and hardware side are expressed with the

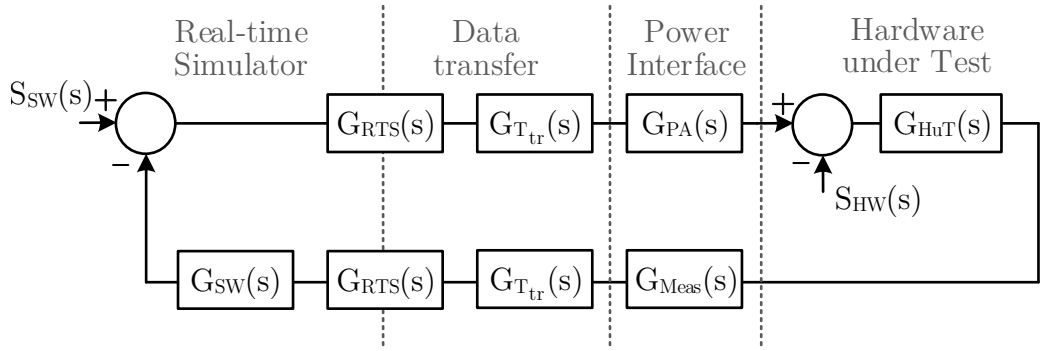

Fig. 3.8: Block diagram for a general PHIL setup in the Laplace domain

transfer functions $G_{\mathrm{SW}}(s)$ and $G_{\mathrm{HW}}(s)$, respectively. The DAC and the ADC of the RTS are modelled with the transfer function in (3.1). Typically, a unity gain is assumed while the delay contribution due to the discrete time-step of the simulation (T_{s}) is considered.

$$G_{\mathrm{RTS}}(s) = e^{-sT_{\mathrm{s}}} \tag{3.1}$$

The delay due to the data transfer from the RTS to the PA as well as the data transfer from the measurement system to the RTS can be assumed to be similar (T_{tr}) and the corresponding transfer function results:

$$G_{\mathrm{T_{tr}}}(s) = e^{-sT_{\mathrm{tr}}} \tag{3.2}$$

The transfer function of the PA (3.3) and measurements system (3.4) can be modelled as second-order Low-Pass Filter (LPF) and first-order LPF, respectively [102], [112].

$$G_{\mathrm{PA}}(s) = \frac{(2\pi f_{\mathrm{PA}})^2}{s^2 + 2\zeta\pi f_{\mathrm{PA}} s + (2\pi f_{\mathrm{PA}})^2} e^{-sT_{\mathrm{PA}}} \tag{3.3}$$

$$G_{\mathrm{Meas}}(s) = \frac{2\pi f_{\mathrm{Sensor}}}{s + 2\pi f_{\mathrm{Sensor}}} \tag{3.4}$$

where:

f_{PA}	PA bandwidth
ζ	Damping ratio
T_{PA}	Delay due to PA drives
f_{Sensor}	Measurements bandwidth

After the identification of the principal transfer functions, stability and accuracy are analysed with respect to the closed-loop system described in Fig. 3.8. However, the depicted system differs according to the adopted IA. Previous works provide a detailed analysis of stability and accuracy for different IAs [113], [106]. As scope of review, stability and accuracy

evaluation is discussed in the following section with the respect to the ITM and DIM within the frequency-domain approach.

3.3.1 Stability of the ITM

Considering the V-ITM (see Fig. 3.6), the resulting block diagram is depicted in Fig. 3.9. The stability analysis is performed with respect to the open-loop

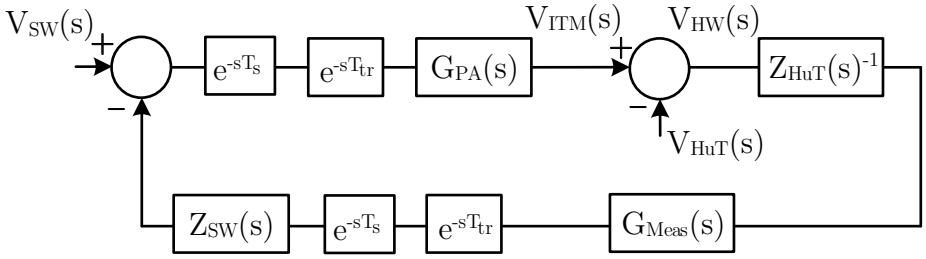

Fig. 3.9: Block diagram for the V-ITM in the Laplace domain

transfer function:

$$G_{\mathrm{OL\_V-ITM}}(s) = \frac{V_{\mathrm{ITM}}(s)}{V_{\mathrm{HW}}(s)} = \frac{Z_{\mathrm{SW}}(s)}{Z_{\mathrm{HW}}(s)} G_{\mathrm{PA}}(s) G_{\mathrm{Meas}}(s) e^{-s2(T_{\mathrm{s}}+T_{\mathrm{tr}})} \tag{3.5}$$

According to the Nyquist criteria, the stability condition for (3.5) is satisfied when $|G_{\mathrm{OL\_V-ITM}}(s)| < 1$. In the case of ideal interface ($G_{\mathrm{PA}}(s) = G_{\mathrm{Meas}}(s) = 1$) the stability condition results:

$$r_{\mathrm{z}} = \left| \frac{Z_{\mathrm{SW}}}{Z_{\mathrm{HW}}} \right| < 1 \tag{3.6}$$

Therefore, the stability strictly depends on the impedance ratio, namely the circuits to be interconnected. The Nyquist diagram in Fig. 3.10 shows the possible conditions for (3.5) depending on different values of the impedance ratio. This dependency can be critical especially when the HuT is not a constant impedance. In this case, Z_{HW} varies dynamically according to the actual operating point of the HuT. Therefore, even an initially stable PHIL simulation might become unstable during the test execution for certain operating points of the HuT.

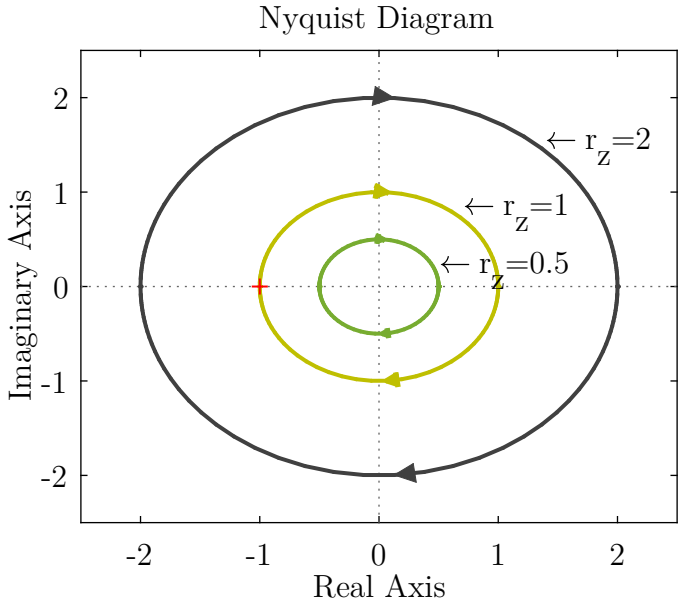

Fig. 3.10: Nyquist diagram for the V-ITM with different impedance ratio: stable condition ($r_z = 0.5$), limit for the stable condition ($r_z = 1$) and unstable condition ($r_z = 2$). First order Padé approximation is used to linearize the delay in (3.5)[1]

Contrary to the V-ITM, the open-loop transfer function for the I-ITM is expressed as follows:

$$G_{\mathrm{OL\_I-ITM}}(s) = \frac{V_{\mathrm{ITM}}(s)}{V_{\mathrm{HW}}(s)} = \frac{Z_{\mathrm{HW}}(s)}{Z_{\mathrm{SW}}(s)} G_{\mathrm{PA}}(s) G_{\mathrm{Meas}}(s) e^{-s2(T_{\mathrm{s}}+T_{\mathrm{tr}})} \tag{3.7}$$

and the stability condition results:

$$r_{\mathrm{z}} = \left| \frac{Z_{\mathrm{SW}}}{Z_{\mathrm{HW}}} \right| > 1 \tag{3.8}$$

Therefore, according to the impedance ratio, the I-ITM might be preferred rather than the V-ITM. However, the possibility to select the V-type rather

[1]First order Padé approximation of the transfer function for a pure time delay τ:

$$e^{-s\tau} \approx \frac{-\frac{\tau}{2}s + 1}{\frac{\tau}{2}s + 1}$$

than the I-type interface can be limited by the nature of the HuT (i.e., when the HuT behaves either as a voltage or current source).

The stability analysis carried out according to the Nyquist method presents some limitations when the contribution of the frequency depending elements (inductive and capacitive reactances) of Z_{HW} are significant with respect to the resistive one. In this case, the conditions in (3.6) and (3.8) are not sufficient to ensure system stability. In [114] an alternative stability assessment method that takes into account the discrete-time representation of impedance from both software and hardware sides is suggested. Other works propose the Routh-Hurwitz criterion as a more suitable stability evaluation method [115], [116]. According to this approach, the stability conditions can be assessed with regard to the exact nature (R, L, C and their combinations) of the hardware and software impedances.

Previous works recommend several interface compensation methods to extend the stability margin of the ITM [106], [117]. The benefit of a PHIL simulation is that those compensation methods can be easily implemented within the simulation by means of additional blocks without need for additional hardware elements. The aim of interface compensation is to improve stability and accuracy without changing the topology of the IA [118]. The authors in [119] suggest a dual-rate interface compensation consisting on partitioning the simulation system into two subsystems with differing sample rates. The subsystem coupling the software to the hardware part is simulated with a small sampling rate, thus the IA in terms of stability and accuracy. Another commonly adopted approach considers the insertion of a LPF in the feedback loop that is virtually implemented within the simulation. However, this solution increases the stability margin but lowers the accuracy with respect to the original ITM. In [116] a dynamically adaptive IA is suggested. This combines the application of the V-ITM and I-ITM that can be online switched according to the actual impedance ratio. However, for the practical implementation of this method two groups of PAs must be available. Moreover, the synchronous commutation between the two

amplifiers output might be challenging in practice. A promising approach is presented in [120] where an additional voltage measurement together with control functions to compensate the undesired interfacing effects are applied to the V-ITM. Although this method improves the stability of V-ITM, a proper r_z is still a prerequisite to ensure system stability.

3.3.2 Stability of the DIM

The DIM can be intended as an advanced implementation of the ITM that aims to improve the PHIL stability by reducing the impact of the impedance ratio. Fig. 3.11 shows the block diagram for the V-DIM obtained from the equivalent circuit previously introduced (see Fig. 3.7). The open-loop

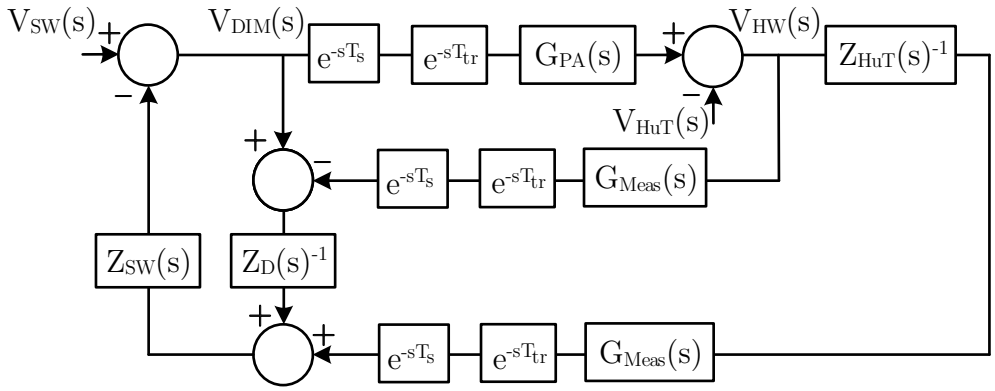

Fig. 3.11: Block diagram for the V-DIM in the Laplace domain

transfer function is obtained as follows:

$$\begin{aligned} G_{\mathrm{OL\_V-DIM}}(s) = \frac{V_{\mathrm{DIM}}(s)}{V_{\mathrm{SW}}(s)} &= \frac{Z_{\mathrm{SW}}}{Z_{\mathrm{HW}}(s)} \left(\frac{Z_{\mathrm{HW}}(s) - Z_{\mathrm{D}}(s)}{Z_{\mathrm{SW}}(s) + Z_{\mathrm{D}}(s)} \right) e^{-s2(T_{\mathrm{s}}+T_{\mathrm{tr}})} \\ &= G_{\mathrm{OL\_V-ITM}}(s) \frac{Z_{\mathrm{HW}}(s) - Z_{\mathrm{D}}(s)}{Z_{\mathrm{SW}}(s) + Z_{\mathrm{D}}(s)} \end{aligned} \tag{3.9}$$

According to (3.9), a particular condition is obtained when Z_{D} is equal to Z_{HW}. In this case, the open loop transfer function is equal to zero and the PHIL system will always be stable. Therefore, in contrast to the ITM, the system stability would not depend anymore on r_z. However, depending

on the nature or the complexity of the HuT, the correct design of Z_{D} is challenging issue. Also additional elements such as cable or connectors needed to implement the PHIL setup can lead to inaccurate estimation of Z_{D}. As suggested in [108], the matching error of the damping impedance (ε_{z}) can be defined to evaluate the effects of a improper design of the damping impedance to the overall system stability:

$$\varepsilon_{\mathrm{z}} = \left(1 - \frac{Z_{\mathrm{D}}}{Z_{\mathrm{HW}}}\right) \cdot 100 \tag{3.10}$$

Fig. 3.12 shows a comparison between an unstable PHIL with ITM and the improvements of the DIM to the stability. It can be observed that the DIM improves the stability margin even in case of considerable ε_{z}. However,

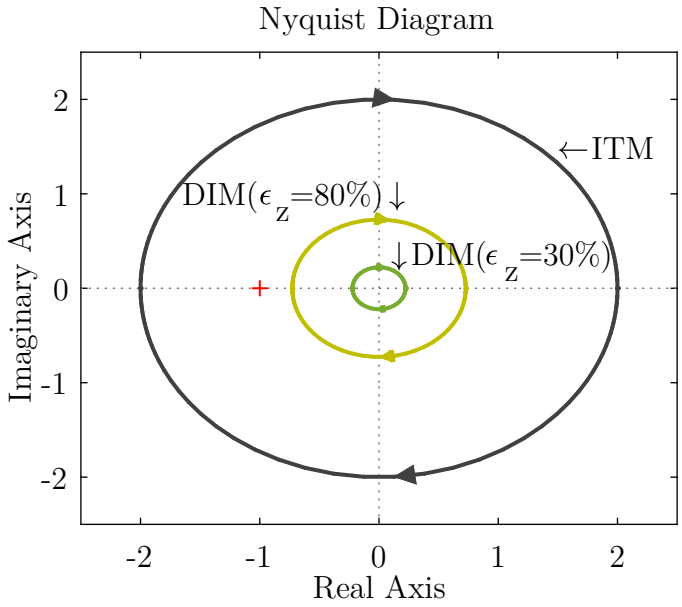

Fig. 3.12: Stability margin comparison between ITM and DIM: unstable V-ITM with $r_z = 2$, V-DIM with $\varepsilon_{\mathrm{z}} = 30\%$ and V-DIM with $\varepsilon_{\mathrm{z}} = 80\%$. First order Padé approximation is used to linearize the delay in (3.5) and (3.9)

high values of ε_{z} reduce the DIM accuracy. Therefore, the design of Z_{D} requires to be accurate enough in order to meet the predefined accuracy requirements. Several approaches can be applied in order to improve the design of Z_{D}. A simple option suggested in [104] considers the approximation of Z_{D} from the historical simulation data. In [121], [122] online estimation

algorithms are suggested. According to those methods, Z_{D} is estimated within the simulation according to the actual measurements. However, those methods only provide the impedance at a particular operating frequency. Furthermore, cannot be effectively applied to a PHIL simulation of a DC system. In [123] wideband system identification techniques are applied to estimate Z_{D}. According to this approach, a small-signal, white noise perturbation is injected into the HuT by using the switching PA acting as the power interface. Cross correlation methods are applied to construct a wideband estimation of Z_{D} that can be online updated afterwards.

3.3.3 Accuracy concerns

Evaluation of PHIL accuracy, is typically carried out by comparing the analytical expression of the PHIL quantities in case of ideal and non-ideal PHIL interface [108, 109, 124]. The former is also known as Naturally Coupled System (NCS) and intends the ideal situation in which the hardware and software parts are ideally coupled without any IA. The latter refers to the actual PHIL using an IA an its related non-idealities. This comparison can also be expressed in the frequency-domain by defining error functions as in the form of (3.11) [119]. This approach allows a more realistic accuracy evaluation throughout the frequency range of interest [117].

$$\varepsilon(s) = \left| \frac{G_{\mathrm{OL\_NCS}}(s) - G_{\mathrm{OL\_IA}}(s)}{G_{\mathrm{OL\_NCS}}(s)} \right| \tag{3.11}$$

Another approach is suggested in [104] where accuracy is evaluated by means of two error functions representing system perturbations defined as transfer function perturbation and noise perturbation. In this case, those error functions are expressed in a form as (3.12) where $\Delta G(s)$ is the given perturbation. The authors in [125] demonstrate that unless small differences, (3.11) and (3.12) are equivalent. Further accuracy evaluation methods are mentioned in [118]. However, due to the complexity of those

methods they are rarely applied in practice.

$$\varepsilon(s) = \left| \frac{1}{1 - G_{\mathrm{OL\_IA}}(s)} \right| |\Delta G(s)| \tag{3.12}$$

Time-domain approach can also be used for accuracy evaluation. Although it can be used for preliminary accuracy evaluation, this approach is better applied to determine the accuracy of the final PHIL experiments. Basically this method is based on the comparison between the relevant instantaneous waveforms from the simulation and the actual measurements from the HuT. The comparison is typically performed in terms of amplitude deviation and phase shift. Practical methods and metrics for verifying the absolute accuracy of a PHIL simulation are presented in [120]. However, at the current state no standard metrics are defined. Therefore, different comparison methods can also be applied.

3.4 Test procedure

At the current state, there does not exist any standard for approaching PHIL and more in general HIL simulation. However, the research community is currently working in that direction. The forthcoming IEEE P2004 Recommended Practice [126] intends to provide established practices for the use of HIL simulation–based testing of electric power apparatus and controls also in compliance with testing standards. However, up to now, different guidelines and recommendation are established out of the experience gained with practical applications. A straightforward test procedure for both CHIL and PHIL simulations is given in [127]. An exemplary application of a test procedure for PHIL based on preliminary simulation is given in [128].

Considering that PHIL simulation involves power components, additional protection requirements are needed for the secure and safety operation in order to preserve components integrity and personnel health, respectively. In [50], the adoption of software protection measures is suggested as good

practice besides classical protection systems for the hardware components. Using the existing simulation environment, protection algorithms can be easily implemented at the software level to prevent undesired setpoints for the power interface that might bring to uncontrolled and dangerous power outputs.

For a given test case a largely accepted test procedure for PHIL simulation includes the following steps:

— definition of the appropriate IA
— selection of the required hardware and software components
— model implementation of the overall components
— verification of offline model system stability
— stability and accuracy evaluation in the frequency-domain
— implementation of the actual PHIL setup
— verification of hardware and software security and possible issues concerning safety
— execution of the real-time PHIL test

Further two practical issues related to PHIL execution are system initialisation and synchronisation [129]. Within a given PHIL test, the power interface is connected with the RTS in a closed loop. However, these two systems cannot be initialised simultaneously. This asynchronous activation might lead to erroneous measurements and signals exchange that might cause system instability. Therefore, a good practise is to provide defined feedback values within the simulation and switch to the actual measurements after the initialisation phase.

Chapter 4

Analysis of laboratory design and operation

Facilities for advanced laboratory testing require a proper architectural design as well as diverse types of components with different features. The former is essential for the effective operation of the facility while the latter ones mainly determine test capability and test targets. In the following part of this chapter, the major design requirements to enhance advanced laboratory testing especially with HIL approach are analysed. An architectural classification of the elemental laboratory equipment is also proposed. As essential element within an advanced laboratory facility, major design concerns for PHIL systems are also discussed. Finally, the fundamental operational use-cases for CHIL and PHIL testing are formulated.

4.1 Functional requirements

Functional requirements refer to the specific functions that the overall test facility must be able to perform. Therefore, the functional requirements are strictly related to the individual targets of a given test facility. However, a more generalized definition of the functional requirements can be formulated with respect to the possible test approaches. According to the concept

of advanced laboratory testing considered within this work, the minimal functional requirements (denoted by F_R) for such a test infrastructure can be generalized as follows:

F_R1 – Simulation
F_R2 – Co-simulation
F_R3 – HIL testing
F_R4 – Full hardware testing

As these testing methods are extensively discussed within the previous chapters, no further considerations are given in this context. Together with the specific laboratory targets, these requirements also define the characteristics of the necessary laboratory equipment. For instance, a facility targeting testing on Photovoltaics (PV) systems can be equipped with suitable simulators for PV applications to fulfill F_R1 as well as with inverters for PV-systems to fulfill F_R3 - F_R4, and so on.

4.2 Non-functional requirements

Non-functional requirements describe quality attributes that the test facility should meet from an operation capability and performance perspective. Therefore, these requirements are more related to the practical design concerns that enhance the overall facility utilization. Some of these attributes are of particular relevance for enhancing HIL tests (particularly PHIL) while others refer to more general purposes. As a result of the requirements analysis for advanced test facilities, the major recommended non-functional requirements (denoted by NF_R) are summarized below.

NF_R1 – Modularity: modular design of the principal laboratory components would facilitate their integration and operation within the overall test facility. Each component can be operated as stand-alone module for component-level testing or in combination with multiple modules for system-level testing.

NF_R2 – Reconfiguration: the test environment should enable practical and straightforward setup implementation for diverse purposes. In fact, a given test-case might require an execution of the test under diverse scenarios and/or for different use-cases. Therefore, a re-configurable hardware framework that allows for quick, straightforward and safe setup configuration is an indispensable element.

NF_R3 – Flexibility: advanced test facilities covering multiple targets might need very different setup requirements. The test environment should be designed to practically be adapted for multiple test purposes with diverse components. Moreover, a flexible design should also include the possibility for multiple users to perform parallel tests, thus increase laboratory usability.

NF_R4 – Integration: laboratory design should ensure that individual components can be properly integrated within the facility area. Among others, this includes design solutions about devices installation and placement to optimize the utilization of the available space as well as to allow users for comfortable and practical operation of the overall test environment.

NF_R5 – Extensibility: laboratory development often take place in several stages. Typically, possible laboratory extensions are taken into account at each development stage according to planned needs and resources. Therefore, the laboratory should be designed in order to enhance follow-up facility extensions.

NF_R6 – Interoperability: with special regards to the smart grid concept, the laboratory design should ensure the capability for each component module to operate in conjunction with each other. This includes not only their electrical interconnection but also the exchange of information data that is essential for system level-testing.

NF_R9 – Conformity: technical standards are essential for the the interoperability of power equipment and communication devices. Therefore, test facilities should be developed to ensure conformity to the existing standards. Furthermore, when possible, standards should

also be applied as testing procedure, thus enhancing test reproduction along with a larger community acceptance of test results.

NF_R7 – Monitoring: one of the practical issues by testing with multiple components from different manufacturers is that each one usually operates with its own control platform. This makes it difficult for test engineers to coordinate the operation and monitoring actions during the experiments. For this purpose, flexible monitoring tools are required to integrate the main visualization and basic control functionalities of the operated components.

NF_R8 – Data repository: a central data storage system is essential to collect results and to share them with multiple laboratory users. Data repository might also be beneficial to collect information about prior users know-how for complex components operation. This can benefit follow-up users for a better understanding and effective operation of the overall components.

NF_R10 – Safety: often laboratories are intentionally operated to reproduce abnormal system operations in order to test under worst-case scenarios. Therefore, safety requirements must be formulated also to allow abnormal test conditions without any risk for personnel and components. This requirement is particularly important in case of testbeds for innovative prototypes for which the operation might result in unexpected behaviors.

NF_R11 – Security: a proper security level is essential to guarantee adequate protection against cyber attacks that might compromise the secure operation of the facility or access to confidential information within local repositories.

NF_R12 – Stakeholder engagement: to better meet components or system requirements for smart grid applications, the cooperation with stakeholders including utilities, manufacturers and consumers is a valuable practice. Therefore, such test infrastructures should also promote joint activities that involve various stakeholders during the different stages of development and testing.

4.3 Architecture and testing equipment

Advanced laboratory infrastructures for smart grid applications are complex facilities that include different components. Some of these components represent the object of the test while further equipment is needed to provide suitable test scenarios to prove the HuT. Further equipment is needed as auxiliary systems to perform tests. An architectural classification of testing equipment is given in this section. This classification is intended to be applied to smart grid test infrastructures with a particular focus on power system operation. It must be underlined that a general and full exhaustive inventory of the required equipment is an ambitious task. The different nature and diverse target of a test infrastructure make it almost unique. However, the overall equipment can be classified into specific typologies according to their function while performing a test. A visual conception of the proposed classification is depicted in Fig. 4.1. The overall equipment can be split into three main typologies. Each component type is equally important and it is considered as necessary part to accomplish the test purposes.

> **Type I** components are the essential tools required to simulate and/or emulate the desired test scenarios. Usually, these devices are not the object of the test but are operated to test other components

Concerning the power system, test scenarios represent the simulation or emulation of specific load or generation conditions. Usually, these scenarios refer to abnormal operating circumstances such as overload, overvoltage, undervoltage or frequency deviation. For advanced test infrastructures the possibility to perform those test scenarios by combining both full simulation and full hardware approach is a prerequisite. Therefore, components such as RTSs and PAs belong to this group. The former ones can be used in case of full simulation while the latter ones can be used for full hardware tests to emulate specific voltage and current scenarios. The proper design of these two components result in a HIL system that can be used for both CHIL

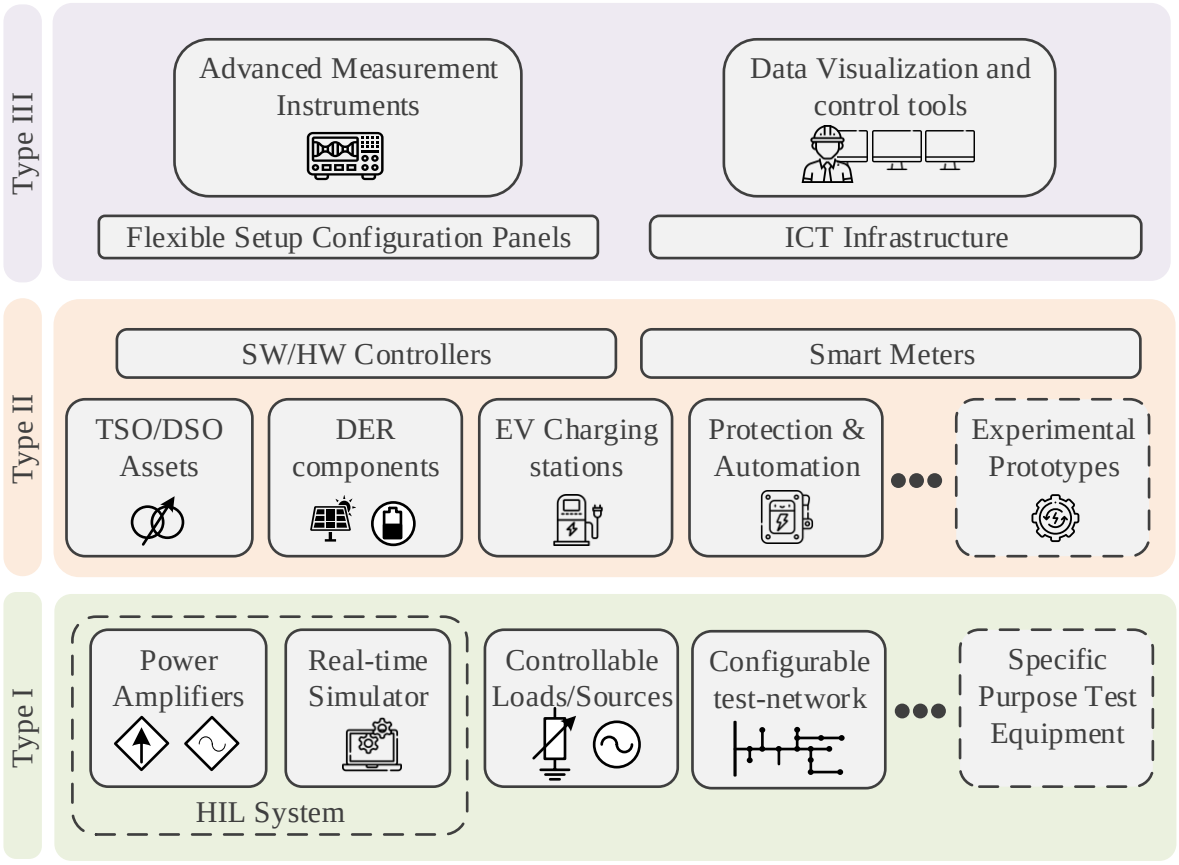

Fig. 4.1: Proposed architectural classification of advanced laboratory–based test infrastructures

and PHIL tests. Beside of those components, auxiliary modules such as controllable loads or generators can also be used to emulate specific scenarios for the given test purposes. A configurable test-network can be required to emulate specific network topologies. For instance, tests on the area of voltage control might require the emulation of voltage variation within several nodes. In that case, real cables or hardware cable emulators can be used to emulate a grid portion. In case of particular needs, further specific equipment can also be included. For instance, fault emulation systems such as short circuit emulators require a special machine design.

Type II components represent the HuT or the elements required to properly test a third component. This equipment is optionally selected according to the predefined targets of the test facility

According to the given definition, type II components identify the specific focus of the test facility. Regarding smart grid testing, typical applications are confined to MV and LV distribution grids. However, applications related to the transmission network are also possible. Type II components can be power devices, controllers, protection, meters or further prototypes. The power components can be of different nature such as grid operator's assets (e.g., On-Load Tap Changer (OLTC) transformers) or DER such as PV systems and Battery Energy Storage System (BESS) or further technologies. Some of these type II components can either be used as HuT or operated to test a further component that is the main object of investigation. For example, testing a controller for voltage regulation with OLTC evidently presupposes the use of an OLTC even though this is not itself the object of the test.

> **Type III** components include all the equipment needed to support test execution, monitoring, and data acquisition

Auxiliary elements such as flexible hardware frameworks that enable a straightforward setup configuration, suitable measurement instruments, data visualisation and control tools are some of the possible type III components. According to the facility targets, the ICT infrastructure can also be assumed as an auxiliary element. In this case, ICT is not the object of investigation but still essential for test execution. For instance, the communication network can be required for controlling type II components during a test. Further physical ICT components such as repository servers also belong to this category and are essential for offline activities.

The suggested classification aims to provide a structural and modular approach to identify the fundamental type of components and their role within a test facility. On the one hand, this can favourite the design process of an overall complex test infrastructure. On the other hand, this approach provides a method for describing the applied devices and their functions within a given test setup.

4.4 Design concepts of PHIL systems

The design of a PHIL system involves formulation of the requirements for both RTS and PAs. Some of these requirements are needed for the use of both components as stand-alone devices while others are needed for a comprehensive utilization of the two components as a whole PHIL system. PHIL system requirements are here formulated with respect to the following suggested categories.

4.4.1 Simulation requirements

Simulation requirements mainly refer to the fundamental prerequisites that a RTS must provide for the given simulation purposes. The simulation bandwidth ($f_{\mathrm{Sim_{BW}}}$) defines the range of capable applications and represents the main functional requirement to be defined. The bandwidth of the RTS must be selected according to the simulation bandwidth that is usually expressed in terms of minimal time-step that the RTS can perform. The admissible time-step is obtained by the practical application of the Nyquist-Shannon theorem, as in 4.1. By practice, a factor $k_{\mathrm{BW_I}}$ between 10 and 30 samples per cycle is usually considered as suitable margin for the proper discrete representation a continuous sine waveform over one period.

$$T_{\mathrm{S}} < \frac{1}{k_{\mathrm{BW_I}}} \frac{1}{f_{\mathrm{Sim_{BW}}}} \tag{4.1}$$

Beside the specification imposed by the simulation bandwidth, the definition of a target simulation size should be also considered to determine the needed computation capacity. The larger is the size and the complexity of the simulated model, the higher is the computation capacity needed to perform the simulation within the defined bandwidth. Concerning power system simulation, in case of CPU based RTSs, the simulation size is typically given in terms of theoretical number of nodes per CPU. However, the required computation capacity might vary also according to the complexity of the implemented models. For instance, depending on the test purpose, a

simplified model of a specific component can be preferred to a more detailed one. This will reduce computation, thus permitting larger simulations.

A practical non-functional requirement to be further considered is the modelling tool. Some commercial RTSs include their own dedicated modelling software in order to improve simulation performance and reduce third parties dependencies. From a practical prospective, this solution poses some limitations such as complicating the inclusion of existing projects implemented with conventional tools and reducing projects exchange between users. Furthermore, users starting to approach real-time simulation need to be prior trained to properly operate such specific modelling tools. Therefore, RTSs that adopt modelling tools based on typical power system software can be considered as more effective solution.

4.4.2 Requirements for hardware interfacing

Hardware interfacing for HIL simulations is made possible by the I/O board. This can be either an embedded component of the RTS or an external unit. The formulation of the I/O board's requirements is strictly related to the application purposes. Analog and digital I/Os might be required for interfacing a physical controller within the CHIL approach. Particularly, for communication based CHIL, additional physical connection ports together with dedicated software interfaces are needed for the emulation of a specific communication protocol.

The main requirements can be formulated by considering:

- Number and types (digital/analog) of I/O
- Resolution
- Bandwidth
- ADC/DAC conversion time
- Rating of voltage and current signals
- Communication interfaces

The aforementioned requirements mainly refer to the prerequisites of the I/O board of the RTS. However, when considering PHIL simulations, the requirements for hardware interfacing also refer to the common communication link between the RTS and the PAs. When those components are committed as separate items, it must be verified that both include a compatible communication link that meets the performance requirements discussed in the follows.

4.4.3 PHIL dynamic requirements

Dynamic requirements aim to assess the required dynamic performance of the PAs as well as the performance of the communication link between the RTS and the PAs. The dynamic requirements are formulated with respect to the frequency-domain model of a PHIL setup prior introduced in Chapter 3 and taking into account the suggested approach in [130]. As a fundamental requirement, the PA bandwidth should be higher than the simulation bandwidth of a factor $k_{\mathrm{BW_{II}}} > 1$, as expressed in (4.2). As recommended practice, k_{BW} should be set in order to provide an open-loop phase shift under $-30°$ [130].

$$f_{\mathrm{PA_{BW}}(-3dB)} > k_{\mathrm{BW_{II}}} f_{\mathrm{Sim_{BW}}} \tag{4.2}$$

The time delay of the open-loop transfer function (T_{OL}) for a given frequency can be expressed in term of phase shift as shown in (4.3). The phase shift can be further expressed by the phase margin (m_ϕ) as given in (4.4):

$$T_{\mathrm{OL}} = \frac{\varphi}{2\pi f} \tag{4.3}$$

$$m_\phi = \pi - \varphi \tag{4.4}$$

Therefore, the maximum open-loop delay can be designed by specifying the admissible phase margin for the open-loop transfer function at the designed

simulation bandwidth:

$$T_{\mathrm{OL}_{\max}} = \frac{\pi - m_\phi}{2\pi f_{\mathrm{Sim}_{\mathrm{BW}}}} \tag{4.5}$$

Considering the Nyquist's stability criterion, the phase margin must be greater than 45°. Finally, the contribution of the looped parts to the overall open-loop delay must satisfy (4.6):

$$T_{\mathrm{PA}} + 2(T_{\mathrm{s}} + T_{\mathrm{tr}}) < T_{\mathrm{OL}_{\max}} \tag{4.6}$$

Therefore, considering the admissible T_{s} deduced from (4.1), the delay due to the PA drive (T_{PA}) as well as the latency of the communication link between the RTS and the PAs (T_{tr}) must meet the condition in (4.6).

4.4.4 Electrical design and safety aspects

Beside the specifications for PHIL simulation, the PA system must meet electrical and safety requirements. Typically, these requirements are formulated in compliance with the characteristics of the given laboratory infrastructure. However, the general requirements to be defined can be summarized as follows:

- PA technology
- Installed power
- Power operating quadrants
- Operation mode (DC, AC, DC & AC)
- Voltage range
- Current range
- Frequency range at full output voltage
- Frequency range for small signals
- Protection devices
- Cooling system

Among others, protection and safety requirements represent an important aspect. Compared to conventional electrical components, PAs can be operated at variable frequency, voltage and current ratings which differ from the nominal ones. However, protection components are typically designed for a specific operating mode (AC or DC) and for specified ratings. This makes the design of the protection system more complex. For switched-mode PAs, additional concerns should be considered with respect to the output filters. In fact, possible leakage currents due to the output filters might affect the operation of the residual current protection that must be properly selected in order to avoid undesired trips (see Section 5.4). Moreover, the filters should meet the Electromagnetic Compatibility (EMC) requirements. To achieve functional safety, the PA system should additionally be equipped with Safety Instrumented Systems (SISs). These include a number of sensors, actuators and control logic to enable the required safety functions such as emergency system shutdown. SISs are designed depending on the required Safety Integrity Level (SIL) (as defined in IEC 61511) that is usually defined according to the test facility requirements.

4.5 Fundamental operational use-cases

A schematic description of the fundamental operational use-cases of HIL techniques within an advanced laboratory infrastructure is provided in the following. The given formulation does not consider all the possible use-cases but only the practice–relevant ones. For the formulated use-cases the concept of HuT is extended by considering its nature as component or system. As depicted in Fig. 4.2, a component is considered as a subsystem including four main units: control, measurement, communication and power elements. According to this organization, component-level testing is considered when a single or multiple units of a component are involved within the test. A test including multiple components connected together and interacting within a common setup is assumed as system-level testing.

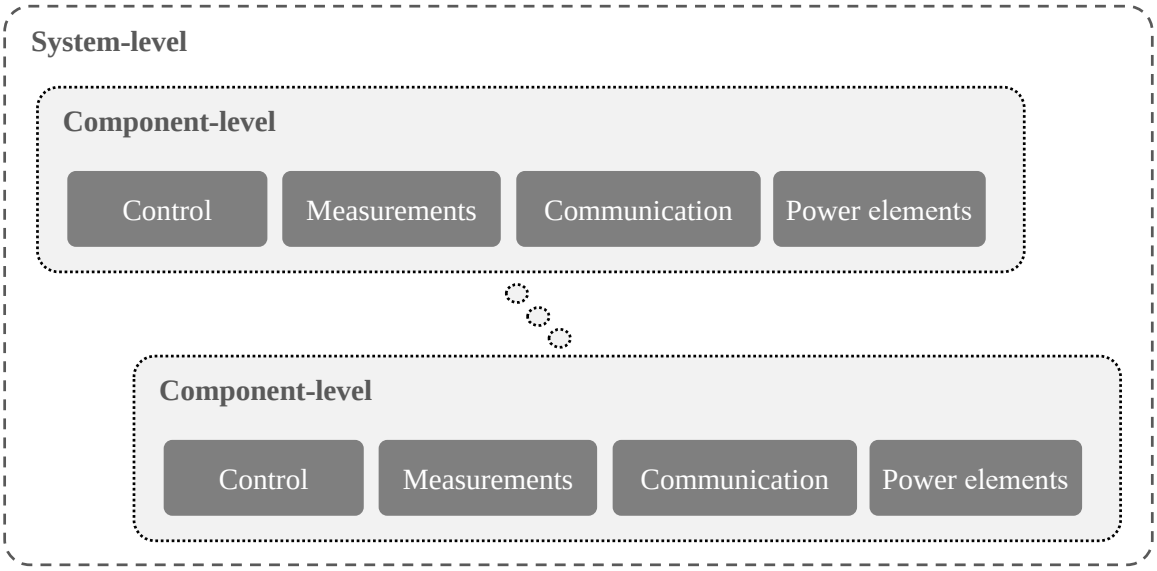

Fig. 4.2: Elements involved in testing at the component and system level

The layout of the formulated use-cases is shown in Fig. 4.3. On the left-hand are included the possible approaches for advanced laboratory–based testing. For each testing approach a set of fundamental use-cases is defined. On the right-hand, the typical testing targets for each use-cases is also considered. According to the test purpose, multiple use-cases can be combined and applied to a conjunct setup. Co-simulation represent a promising testing approach for both full-simulation or HIL testing, as prior discussed in Chapter 2. Within the suggested use-cases formulation, co-simulation is distinguished between local and remote. The former refers to the case in which multiple simulation platforms are involved within a common test setup that is confined to a local test facility. The latter is intended as the coupling of multiple tools from different test facilities interacting together for the overall test objective. The implementation of local and remote co-simulations has a relevant impact on the setup configuration as well as on the performance requirements. However, co-simulation is not further analyzed in the follows as this approach is not explored within this work. For completeness, the application of full real-time simulation is also included as testing approach. Particularly, the possible application of real-time simulation running on a single simulation platform (UC1) as well as the application of co-simulation locally or remotely performed

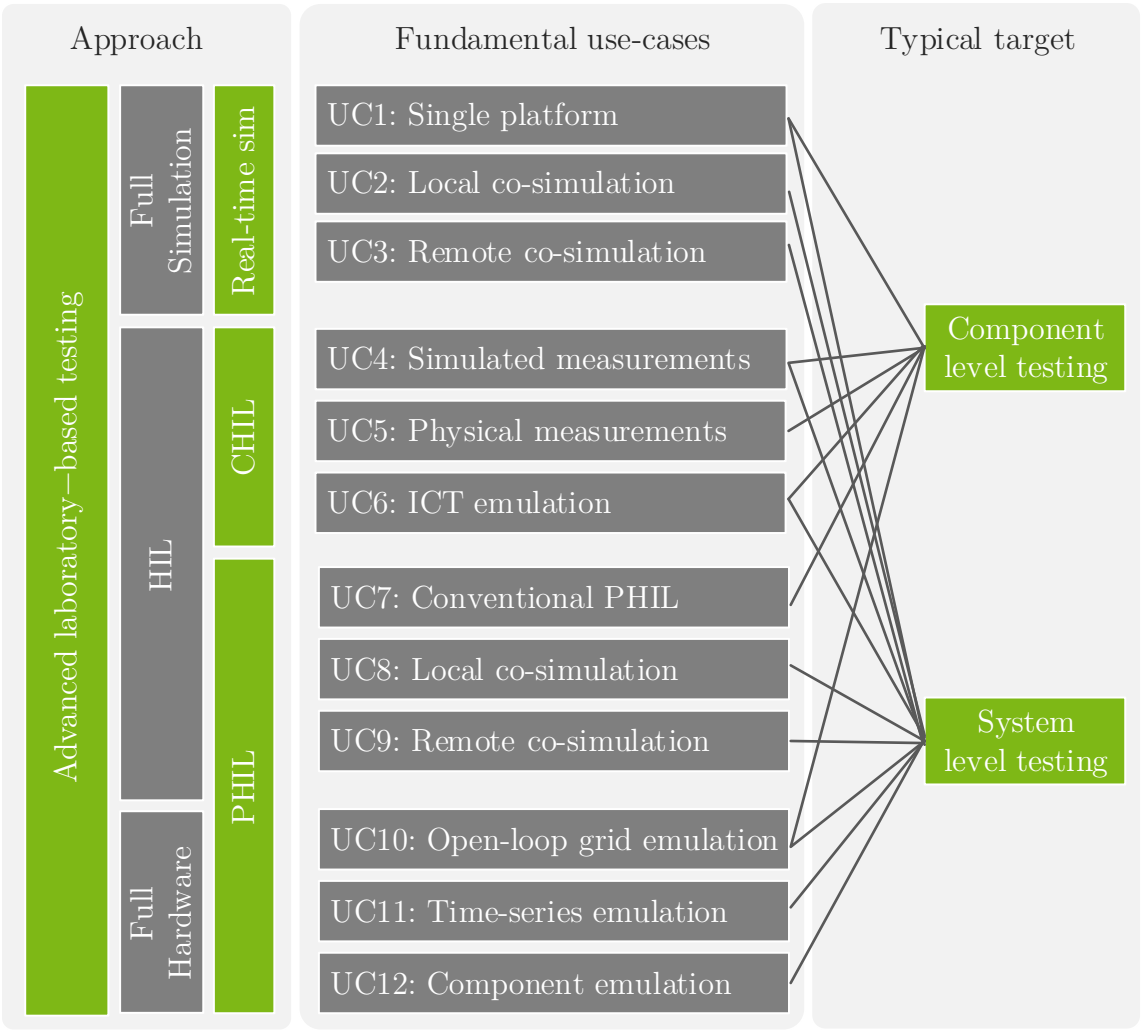

Fig. 4.3: Fundamental operational use-cases for advanced laboratory–based testing

(UC2 and UC3, respectively) is highlighted. CHIL and more particularly PHIL are considered as most relevant approaches for the purpose of this work. Therefore, a more detailed description of the formulated use-cases is given in the following section with particular emphasis on CHIL and PHIL approaches.

4.5.1 Use-cases for CHIL

The use-cases for CHIL are defined according to the different distribution of the component's units between the simulated parts and the physical ones. As common pattern for each defined use-case, the power elements

of the component that implements the electric plant are always modelled within the simulation while the control unit is a physical part. However, measurements and communication units can either be simulated or physical parts. Fig. 4.4 shows the block diagram for each respective use-case.

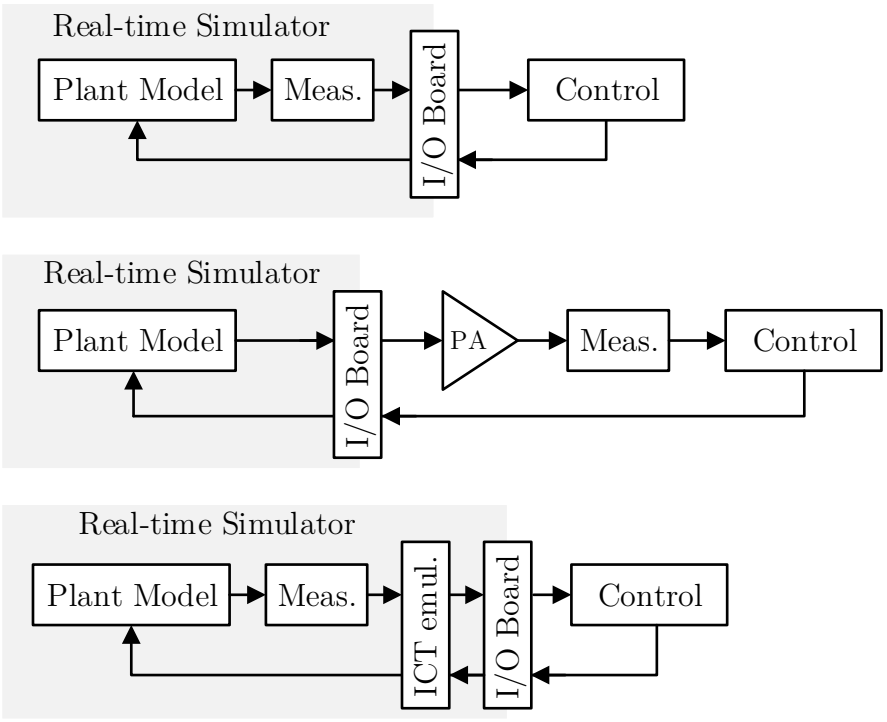

Fig. 4.4: Block diagram of the principal CHIL use-cases – from top to bottom: Simulated measurements (UC4), Physical measurements (UC5), ICT emulation (UC6)

UC4: describes the situation in which the control unit (and eventually the communication unit) is the only HuT while the measurement unit is included within the simulation. In this case, the analog measurements from the power plant model are obtained by virtual current and voltage probes. These signals are scaled down with respect to the allowed range of the I/O board of the RTS and provided to the control unit.

UC5: if the measurement unit is also included within the HuT, PAs are needed to scale up the measurements from the simulated plant. When the measurements unit also includes current measurement, a setup involving two PAs is required in order to emulate the current flow, as

depicted in Fig. 4.5. PA 1 is operated as voltage source (V-Mode) and emulates the voltage from the plant model. PA 2 operates as current sink and emulates the current from the plant model. The two PA are parallel-connected thereby allowing a current flow between them. The physical measurement unit is installed in between and provides the measured signals to the control unit. A typical application is the test of a protection device that can be supplied with full-rate voltage and current to validate its protection algorithms.

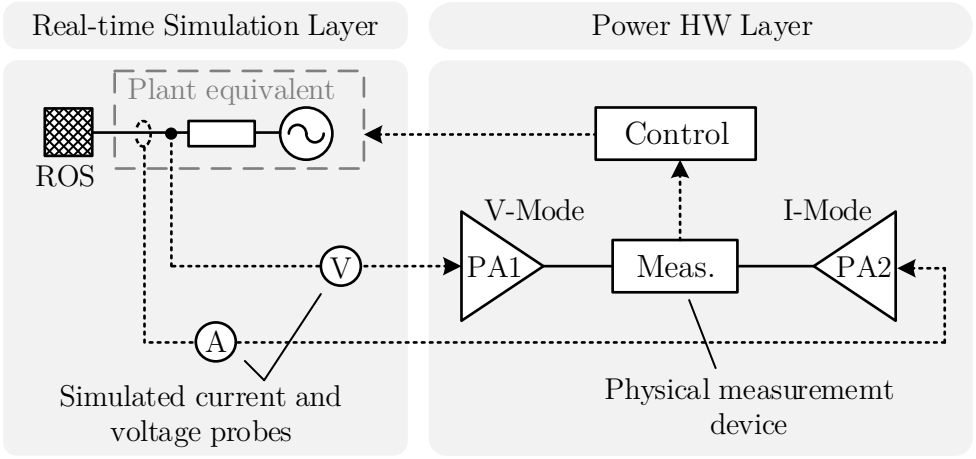

Fig. 4.5: Setup configuration for CHIL within UC5

UC6: refers to the situation in which a physical controller exchanges setpoints and measurements exclusively via a communication link. In this case, the measurement unit is included within the simulation and the simulator is set to exchange digital data via a defined communication protocol. With reference to Fig. 4.4, the ICT emulator block represents the implementation of the needed configuration settings for the communication protocol to be enabled.

These formulated use-cases can be implemented individually or in combination. For instance, combining UC5 and UC6 a physical measurement units can be included within the setup while the control unit send the setpoints to the plant model via a selected communication link.

4.5.2 Use-cases for PHIL

Referring to Fig. 4.3, UC7 to UC9 belong to the classical understanding of PHIL simulation and co-simulation as frequently discussed in the literature. Additionally, UC10 to UC12 are formulated in consideration of the test capability that the combined operation of RTSs and PAs can provide as a whole system. For these use-cases, the PHIL system is mainly operated for full hardware tests in addition to further type I equipment. Fig. 4.6 shows the block diagram of the aforementioned use-cases with exception of the co-simulation use-cases (UC8 and UC9) as their application is not explored within this work in detail.

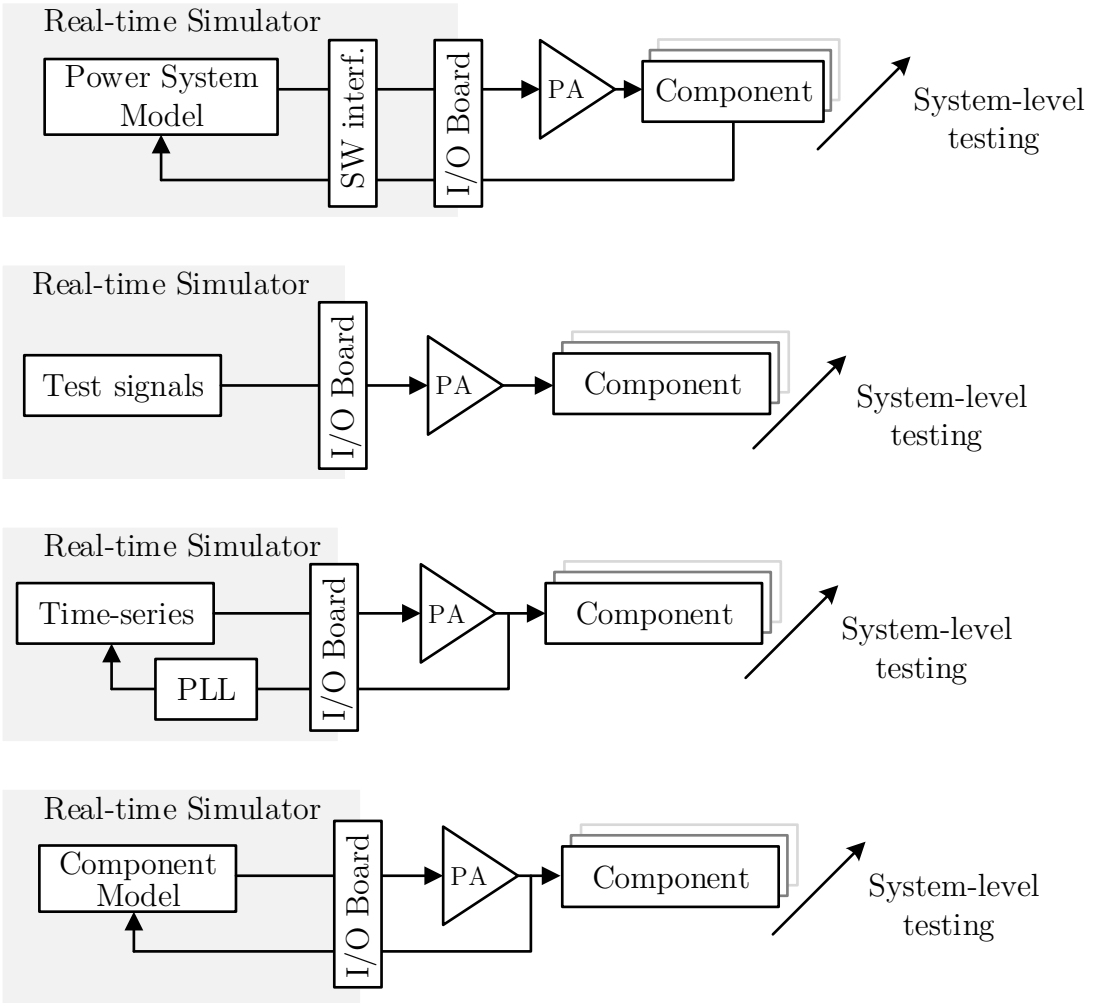

Fig. 4.6: Block diagram of the main PHIL use-cases – from top to bottom: Conventional PHIL (UC7), Open-loop grid emulation (UC10), Time-series emulation (UC11), Component emulation (UC12)

UC7: refers to the classical understanding of PHIL simulation where the RTS is used for grid simulation while the PA is used to emulate the grid for testing the HuT. Typically, the HuT is a single component. However, PHIL with multiple components are also possible. From a practical perspective, the type of the electrical connection of the HuT determines diverse interface approaches. Parallel-connected components are the most common applications. In this case, a single PA group is sufficient for emulating the power terminal of the simulated component. Series-connected components require the emulation of two power terminals, thus increasing the setup complexity. Fig. 4.7 shows two suggested setups for interfacing a physical component which is connected in series between two portions of a simulated grid (both indicated as ROS). The physical component can be assumed as its Thévenin equivalent model. Fig. 4.7a depicts the case of voltage type interface where two groups of PAs operate in voltage mode (V-Mode) to emulate the voltage at the connection terminals of the physical component. The initial voltage difference between the two connection points favourites the current flow through the physical component. The current is measured and sent back to the RTS where the com-

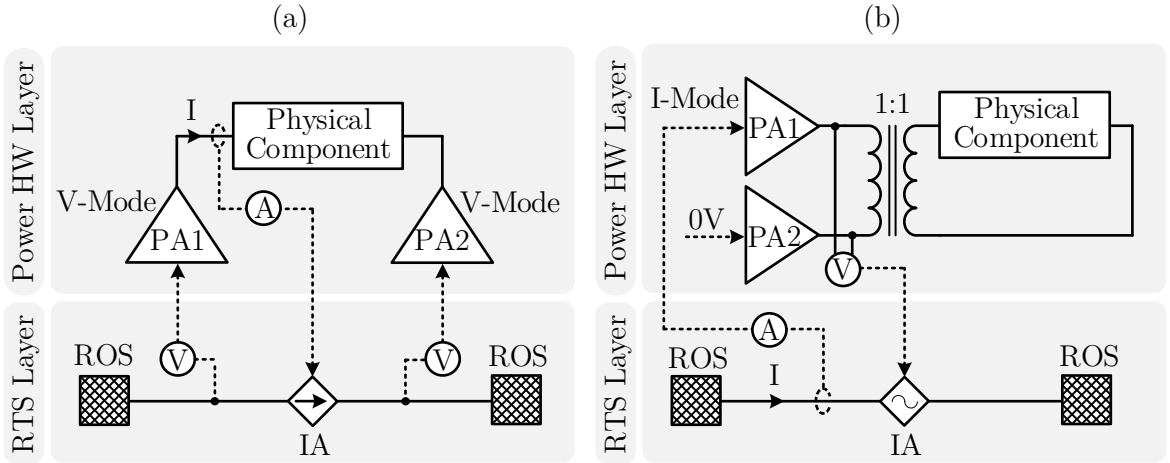

Fig. 4.7: PHIL setup for interfacing a series-connected component to a simulated grid – (a) Emulation of terminal's voltage with PAs, (b) Current–based emulation via unity ratio transformer

ponent is simulated by a series-connected current source. A second option based on current type interface is depicted in Fig. 4.7b. In this case, a transformer is optionally included as additional setup element. This is particularly effective to adapt voltage and current in case that the ratings of the physical components exceed the PA capability. The reference signals as well as the feedback measurements require to be properly scaled within the RTS according to the transformer ratio. Fig. 4.7b includes a unity ratio transformer in order to simplify the diagram. The physical component is connected at the secondary side of the transformer in a closed circuit. PA 1 operates in current mode (I-Mode) and supplies the primary side of the transformer according to the reference from the simulated grid. PA 2 can be used to emulate the neutral voltage at the primary side of the transformer. In case of a symmetrical three-phase component and depending on the connection (Delta or Star) the second PA can be omitted. Finally, the voltage measured at the primary side is sent back to the RTS where the component is simulated by a series-connected voltage source.

The first setup is realized without additional elements. However, according to the nature of the physical component (especially for small impedance components) the stable operation of the parallel V-Mode PAs might be an issue. The second setup can include transformers as additional elements. This will affect the overall stability and accuracy of the setup. However, compensation schemes can be implemented within the simulation in order to compensate the additional impedance of the transformer (see Section 7.2).

UC10: open-loop grid emulation is applied under the assumption that the operation of the HuT, either a component or a system, does not affect the behavior of the simulated grid. Therefore, the feedback from the HuT is not needed to be fed back to the simulation. In this case, the objective of the test is to prove how the HuT reacts to specific inputs.

The selected grid conditions can be modelled in a form of test signals within the RTS and emulated by operating the PAs in open-loop.

UC11: time-series emulation is applied to emulate selected time varying signals to reproduce suitable test scenarios for the HuT. A particular application is the emulation of active and reactive power profiles. In this case, the PAs need to be operated in closed-loop. In contrast to conventional PHIL simulation, the feedback is needed for the correct computation of the reference signals for the PAs. To compute the power reference, PAs are operated in current mode and the voltage feedback is used to implement the Phase Locked Loop (PLL) algorithm for calculating the correct phase of the instantaneous currents.

UC12: describes the case where the PHIL system is used to emulate the operation of a simulated power component with the aim of testing the actual HuT. In this case, the PHIL system emulates the behavior of power system components that otherwise would not be available as physical components for the testing purpose. This use-case can be intended as the dual application of UC7 where the simulated grid is replaced with a physical test environment while the physical component is substituted by a simulated model. Similarly to UC7, diverse interface approaches can be implemented according to the electrical connection of the emulated component. Fig. 4.8 shows two suggested setups for the specific case of series-connected components. Particularly, the component is connected in series with a hypothetical physical test network (indicated as ROS). Also in this case, the component model can be assumed as its Thévenin equivalent. According to the solution depicted in Fig. 4.8a, the insertion of the simulated model into the physical setup is virtually realized by two PAs groups. PA 1 guarantees the current continuity for the ROS on the left-side while PA 2 emulates the voltage at the output terminal of the simulated component. The operation of the simulated component is implemented by the injection of the voltage ΔV in addition to

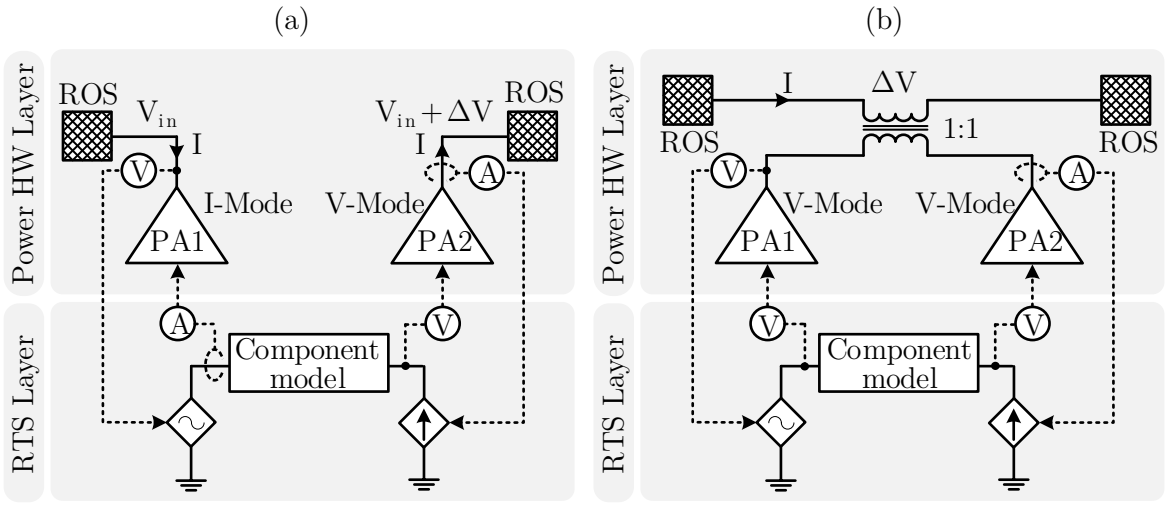

Fig. 4.8: PHIL setup for emulation of a series-connected component within a physical test network – (a) Virtual series connection with PAs, (b) Physical series connection via unity ratio transformer

the input voltage V_{in} by PA 2. Fig. 4.8b, shows a different solution where the current continuity is obtained by means of an additional unity gain transformer that is connected in series with the ROS. The primary side of the transformer is supplied by two PAs that emulate the voltage at the terminals of the simulated component. Despite internal voltage drops of the transformer, the voltage from the PAs is transferred to the secondary side thereby emulating the behavior of the simulated component within the physical environment. Also in this case, a transformer with a suitable ratio can be selected to scale voltage and current according to the ratings of the physical test network.

4.6 Remarks

The minimal requirements for the design of advanced smart grid test facilities are analyzed. Particularly, a number of non-functional requirements are identified as essential attributes to enhance the operation and the performance of such advanced infrastructures. A possible laboratory architecture based on the classification of the principal test equipment is

also suggested. This considers three main typologies of components that are identified according to their function within a test. The major design concepts for PHIL systems are also analyzed. Beside the typical dynamic requirements, complementary features for RTSs and PAs are given for their use as individual components. Finally, a set of practice-relevant operational use-cases is formulated with respect to the principal testing approaches for advanced laboratory infrastructures. Particular emphasis is given to describe the fundamental use-cases involving CHIL and PHIL techniques as main object of this work.

Chapter 5

Case-study: the Smart Grid Technology Lab

The existing Smart Grid Technology Lab (SGTL) [1] infrastructure at TU Dortmund University is considered as reference to prove the design and operational concepts formerly introduced in Chapter 4. First, a description of the laboratory with respect to the research targets and architecture is given. Subsequently, practical aspects and challenges in designing and integrating a PHIL system into the SGTL facility are discussed in detail since it is the principal focus of this work.

5.1 Research targets

The SGTL is the advanced laboratory infrastructure of the Institute of Energy Systems, Energy Efficiency and Energy Economics (ie^3) at TU Dortmund University for testing and validation of smart grids applications. The main activity of the laboratory consists of practical research projects carried out with partners from different sectors, such as Distribution System

[1] The laboratory realisation was carried out by others in the course of the project SGTL (FKZ: 03ET7550) funded by the *German Federal Ministry for Economic Affairs and Energy (BMWi)*. The existing facility including a PHIL system is employed to prove design and operational concepts suggested in this work.

Operators (DSOs), component manufacturers and public institutions. It provides a way to transform the theoretical know-how from the academy to serve the needs of the industry. The laboratory was initially developed to provide a testbed for electromobility applications. Particularly, thanks to the collaboration between specialists in different fields related to electromobility, the laboratory was promoted as Competence Center for Electromobility and Network Integration. The laboratory provided a suitable test environment for both grid operators and charging infrastructure manufacturers for evaluating new products and their interoperability within a distribution grid. Today, this center of excellence is still an active part of the current facility. Later on, the need to extend laboratory capability for testing and validation in a more holistic manner has led to further laboratory expansions for practical experiments in the wider area of smart grids. At the current state, the SGTL offers suitable test capability in the area of DER, Distribution Automation, Grid Management, Electromobility and Energy Storage.

The test facility is designed to perform advanced laboratory testing that includes full simulation, full-scale hardware testing and HIL simulation. This allows for experimental tests with commercial products of diverse nature and from different manufacturers also including ICT. Those testing approaches are mainly applied for studies of distribution grids with a particular focus on voltage control, distribution grid state estimation, congestion management, ancillary services with DER as well as innovative controllers and power components prototyping.

The SGTL also provides an advanced infrastructure for teaching purposes. TU Dortmund University offers a novel master-level course exclusively focusing on smart grids. The format of the course includes active frontal lectures focusing on current research topics along with practical trials. In this context, the laboratory is used for practical demonstrations and hands-on experiments. This provides students firsthand experience on modern laboratory tools and smart grid technologies.

5.2 Laboratory architecture

The SGTL is located within the Dortmund Science and Technology Campus close to the campus area of TU Dortmund University. The overall laboratory is implemented within an industrial hall that covers a total area of about 400 m^2. Fig. 5.1 shows a portrait of the facility area.

Fig. 5.1: The Smart Grid Technology Lab at TU Dortmund University

The laboratory architecture gives an immediate application of the requirements and design concepts prior discussed in Chapter 4. It consists of an extensive LV test network equipped with several components integrated as modular elements within the facility area. A pseudo schematics of the SGTL architecture is given in Fig. 5.2. The diagram refers to a representative topology including the major laboratory components and their principal electrical features. In compliance with the architectural classification proposed in the previous chapter, all the components can be associated to a specific typology. This classification is also highlighted within Fig. 5.2 where the various components are mapped by different colors accordingly.

As major type I components the laboratory includes the PHIL system (being integrated) together with further stand-alone PAs and controllable resistors. Furthermore, a desired network topology can be implemented by configuring available segments of typical cables for LV grids. Otherwise, cable emulators consisting of adjustable resistors and inductors can be proper configured to emulate a specific cable. A total number of 8 busbars allows to connect components to the different nodes of the configured grid. If needed, a secondary substation connects the test network with the utility grid. Otherwise, PAs can be used for grid emulation or to emulate specific island operations. The secondary substation is particularly designed for testing in the area of voltage control. For that purpose, two series-connected OLTCs are allocated rather than a single unit. Particularly, a 10/10 kV OLTC operates as type I component in order to emulate voltage deviations from the MV side of a second 10/0.4 kV OLTC. The former has a specialized design and consists of a nominal unity ratio while the latter has a conventional design as MV/LV distribution transformer and is used in the form of type II component. Both OLTCs provide a regulation range of $\pm 10\%$ with respect to the nominal secondary voltage.

Besides the OLTC and in line with the research targets, the laboratory is further equipped with several type II components. A testbed including a number of commercial AC charging stations along with commercial EVs is available for studies on Electromobility. As major BESSs, a Vanadium Redox flow storage along with smaller size Li-ion BESS are also part of the facility. The laboratory also includes a testbed for DER that can host power converters while the PHIL system can be used to emulate the specific technology such as PV-systems. Additional type II components are often interfaced with the main test network according to the individual research needs. Among others, specific prototype components such as the line voltage regulator included within the schematics. Furthermore, according to the test purpose, different forms of hardware controllers are also part of the setup as type II components.

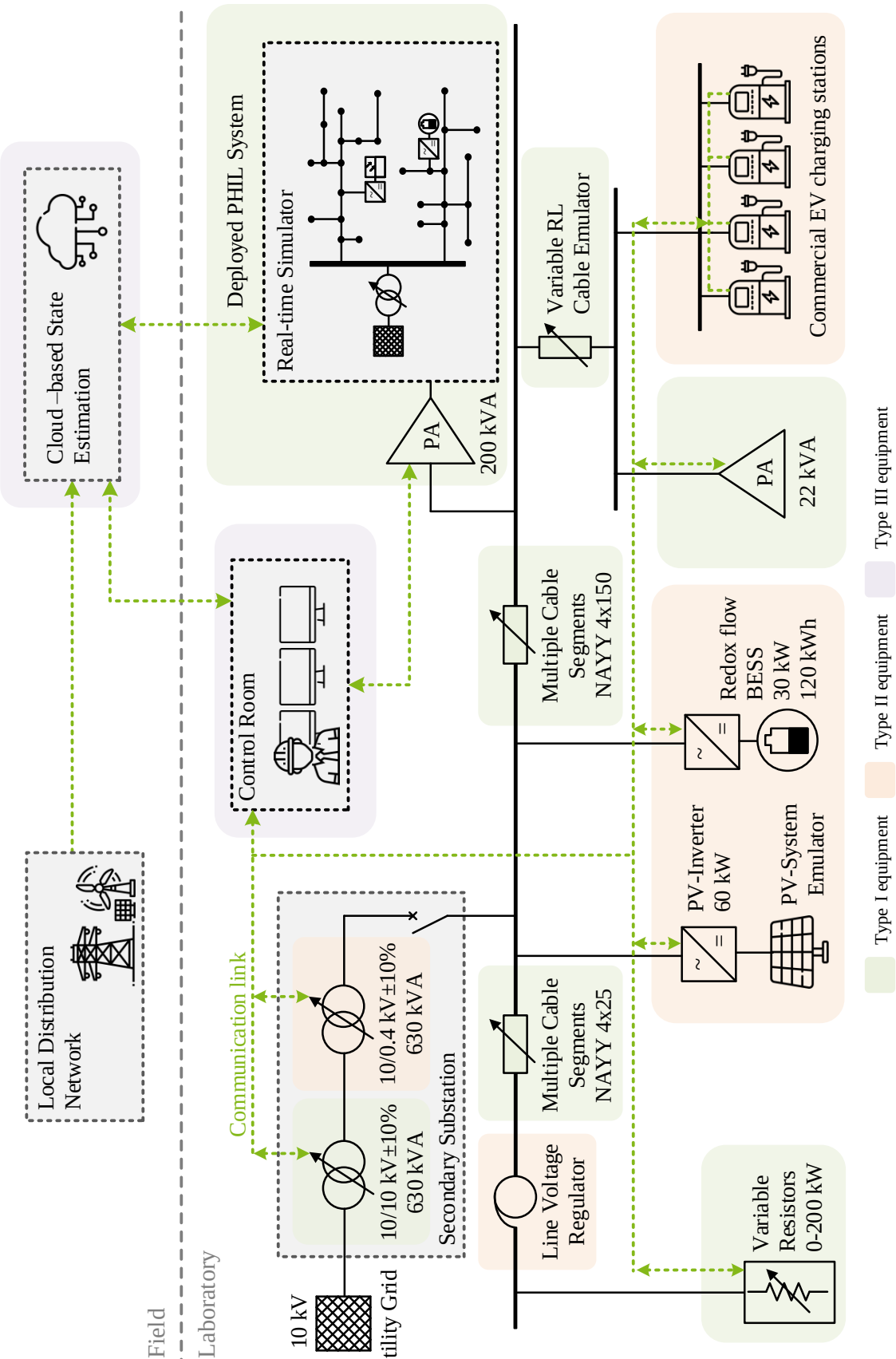

Fig. 5.2: Demonstrative schematics of the SGTL architecture

Among the major type III components, the ICT infrastructure ensures a communication link between the various components for monitoring and control. Standard industrial communication protocols such as Modbus as well as innovative communication protocols such as 5G are used for testing including ICT. Another remarkable feature of the laboratory is the close-to-real-time data stream from the several DSOs. This enables the test network behave as if it was a real low voltage network. In other words, realistic load conditions can be reproduced in the laboratory. This is extremely valuable in order to verify that the developed control strategy or a prototype behaves in the required way under real network conditions. Secondly, the system gives the researchers an access to a valuable amount of grid data that will support various studies. Finally, a control room hosts the main laboratory server also used for running control, visualization and analysis tools that are essential elements for testing.

5.3 PHIL system architecture

The PHIL system is designed to meet the laboratory targets and the requirements of the existing hardware devices that compose the SGTL facility. The deployed PHIL system is following described with particular emphasis on the key attributes of the selected RTS and PAs.

5.3.1 System specifications

System specifications are in the following formulated in compliance with the general PHIL system design concerns prior discussed in Section 4.4. Although most of the specifications are stated in order to fulfil technical requirements, some of them are also guided by unavoidable cost aspects.

Simulation – According to the research targets discussed in the previous section, a maximal simulation bandwidth of 2 kHz is selected. This allow EMT as well as RMS simulations for a wide range of power system applications, as shown in Fig. 5.3. The selected simulation bandwidth

also provides an effective compromise between simulation capability and cost of the required equipment. As the principal function of the

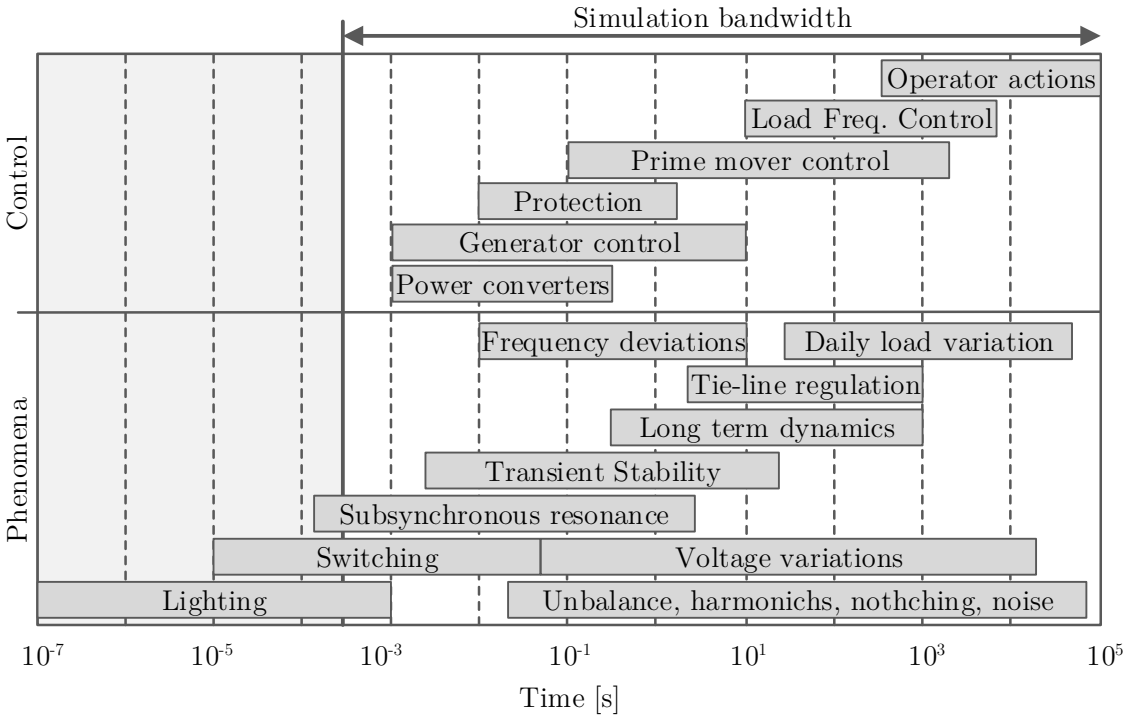

Fig. 5.3: Designed simulation bandwidth and principal power system applications (adapted from [21])

system is PHIL testing, detailed simulations of small-size grids are prioritized rather than larger ones. Therefore, computation capability of 80 to 100 nodes is considered as reference. Moreover, multi-core CPU–based simulation is also selected for performing parallel model execution.

Hardware interfacing – Testing hardware controllers or protection devices also belong to the SGTL targets. Therefore, a set of analog and digital I/Os is required. A further important aspect of the test facility is also the capability to perform tests including ICT. Therefore, besides conventional analog and digital I/Os, emulation of standard communication protocols is also required. As the minimum requirement, the system is specified to emulate Modbus TCP/IP along with IEC 60870-5-104 protocols. The former is selected as the majority of the installed type II components are commercial products that include

Modbus TCP/IP as a standard industrial communication protocol. The latter is the major standard for power substation communication, supervisory control and system automation. Concerning communication between RTS and PAs for PHIL applications, an optical fiber link is selected as most suitable option to minimize communication latency, thus enhance PHIL stability.

PHIL dynamics – Considering the specified simulation bandwidth and according to equations (4.1), (4.2) and (4.5) (see Section 4.4), the major dynamic specifications for PHIL are defined. Particularly, the following design factors are taken into account:

- $k_{\mathrm{BW_I}} = 25$
- $k_{\mathrm{BW_{II}}} = 1.5$
- $m_\phi = 60°$

A graphical representation of the system dynamic specifications is depicted in Fig. 5.4 where the main design parameters are represented as a function of the simulation bandwidth. The specified simulation bandwidth ($f_{\mathrm{Sim_{BW}}}$) of 2 kHz defines the performance specifications for the PA system essential for PHIL simulation.

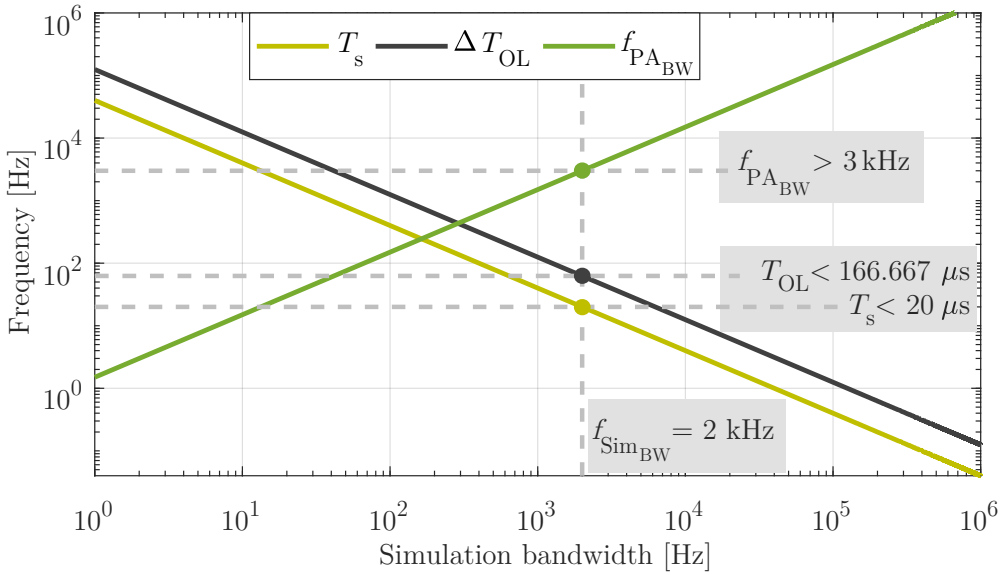

Fig. 5.4: Graphical representation of the PHIL system specifications for the selected simulation bandwidth of 2 kHz (inspired by [130])

Particularly, the RTS must be capable of discrete EMT simulations with a minimal time-step of 20 µs. The PA system requires a minimal bandwidth of 3 kHz. Moreover, in order to meet the designed margin of stability, the open-loop delay should be limited to about 167 µs.

Power and safety – The PA system is designed as 4-Quadrant system in order to allow bidirectional power flow and full emulation of generation and load components. Three-phase AC operation is the principal application. Therefore, the major specifications are formulated accordingly. However, DC operation is also planned to provide DC-link for inverter–based DER as well as for direct testing of further DC components. The power rating is selected according to the rating of the actual test facility, as shown in (5.1). Particularly, the system is designed to substitute the secondary substation for supplying a given test-network that includes the available type II components. However, the PA system rating must not exceed power rating of the secondary substation, thus avoiding overload conditions when operating at full range.

$$S_{\mathrm{OLTC}} \geq S_{\mathrm{PA}} \geq k_{\mathrm{g}} \sum_{n \in N} S_{\mathrm{n}} \tag{5.1}$$

where:

S_{PA}	apparent power of the PA system
S_{OLTC}	apparent power of the OLTC transformer
k_{g}	global contemporary factor (≤ 1)
N	Type I + Type II power components (OLTC excluded)

The minimum installed power of 200 kVA is selected as suitable design for this given application. As further design option, the total required power is split into two groups of PAs for a more flexible utilization and also to allow PHIL setups with series components (see UC5, UC7 and UC12). According to the designed power rating for the PA system

along with the relative small required bandwidth, switched-mode PA technology can be selected rather than a linear one.

Concerning voltage specifications, the system must provide a nominal phase-to-ground voltage of $230\,V_{RMS}$ according to the rating of the existing facility. Moreover, in compliance with the laboratory targets, the maximum AC voltage is designed to perform overvoltage tests and therefore must be higher than 10 % of the nominal voltage.

Particularly important is the design of the PA output filters. This affects the dynamic performance for PHIL and the quality of the power output directly. Moreover, the output filter must meet the current regulation on EMC. Further aspects must be also considered when interfacing the PA system with specific power components. For instance, the designed PA system is planned to be also operated as DC emulator for inverter–based DER. Therefore, the PA system must meet the connection requirements to be proper interfaced with power inverters. These requirements are particularly selective when operating with commercial inverters. In fact, commercial inverters are set to fulfill typical connection requirements for field installations that might include rigorous safety standards. For instance, in case of commercial PV inverters, insulation resistance must be kept above a specified threshold to allow inverter operation. The output filters of switched-mode PAs include capacitors that contribute to system leakage currents. Therefore, as additional specification, PA filters must be proper designed in order to guarantee an adequate insulation level according to the inverter requirements.

Further power and safety considerations will be discussed in the following Section 5.4.

5.3.2 Selected real-time simulator

As design solution, a RTS from Opal-RT is selected for the developed PHIL system. A picture of the system architecture is shown in Fig. 5.5. The overall system includes two units: the target PC (OP5030) and the

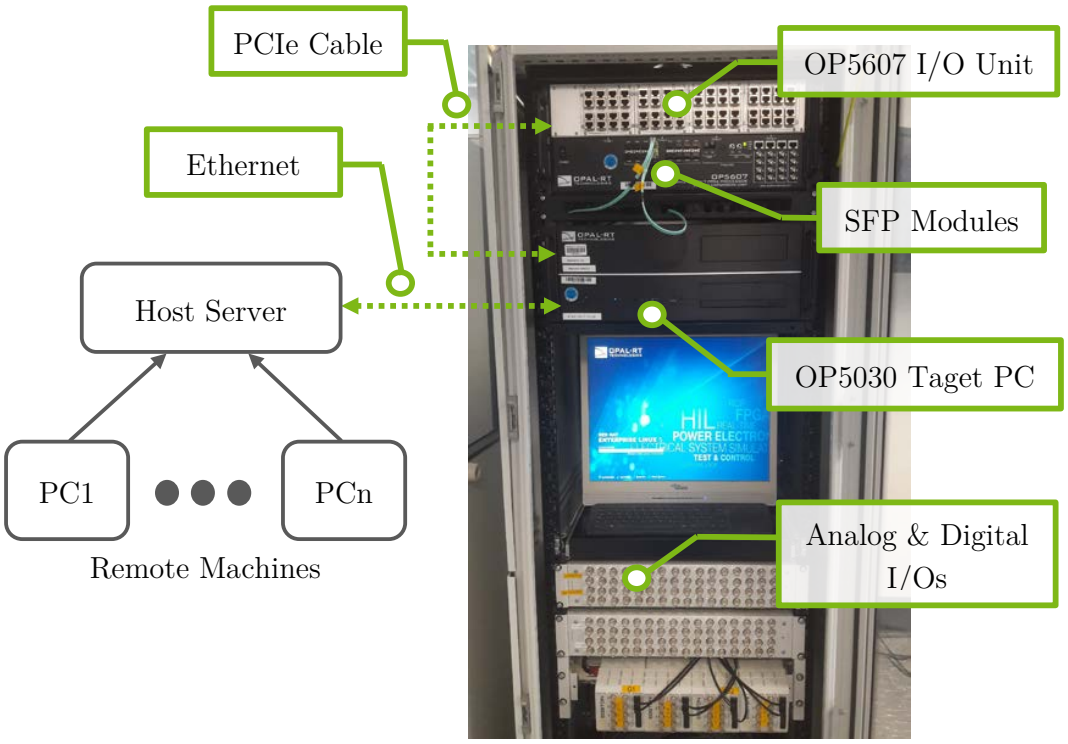

Fig. 5.5: Installed real-time simulation system at Smart Grid Technology Lab

I/O extensions unit (OP5607) for HIL simulations. In addition, the main laboratory server is used as host PC. It consists of a Windows OS running on a virtual machine where the simulation control platform is installed. This solution allows for multiple users to remotely access to the simulation platform. The target and the I/O unit are connected together via PCIe Gen.2 cable while the host server communicates with the target via Ethernet within the local laboratory network.

The target unit includes all the computation parts and mainly consists of an Intel processor with 8 cores at 3.2 GHz. This enables to split complex models up to 8 parts for parallel computation. The principal hardware specifications of the OP5030 are summarized in Table 5.1. As main peripheral, the

Table 5.1: Principal specifications of the OP5030 real-time target PC

Computation	
CPU	1 Intel processor, 8 cores at 3.2 GHz
Communication systems	4 PCIe slots
Operating System	Linux RedHat, 32-bit
Peripheral	
Intel EXPI9404PTL PT adapter	
Number of Ethernet ports:	4
Data rate(s) supported per port:	10, 100 and 1000 Mbit/s
Bus Type:	PCIe 1.0a
Bus width:	lane PCIe (x4)
Bus speed (x4, encoded rate):	10 Gbit/s uni-directional 20 Gbit/s bi-directional
Communication protocols	
Ethernet–based protocols	Modbus TCP/IP Slave IEC 60870-5-104 Slave
Total number of data points	2100

Intel EXPI9404PTL PT is also used as physical Ethernet port for the emulation of the required TCP/IP–based communication protocols. This is particularly required for CHIL simulations including ICT emulation (UC6). According to the current system license, a total number of 2100 data points for Ethernet–based communication protocols is enabled. In line with the RTS requirements, Modbus TCP/IP slave and IEC 60870-5-104 slave are the activated protocols. The configuration of the communication protocol is performed via the provided real-time simulation management platform. If multiple slaves are simulated in the same model on the target IP address, the device driver will attempt to create an IP aliases on the network interface and attach each slave to the related alias. In this case, an external master device will be able to reach the slaves using the alias IP address. This functionality is useful to simulate different slaves in the same model and have each of them being reachable using their own IP address. The I/O expansion unit is equipped with a number of analog and digital I/Os for conventional CHIL simulation (UC4). Moreover, the embedded Xilinx Virtex-7 FPGA provides additional high speed Small

Form-factor Pluggable (SFP) communication ports. These can later be used to link the RTS with the PA system to fullfill the PHIL requirements. The main specifications of the OP5607 I/Os expansion unit are given in Table 5.2.

Opal-RT provides a set of software specialized for power system simulation at different levels. An overview of the software solutions together with their main features is given in Table 5.3. According to the simulation purpose, a suitable software can be selected. In line with the SGTL targets the eFPGASIM is not included within the selected RTS. In case of full-simulations (UC1–UC3), ePHASORSIM and HYPERSIM can be preferred especially for large scale power system models. However, both solutions require dedicated editing approaches and tools. For reduced power system or component models to be applied to PHIL tests, the eMEGAsim provides a more suitable solution. Within eMEGAsim, model editing is performed on Simulink [131]. Precisely, the simulation control platform RT-LAB [132], [133] is used to combine the power system toolbox from the Simscape Electrical library of Simulink with specialized libraries for real-time simulation. Therefore, prior models developed in Simulink can be quickly imported and adapted for real-time execution. This feature is particularly valuable considering that MATLAB and Simulink are largely used in the academic context. As additional feature, eMEGAsim provides accurate solvers for enabling real-time EMT simulation. Among others, ARTEMiS and ARTEMiS-SSN solvers and algorithms eliminate artificial delays in case of parallel computation, by using advanced decoupling techniques for added speed and efficiency. Besides model editing functionalities, RT-LAB is also used to compile, load, execute and analyze models [134]. As additional feature, the RT-LAB platform also includes an API based on Python or C programming language. Among others, this enhance user customization as well as automatic tests execution.

Table 5.2: Principal specifications of the OP5607 I/O extension unit

FPGA	
Model	VIRTEX 7 FPGA
FPGA Slices	75900
Digital Signal Processing (DSP) slices	2800
Analog Input Card (ADC) OP5340-1	
Number of channels	16 differential
Resolution	16 bit
Max. sampling frequency	500 kHz
Min conversion/acquisition time	2.5 µs per channel
Nominal input ranges	±20 V to ±120 V
Analog Output Card (DAC) OP5330-1	
Number of channels	16 single-ended
Resolution	16 bit
Default range	± 16 V
Maximum current	15 mA
Max. sampling frequency	1 MHz
Min conversion/acquisition Time	1 µs per channel
Maximum noise	20 mV peak-to-peak
Maximum offset	± 80 mV
Digital Input Card OP5353-3	
Number of channels	32 digital inputs
Isolation	Optical isolator
Input current	3.6 mA, current limiting diode
Voltage range	4 to 50 V_{DC}
Delay low-to-high	110 ns
Delay high-to-low	60 ns
Rise/fall time	6 ns/6 ns
Digital Output Card OP5360-1	
Number of channels	32 digital outputs
Isolation	Galvanic isolator
Reverse voltage limit	maximum 30 V_{DC}
Voltage range	5 to 15 V_{DC}
Delay Low-to-High	$\leq$ 50 ns
Delay High-to-Low	$\leq$ 50 ns
Rise/Fall times	$\leq$ 15 ns
Communication	
PCIe Gen2 (x4) SFP connectors with speeds from 1 to 5 Gbit/s (x16)	

Table 5.3: Overview of software solutions for the deployed RTS [135]

	ePHASORSIM	**HPERSIM**	**eMEGAsim**	**eFPGASIM**
Typical Application	Large-Scale Electromechanical Power System Simulation	■ Power Systems ■ Power Electronics ■ Control	■ Power Systems ■ Power Electronics ■ Control ■ Protection	■ Power Electronics ■ Control
Simulation type	Phasor	EMT	EMT	EMT
Time-step	1-10 ms	■ Network solution: 5-100 µs ■ Switches and converters: 0.2–2 µs	■ Network solution: 10-100 µs ■ Switches and converters: 0.2–2 µs	0.2–2 µs
Model editing	■ Simulink ■ Excel ■ ETAP ■ PSS®E ■ CYME ■ PowerFactory ■ Open Modelica ■ Dymola	HYPERSIM	■ Simulink ■ Simscape Power System	■ Simulink ■ Simscape Power System ■ PLECS ■ PSIM ■ NI Multisimend
Grid size	108,000 1-phase nodes	9,000 3-phase nodes	300 3-phase nodes	288 states/128 switches
Capability per CPU core	10,000 nodes @ 10 ms	75 3-phase	120 nodes	
Features	API: Python	API: Python	Dedicated SSN solver, Multi-physical domain simulation, API: Python, C, Java, LabVIEW	Automatic scripting, FPGA compilation not required, 200 kHz PWM I/O, Rich library of electrical motors

5.3.3 Selected power amplifier system

The PA system is selected taking into account both the dynamic specifications for PHIL purpose as well as the electrical specifications with regards to the existing laboratory components. The commercial PA product CSU200-2GAMP4 by EGSTON Power Electronics [136] is selected as suitable solution to fullfil the stated specifications. A picture of the deployed system is shown in Fig. 5.6. The overall system is implemented

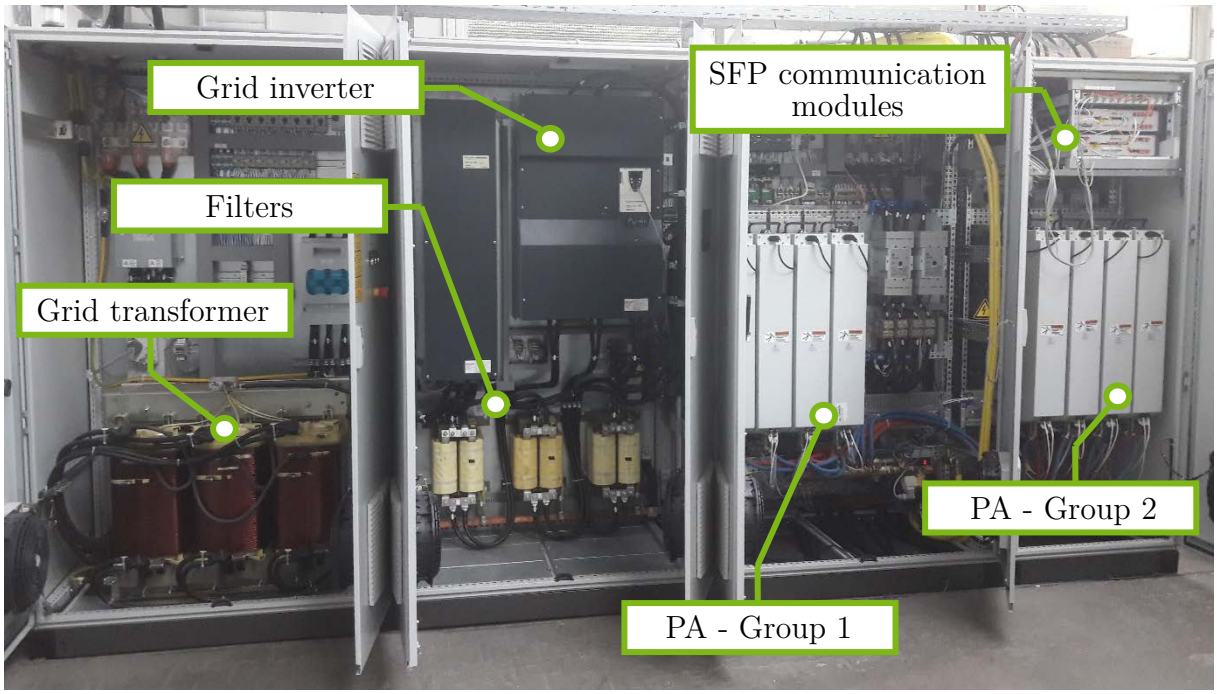

Fig. 5.6: Architecture of the power amplifier system

within a total number of four cabinets that also include control, protection and cooling systems. By design, the overall system capability is split in two similar groups with a power rating of 100 kVA and each one including four PA modules. Each module is a 4-Quadrant switched-mode PA working as 6 legs buck-boost converter. Every leg is commuted at rate of 20.833 Hz, thus providing an effective switching frequency of 125 kHz. Both PA groups are supplied by the same grid conversion system that consist of a galvanic isolated transformer together with a bidirectional power converter. The isolating transformer provides galvanic isolation between the DC-link and the external AC grid that supplies the overall system. Each PA group also includes a dedicated communication unit equipped with SFP connectors

to enable fiber optic communication with the OP5607 unit. A simplified diagram of the communication flow between the RTS and the PA system is depicted in Fig. 5.7. The PHIL loop is realized via the fiber optic link between the OP5607 unit and the SFP communication module of the PA system. The amplifier control loop consists of a high-speed real-time link (RT-link) to drive the PA with a setpoint frequency of 250 kHz, thus providing a minimal transfer delay. The embedded probes for voltage and current measurements together with the ADC are aligned to minimize measurement inaccuracy. Current measurements give 1.1 % error over a range of ±200 A with a 15 bit ADC resolution while voltage measurements provide 0.3 % error over a range of ±1000 V with 16 bit ADC resolution.

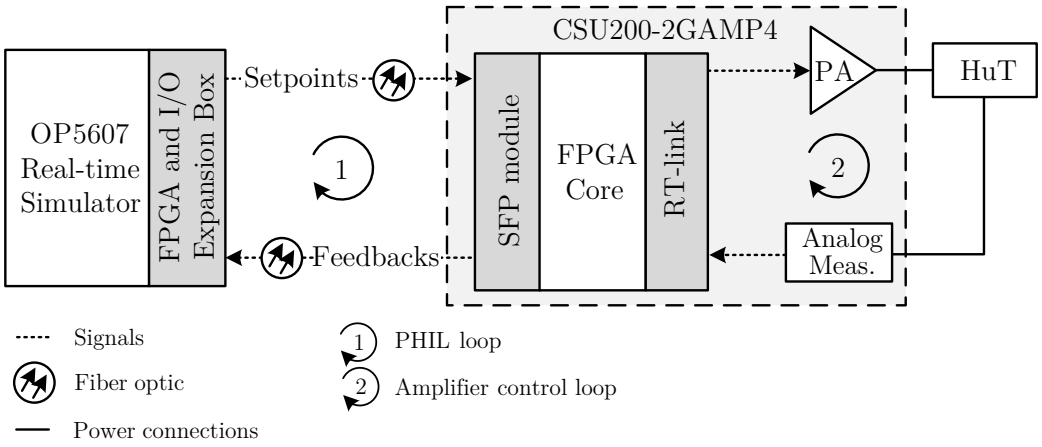

Fig. 5.7: Communication architecture of the PHIL system

Each PA group can be operated independently and simultaneously with the selected operating mode. The two groups can be contemporary operated also for diverse test purposes. For instance, one group can be used for emulating a power component while the second groups operates as grid emulator at the same time. According to the operating mode, each PA group is differently configured, as depicted in Fig. 5.8. Within the "Free Amp mode" each PA module can be operated independently according to the reference signal. However, all the four PA modules can be operated either in voltage mode or current mode. In case of "3ph+N mode" the PA group operates as three-phase system where the fourth module emulates the

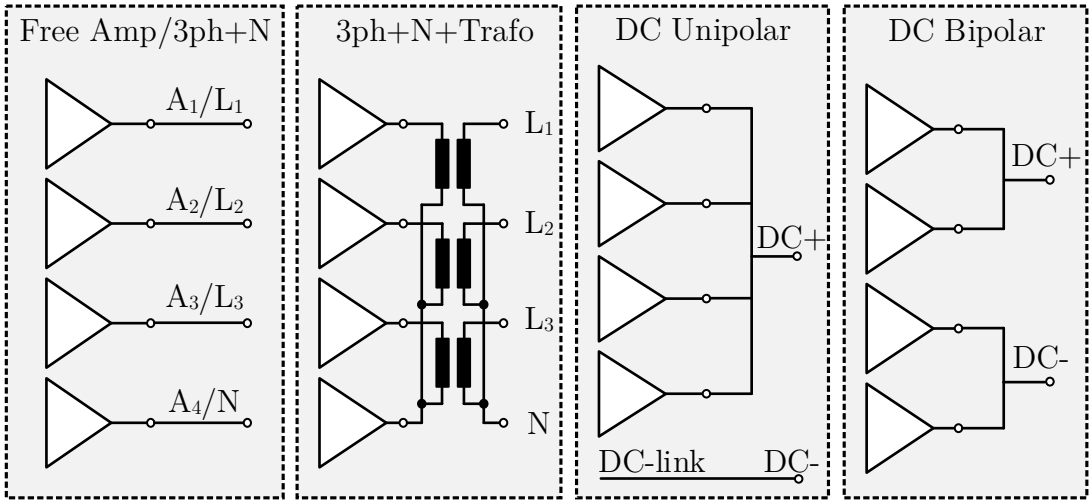

Fig. 5.8: PA system operating modes – from left to right: Free Amplifiers and three-phase plus neutral mode; Three-phase plus neutral with transformers; DC Unipolar; DC Bipolar

neutral conductor. This operating mode can be also applied as voltage mode or current mode. In the second case, three PA operate in current mode while the fourth PA is still operated in voltage mode. Three single-phase transformers are also part of the system and can be eventually included at the output of the PAs, thus providing galvanic isolation ("3ph+N+Trafo mode"). DC operation can be configured either in "DC Unipolar mode" or "DC Bipolar mode". The former consists of the parallel connections of all the PA modules in order to emulate the positive DC pole while the negative pole is obtained by accessing the DC-link ground. This configuration is more effective when a higher current range is required. Within the DC Bipolar mode, each pair of PA modules is connected in parallel. Each couple of PAs is controlled to symmetrically emulate the positive and negative DC poles. All the operating modes are manually set by the user via the provided system Supervisory Control and Data Acquisition (SCADA). A basic Simulink library is also provided to establish real-time communication with the simulated model running into the RTS.

A summary of the principal specifications of the deployed PA system is given in Table 5.4.

Table 5.4: Principal specifications of the deployed PA system

Electrical supply	
Input voltage	400 V_{RMS} ±10% (50 Hz)
Input current	332 A_{RMS}
Input power	230 kVA
Output power	200 kVA
DC-link voltage	770 V
Single Power Amplifier	
Switching frequency	125 kHz
Current overload capability	10% (1 min)
Output frequency	DC to 5 kHz sine wave (-3 dB) up to 15 kHz (small signal)
Output ripple voltage	< 2.5 V_{Peak} ($V_{DC\text{-}link} = 770$ V)
System Operating Modes	
– **Free Amp Mode (per Amplifier)**	
AC Mode	
AC Power rating	31.5 kVA
Voltage Offset	380 V
AC Voltage range	0-250 V_{RMS}
AC Current range	0-126 A_{RMS}
DC Mode (unipolar)	
DC Power rating	100 kW
DC Voltage range	20-732 V
DC Current range	0-150 A
– **AC 3ph+N Mode**	
Maximum Power	94.5 kVA
Voltage range	0-250 V_{RMS}
Current range	0-126 A_{RMS}
– **DC Unipolar Mode**	
Maximum Power	100 kW
Voltage range	20-732 V
Current range	0-600 A
– **DC Bipolar Mode**	
Maximum Power	100 kW
Voltage range	±713 V
Current range	0-300 A
Cooling System	
Water cooling	8 kW
Air cooling	11 kW
Communication	
Real-time link to drive each amplifier	$f_{setpoint} = 250$ kHz (setpoint frequency)
SFP module	5 Gbit/s
SCADA link	100 Mbit/s optical, UDP

5.4 System integration

The overall laboratory components must be properly integrated into the test facility especially to fulfill the non-functional requirements, as discussed in Section 4.2. Among others, modularity and reconfiguration are considered as fundamental requirements for the flexible operation of the overall facility. Therefore, each component is deployed as single module that can be operated as stand-alone device for component-level testing as well as in connection with further components for system-level testing.

Due to logistical reasons, the laboratory components are distributed at different places within the facility area. Therefore, configuration cabinets are designed in order to converge the output power terminals of each modular component. According to the architectural classification proposed within this work, this kind of equipment is intended as type III components and therefore, essential elements also for supporting setup implementation and test execution. For example, a configuration cabinet is designed to implement a re-configurable grid topology by combining multiple physical cable segments. In this case, several cable segments with different lengths are placed along the basement of the laboratory area, as shown in Fig. 5.9. Available cables are of type NAYY 4x150 mm^2 and NAYY 4x25 mm^2 which

Fig. 5.9: Re-configurable test network available at SGTL – cables installation along the basement of the laboratory area (left-middle) and configuration cabinet for manual network topology implementation (right)

are common in German LV grids. The terminals of each cable segment are made available into the configuration cabinet where, by means of auxiliary

power patch cables, the user can manually configure a desired topology. The configuration cabinet also include four individual busbars that can be also connected to the rest of test facility.

Similar to the design solution for the re-configurable network, further configuration cabinets are adopted for interconnecting all the remaining component modules. A schematics of the overall implementation is depicted in Fig.5.10. Particularly, the AC test environment includes two similar configuration cabinets (AC-Cabinet A and B) each one hosting the output terminals of the main AC components together with an independent

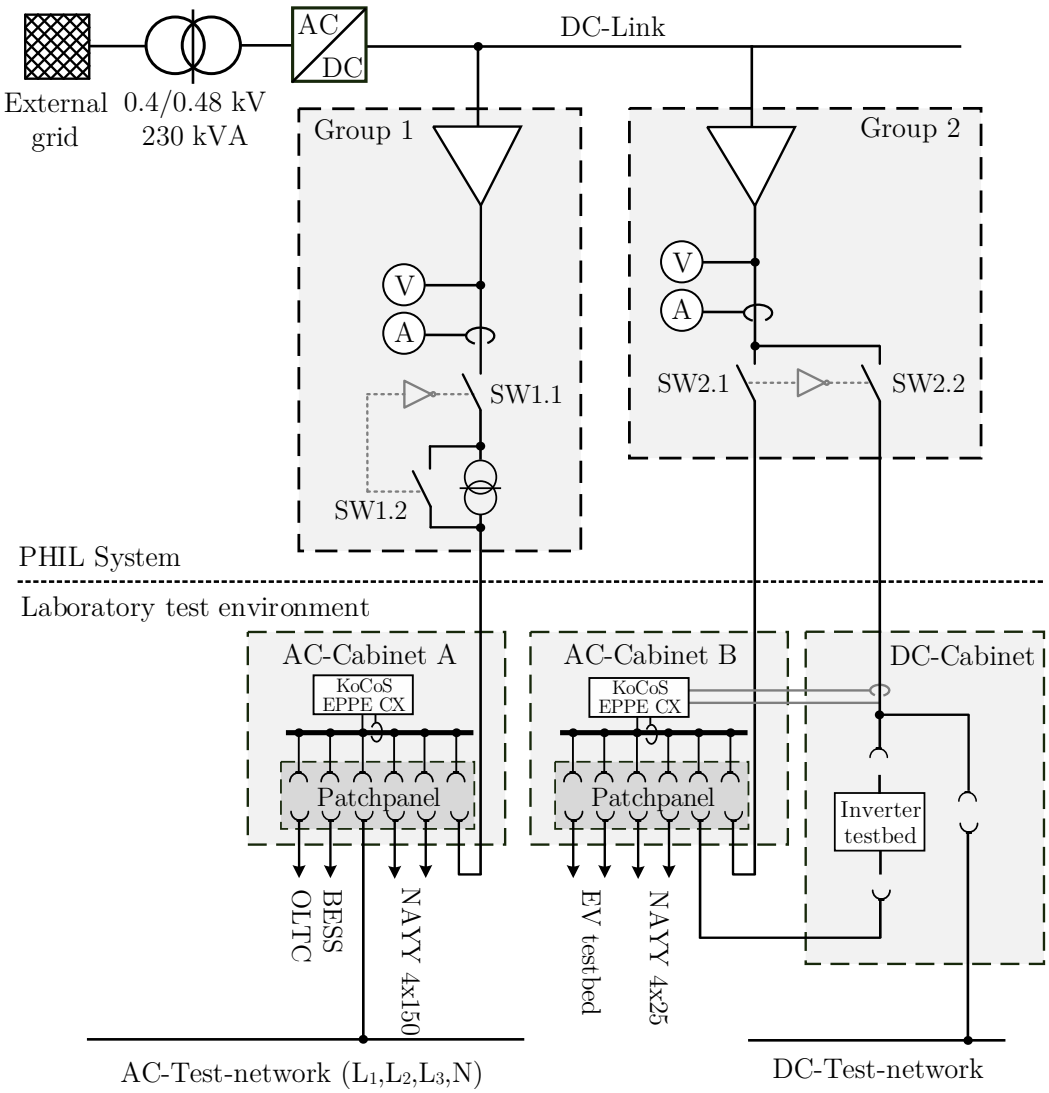

Fig. 5.10: Simplified electrical diagram of the selected design solution for the practical integration of modular power components including the PHIL system within the test facility

busbar. These two busbars can eventually be connected together within a common setup or operated individually, thus allowing parallel testing for different users. A separate configuration cabinet is designed for testing DC components and grid-connected inverters. The DC-Cabinet also includes a busbar equipped with all the required protection devices suitable for a DC supply system. A picture of the deployed cabinets is shown in Fig. 5.11.

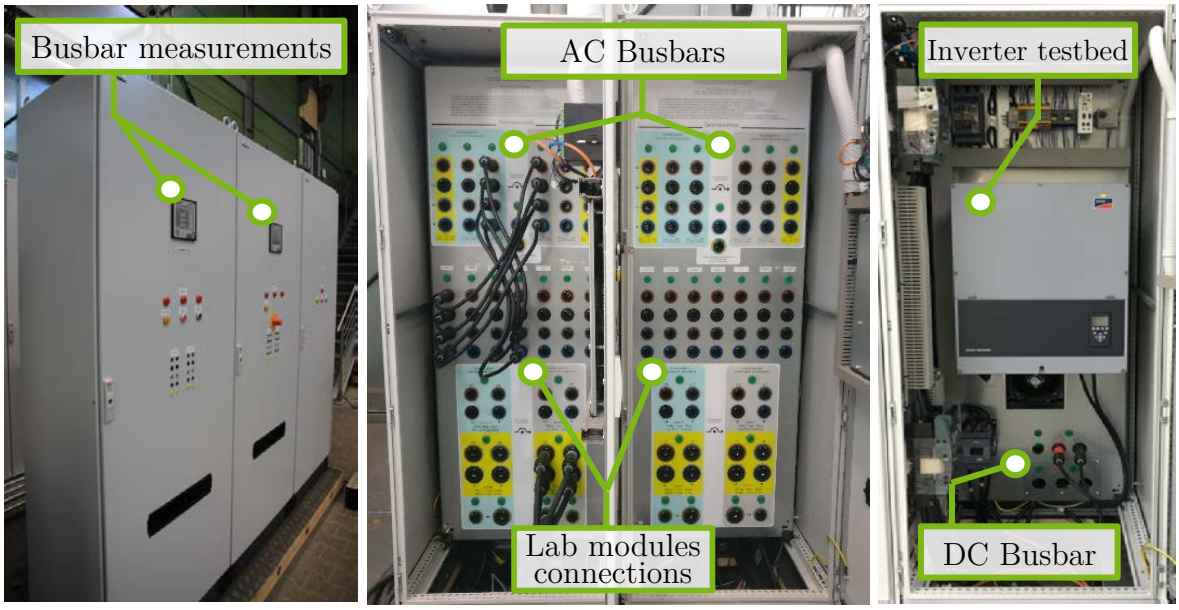

Fig. 5.11: Deployed configuration cabinets – outer view (left); inner view of the two similar AC cabinets (middle); inner view of the DC cabinet (right)

Both AC and DC cabinets are also designed to host the power outputs of the PA system. However, for practical needs the PA system is installed on the opposite side of the laboratory's perimeter with respect to the position of main configuration cabinets. Therefore, additional stationary cables with a length of about 80 m are installed to link PA outputs to the configuration cabinets. This will contribute to the total output impedance of the PA system and should be taken into account for PHIL stability analysis. Moreover, the adopted implementation solution leads to reworking concerns of the PA system. On the one hand, a dedicated commutation logic must be integrated to connect PAs outputs to the proper configuration cabinet according to the selected operating mode (AC or DC operation). On the

other hand, also different types and sizes of cables should be installed according to the specific operating mode. Also within a given operating mode (e.g., DC operation), current ratings can vary significantly (as between DC Unipolar and DC Bipolar), thus resulting either in cable oversizing or in the impractical installation of multiple cable paths for the given operating modes. In light of these considerations, additional design concerns (including a trade-off between requirements and implementation costs) have led to the conclusion of limiting the PA system configurations in favor of a more cost effective and task-oriented design. Particularly, PA Group 1 is designed to operate only in AC mode as major operating target of the facility. In this way, a single three-phase connection to the AC-Cabinet A is implemented. Moreover, the outputs of PA1 can be ether directly connected to the AC-Cabinet A (Free Amp/3ph+N mode) or connected through the insulated transformer (3ph+N+Trafo mode). By contrast, PA Group 2 is employed for both AC and DC operating modes. However, DC operation is restricted to DC Bipolar mode as no high currents are required. With respect to Fig.5.10, the embedded Programmable Logic Controller (PLC) of the PA system controls SW 2.1 and SW 2.2 complementary to connect the PA outputs either to AC-Cabinet B or to the DC-Cabinet according to the selected operating mode. Furthermore, PAs within a group are controlled as comprehensive system and connected to the configuration cabinets by 4-pole breakers; this limit the possibility to use a single PA group in a more flexible way. In fact, each PA group can be operated either in current or voltage mode but not in a mixed form.

The allowed operating modes for each PA group after the configuration reworking are summarized in Table 5.5.

Table 5.5: Allowed PA operating modes after system integration

	Operating modes				
	Free Amp	3ph+N	3ph+N+Trafo	DC Unipolar	DC Bipolar
PA Group 1	✓	✓	✓	✗	✗
PA Group 2	✓	✓	✗	✗	✓

Besides the aforementioned operational concerns, further aspects such as protection, measurements and safety are also of relevance for the proper system integration. The developed configuration cabinets as well as the installed PA system are equipped with typical protection devices for AC and DC systems in line with the possible operating modes. Particularly, each AC cabinet is equipped with usual overcurrent and overvoltage protection devices for three-phase systems with special regards to the residual current protection relays. In fact, due to the connection with the PA system (or further power electronics–based components), the Residual Current Device (RCD) must be properly selected in order to avoid undesired trips due to leakage currents or, even worst, missing detection of residual currents. In contrast to residual current, leakage current does not represent a fault situation (see Fig. 5.12).

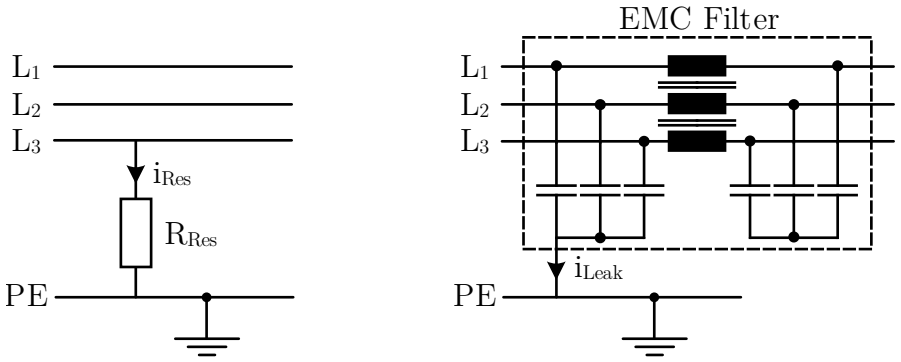

Fig. 5.12: Concept of residual current (left) and leakage current (right)

Typically, leakage currents are caused by capacitive currents to ground during normal operation due to filters or the capacitance of long cable connections. However, leakage currents must be limited within specific thresholds (0.4 times the rated residual current of the residual current operated protective device [137]). In fact, conventional RCDs cannot distinguish between residual currents and leakage currents. In case of high leakage current the RCD might trip even though there is no fault (residual current) in the system [137]. Furthermore, switch-mode power converters may produce a smooth DC residual current in case of fault at the DC-link or at the load side [138]. In conventional RCDs (such as type A), this

DC residual current saturates the magnetic core, thus leading to improper operation of the circuit breaker that may not trip in case of fault.

In compliance with EN 50178, type B RCDs must be used to provide protection against direct and indirect contact if electric equipment may produce a smooth DC residual current in the event of a fault. In facts, the specialized design of type B RCD includes an additional magnetic core for the detection of DC residual currents, thus guarantee a proper degree of protection especially by operating power converters [138].

As principal busbar measurements, the power quality analyzer EPPE CX by KoCoS [139] is included within each AC-cabinet. Besides conventional measurements, this device provides advanced functions such as Total Harmonic Distortion (THD) calculation or fault recording. In contrast to conventional measurements devices, the EPPE CX also allow to implement and to execute user-defined control functions. In fact, the device is equipped with analog and digital I/Os to interact with hardware components. Furthermore, a communication module including diverse standard protocols is also available for communication–based control. Therefore, the device can also be operated as type II component according to the individual test purposes.

As further system integration concerns, the implemented configuration cabinets as well as the integrated PA system are designed to provide a SIL 2, thus fulfill the actual safety level of the existing facility. In practice, this is achieved by installing additional SISs such as position and safety switches or emergency shutdown buttons. These parts are integrated within the emergency shutdown system of the existing facility. In case of manual stop or trip of protection devices, the overall test environment is shutdown and a manual restart of the system is required. This is also essential to avoid unintentional operations under voltage during setup re-configuration.

5.5 Remarks

The existing SGTL facility is presented and considered as case-study to describe the principal features and the main challenges by designing and developing such advanced laboratory infrastructures. Particularly, the overall laboratory is described according to the architectural classification suggested within this work. Particular emphasis is given to describe the PHIL system as principal element considered in this work. Finally, system integration aspects are discussed to provide an overview of the possible issues when applying the major non-functional requirements in practice.

In the next two chapters the SGTL facility and particularly the integrated PHIL system are used to prove the operational concepts formerly introduced in Chapter 4.

Chapter 6

Test of the elemental PHIL system functionalities

In this chapter preliminary tests are performed on the deployed PHIL system in order to prove its elemental functionalities. These provide a practical application of parts of the operational use-cases for PHIL applications introduced in Section 4.5. First, preliminary tests are performed to determine the dynamic model of the PA system and to assess the principal Interface Approaches (IAs) for conventional PHIL simulation. Later, the overall PHIL system is operated to emulate typical grid disturbances. Finally, a setup for the emulation of power profiles is implemented and applied to reproduce scenarios based on time-series within a test network.

6.1 Conventional PHIL test

PHIL setups require to be formerly analyzed in order to prove setup stability and accuracy before their practical implementation. In this regard, accurate models of the main looped components can be required. The dynamic model of the PA system together with the behavioral model of the specific IA represent the major elements to be considered. Therefore, preliminary tests are performed to assess both PA system model and IAs performance with respect to the deployed PHIL system.

6.1.1 PA dynamic model evaluation

PAs are usually modelled as second order transfer functions due to the LC output filters and including a time delay that represents the internal drives. The mathematical expression of this transfer function was introduced in Section 3.3 and reported in (6.1).

$$G_{\mathrm{PA}}(s) = \frac{(2\pi f_{\mathrm{PA}})^2}{s^2 + 2\zeta 2\pi f_{\mathrm{PA}} s + (2\pi f_{\mathrm{PA}})^2} e^{-sT_{\mathrm{PA}}} \tag{6.1}$$

In the following, the PA system is tested in both frequency and time domain to determine the proper parameters in (6.1). In both cases, the PA system is configured as three-phase voltage source operating at the maximum output voltage. A resistive load of 3.2 Ω is used to operate at about 50 % of the maximum current. Fig. 6.1 shows the results of the frequency response tests. The physical PA system is tested with frequencies up to 10 kHz. First, the measurements are compared with simulation results based on the application of the datasheet specifications for the parametrization of

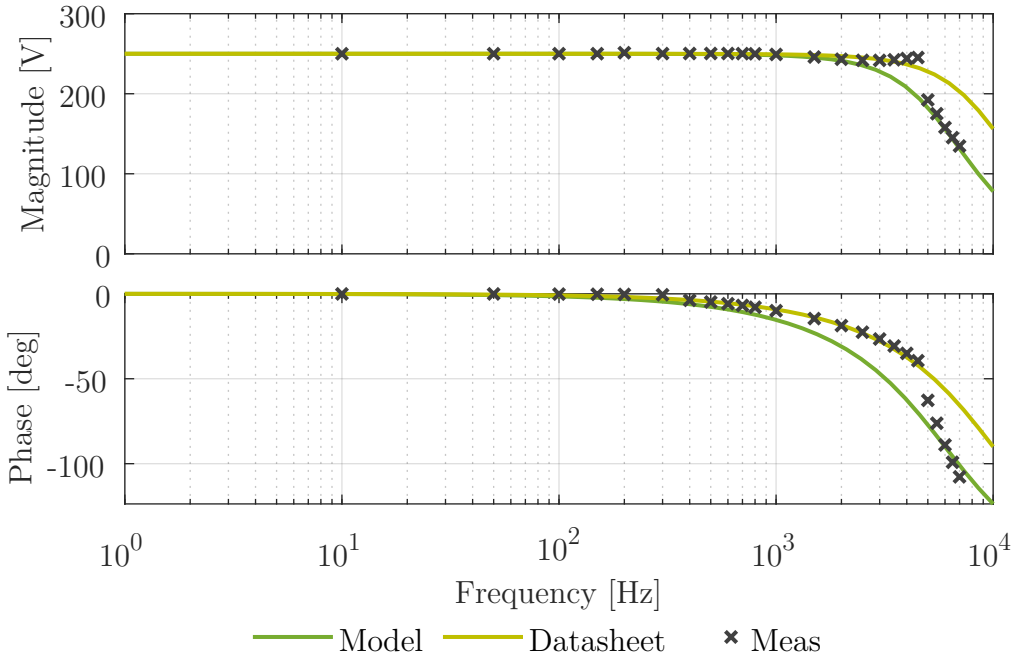

Fig. 6.1: Frequency response: comparison between the simulated model and measurements from the physical PA (test at max voltage output with 3.2 Ω Y-connected load)

(6.1). Results show a proper response approximation for frequencies up to 5 kHz. However, for higher frequencies the model outcomes deviate from the actual measurements. Therefore, the model parameters are further tuned to improve the model outcomes afterwards. The final model results in a transfer function characterized by a cut-off frequency $f_{\mathrm{PA}} = 6\,\mathrm{kHz}$, a damping factor $\zeta = 0.8$ and a time delay $T_{\mathrm{PA}} = 30\,\mu\mathrm{s}$.

Similar test conditions are reproduced also to evaluate the time response of the PAs to a step reference signal. The measurements are compared with the response of the determined model with respect to the similar reference signal, as shown in Fig. 6.2.

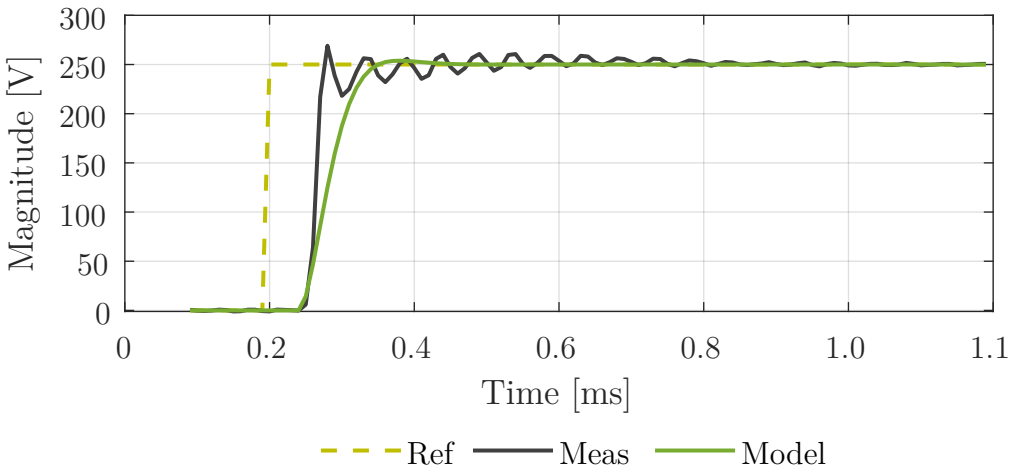

Fig. 6.2: Step response: comparison between the simulated model and measurements from the physical PA (zero to max voltage output with 3.2 Ω Y-connected load

The identified model provides an acceptable approximation of the actual physical system. However, the application of (6.1) as a reference model results in an inexact behavior with respect to the measurements of the physical system. The actual response of a physical PA also depends on the control parameters of the inner PI (proportional plus integral) regulator. This contribution is not included in the generally adopted dynamic model. Therefore, the frequency response of the closed-loop physical system differs from the resulting second order dynamic model. Furthermore, PI parameters can be adjusted according to the application requirements. Therefore, PA

system response can vary accordingly. Moreover, further aspects related to the actual operating conditions such as the load level (in closed circuit operation) also affect the dynamic performance. Therefore, the exact determination of the PA model should be performed also considering those aspects. The determined dynamic model is in line with the community accepted modeling approach and results in a sufficient approximation of the actual PA system response. However, in case of particular PHIL applications where the stability conditions are close to the limits a more detailed evaluation of the dynamic model is recommended.

6.1.2 Interface assessment

A basic setup is implemented for the development and assessment of the IAs required for PHIL testing. The principal software interfaces are implemented for both Ideal Transformer Method (ITM) and Damping Impedance Method (DIM) as main ones applied for PHIL testing. Particularly, the implementation of the DIM is given with a fixed damping impedance as well as with online estimated damping impedance. The latter implements the algorithm suggested in [121] to adjust the damping impedance according to the actual impedance of the HuT, as shown in Fig. 6.3. This algorithm can be applied to a RL (resistive and inductive) type HuT where the resistive part (R_D) and the inductive part (L_D) are obtained in real-time from the voltage and current measurements ($v(t)$ and $i(t)$, respectively) of the HuT.

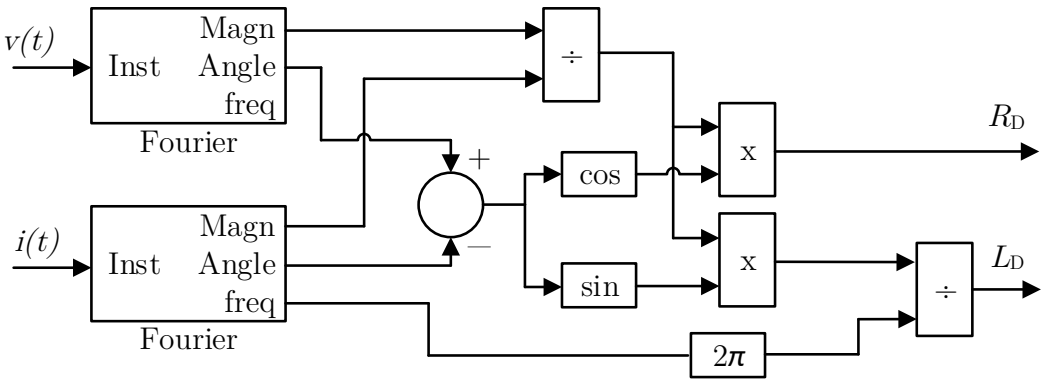

Fig. 6.3: Algorithm for the online damping impedance estimation [121]

All the implemented IAs are tested on a similar setup, as shown in Fig. 6.4. Two similar circuits are simultaneously simulated within the RTS. These can be intended as Thévenin equivalent circuits of more complex grids. The simulated impedance Z_{HuT} is connected to the circuit on the top-side, thus forming the NCS. This represents the ideal implementation of the actual PHIL setup that is realised with the circuit on the bottom-side. Physical variable resistors are used as HuT for the actual PHIL setup. The simulated impedance Z_{HuT} is set with resistance values similar to the physical resistors used for the PHIL setup. Lastly, a group of PAs is operated as voltage source (*3ph+N V-Mode*) to emulate the Point of Common Coupling (PCC) of the simulated circuit. The software impedance (Z_{SW}) and the hardware resistor are selected in order to ensure a stable PHIL simulation.

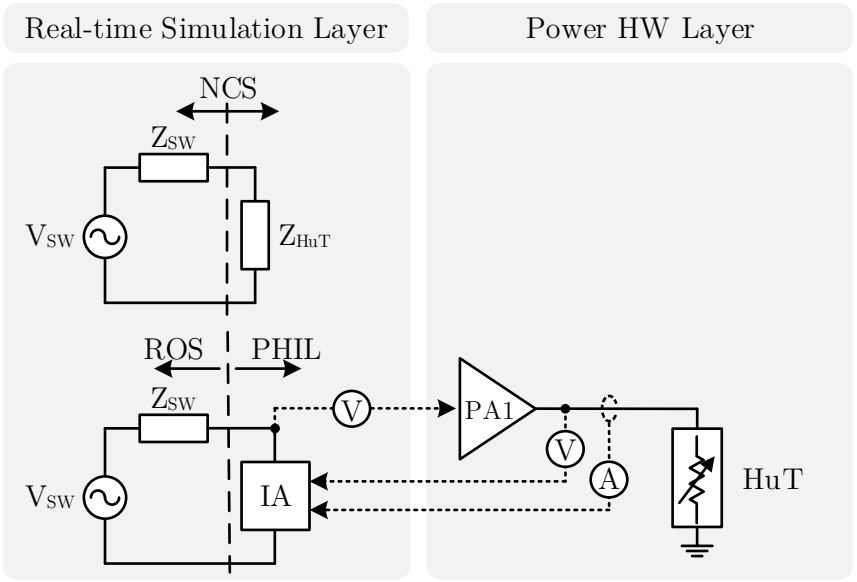

Fig. 6.4: PHIL setup in case of emulated HuT

Fig. 6.5 shows the test results for the various IAs as well as for the NCS with particular emphasis on the amplitude and phase shift between the relevant waveforms. As suggested in [108], these results can be compared in terms of amplitude error and phase shift with respect to the NCS case where the HuT is modelled within the RTS. However, this approach might lead to erroneous interpretation of the results. In fact, the NCS simulation only considers a fixed and pure resistive HuT. However, the resistance of the physical HuT is varying due to external factors such as the actual operating

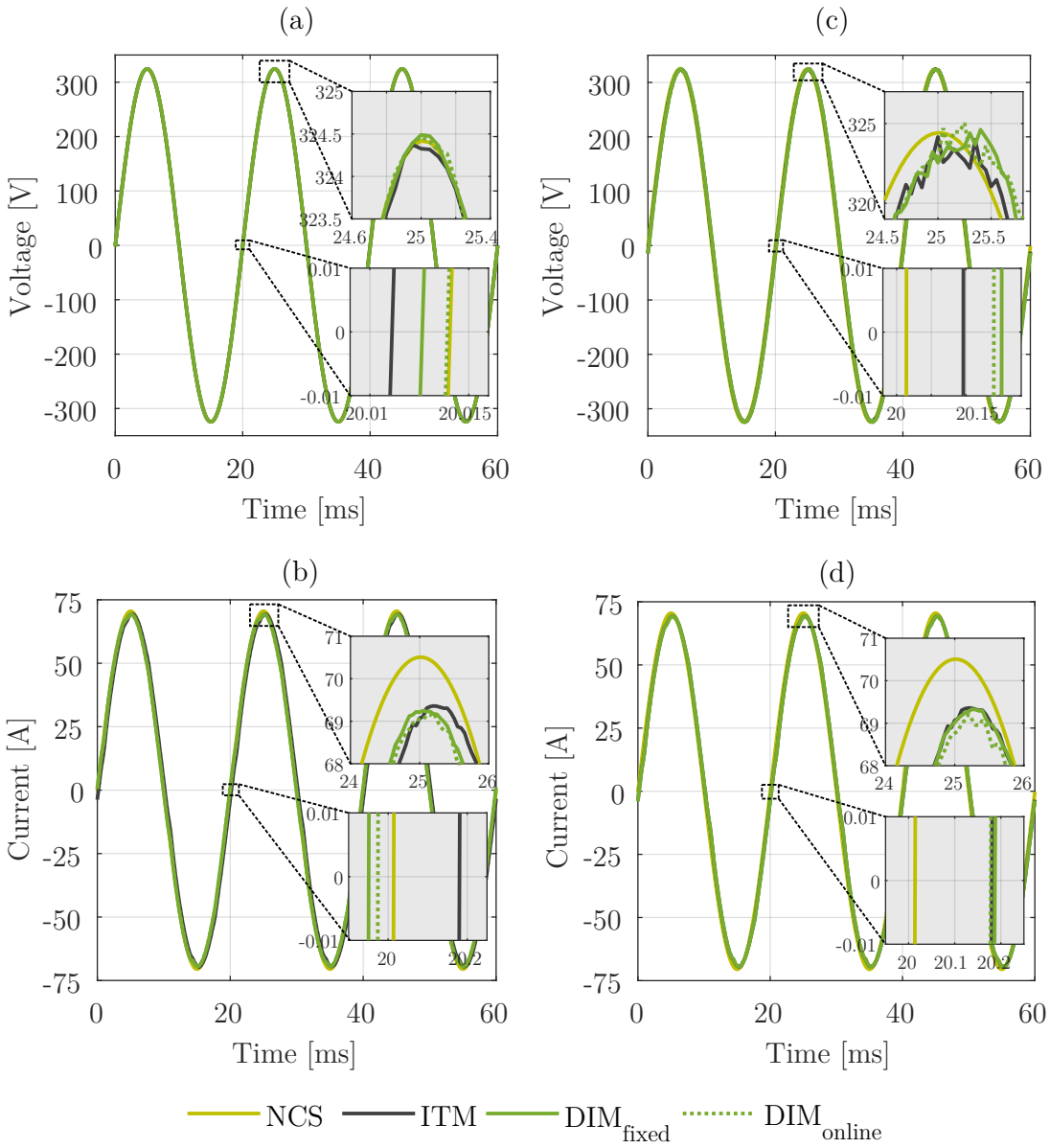

Fig. 6.5: Waveform comparison between NCS, ITM, DIM with fixed Z_D and online Z_D estimation – (a) voltage of the ROS, (b) current of the ROS, (c) voltage of the HuT, (d) current of the HuT

temperature. This, together with additional cable connections needed for the setup implementation, contribute to the actual impedance of the HuT. Moreover, the resulting impedance of the HuT also includes parasitic reactive parts that contribute to the load angle. Therefore, the accuracy evaluation based on the comparison of the outcomes with respect to the simulated NCS is not a viable solution in case of practical implementations. To proper perform such comparison the compensation of the aforementioned issues should be formerly considered.

An alternative approach is to consider instantaneous error functions to compare the results between HuT and ROS, as suggested in [120]. The instantaneous error functions can be defined for both voltage (6.2) and current quantities (6.3).

$$\varepsilon_{\mathrm{V}}(t) = \frac{V_{\mathrm{ROS}}(t) - V_{\mathrm{HuT}}(t)}{\sqrt{2}\, V_{\mathrm{ROS_{RMS}}}} \tag{6.2}$$

$$\varepsilon_{\mathrm{I}}(t) = \frac{I_{\mathrm{HuT}}(t) - I_{\mathrm{ROS}}(t)}{\sqrt{2}\, I_{\mathrm{HuT_{RMS}}}} \tag{6.3}$$

The application of (6.2) and (6.3) results in to the instantaneous quantities shown in Fig. 6.6. A better accuracy of the ITM can be observed especially with regard to the current error. Minimal accuracy improvements can be detected for the application of the $\mathrm{DIM_{online}}$ compared with the $\mathrm{DIM_{fixed}}$. The former, however, should result more effective in case of online variations of the HuT.

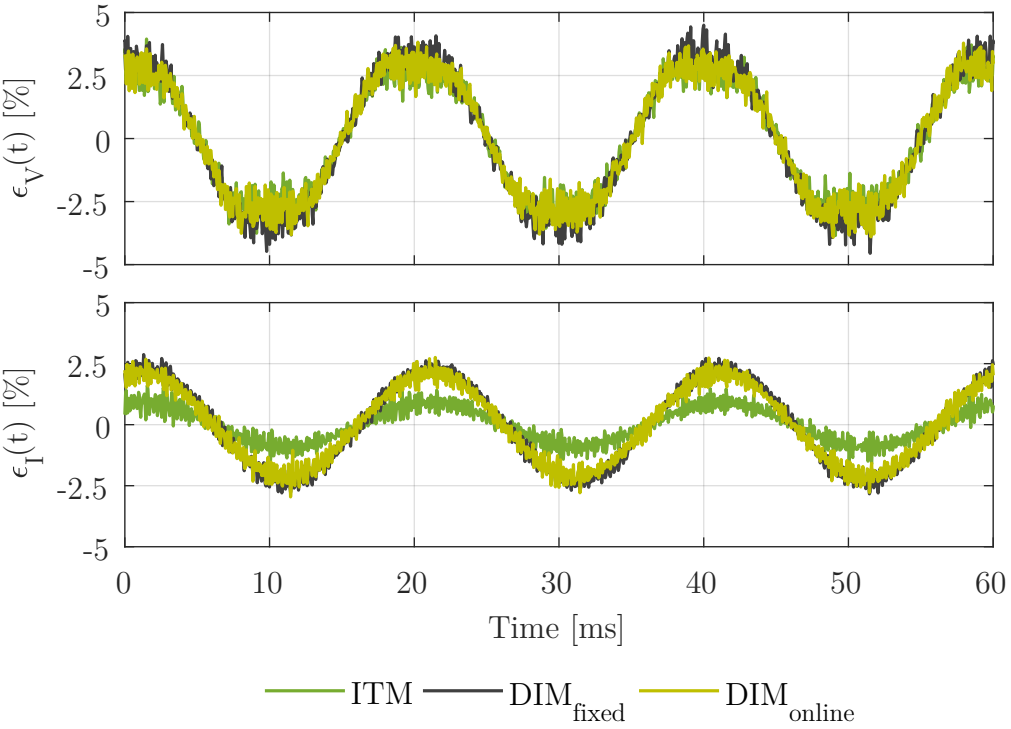

Fig. 6.6: Instantaneous error functions for the different IAs – instantaneous voltage error (top); instantaneous current error (bottom)

The steady-state error can be quantified by considering the RMS value of the instantaneous error, as reported in Table 6.1. Although the ITM

Table 6.1: RMS error for the different IAs

Error	**ITM**	**DIM$_{\text{fixed}}$**	**DIM$_{\text{online}}$**
$\varepsilon_{\mathrm{V_{RMS}}}$[%]	1.961	2.446	2.246
$\varepsilon_{\mathrm{I_{RMS}}}$[%]	0.622	1.681	1.589

provides more accurate results its stability highly depends on the setup parameters (see Section 3.3). In contrast, the DIM provides lower accuracy due to estimation errors of the damping impedance. However, DIM does not require detailed stability analysis to be performed every time as stability does not depend on the parameters of the circuits. Therefore, the use of the DIM (particularly the DIM$_{\text{online}}$) can be encouraged in case of PHIL setups that do not require high level accuracy or to speed up the development of "prove of concept" setups. To better assess the performance of the implemented DIM$_{\text{online}}$, a variable RL load is required as HuT. For this purpose, an exemplary test is performed by emulating the HuT with a second PA group, as depicted in Fig. 6.7. The current on Z_{HuT} drives PA 2 in order to emulates its behavior on the power hardware layer. Therefore,

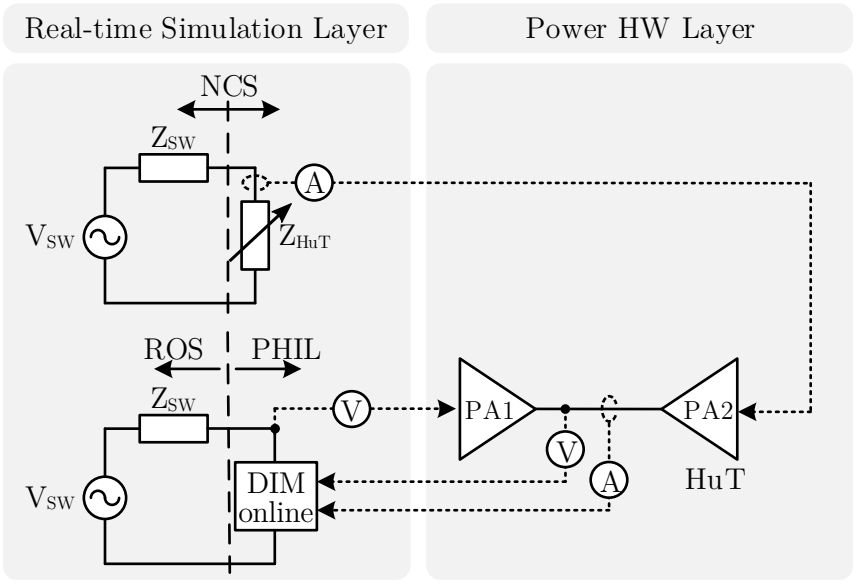

Fig. 6.7: PHIL setup in case of emulated HuT

PA 2 acts as HuT for the PHIL simulation that involves the simulated network on the bottom realized by PA 1. This solution can be generally applied to emulate power components otherwise not available as physical ones (see UC12). In this case, the emulated impedance provides a variable RL load, thus allowing to test the online estimation of both resistive and inductive parts. A qualitative comparison between the simulation results of the NCS and PHIL is given in Fig. 6.8. Particularly, between 40 and

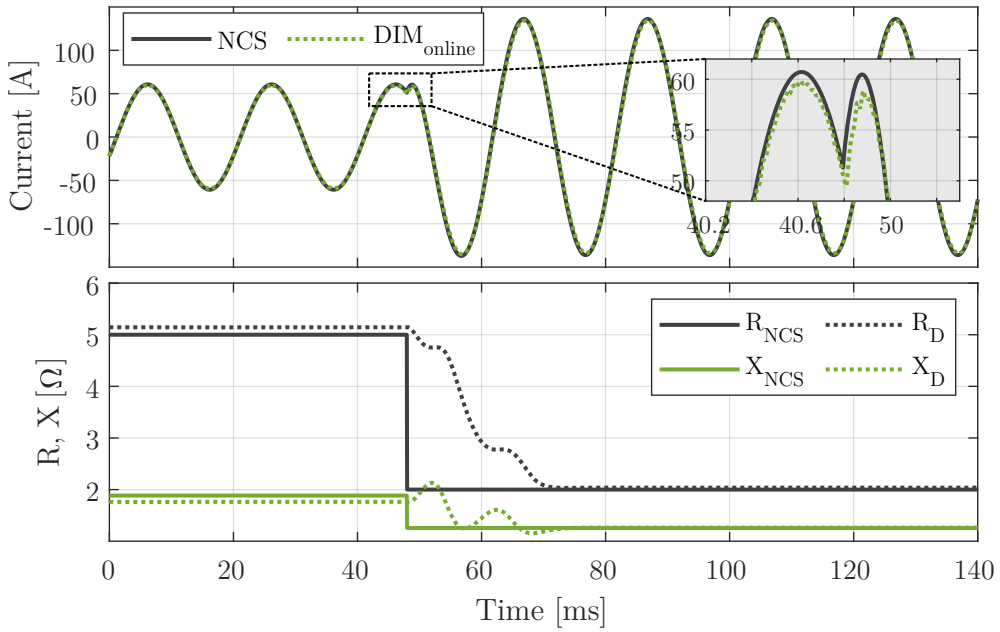

Fig. 6.8: Comparison between NCS and online $\mathrm{DIM}_{\mathrm{online}}$ in case of emulated impedance as HuT – Instantaneous current (top); set and estimated resistance and reactance (bottom)

60 ms the resistance and the inductance of the simulated impedance Z_{HuT} is varied step-wise. Results show the ability of the implemented algorithm to estimate the actual impedance within 20 ms. Moreover, a lower estimation error is detected for higher current values. However, as formerly mentioned, this comparison is considered for qualitative evaluations only. In fact, in contrast to the simulated impedance Z_{HuT}, the impedance estimation also includes the contribution of additionally looped elements such as PA filters and connection cables. However, the implemented $\mathrm{DIM}_{\mathrm{online}}$ behaves as expected and can be further applied according to the given PHIL setup requirements.

6.2 Open-loop grid emulation

The PHIL system is tested to prove its capability to emulate typical voltage disturbances in power system according to the operational use-cases UC10 suggested in Section 4.5. In this case, the RTS is used as a flexible signal generator while the PA system provides the full-scale outputs to the laboratory test environment. Compared to conventional signal generators, the use of a RTS provides more practical benefits in term of flexible and straightforward signal editing. Steady-state as well as dynamic signals can be programmed as mathematical functions and real-time executed. Moreover, a test routine including different signal parametrization can be automatically performed, thus improving the execution of multiple tests. A block diagram of the overall setup is depicted in Fig. 6.9. A set of test

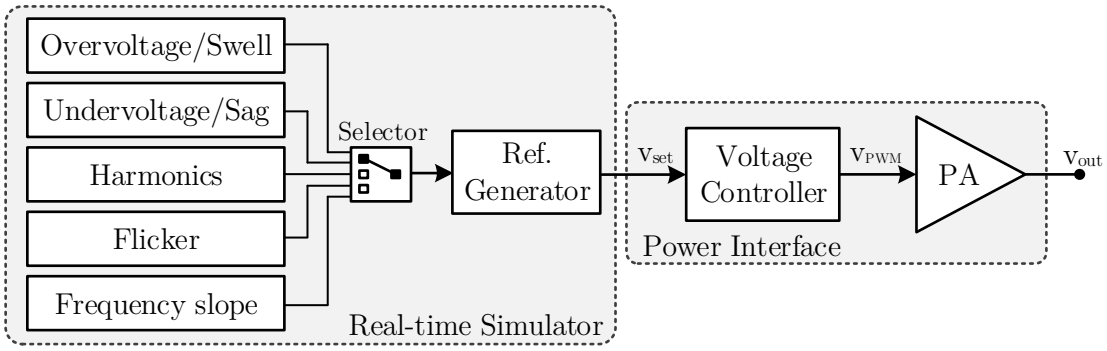

Fig. 6.9: Setup for grid disturbance emulation

functions is selected and implemented within the RT-Lab environment and running on the RTS. These functions can be individually selected and converted into instantaneous reference signals that are sent to the PA system via a SFP link. The developed test functions aim to emulate typical power quality disturbances according to the standard IEEE-1159 [140]. However, due to the minimal simulation time-step and the maximum PA's bandwidth, transients such as impulses and oscillations are neglected. The test functions include steady-state disturbances such as harmonics or flicker as well as long and short time duration events such us undervoltage or

overvoltage conditions. Exemplary applications for each developed test function are given in the follows.

Undervoltage/Sag

As suggested in IEEE-1668 [141], depending on the recorded frequency of sag events in the field, three main common sag types can be defined. These are considered as reference and implemented within the RTS. Their mathematical implementation is summarized in Table 6.2. Particularly, type I and type II refer to asymmetrical voltage sags while type III refer to symmetrical ones. Undervoltage conditions can be emulated as long duration sags. For instance, symmetrical undervoltage emulation can be obtained by long duration type III voltage sags.

Table 6.2: Voltage sag emulation – selected test vectors according to [141]

Voltage sag	**Description**	**Equations***	**Vector diagram**
Type I	Voltage sag in which a drop in voltage takes place mainly in one of the phase-to-ground voltages	$\overline{V}_1 = a\overline{E}_1$ $\overline{V} = -\frac{1}{2}a\overline{E}_2 - j\frac{\sqrt{3}}{2}\overline{E}_2$ $\overline{V}_3 = -\frac{1}{2}a\overline{E}_3 + j\frac{\sqrt{3}}{2}\overline{E}_3$	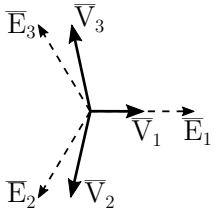
Type II	Voltage sag in which a drop in voltage magnitude takes place mainly in one of the phase-to-phase voltages	$\overline{V}_1 = \overline{E}_1$ $\overline{V}_2 = -\frac{1}{2}\overline{E}_2 - j\frac{\sqrt{3}}{2}a\overline{E}_2$ $\overline{V}_3 = -\frac{1}{2}\overline{E} + j\frac{\sqrt{3}}{2}a\overline{E}_3$	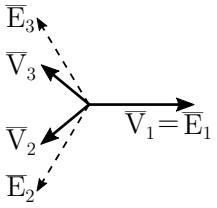
Type III	Voltage sag in which there is a drop in voltage magnitude that is equal for each voltage	$\overline{V}_1 = a\overline{E}$ $\overline{V}_2 = -\frac{1}{2}a\overline{E}_2 - j\frac{\sqrt{3}}{2}a\overline{E}_2$ $\overline{V}_3 = -\frac{1}{2}a\overline{E}_3 + j\frac{\sqrt{3}}{2}a\overline{E}_3$	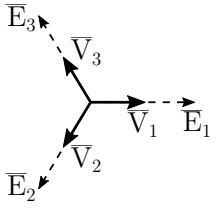

* Where: a = sag voltage factor ($a < 1$); $\overline{E}_1$, $\overline{E}_2$, $\overline{E}_3$ = pre-sag phase-to-ground voltages; $\overline{V}_1$, $\overline{V}_2$, $\overline{V}_3$ = actual phase-to-ground voltages

Results of voltage sag emulation with different sag voltage factors (a) and different time intervals (ΔT) for each selected sag type are shown in Fig. 6.10.

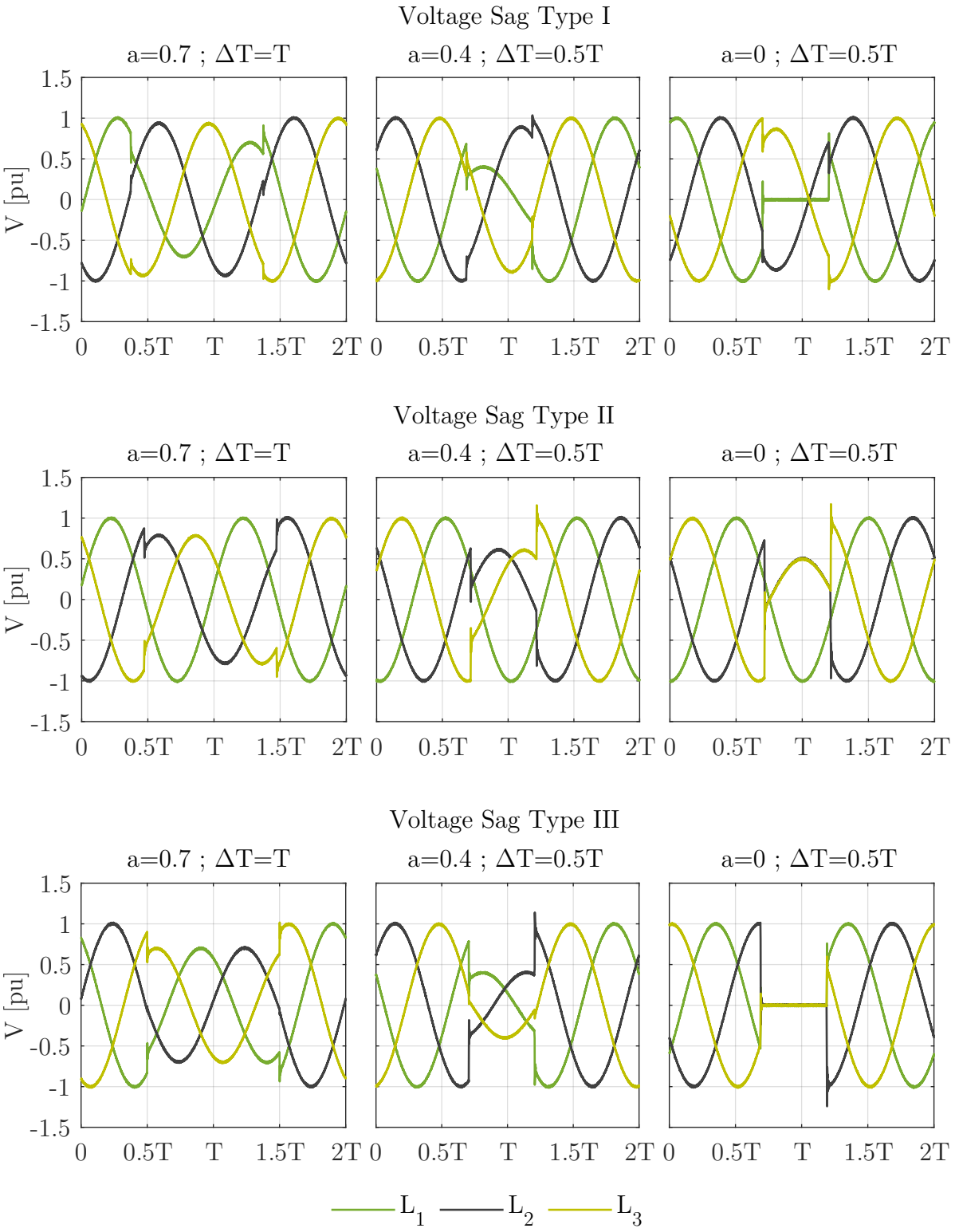

Fig. 6.10: Emulation of different types of voltage sags at different time intervals ΔT expressed as a fraction of the fundamental period T (pu values refer to a fundamental sine waveform at 50 Hz and 230 V_{RMS} phase-to-ground)

Overvoltage/Swell

According to the limits specified by EN 50160, overvoltage in LV distribution grids is defined for voltage increase above 10 % of the nominal voltage. However, the PA system is designed to provide a maximum output voltage of 250 V_{RMS} phase-to-ground according to the available DC-link voltage. Therefore, the maximum sinusoidal output achievable within the linear region of PWM modulation corresponds to +8.7 % with respect to the nominal voltage of 230 V_{RMS} (typical of LV grids). For setpoints higher than 250 V_{RMS} the PWM converter operates in overmodulation, thus distorting the output waveform. This situation is shown in the top-side of Fig. 6.11. Starting from a nominal voltage of 230 V_{RMS}, the voltage is increased of 25 %. For setpoints above 8.7 %, the output waveform is truncated due to the limited DC-link voltage. To better exploit DC-link voltage, a

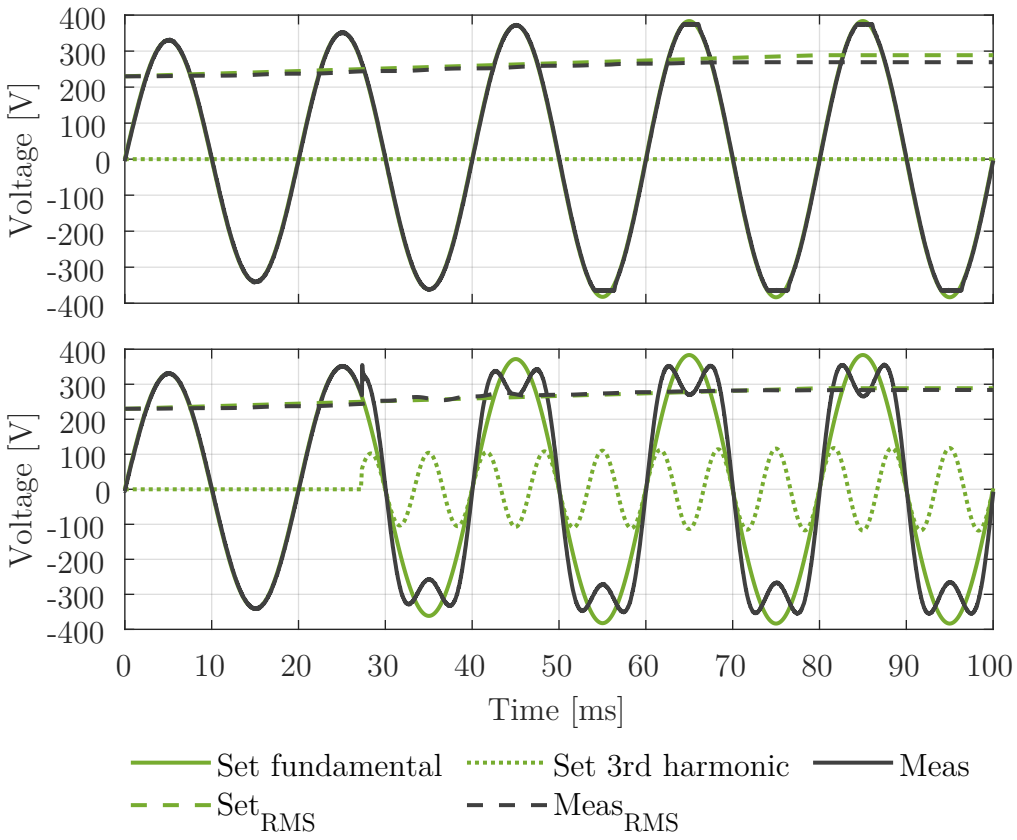

Fig. 6.11: Overvoltage emulation test with phase-to-ground voltage slope from 230 V_{RMS} to 287.5 V_{RMS} (+25 %) – overvoltage without third harmonic injection (top); overvoltage with automatic third harmonic injection (bottom)

third harmonic component can be injected in addition to the fundamental waveform. This provides an increase of 15 % with respect to the maximal output voltage with a minimal harmonics content. Therefore, a total overvoltage of 25 % can be achieved. For this purpose, the reference voltage is generated by an algorithm that automatically injects a third harmonic component in addition to the fundamental waveform. The resulting output waveform in case of an automatic injection of third harmonic components is shown in the bottom-side of Fig. 6.11. The waveform distortion due to the third harmonics is observable within the phase-to-ground voltage while it does not affect the phase-to-phase voltage where the third harmonics are cancelled.

Flicker

The flicker emulator generates a sinusoidal waveform modulated with a defined signal. Three different modulating signals are considered to shape the flicker disturbance as: sine flicker, sawtooth flicker and square flicker. Fig. 6.12 shows the test results of flicker emulation for the aforementioned modulating signals in case of similar modulation amplitude and frequency.

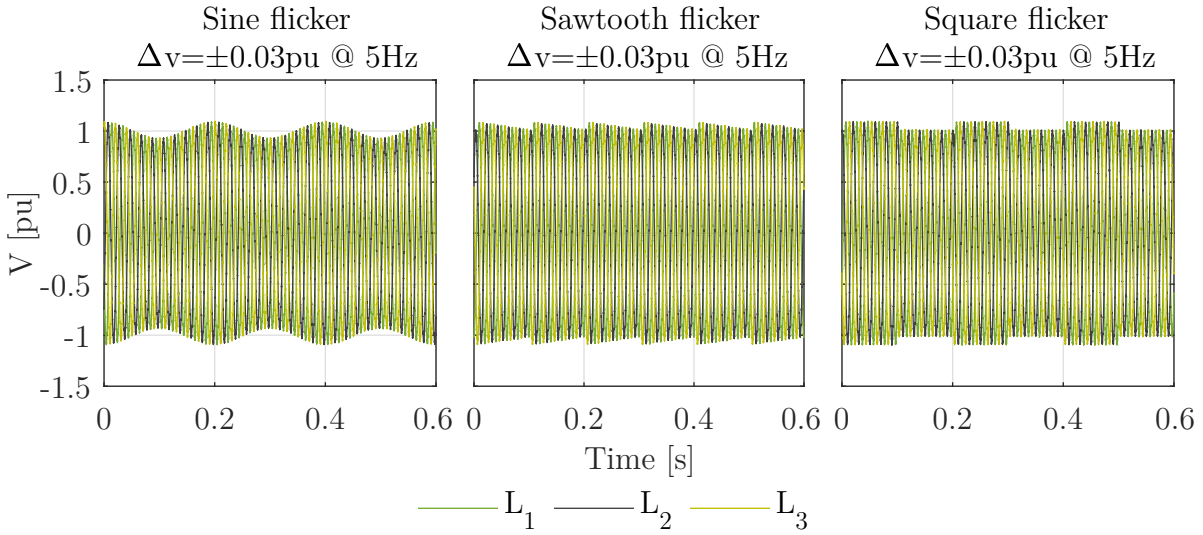

Fig. 6.12: Flicker emulation test with different modulating waveforms in case of similar modulation amplitude and frequency (pu values refer to a fundamental sine waveform at 50 Hz and 230 V_{RMS} phase-to-ground)

Harmonics

The harmonics emulation includes the possibility to set a desired harmonic order with a defined amplitude with respect to a defined fundamental waveform. Multiple harmonics can be simultaneously applied to each phase while the PAs operate as a symmetrical three-phase system. Otherwise, the individual setpoints of the harmonics can be provided for each phase independently. These operation options are tested according to the parameters reported in Table 6.3.

Table 6.3: Harmonics emulation – Test cases and parameters

Test case		**Harmonics**	
		Order*	**Amplitude*** [%]
Low-frequency	Symmetrical system	3 5 7	30 20 20
High-frequency	Symmetrical system	21 23	10 10
Individual phase	Phase 1 (L_1)	3	35
	Phase 2 (L_2)	3 7 11	10 10 10
	Phase 3 (L_3)	23 25	10 5

* with respect to a fundamental sine waveform at 50 Hz and 230 V_{RMS}

Fig. 6.13 shows the resulting output voltage measured at the PA's terminals. The implemented model is performed without overruns with a fixed simulation time-step of 10 μs. Therefore, the simulator is able to provide a good quality of the signal waveforms for harmonics up to 4 kHz (see Equation 4.1). However, the PA system is limited to 2.5 kHz harmonics when operating at full output voltage. Therefore, harmonics emulation at full output voltage can be performed up to 50^{th} harmonic order with respect to the fundamental frequency of 50 Hz.

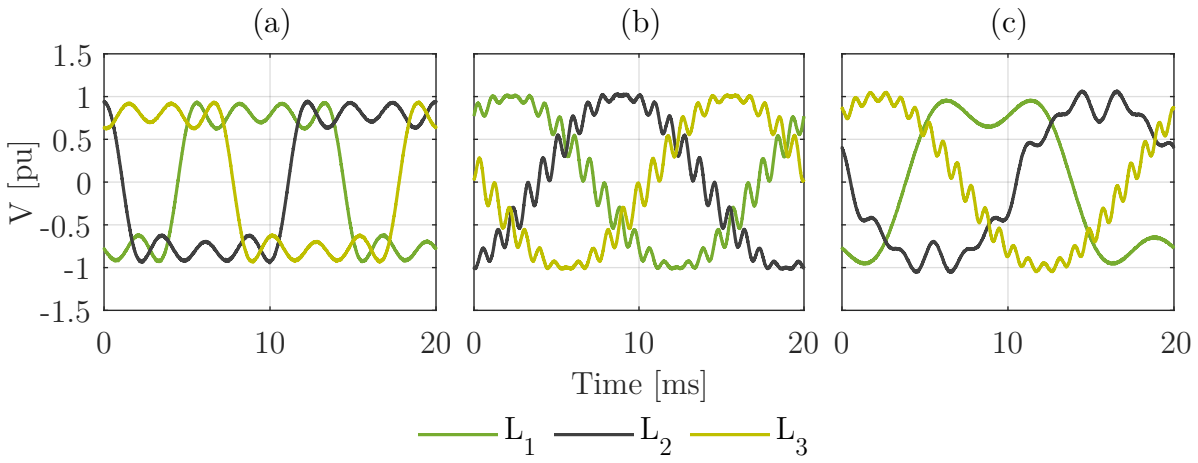

Fig. 6.13: Harmonics emulation test with a fundamental sine waveform at 50 Hz and 230 V_{RMS} phase-to-ground – (a) Low frequency harmonics; (b) High frequency harmonics; (c) Individual phase harmonics

Frequency slope

The frequency slope emulator implements a set of three-phase voltage signals with a desired frequency modulation. Fig. 6.14 shows the results frequency slope emulation for different frequency setpoints in both underfrequency and overfrequency case.

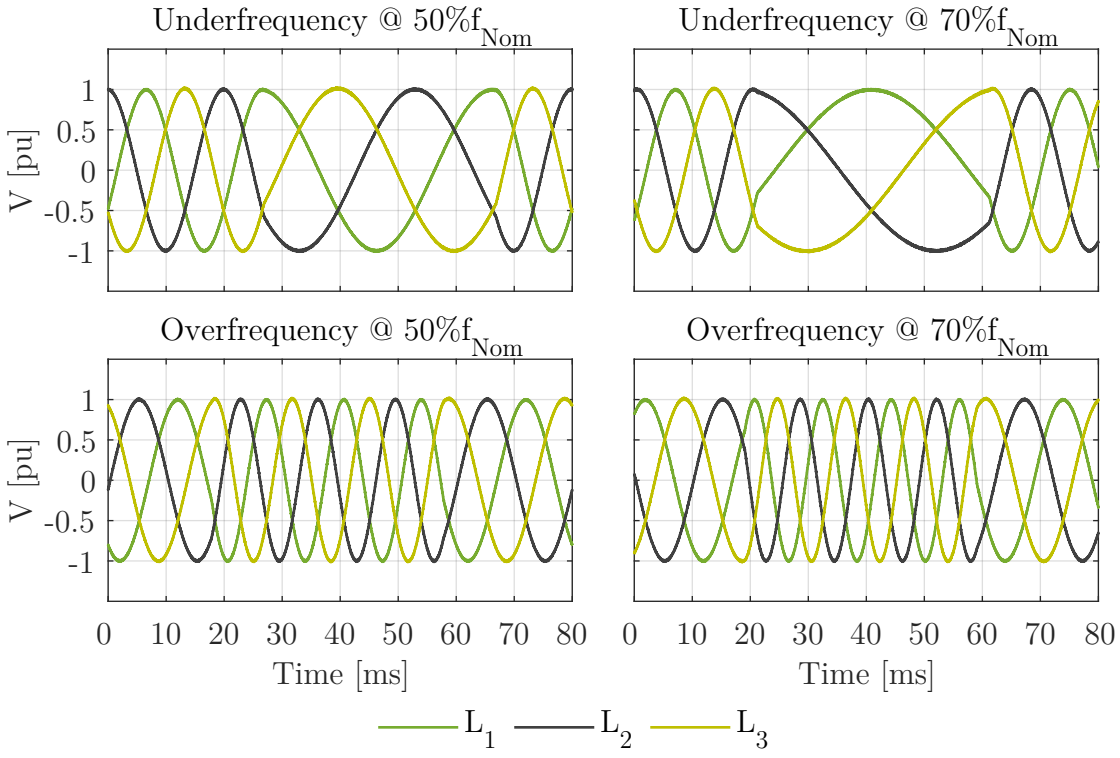

Fig. 6.14: Frequency slope emulation

6.3 Power profiles emulation

Besides the emulation of desired voltage waveforms, the PHIL system can be used to emulate generation feed-in and load consumption within the laboratory test environment. In this case, the PA system is operated in current mode (I-mode) and the reference currents are provided by the RTS. Of particular interest is the emulation of power profiles (see UC11). In this case, the reference active and reactive power values must be converted in to instantaneous currents and sent as setpoints to the PA system. For this purpose, a PLL algorithm is implemented within the RTS, thus providing a closed-loop setup, as shown in fig. 6.15. The amplitude and the angle of the instantaneous currents are computed within the reference generator block according to the outcomes of the PLL and the reference power. Active and reactive power setpoints can be derived from an external data source as time-series format. In this case, the scenario interface implements a python–based script that uses the API of the RTS to transfer power references from an external data source.

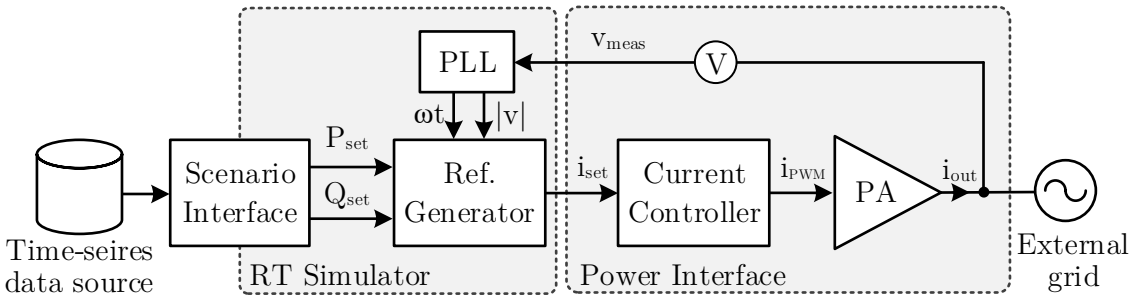

Fig. 6.15: PHIL setup for emulation of power profiles based on time-series

An exemplary application of this operational use-case is depicted in Fig. 6.16. A cloud–based state estimation tool is installed within a LV network in the city of Dortmund and integrated into the SGTL infrastructure. The state estimation tool is a commercial product called Venios Energy Platform (VEP) by company Venios [142]. At field level, VEP performs grid estimation based on the measurements at the secondary substation of the selected LV grid. VEP is interfaced at laboratory level by using the mentioned scenario

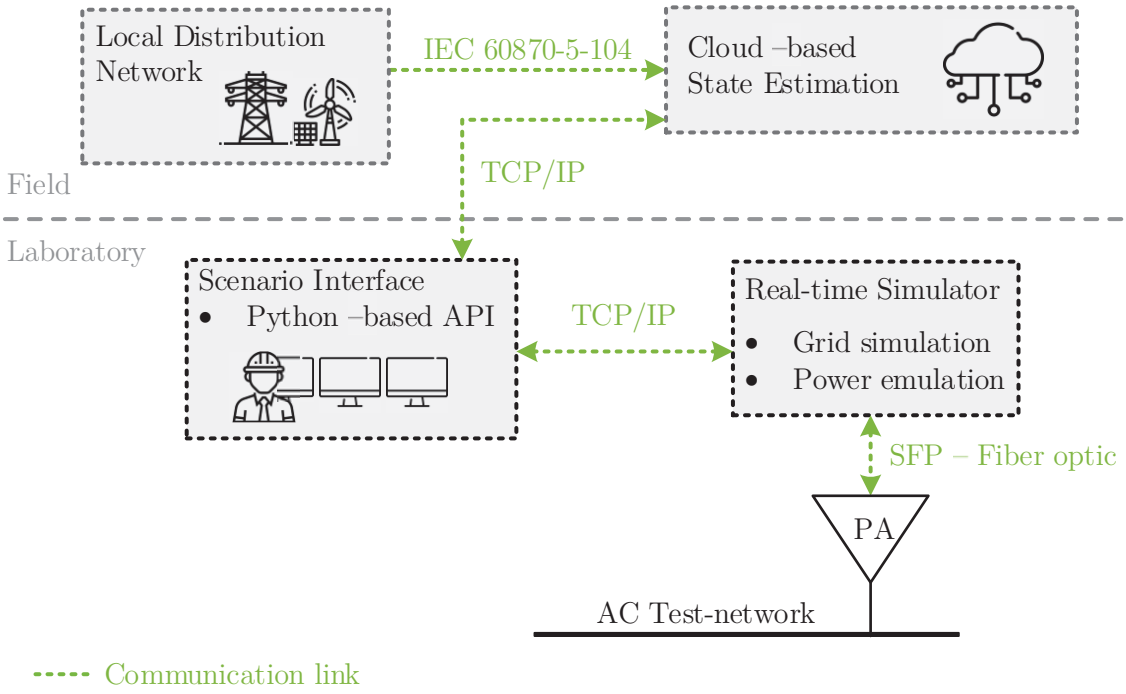

Fig. 6.16: Setup for laboratory–level power emulation based on field measurements and state estimation outcomes

interface. This transfers field measurements as well as the outcomes of the state estimation to the RTS. Finally, the PA system is used to emulate the resulting power profiles within the laboratory test network thereby providing realistic scenarios for the given test purposes.

The selected LV grid covers a residential area close to the campus of TU Dortmund University with a total number of 97 nodes. The grid includes 20 PV units for a total installed power of 81 kWp. An illustration of the selected LV grid is shown in Fig. 6.17. Measurements and communication modules are installed at the secondary substation as shown in Fig. 6.19. A voltage measurement is installed at the 0.4 kV busbar while current sensors are installed in each feeder. A commercial rooter is included on a Virtual Private Network (VPN) and used to transfer measurements from the secondary substation to VEP via IEC 60870-5-104 communication.

The scenario interface is running on a local terminal of the laboratory and performs TCP/IP requests to the server of VEP in order to acquire specific data from the field. This allows for collecting measurements and

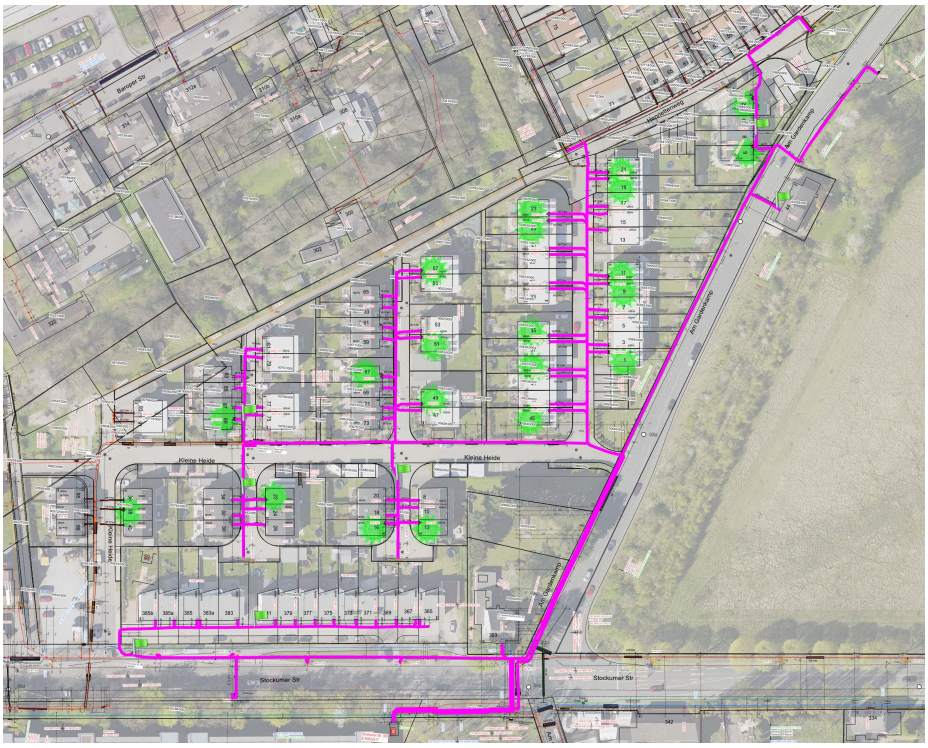

Fig. 6.17: Selected LV grid in Dortmund City – grid topology (magenta lines); roof PV-system installations (green marks)

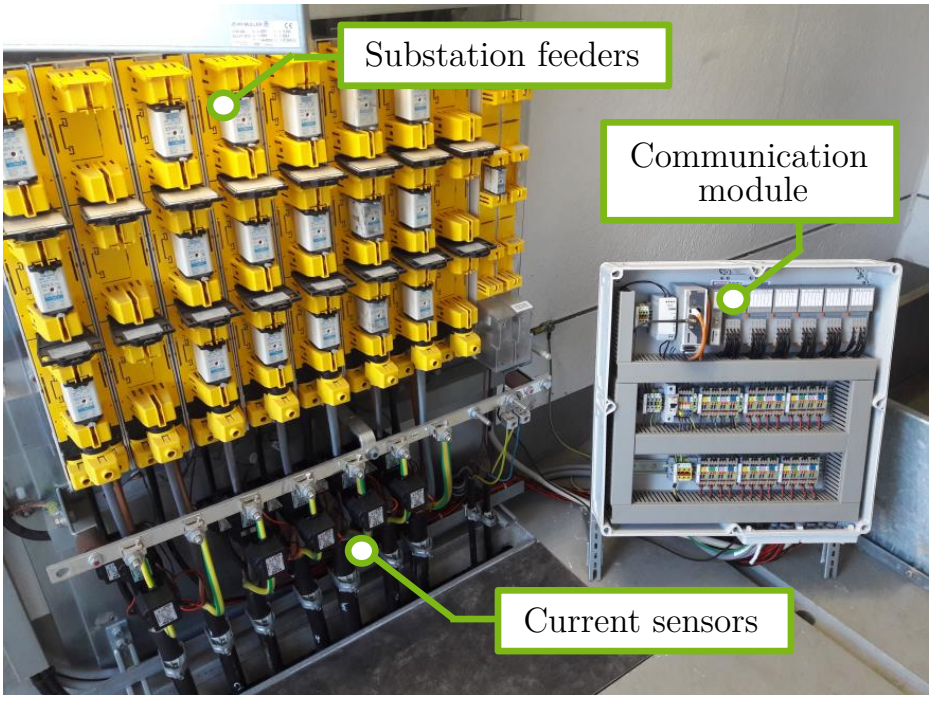

Fig. 6.18: Measurements and communication module installed at the secondary substation

state estimation outcomes either in real-time or for a specified time window. The latter, can be used to select and simulate specific and interesting grid scenarios recorded in the past. These data are collected into a local database and transferred to the RTS with a specified time-step. Fig. 6.19 shows power emulation outcomes from field measurements of the selected LV grid during a summer day. Particularly, field data acquired with 1 min time resolution are emulated within the laboratory test-network with a time-step of 1 s, thus speeding up the execution.

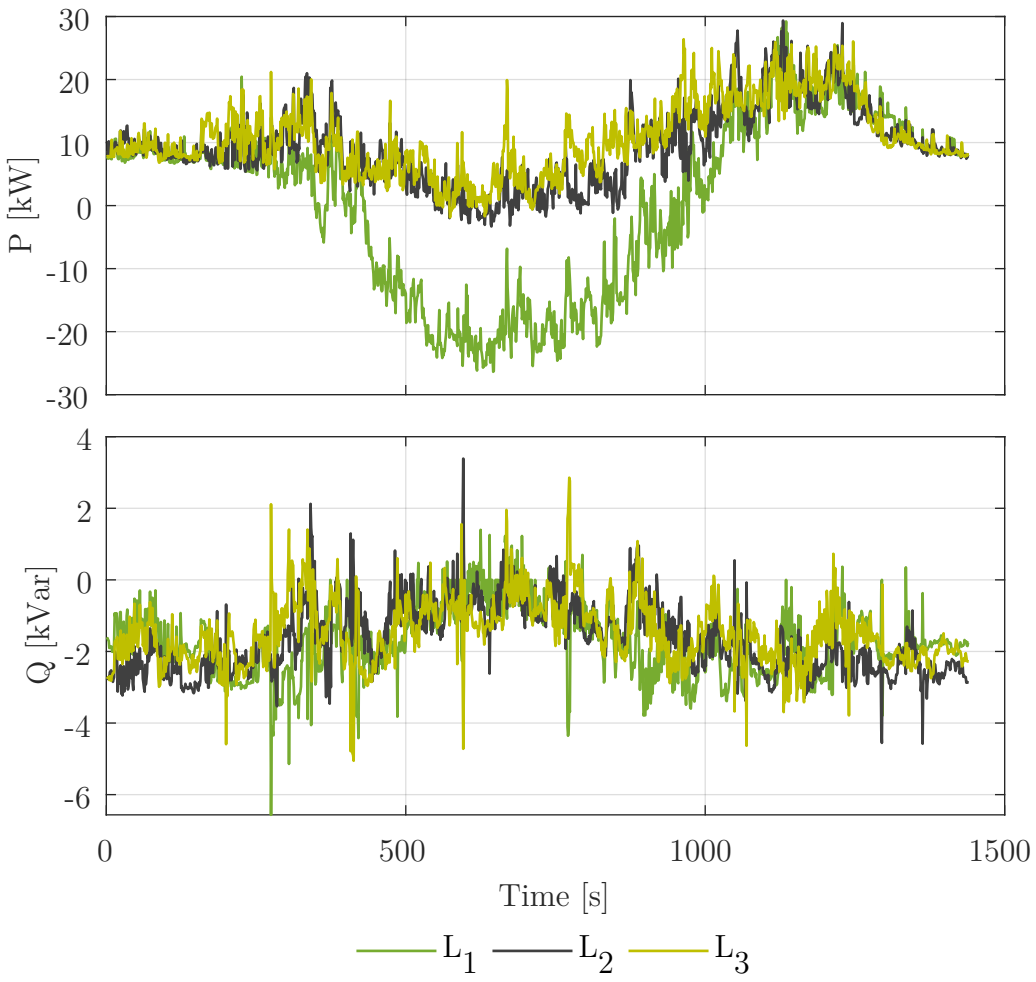

Fig. 6.19: Power profile emulation based on time-series from field measurements

6.4 Remarks

A number of basic setups are developed to prove the elemental test functionalities of the deployed PHIL system. First, the dynamic characteristics of the PA system are evaluated in terms of frequency-domain and time-domain response. As result of these tests, a dynamic model of the PA system is identified in line with the second order transfer function model found in the literature. Although this model provides an acceptable representation of the physical PA system, experimental tests show that the actual system response is described by a more complex model that should consider the actual operating conditions of the PAs. Later, conventional PHIL tests are performed by using a simplified setup in order to develop and assess the properties of the major IAs. The software interfaces of the ITM and DIM are successfully developed and tested. Particularly, the DIM is implemented for both fixed damping impedance and online estimated damping impedance. The latter provides an acceptable impedance estimation during real-time impedance variations of the HuT. However, the implemented algorithm is applicable for RL type HuT only. Enhanced accuracy is observed by applying the ITM. Therefore, the ITM is considered as primary IA within the rest of this work. For an effective application of the DIM additional improvements of the online impedance estimation algorithm are needed. However, the actual $\mathrm{DIM}_{\mathrm{online}}$ can also be applied for fast development of "proof of concept" setups of for those applications that do not require high level accuracy.

Further tests are performed to prove PHIL capability to emulate typical power system disturbances. In this case, the PHIL system is open-loop operated to reproduce reference signals modelled within the RTS into the physical laboratory test environment. A number of test functions are selected and tested in line with the PHIL capability. In contrast to conventional signal generators, the use of a RTS provides more practical benefits in terms of flexible and straightforward signal editing. On the other hand, the limited time-step of the RTS confines signals generation to lower

bandwidth ones compared to conventional signal generators. However, the overall system is able to emulate major grid disturbances as expected and in accordance with its design specifications. Major constraints are detected for overvoltage emulation due to the limited DC-link voltage. However, automatic third harmonics injection is effectively implemented to overcome this limitation.

Finally, a setup for the emulation of power profiles is implemented. This consists of a closed-loop setup where the active and reactive power setpoints are converted to instantaneous currents using a PLL algorithm and provided as references to the PA system. Additional software interfaces based on the API of the RTS are implemented to dynamically update power setpoints during real-time simulation, thus enabling scenarios emulation based on time-series. This setup is successfully applied to emulate power profiles based on field measurements and grid state estimation from a local LV grid. In addition to the time-series emulation function, the implemented software interfaces are also extended to facilitate the interactions with external tools involved within the setup. As further improvements, interpolation functions can be applied in case of time-series data with large time resolution. In fact, many sources of data are often based on 5 min or 15 min time resolution. However, the PHIL system emulates power profiles in real-time. For a more realistic power emulation, interpolation functions can be implemented to avoid wide constant power intervals during time-series emulation.

Chapter 7

PHIL setups for practical applications

This chapter provides a number of collected experiences based on the use of the deployed PHIL system for practical research needs in the area of smart grids. These representative test-cases are considered as exemplary applications to evaluate test capability and challenges in case of practical implementations. First, some of the operational use-cases for PHIL defined within this work are applied for testing hardware devices at component-level. Lastly, a test-case including multiple physical components is implemented as representative setup for system-level testing.

7.1 Testbed for PV-systems emulation

Emulation of PV-systems is one of the most common applications of PHIL. The behavior of a PV-system can be modelled within the RTS while its power output is emulated by PAs. In contrast to physical systems, PV emulations allows for a more flexible test execution as the desired operating conditions can be reproduced in a controlled manner, thus avoiding dependencies of actual weather conditions. Furthermore, the possibility to interface physical PV-inverters enables to test special functionalities such as voltage or frequency support under close to real-world conditions.

7.1.1 Description of the setup

The overall testbed consists of a PHIL setup where a group of PAs is used to emulate the DC output of a simulated PV system implemented within the available RTS. Then, the PAs is interfaced with a physical inverter to complete the overall testbed. The inverter design must be compatible with the electrical characteristics of the PA system. Therefore, the correct design should consider inverter's operating ranges below the voltage and current limits of the looped PA system. A commercial 60 kVA PV-inverter by SMA is selected and integrated as part of the overall testbed. The inverter is also equipped with a communication module based on Modbus TCP, thus favoring its integration within the laboratory ICT infrastructure.

The PV-system model is based on Matlab/Simulink and is implemented within the RTS[1]. A block diagram of the simulated model is shown in Fig. 7.1. It takes technical parameters such as number of series/parallel connected cells/modules and solar cell technology as offline inputs in order to design the required PV-system. Weather data such as solar irradiance (E) and local temperature (T) are used as online inputs during the simulation. These can be set either as constant values or time-series according to the

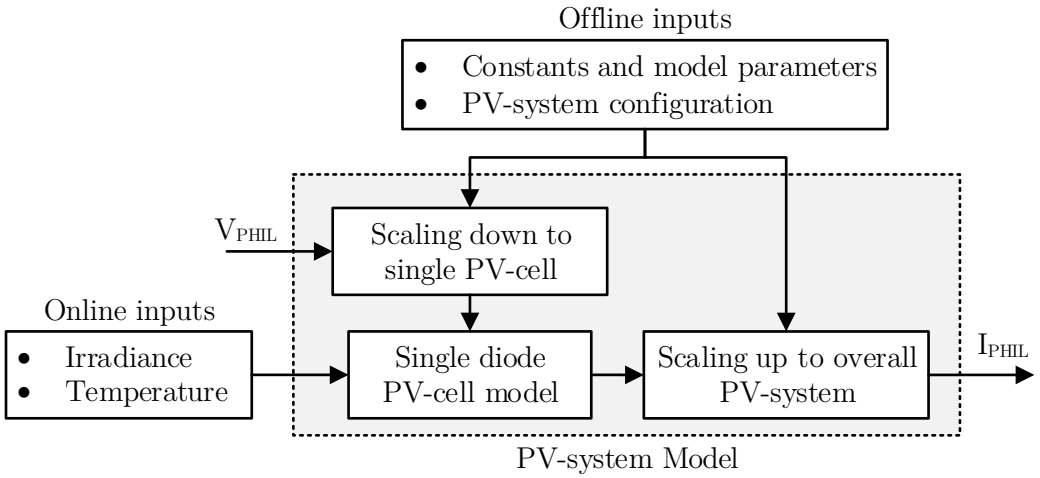

Fig. 7.1: Block diagram of the implemented PV-system model

[1]Model developed as a part of a supervised student's thesis: J. Spinneken, "Modellierung eines Photovoltaikmoduls auf einem Echtzeitsimulator für netztechnische Untersuchungen von PV-Anlage mittels PHIL Verfahren", Bachelor thesis, July 2018.

test purpose. The elemental behaviour of the PV-system is based on the single diode PV-cell model. A detailed description of this model and its parameters is given in the Appendix. The resulting DC output current (I_{PHIL}) provides the reference signal for the PA that is operated in DC Bipolar mode. The measured DC voltage at the PA's terminals is fed back to the model for the correct simulation of the IV characteristics of the PV-cell model.

According to the needs of the test, the implemented testbed can be operate in two different operation modes: Lab-connected mode and Full PHIL mode, as depicted in Fig. 7.2a and Fig. 7.2b, respectively. Within the

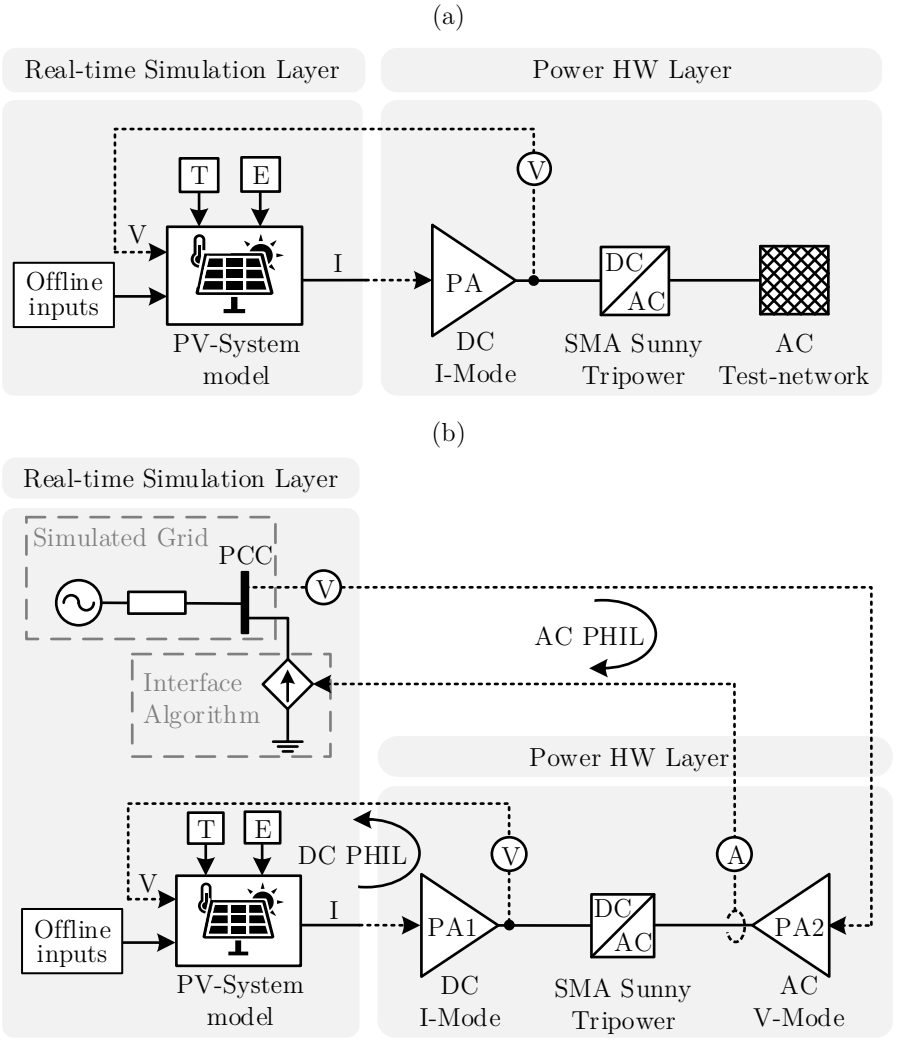

Fig. 7.2: Setup configuration for the PV-systems emulation testbed – (a) Lab-connected mode, (b) Full PHIL mode

Lab-connected mode, the PV-testbed is used for running tests on the laboratory test network. In this operation mode, the PV-system is the only simulated part. The AC-side of the inverter connects the overall system to the rest of the laboratory test network. Optionally, the physical inverter can also be excluded from the setup. In that case, the PV-system model includes an inverter model that provides the AC current references to the PA which is operated as three-phase current source. However, a configuration which includes the hardware inverter is preferred to provide more realistic outcomes. The full PHIL mode is used to execute network simulations in which a detailed behavior of PV-systems is required. In this case, the grid model as well as the PV-system model are implemented within the same simulation and executed in parallel. In contrast to the previous configuration, a second group of PAs (PA 2) is required to implement the AC PHIL. The voltage measurement at the PCC is used as a setpoint for PA 2 while the current output from the AC-side of the inverter is reproduced into the simulated grid by the IA.

7.1.2 Test-cases and results

A number of tests are performed in order to prove the effectiveness of the implemented testbed. First, steady-state operations are tested for constant values of irradiance and temperature. Later, exemplary irradiance profiles are used to prove testbed capability for PV-system emulation based on time-series. All these tests are performed operating the testbed in the Lab-connected mode (see Fig. 7.2a) where the AC-side of the PV-inverter is connected to the laboratory secondary substation.

Steady-state tests

Preliminary tests are performed in order to assess the steady-state performances of the designed testbed. Particularly, the measurements of the Maximum Power Point (MPP) obtained with the hardware inverter are compared with the outcomes of the simulated model. A number of tests

are performed for different values of irradiance and temperature, as shown in Fig. 7.3. As a major outcome, the operation of the internal Maximum Power Point Tracking (MPPT) algorithm of the hardware inverter is able to follow the theoretical MPP of the simulated model with acceptable accuracy. Therefore, the physical inverter behaves as it is connected to a physical PV-system. This confirms the correct implementation of the PV-system emulation via PHIL.

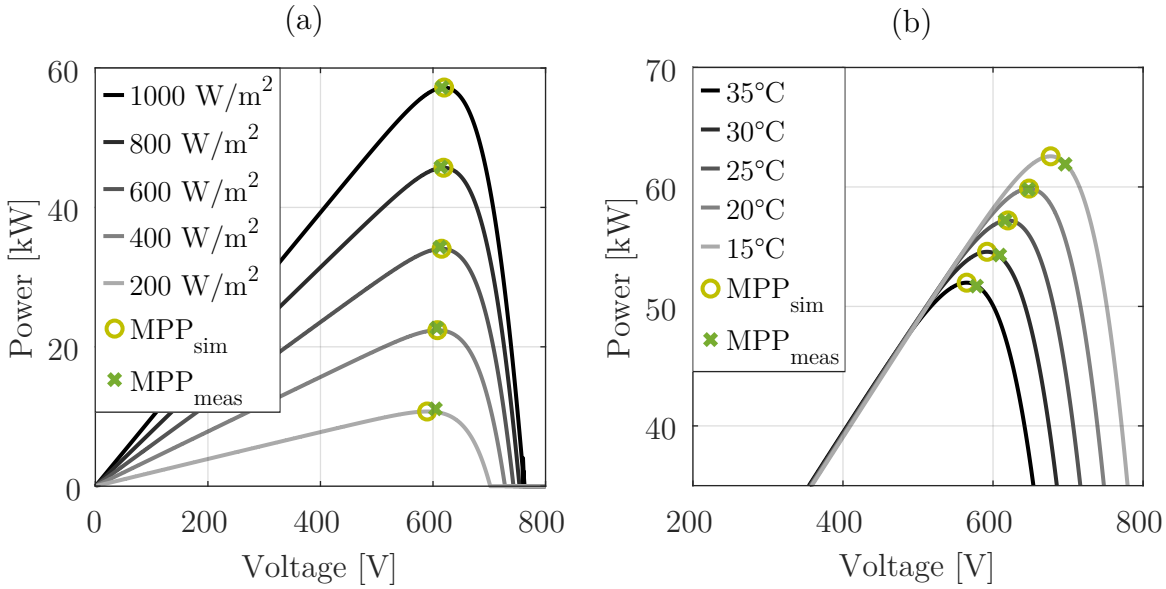

Fig. 7.3: Comparison between the theoretical MPP of the simulated model and the MPP measured – (a) P(V) for variable irradiance at 25°C, (b) P(V) for variable temperature at 1000 W/m^2

Time-series tests

Further tests are carried out to prove the testbed capability to perform PV-systems emulation based on time-series. Two different time-series data sources of irradiance are calculated from the power measurements of a real-world PV-system installed close to Dortmund City and used as reference. Both profiles are based on daily measurements with a resolution of 15 min. To speed up tests execution, the irradiance profiles are scaled within a time range of 11 min. Fig. 7.4 shows the test results for a sunny day with sporadic large irradiance gradients. The simulation starts with the initialisation of the PHIL simulation where the real-time model of the PV-system is first

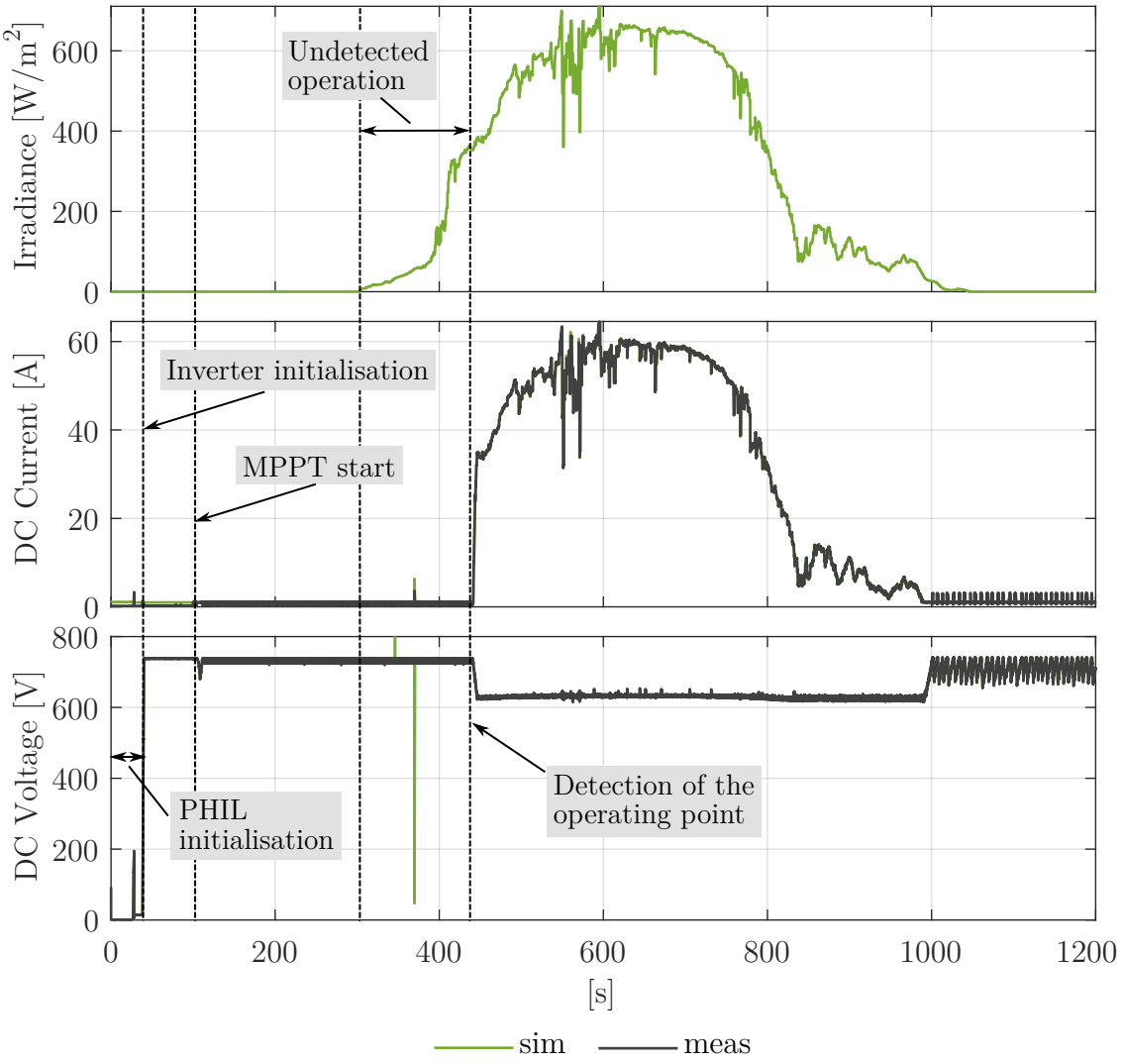

Fig. 7.4: Time-series PV-system emulation – simulation scenario with low irradiance gradients

executed in open-loop in order to check the effectiveness of the reference currents to be sent to the PA. Later, the breakers of the PA are closed thereby supplying the DC side of the PV-inverter. The inverter starts its initialization process where all the required parameters are checked before enabling the feed-in operation. Later, the MPPT algorithm starts varying the DC voltage of the PA, thus searching the MPP. The simulation starts with initial irradiance equal to zero. Therefore, no current flow is provided as expected. However, during the initial increase of irradiance the MPPT is not able to detect the potential power feed-in from the simulated model. It is not able to adapt the DC voltage to allow the current flow from the

simulated model according to its IV curve. Only at about 420 s of the simulation the MPPT controls the DC voltage properly and the current flow starts accordingly. As a major outcome, the testbed is able to operate according to the simulated irradiance profile excepted for the observed time interval in which it is not able to detect model operations.

A similar test is repeated with a different irradiance profile that includes recurrent and large irradiance gradients, as shown in Fig. 7.5. Also within this test scenario the unexpected MPPT operation interferes with the simulation, thus neglecting part of the simulated behavior. Particularly, undetected operations can be observed within both the initial part and

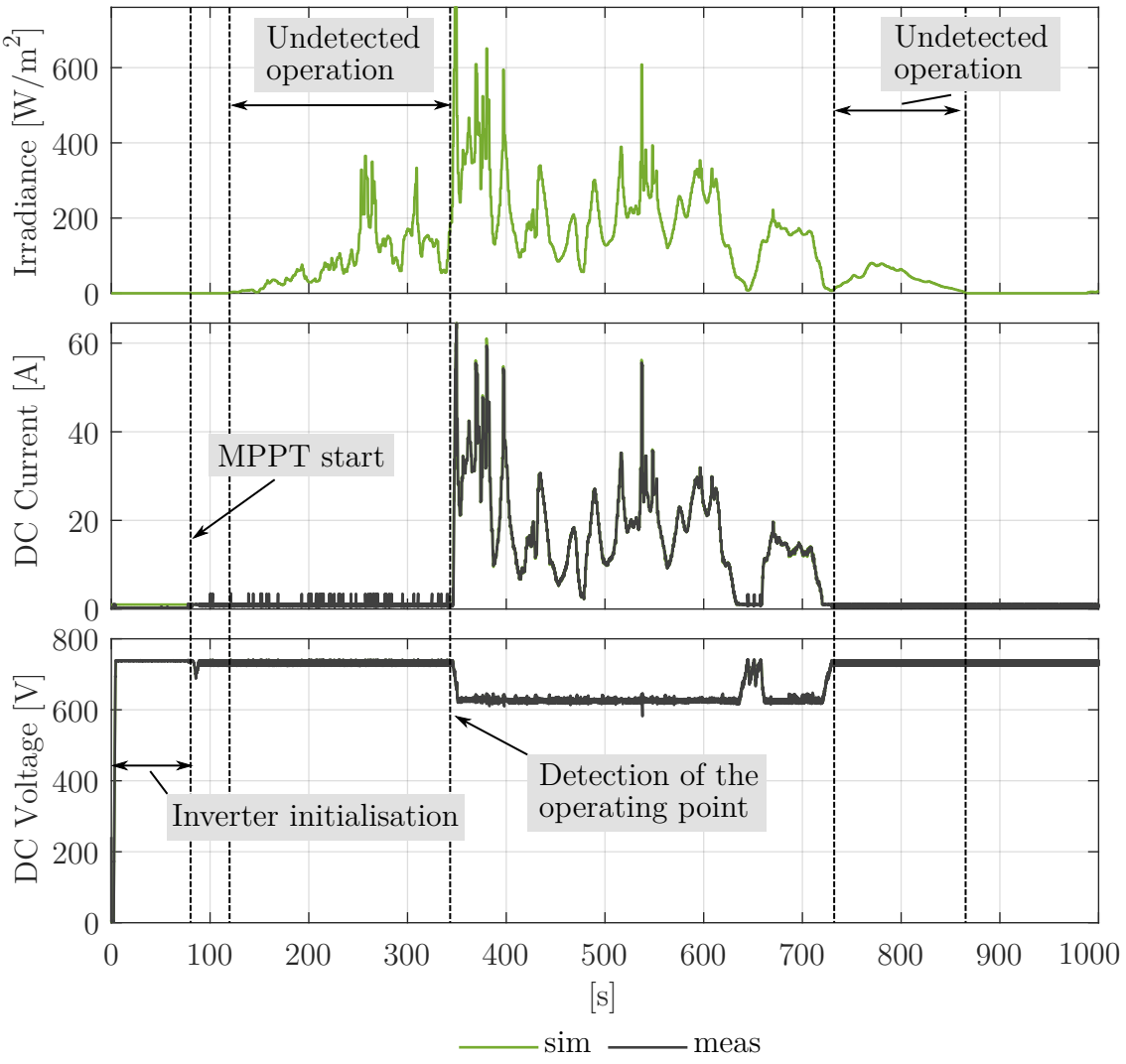

Fig. 7.5: Time-series PV-system emulation – simulation scenario with high irradiance gradients

the final part of the simulation. It is observed that this behavior most frequently occurs when the reference irradiance is close to zero. However, after the detection of the operating point the PV-testbed is able to follow the irradiance input even in case of fast dynamics.

A possible cause of this improper behavior can be due to the fast irradiance variations. In fact, in both previous tests the daily irradiance profiles are scaled within a time range of 11 min, thus providing fast changes in irradiance compared to the real-world case. The higher dynamic of the input irradiance might be in contrast with the more slower dynamic of the MPPT. Therefore, a further test is performed considering slower irradiance variations. Tests results are shown in 7.6. The irradiance profile is voluntary kept higher than zero to exclude further abnormal behaviors. Results show partial improvements as the testbed operates according to the entire iradiance profile. However, undesired voltage and current oscillations due to MPPT operations still occur. Additional LPFs can be implemented within the RTS to smooth the voltage oscillations at the input of the PV-system model. Consequently, lower oscillations of the reference DC current

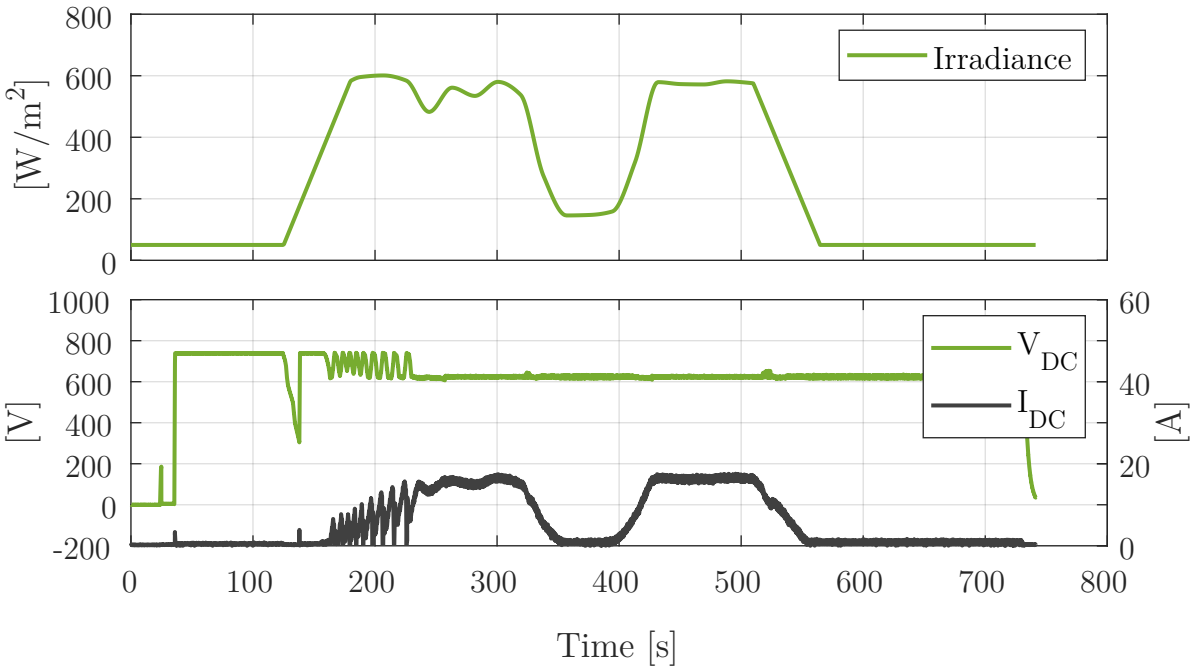

Fig. 7.6: Time-series PV-system emulation – simulation scenario whit slower irradiance variation

can be expected. However, the additional delay introduced by LPFs might lead to possible disturbances of the MPPT operation. Therefore, further investigations are required to properly assess this behavior.

7.1.3 Remarks

A PHIL setup is implemented to perform PV-system emulation including physical PV-inverters. The overall testbed can be operated either for full hardware tests (Lab-connected mode) or for conventional PHIL simulations (Full PHIL mode) according to the specific test purpose. PV-system model parameters can be adjusted to configure a desired PV-system. However, it must be ensured that electrical parameters are set in compliance with the electrical characteristics of the PAs. Simulation inputs are given in the form of temperature and irradiance. These can be provided as stationary values or profiles based on time-series.

Results show that the implemented testbed behaves as expected under stationary irradiance and temperature inputs. However, results of time-series tests show unexpected behaviors due to the operation of MPPT of the hardware inverter. Further tests performed considering irradiance profiles executed within a realistic time range show outcomes improvement. However, high voltage and current oscillations due to the MPPT operation are still detected. Also additional simulation tests performed with similar irradiance profiles but replacing the hardware inverter with a simulated model exclude erroneous behaviors of the simulated PV-system. Therefore, the observed undetected operation should be investigated within the MPPT of the hardware inverter. However, component manufacturers often do not allow access to specific information such as detailed device operation settings. This makes such investigations more challenging. Further tests are also planned with physical inverters from different manufacturers to verify similarities or improvements with respect to the results obtained with the actual hardware setup.

7.2 Testbed for Distributed Series Reactors

A PHIL setup is designed for laboratory testing of physical Distributed Series Reactors (DSRs). This is a particular application in that these devices are typically applied to High-Voltage (HV) transmission systems while the test facility is designed for LV grid applications. Therefore, this setup demonstrates how flexible can the PHIL system be operated to meet such atypical test requirements. Moreover, as DSRs are series-connected components, special design concerns are assessed, thus providing an exemplary application of the solutions suggested in Section 4.5.

A DSR is mounted directly onto a conductor of a power line and injects additional series reactance upon activation [143]. It behaves similarly to a single-turn transformer with the conductor as the primary winding, as shown in Fig. 7.7. While a single DSR can only inject 10-40 mΩ, the combined additional reactance of multiple devices installed in series enables functionalities such as current limiting and shifting power flows into parallel lines. PHIL simulations allow testing of DSRs in settings that are closer to reality than pure software simulations but at lower costs than field installations.

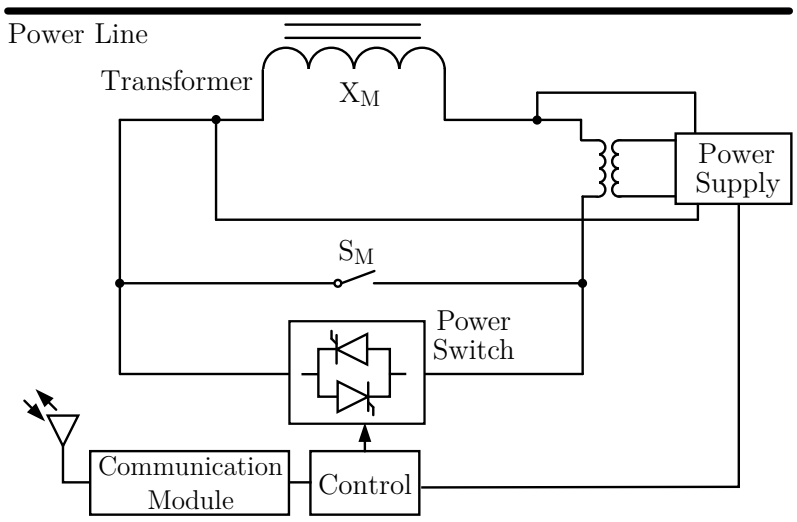

Fig. 7.7: Schematic of a Distributed Series Reactor [143]

The proposed PHIL testbed is applied for testing full-scale DSRs and it is designed to satisfy the following elemental requirements:

- Emulation of realistic current ratings
- Suitable tests capability even with limited number of DSRs
- Multiple device configurations

To meet the stated requirements, the design of the overall PHIL setup considers two main aspects. On the one hand, scaling solutions are implemented from the hardware side to meet the usual rating for the DSRs. On the other hand, a suitable IA is considered to couple the DSRs with the simulated network. The selected IA has a relevant impact not only within the simulation but also for the hardware setup, thus determining the configuration needed for the PAs. Finally, the developed configuration cabinets are used to connect the power terminals of the DSRs with the PAs. This allows for a more flexible implementation of the required setup configurations.

7.2.1 Description of the setup

The HuT consists of three DSR modules of the type PowerLine Guardian SD4-700 by Smart Wires Inc. [144]. These devices are usually used in medium to high voltage (10-400 kV) networks. The DSRs reach nominal operation at 300 A and are rated up to 700 A. A laboratory–scale emulation of a transmission system power line is implemented in order to host the DSRs under test, as shown in Fig. 7.8. The power line consists of three short segments of overhead conductors of the type Al/St 265/35, which is commonly found in German 110 kV networks.

The overall setup is virtually connected to a simulated model of a 110 kV network running into the RTS. The simulation provides the voltage/current reference to the PA that supply the overall HuT. However, the PAs are designed for current and voltage ratings typical for LV applications. Therefore, the reference signals are scaled to meet the voltage/current ratings

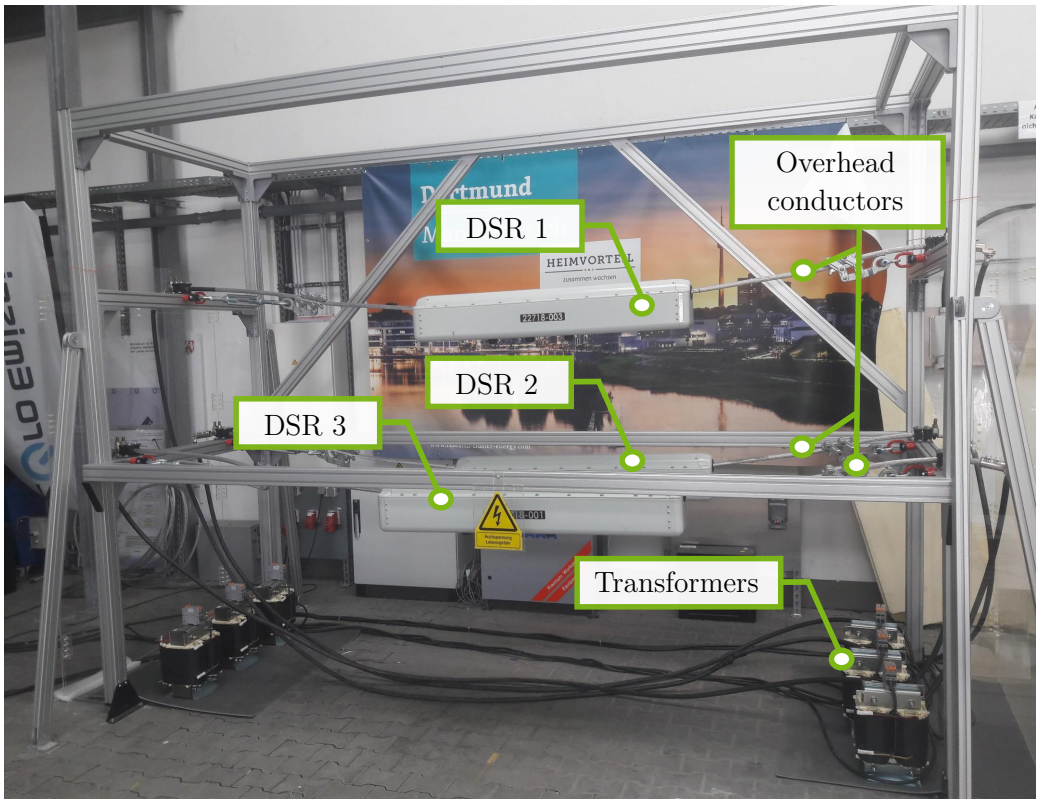

Fig. 7.8: Laboratory–scale emulation of a transmission system power line with three overhead conductors equipped with PowerLine Guardian DSRs [2]

of the PAs. To overcome this limitation a power transformer is included to step the output current from the PAs up to the rating current of the HuT. Consequently, the output voltage from the PAs will be scaled down to unusual operating points for the HuT. However, the DSRs functionality is not influenced by the voltage because the devices are on the same electrical potential as the conductor they are installed on; they only react to the current through the conductor. The low voltage also facilitates the hardware setup due to low insulation requirements. This is especially useful for the structure holding the conductors and DSRs. The conductors are at different electrical potentials while the aluminum structure is at ground potential. Insulation is achieved through simple support insulators, with ratings below 1 kV and air gaps of a few centimeters.

[2]The realisation of the depicted setup was carried out by others in the course of the project IDEAL (FKZ: 03ET7557A) funded by the *German Federal Ministry for Economic Affairs and Energy (BMWi)*. The PHIL interfacing issues of the overall testbed are analyzed and assessed as a part of this thesis.

Proposed PHIL Architecture

As mentioned in the previous section, the main requirement for testing the DSRs is to operate the PHIL setup with similar current magnitudes of the simulated 110 kV network. This requirement together with the usual requirements for a PHIL simulation (stability and accuracy) determines the proper IA to be implemented. Fig. 7.9 shows two main design options that are considered for the implemented setup with respect to the operational use-cases UC7 (see Section 4.5). Particularly, Fig. 7.9a shows the implementation of the voltage type ITM. The DSR is simulated by

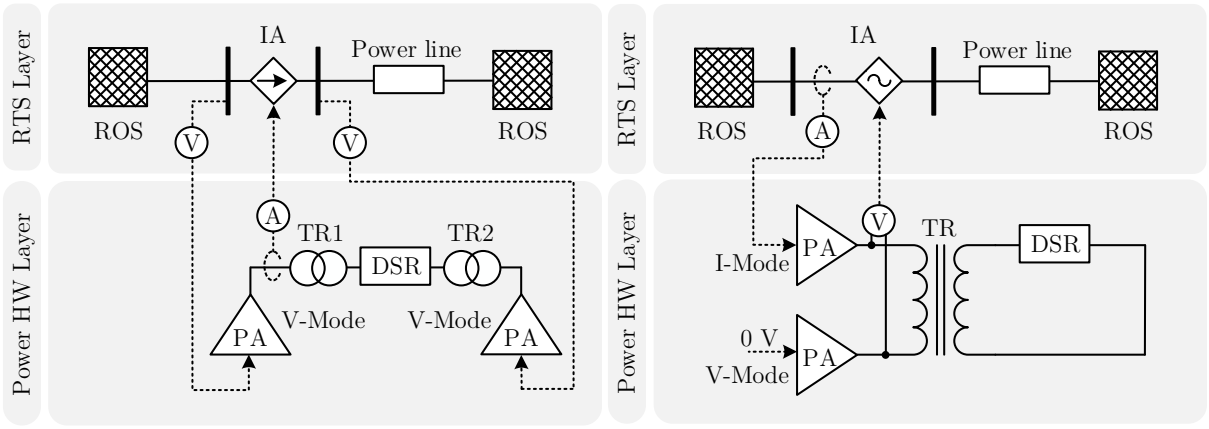

(a) Voltage type ITM **(b)** Current type ITM

Fig. 7.9: PHIL setup configuration options

a controlled current source that takes the current measurement from the DSR as setpoint. The configuration requires two PA groups along with two power transformer groups that emulate the input and output voltage at the connection points. The difference in magnitude and angle between the input and output voltage of the PAs results in current flow. Once the DSR turns on, the current is reduced and sent back to the simulated network thereby closing the loop. The current flowing through the DSR only depends on the voltage difference at the connection points. However, because of the limited ratings of the PAs the magnitude of the voltage references is scaled down to the maximum voltage of the PAs. This scaling affects the resulting current magnitude that would not match the current otherwise flowing within the simulated network. The voltage setpoints could

be further manipulated in order to get the required current magnitude. However, possible manipulations of voltage magnitude and angle should be dynamically applied at each operating point, thus leading to a complex control algorithm. This setup also foresees the PAs to be operated as parallel connected voltage sources. This operating mode makes it likely to experience current oscillations even due to small errors in the PA output voltage. Lastly, considering the stability condition for the voltage type ITM, further improvements to ensure system stability are required [106]. In fact, the equivalent impedance of the simulated network is expected to be higher than the impedance of the DSR. The simplified DIM could be considered as a viable alternative to improve system stability without redesigning the setup [104].

In light of the aforementioned considerations, an alternative setup configuration based on the current type ITM is designed (Fig. 7.9b). In contrast to the previous configuration option, only one transformer per phase is needed. The DSR is connected on the secondary side of the transformer in a closed circuit. The current from the simulation is emulated by operating a PA as a current source (I-Mode). A second PA operates as a voltage source (V-Mode), thus emulating the neutral potential. The current flowing through the simulated power line is scaled down according to the hardware transformer ratio and sent as a setpoint to the PA. This feeds the current to the DSR through the transformer that scales the current up according to its ratio. The voltage measured at the connection point is sent back as reference to the voltage source block that simulates the DSR within the model. With the current type ITM the stability condition is satisfied when the equivalent impedance of the simulated network is greater than the impedance of the DSR. This stability condition fits with the expected range of the simulated network impedance and the DSR impedance.

Stability analysis

The stability of the ITM strongly depends on the ratio between the equivalent impedance of the simulated network (Z_{SW}) and the equivalent impedance of the hardware part (Z_{HW}) [104]. The latter, includes not only the impedance of the HuT but also the inevitable contribution of the hardware parts involved within the setup. Fig. 7.10 shows the equivalent circuit of the hardware parts.

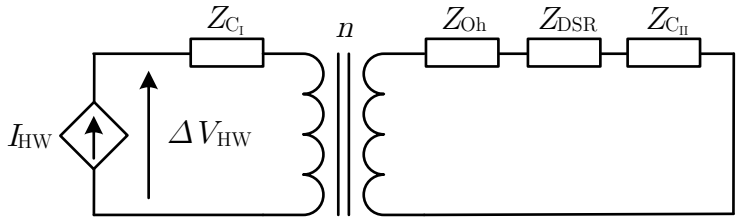

Fig. 7.10: Equivalent circuit of the hardware parts

The total impedance of the hardware implementation seen at the connection point of the PA is obtained as follows:

$$Z_{\mathrm{HW}} = Z_{\mathrm{C_I}} + n^2(Z_{\mathrm{DSR}} + Z_{\mathrm{Oh}} + Z_{\mathrm{C_{II}}} + Z_{\mathrm{T}}) \tag{7.1}$$

where:
$Z_{\mathrm{C_I}}$: Cable impedance of the primary side connection
$Z_{\mathrm{C_{II}}}$: Cable impedance of the secondary side connection
Z_{Oh}: Impedance of the of the overhead conductor
Z_{T}: Impedance of the transformer
Z_{DSR}: Impedance of the DSR
n: Transformer ratio

The total impedance contribution due to the setup can be expressed as follows:

$$Z_{\mathrm{Setup}} = Z_{\mathrm{C_I}} + n^2\,(Z_{\mathrm{Oh}} + Z_{\mathrm{C_{II}}} + Z_{\mathrm{T}}) \tag{7.2}$$

so that the total impedance of the hardware implementation is:

$$Z_{\mathrm{HW}} = Z_{\mathrm{Setup}} + n^2 Z_{\mathrm{DSR}} \tag{7.3}$$

When the DSRs are not in the injecting mode $Z_{\mathrm{DSR}} \approx 0\,\Omega$ but still a small voltage is injected into the simulation due to the contribution of Z_{Setup}. However, this inaccuracy can be compensated within the simulation as follows. Figure 7.11 shows the block diagram in the Laplace domain of the overall PHIL setup. The diagram also includes the delay due to the discrete simulation with time step T_{s} along with the transfer function of the PA and the transfer function of the measurement system, $G_{\mathrm{PA}}(s)$ and $G_{\mathrm{Meas}}(s)$ respectively. On the upper part of the diagram the setup impedance compensation algorithm is depicted. The algorithm takes as inputs both the current and the voltage measurements from the hardware to estimate the equivalent impedance. During the initialisation of the PHIL simulation, the DSRs do not inject any voltage so that $Z_{\mathrm{DSR}}(s) \approx 0$. In this condition, the voltage measured corresponds to $\Delta V_{\mathrm{Setup}}(s)$ and $Z_{\mathrm{Est}}(s) = Z_{\mathrm{Setup}}(s)$. The compensation voltage $\Delta V_{\mathrm{Comp}}(s)$ is obtained by multiplying $Z_{\mathrm{Est}}(s)$ with I_{SW}. By adding $\Delta V_{\mathrm{Comp}}(s)$ in the loop the aforementioned voltage injection caused by Z_{Setup} is effectively compensated. The estimation of Z_{Setup} is also the suitable method to properly quantify the impedance of the

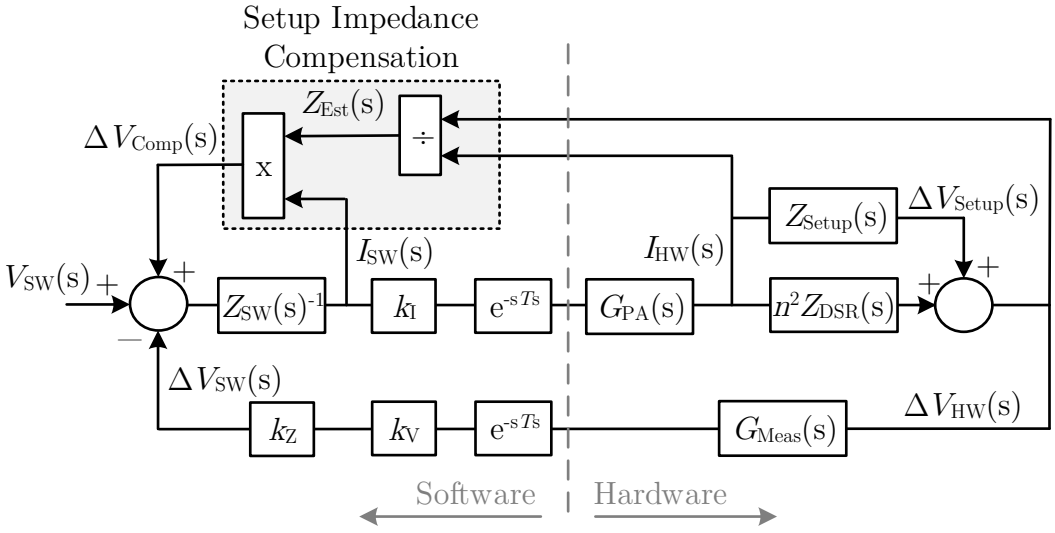

Fig. 7.11: Block diagram of the PHIL setup

looped components in case of lack of data. Furthermore, by comparing Z_{Est} with Z_{SW} it is possible to evaluate the stability of the system online.

With the setup impedance compensated, the overall system stability can be evaluated. In case of ideal interface ($G_{\mathrm{PA}}(s) = 1$ and $G_{\mathrm{Meas}}(s) = 1$) the stability condition for the open loop transfer function is expressed as follows:

$$G_{\mathrm{OL}}(s)^{*} = k_Z k_I k_V \frac{Z_{\mathrm{HW}}(s)}{Z_{\mathrm{SW}}(s)} e^{-s2T_{\mathrm{s}}} = \frac{Z_{\mathrm{HWeq}}(s)}{Z_{\mathrm{SW}}(s)} e^{-s2T_{\mathrm{s}}} \tag{7.4}$$

According to the Nyquist criterion, the resulting stability condition is given by:

$$\frac{Z_{\mathrm{HWeq}}(s)}{Z_{\mathrm{SW}}(s)} < 1 \tag{7.5}$$

The current factor k_{I} and the voltage factor k_{V} are set according to the transformer ratio n with the relation $k_{\mathrm{V}} = k_{\mathrm{I}}{}^{-1} = n$. In this condition these scaling factors do not affect the system stability and the current flowing through the DSRs corresponds to the current of the simulated power line. The impedance scaling factor k_{Z} can be arbitrarily set to manipulate the DSR impedance within the simulated network. If $k_{\mathrm{Z}} = 1$, the equivalent hardware impedance seen within the simulation ($Z_{\mathrm{HW_{eq}}}$) is equal to $n^2 Z_{\mathrm{DSR}}$ because of the transformer connection. The simulated network receives the contribution of n^2 series connected DSRs instead of a single one. Setting $k_{\mathrm{Z}} = n^{-2}$, the contribution of the transformer to the total impedance is neglected. However, k_{Z} impacts the system stability so that it must be limited according to (7.5). In the event that (7.5) is widely satisfied, the contribution of $G_{\mathrm{PA}}(s)$ and $G_{\mathrm{Meas}}(s)$ does not compromise the evaluated stability considering $G_{\mathrm{OL}}(s)^{*}$. However, if operating close to the stability limit or if additional elements such as filters are needed to improve the quality of the feedback signal, a more detailed stability analysis is required.

7.2.2 Test-cases and results

The simulated network is a simplified 5-Bus system based on an existing 110 kV network implemented into a MATLAB Simulink model running on the OP5607 RTS with a time step of 50 μs. The generators are modelled as three-phase voltage sources while the loads are modelled as RL-parallel loads. The power lines are modelled as π–sections with typical parameters of the Al/St 265/35 conductor. According to Fig. 7.9b, the DSRs are modelled as controlled voltage sources that inject the voltage feedback from the hardware setup. Three main DSR configurations are considered, as shown in Fig. 7.12. Within Configuration I the DSRs operate as a three-phase system connected to a simulated three-phase power line. Additionally, the DSRs can be either operated as series connected on the same single-phase line (Configuration II) or on three different single-phase lines (Configuration

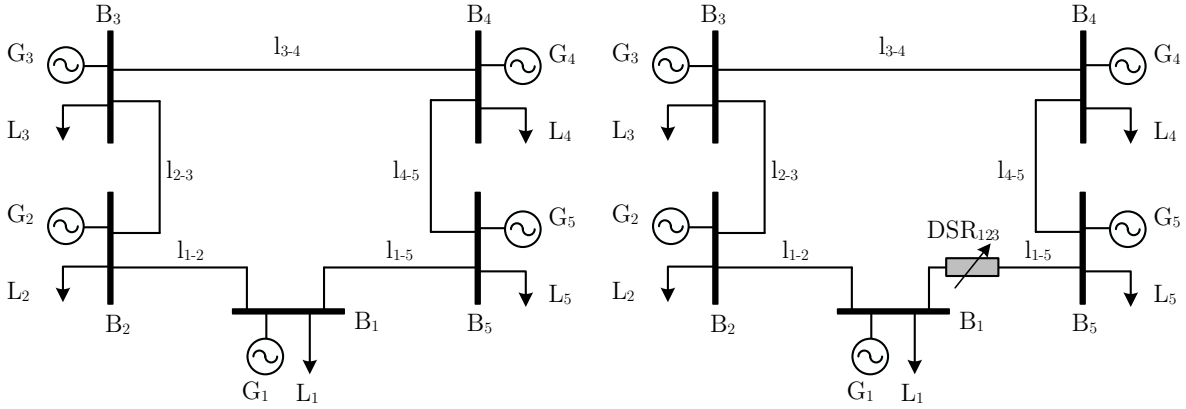

(a) Original test network

(b) DSRs – Configuration I

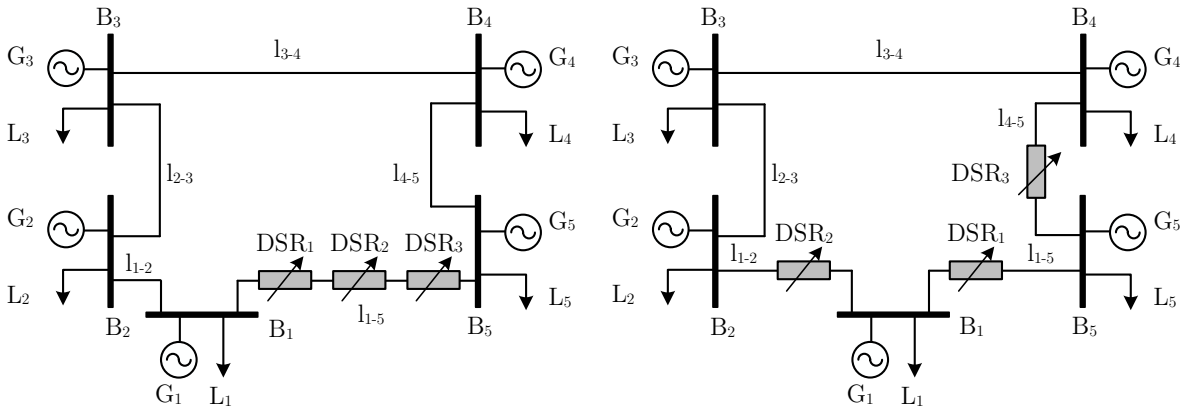

(c) DSRs – Configuration II

(d) DSRs – Configuration III

Fig. 7.12: Test network topology and selected DSR configurations

III). In both Configuration II and III, the DSRs operate on a single phase even if the simulated network is a three-phase system. However, based on the measurements of the phase where the DSR is connected, the injected voltage on the remaining two phases is generated within the simulation. The voltage and current measurements from the hardware setup refer to the PA measurement system that takes measurements from the primary side of the transformers, as shown in Fig. 7.9b.

Test results – Configuration I

The simulation results related to Configuration I with $k_Z = 1$ are shown in Fig. 7.13. The equivalent software impedance Z_{SW} at the connection point of the DSRs results 33 Ω while the expected Z_{HW} according to the data available of the hardware components is 0.4 Ω. Considering that each DSR injects a voltage that corresponds to a maximum impedance of 20 mΩ, the stability condition expressed in (7.5) is largely satisfied and the simulation results stable as expected. The simulation starts with the power line current of about 501 A that corresponds to reference current of about

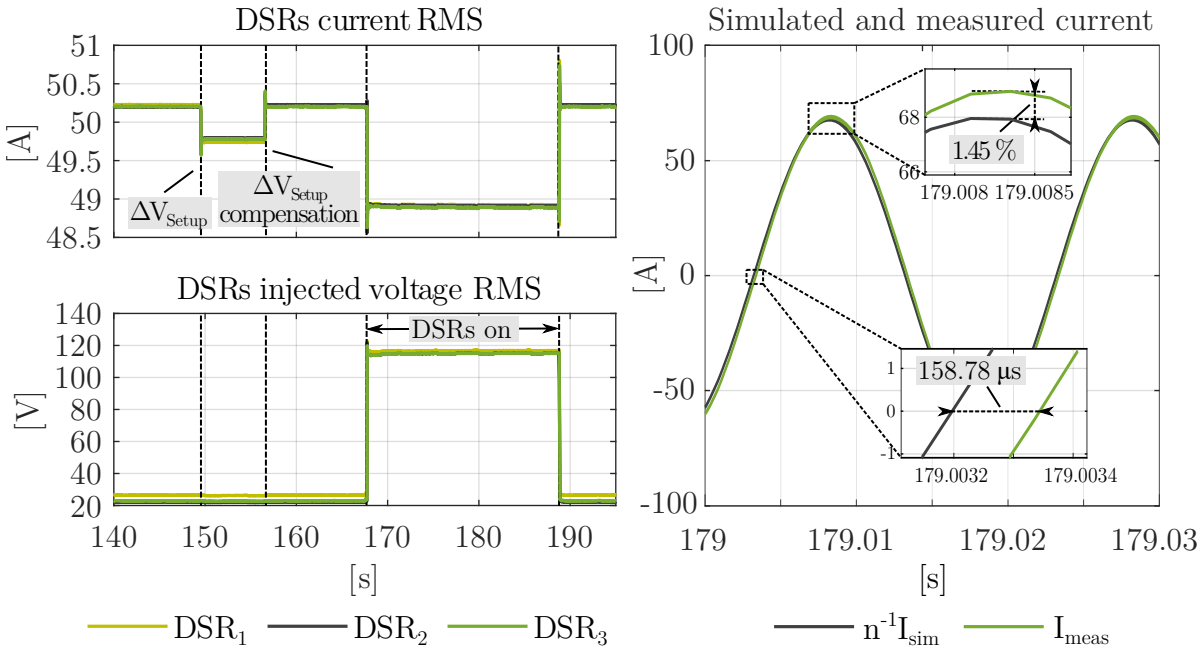

Fig. 7.13: PHIL test Configuration I – DSRs measurements at primary side of the transformer (left-hand); comparison between DSR current within the simulation and DSR current measurement (right-hand)

51 A for the PA, namely the nominal current of the transformer. At 149 s the voltage feedback from the hardware setup is enabled and the current decreases due to $\Delta V_{\mathrm{Setup}}$. At 156 s $\Delta V_{\mathrm{Setup}}$ is almost totally compensated through the impedance compensation algorithm and current returns to around 51 A. However, the measured injected voltage is not affected by the compensation. In fact, the compensation algorithm neglects the voltage drop due to Z_{Setup} within the simulation only. Between 168 s and 189 s, the DSRs are manually activated and inject an additional voltage of 92 V. Consequently, the current decreases by about 1.45 A that corresponds to 14.5 A within the simulation.

Fig. 7.13 (right-hand) shows the measured current of a DSR and the current of one phase of the simulated power line scaled according to the transformer ratio. The DSR current lags the simulation current of about 158.78 μs due to the delay chain of the PHIL simulation. The current amplitude of the DSR exceeds the amplitude of the simulated current, thus giving an error of about 1.45 %. This effect is attributable to an overcompensation of the setup impedance. However, this issue can be fixed by improving the compensation algorithm. A similar test with $k_{\mathrm{Z}} = n^{-2}$ would provide a current drop due to Z_{DSR} of about 0.145 A. Therefore, the contribution of a single DSR is too small to be considered as a meaningful test-case. In fact, real-world applications also consider the installation of multiple DSRs series connected to the same power line to reach the desired current reduction [145].

Test results – Configuration II

According to Fig. 7.12c, the DSRs are now series connected and operating on the same simulated power line. The contribution of Z_{Setup} is expected to be three times higher than the one estimated within Configuration I. This would lead to a higher initial voltage injection that, when summed to the contribution of the DSRs, would exceed the voltage rating of the PAs. This situation is tested with the nominal initial current of 51 A as

shown in Fig. 7.14. After initialising the simulation, the PHIL feedback voltage is enabled and the initial voltage injection due Z_{Setup} of about 100 V is reduces the current to 48.8 A. After the compensation, the current moves back to the initial value. Between 180 s and 290 s the three DSRs are step wise turned on and then off. From the second DSR turn on, the voltage exceeds the PA limit of 250 $\mathrm{V_{RMS}}$. The maximum voltage rise is obtained when all the three DSRs are turned on. In this condition, the PA limits the voltage amplitude, thereby providing almost a square output voltage. Consequently, because of the prevalent inductive nature of Z_{HW}, the current results in a triangle waveform. A reduction of k_{Z} within the simulation would even make the issue worse. In fact, k_{Z} would reduce the DSR impact on the simulated current. Therefore, due to the smaller current reduction the corresponding voltage injection on the hardware side would be larger. A possible solution to overcome this issue is to reduce the initial current, thus limiting the operating range for Configuration II. A current of 377 A is measured and selected as the maximum value that permits to operate all three DSRs within the sinusoidal mode. Considering that the DSRs act in

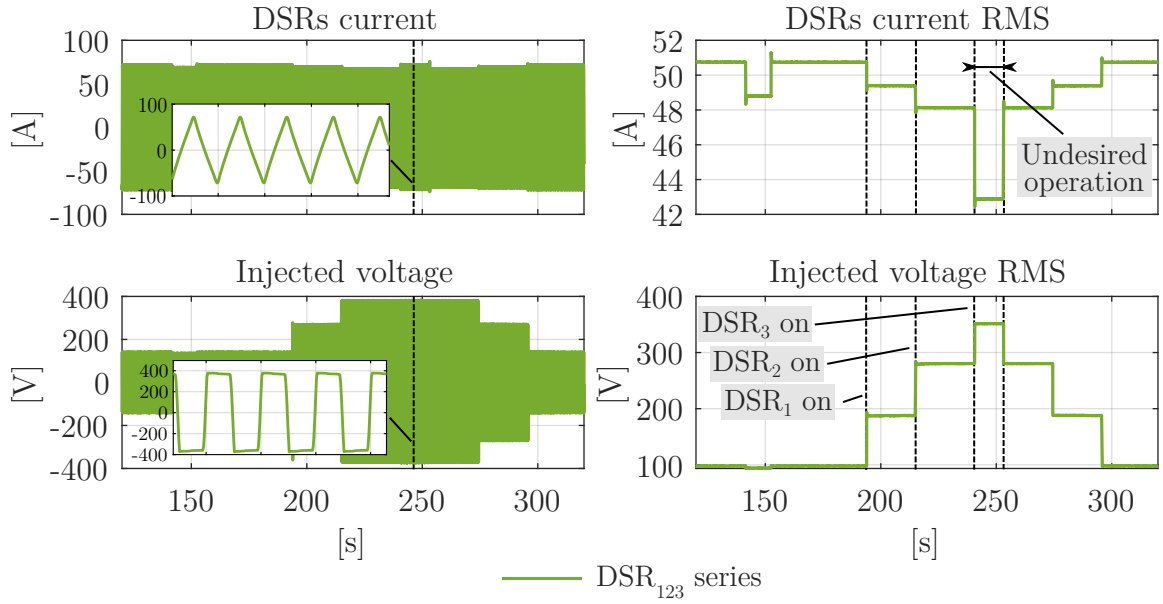

Fig. 7.14: PHIL test Configuration II – DSRs measurements at the primary side of the transformer: instantaneous waveforms (left-hand), RMS values (right-hand)

normal operation for currents higher than 300 A, limiting the current to 377 A is not altering the devices' performance.

Test results – Configuration III

Within Configuration III, each DSR is connected to the first phase of three different simulated power lines (see Fig. 7.12d). The test results are shown in Fig. 7.15. Also within this configuration mode, the PHIL setup is working as expected. Each DSR can be independently operated to reduce the current flow of individual simulated power lines with different current values. Because the DSRs belong to different power lines, the turn on of a single DSR perturbs the current flow on the other two according to the network admittance matrix. Referring to the diagram of the injected voltage on Fig. 7.15, it is possible to distinguish the operation of each DSR.

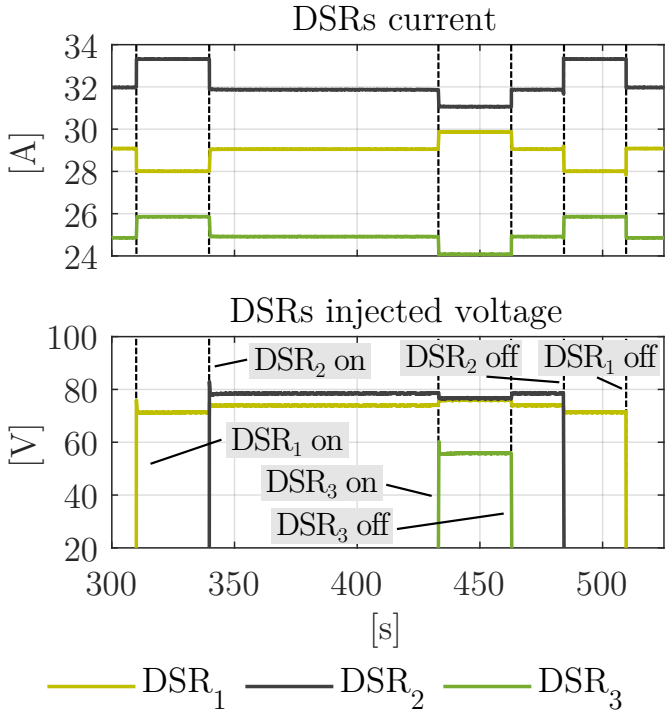

Fig. 7.15: PHIL test Configuration III

7.2.3 Remarks

A PHIL setup for testing commercial DSRs for power flow control in HV grids is successfully designed and implemented. This application confirms the capability of the deployed PHIL system to be operated in a flexible manner also for special needs. Three setup configurations are selected and practically implemented by using the developed configuration cabinets. This allows for a more straightforward restructure of the setup according to the configuration to be proven. The different configurations are used to operate the DSRs under diverse conditions within a simulated network. Results confirm the stability and the robustness of the setup in all the three configurations. The operating current must be limited in Configuration II due to the voltage limit of the PA. However, the resulting limited operating range does not compromise the DSRs performance. The setup impedance is compensated software-wise, thus isolating the contribution of the DSRs within the simulation. Results show that the compensation method can be further improved to prevent significant errors between the measured current and the current within the simulation.

In future works, the setup will be used to test the operation of the DSRs under specific network contingencies. Furthermore, a controller hardware-in-the-loop simulation will be combined with the implemented PHIL setup to validate innovative control algorithms for the DSRs. The final setup will also include a commercial supervisory control and data acquisition interfaced between the simulated network and the hardware DSRs.

7.3 Testbed for decentralized frequency control with DER

A PHIL setup is implemented to evaluate the PHIL system capability to emulate suitable laboratory scenarios for testing and validation of frequency control strategies with DER. Particularly, the PHIL system is used as a type I component to emulate power system events leading to frequency deviations. In contrast to the frequency slope emulator described in Section 6.2, this application requires a closed-loop network simulation. The existing Redox flow BESS at SGTL is used as a type II component and controlled to contribute to the primary frequency control. This application is inspired by a similar work carried out in [146] where experimental tests on decentralized frequency control are performed on a smaller scale Li-ion BESS.

7.3.1 Description of the setup

A simplified schematics of the designed PHIL setup is depicted in Fig. 7.16. A single area network model is implemented within the RTS to simulate the overall power system frequency response together with the primary frequency control from conventional power plants. The model of the power

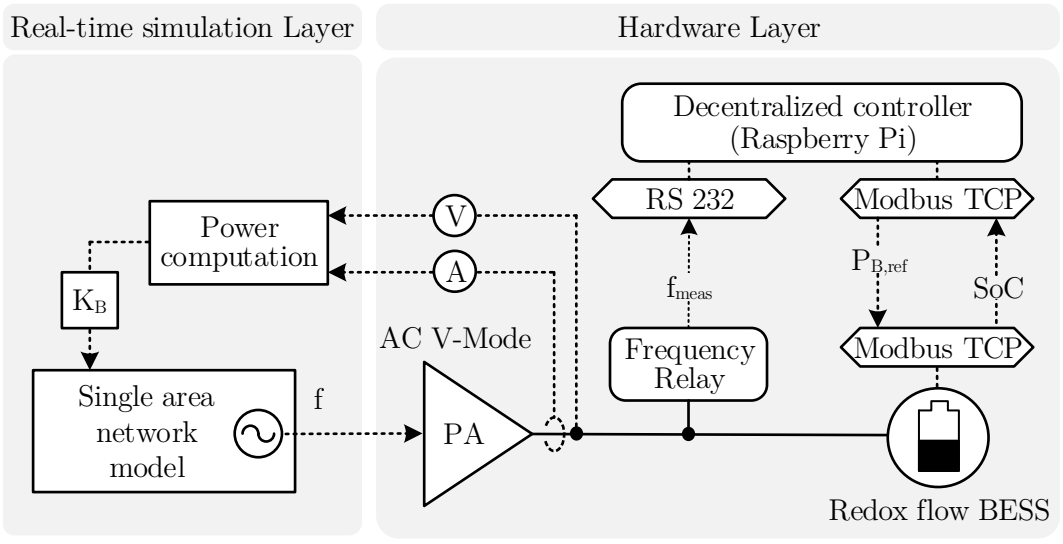

Fig. 7.16: PHIL setup – frequency response emulation

system along with the primary control parameters are selected according to the recommended values by ENTSO-E [147], [148]. The detailed model description is given in Appendix. The single area network model provides the reference frequency to the PA that is operated as voltage source (*3ph+N V-Mode*). In contrast to the PHIL setup suggested in [146], the BESS under test is directly connected to the PA. Therefore, not only the frequency relay but the overall system is subject to the frequency deviations. The current measurements from the PA are sent to the RTS where they are converted to the corresponding power quantities and added to the primary control loop. A gain factor $K_{\mathrm{B}} \geq 1$ can be eventually included to simulate the contribution of the BESS to the primary control in a larger scale.

The BESS under test is a Vanadium Redox flow battery equipped with a total number of 6 stacks. The stacks are split into two groups each one connected to its own grid inverter. The two systems are parallel connected in order to provide a maximum power of 30 kW with a total capacity of 120 kWh. The BESS includes a Battery Management System (BMS) that also allows system monitoring and control. The operating setpoints can be set either locally or remotely via Modbus TCP/IP within the ICT framework of the laboratory. A picture of the overall system is shown in Fig. 7.17.

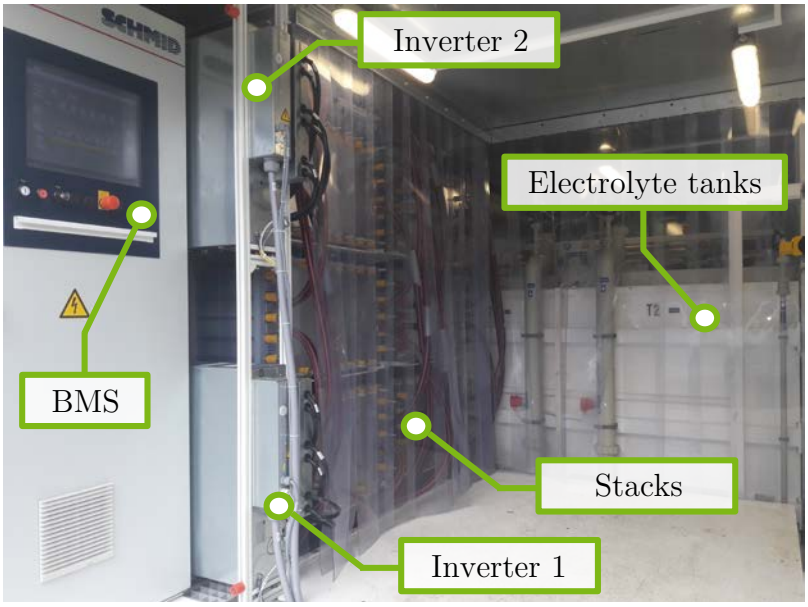

Fig. 7.17: Redoxflow BESS at SGTL facility

A Raspberry Pi is used as an external control platform where different control strategies such as peak-shaving or voltage control are implemented to enable the BESS for multi-task operations. All these control strategies are implemented within the javascript–based platform Node-red by OpenJS Foundation. Among others, this provides a flow–based programming approach including diverse libraries that allows for rapid and straightforward development of communication–based controller prototypes. A droop control similar to the one implemented in [146] is included as an additional control option to perform frequency control. Particularly, the BESS is controlled to charge or discharge in case of frequency deviations up to ±20 mHz with respect to the fundamental frequency. Control actions are performed according to the actual State of Charge (SoC) of the BESS. A detailed description of the implemented algorithm is provided in Appendix. The Raspberry Pi communicates with the BMS via Modbus TCP/IP. A frequency relay developed in [149] is used to acquire accurate measurements of the system frequency with an acquisition rate of 10 ms. The frequency measurements are sent to the Raspberry Pi via a serial communication link based on RS232. Both the frequency relay and the Raspberry Pi are installed within the BESS in addition to the existing BMS, as shown in Fig. 7.18.

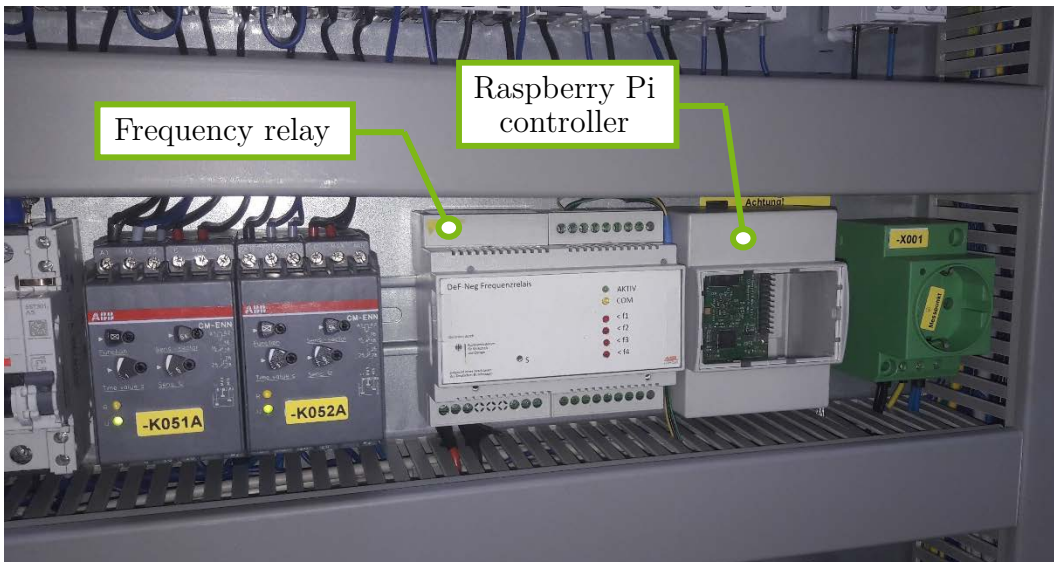

Fig. 7.18: Frequency relay and Raspberry Pi controller installed within the electrical panel of the Redox flow BESS

BESS Response Analysis

Preliminary open-loop tests are carried out in order to evaluate the dynamic response of the deployed Redox flow BESS. Particularly, these tests are performed to determine whether the system satisfies the dynamic performance required to contribute to frequency regulation properly. The usual time to start the primary control is a few seconds after the incident and the deployment time for 100 % of the total primary control reserve is at most 30 s [147]. However, for inverter–based systems as the BESS under test, a much faster response is expected. Fig. 7.19 shows the BESS response for different power setpoints in both charge and discharge operation. Particularly, each diagram compares the trigger signal to set the power reference via Modbus TCP/IP with the actual system response in terms of current. As a major outcome, the limitation of the Redox flow BESS to provide fast response when the initial system's state is in standby (namely not in operation) is detected. In this condition, both charging and discharging operations provide an average delay of about 3.5 s to react to different power setpoints (Fig. 7.19a and Fig. 7.19c, respectively). This behavior does not depend on the inverter dynamics but it is a characteristic of the BESS technology. In fact, the observed delay depends on the time needed to put the electric pumps in operation and transfer the electrolyte to the stacks. However, it is observed that with a minimal initial power setpoint of 4 kW both charging and discharging operations provide a faster average dynamic response of about 1 s (Fig. 7.19b and Fig. 7.19d, respectively). This condition provides a more effective response to the power setpoints and might also represent a more frequent real-world operating condition. In fact, large BESSs can be operated to provide multiple services in order to compensate for the system costs. In this case, the contribution on the primary frequency control can be an additional service on top of daily operations. Therefore, it can be reasonably assumed that the frequency control action starts when the BESS is already in operation.

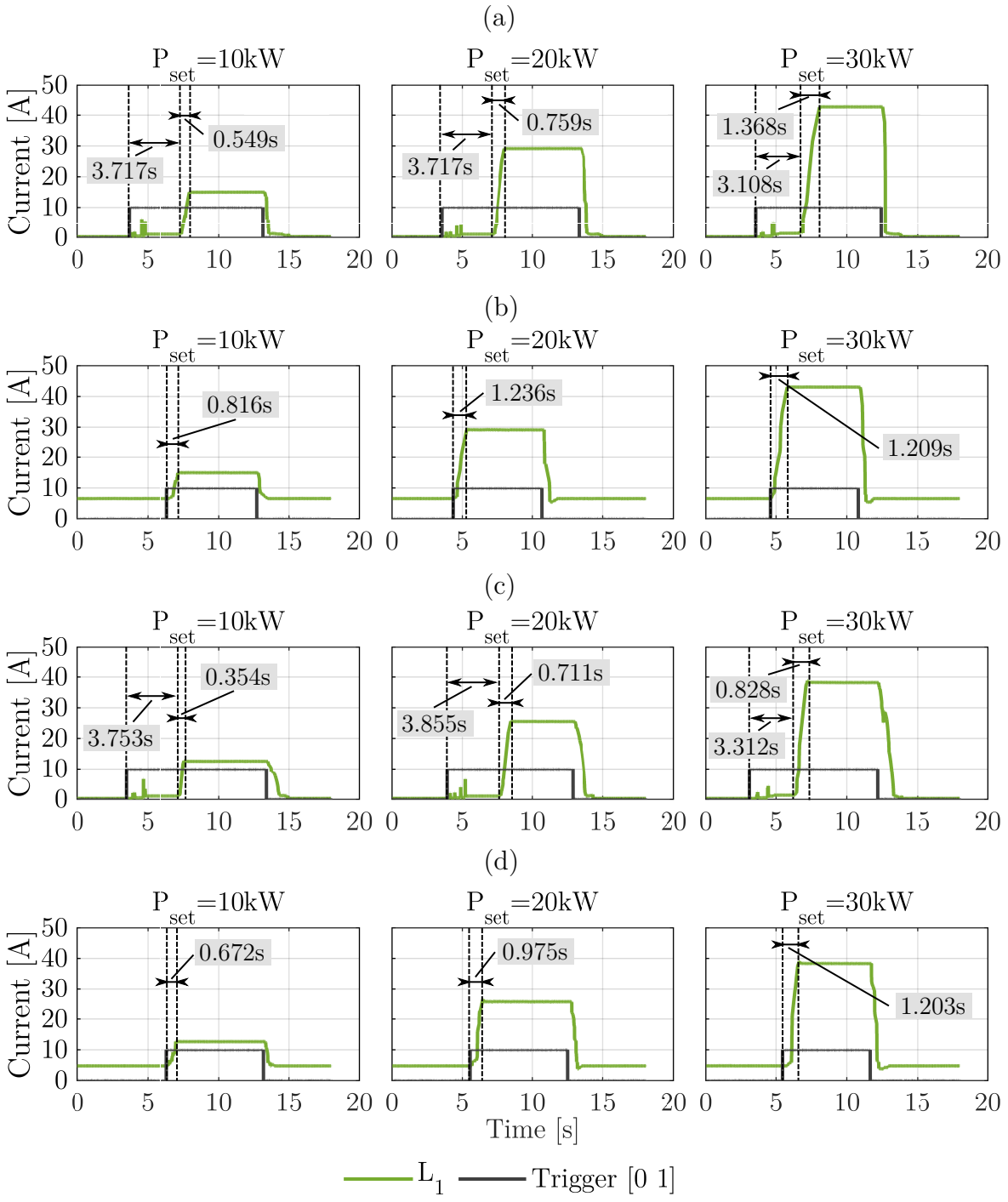

Fig. 7.19: Dynamic response evaluation of the Redox flow BESS under test for charging and discharging operations at different power setpoints: (a) Charging operation from standby condition, (b) Charging operation from initial power setpoint of 4 kW, (c) Discharging operation from standby condition, (d) Discharging operation from initial power setpoint of 4 kW

7.3.2 Test-cases and results

Two test-cases are considered to verify the functionalities of the implemented setup. According to [147], an incident case of 600 MW and 1000 MW of generation loss are taken as reference and simulated within the RTS. Each test-case is performed under three different scenarios. Each scenario includes a diverse contribution of the BESS to the primary frequency control. Particularly, different values of the control reserve from the BESS ($P_{\mathrm{B}_{\mathrm{max}}}$) are simulated by varying the gain K_{B}. The parameters for the selected scenarios are summarized in Table 7.1. All the further power system model parameters are kept constant in all the simulated scenarios.

Table 7.1: Test-cases and scenarios for System response analysis

Test-case	**Scenario I**	**Scenario II**	**Scenario III**
Incident size 600 MW	$K_B = 1e^3$	$K_B = 10e^3$	$K_B = 50e^3$
Incident size 1000 MW	$P_{\mathrm{B}_{\mathrm{max}}} = 1\,\%$	$P_{\mathrm{B}_{\mathrm{max}}} = 10\,\%$	$P_{\mathrm{B}_{\mathrm{max}}} = 50\,\%$

percentages refer to the primary control reserve of 3000 MW from conventional plants

The overall results of the simulation are shown in 7.20. Particularly, both frequency and BESS power (ΔP_{B}) refer to the measurements from the hardware setup while the power from conventional plant (ΔP_{CP}) corresponds to the simulation outcomes. Both the power quantities are expressed in terms of variation from an initial balance condition of the simulated network in which no frequency deviations occur. Results show that the implemented testbed operates as expected and in a stable manner. The PHIL system is able to emulate power system frequency deviations in a closed-loop simulation within the physical test environment. The BESS controller is able to properly detect frequency deviations and to react by commanding BESS for power discharging accordingly. BESS operation improves frequency response of the system in both the simulated test-cases. The maximum frequency deviation as well as the required regulation power from conventional plant are reduced due to the support from the BESS.

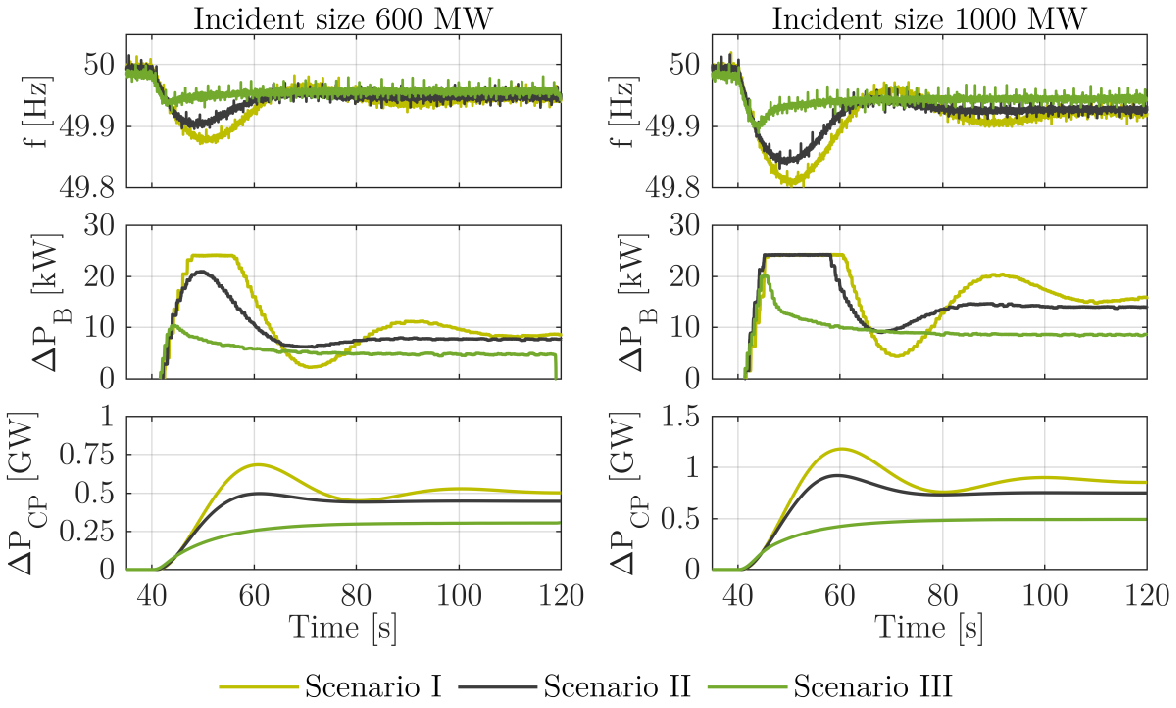

Fig. 7.20: System frequency response for the selected scenarios – test results for a loss of generation of 600 MW (left-hand) and test result for a loss of generation of 1000 MW (right-hand)

As expected, major benefits can be observed within Scenario III where the BESS contribution is scaled up to 50 % of the primary control reserve of the simulated conventional plant. In this case, the resulting maximum frequency deviation is 49.941 Hz and 49.902 Hz for the case of 600 MW and 1000 MW incident size, respectively. Moreover, frequency oscillations are also significantly reduced. Scenario I and II provide minor improvements due to the lower contribution of the BESS compared to the conventional plant. However, these scenarios result in a different stimulation of the BESS controller and, therefore, useful to prove how differently the BESS controller operates.

7.3.3 Remarks

A PHIL setup for testing on the area of frequency control is successfully developed. This emulates frequency deviations as well as the primary frequency control from conventional power plants of a simulated power system. A single area network model is selected as a proof of concept. However, according to the test purpose, a more detailed power system model can be implemented within the RTS. This setup allows for testing local controllers for decentralized frequency control with full-scale physical DER. For this purpose, a Redox flow BESS together with an external controller are used as type II components to prove the major setup functionalities. This exemplary setup demonstrates the valuable contribution of advanced laboratory testing including PHIL systems. In fact, applying PHIL is essential for testing under worst-case scenarios otherwise not viable in field tests. Suitable frequency deviations are successfully emulated in a safe and controlled manner and applied to looped physical components. Moreover, further laboratory features such as the ICT framework enhanced controller testing including the most widely used communication protocols.

Further works can consider extensions of the test setup by involving multiple components for system-level testing. This can be applied to emulate provision of ancillary services from different DER as the approach suggested in [150]. For instance, the developed testbed for PV-system emulation can be combined with the presented setup. In this case, possible interactions between the different components involved for frequency control can be investigated. Furthermore, the implemented setup can also be further deployed for different applications such as testing island operation of microgrids to point operational issues such as grid reconnection.

7.4 System-level testing: coordinated voltage control

A setup to test a coordinated voltage control algorithm is selected as exemplary application to prove the capability of the laboratory test environment to perform testing and validation at the system level. Particularly, this application aims to evaluate the capability of performing tests with different power components from different manufacturers including control systems and ICT. For this test purpose, the PHIL system is operated in order to emulate the required simulation scenarios according to the defined operational use-case UC11.

7.4.1 Description of the setup

The objective is to test a control algorithm implemented in [151] for a coordinated voltage control including the existing OLTC with the support of the Redoxflow BESS also used within the previous experiment. The OLTC under test is a 10/0.4 kV full-scale transformer by Ormazabal included within the secondary substation at SGTL. As shown in Fig. 7.21 (left-hand), the secondary substation also includes an additional 10/10 kV OLTC that is

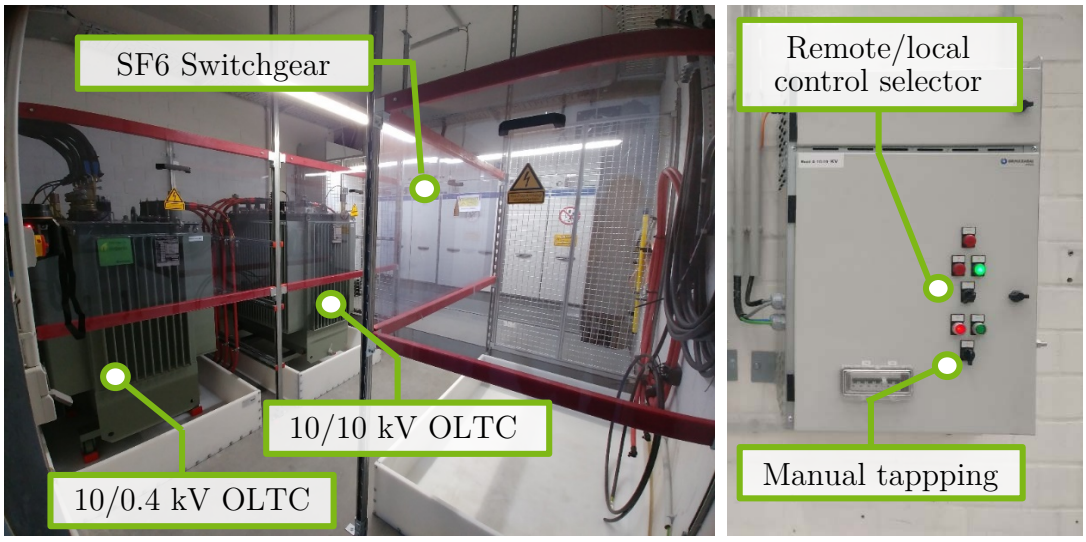

Fig. 7.21: OLTC transformer installed at the SGTL – inner view of the secondary substation (left-hand) and control panel for the OLTC (right-hand)

series-connected to the OLTC under test and used as Type I component to emulate voltage variations from the MV grid. The OLTC operating mode can be set via a control panel installed outside of the transformers room, as shown in Fig. 7.21 (right-hand). The OLTC can be controlled locally as well as remotely. By local control either automatic control or manual tap-triggers can be performed. Remote control is realized via Modbus TCP/IP. In this case, the tap-triggers can be remotely provided by an external controller where customized control algorithms can be implemented. The OLTC allows for voltage regulation within ±10 % of the secondary voltage. This is achieved by adjusting the transformer ratio by a total number of 9 discrete tap positions. Due to the mechanical parts of the tap-changer, consecutive tap variations are only possible with a time delay of 3 s. As additional type I component, the existing re-configurable network based on physical cables provides different grid topologies according to the specific test-case. Finally, controllable resistors are used together with the PHIL system as type I components to reproduce suitable load and generation scenarios.

7.4.2 Control strategies and test-cases

Beside the coordinated control, alternative control strategies are also considered. This aims to demonstrate possible limitations of these solutions that lead to the more favourable application of the suggested coordinated control. Particularly, the following control strategies are considered:

- **Conventional control:** refers to the control strategy provided by the OLTC manufacturer. This consists of control actions based on the voltage measured directly at the secondary side of the OLTC.
- **Advanced control:** OLTC control actions are performed according to the voltage measurements from a number of distributed measurements devices installed at specific nodes within the grid.
- **Coordinated control:** is an extension of the advanced control where additionally DER can be involved in supporting the voltage control.

Particularly, the OLTC is first operated as principal component for voltage control. If voltage deviations exceed the OLTC control range, a support request is sent to the BESS to contribute to voltage control. The detailed description of this control algorithm is given in Appendix.

For each defined control strategy the OLTC operations are defined by three different operating states according to the measured voltage:

- **Tolerance:** defines the range of permitted voltage variations. For voltage magnitudes within the tolerance no control actions are performed and the OLTC remains in standby state.
- **Slow-action:** is enabled in case of small voltage deviations with respect to the tolerance. An internal timer is activated to perform control actions after a predefined time interval. If the voltage magnitude decreases within the tolerance the timer is reset and no tap changes are performed. Otherwise, a number of tap changes are executed to keep the voltage within the tolerance.
- **Quick-return:** is actuated in case of large voltage deviations with respect to the tolerance. In this case, a similar logic as the slow-action is executed. However, due to the severe voltage deviation, the regulation timer is set to ensure a faster control action.

The selected setpoints for the aforementioned control states for the OLTC for each control strategy are summarized in following Table 7.2.

Table 7.2: OLTC control setpoints

Control Mode	**Operating State**					
	Tolerance		Slow-action		Quick-return	
	ΔV [%]	Δt [s]	ΔV [%]	Δt [s]	ΔV [%]	Δt [s]
Conventional control	2	inf	$2 \div 10$	10	> 10	3
Advanced control	10	inf	$10 \div 15$	10	> 15	3
Coordinated control	8	inf	$8 \div 12$	10	> 12	3

Percentages refer to a nominal phase-to-ground voltage of 230 V_{RMS}

The advanced control and the coordinated control strategies are both implemented in Node-red and running on a local computer acting as an external controller. This is connected to the laboratory network to enable communication with the OLTC and the Redox flow BESS via Modbus TCP/IP. The existing meters by KoCoS are deployed as distributed measurement devices for the various test purposes. They are also equipped with communication modules that allow the external controller for the acquisition of the voltage measurements via Modbus TCP/IP.

Two test-cases based on two different network topologies are selected to prove the functionalities of the aforementioned control strategies. Specific load and generation scenarios are emulated within the test network by operating the PHIL system and a controllable resistor bank as type I components. The overall test-plan is summarized in Table 7.3.

Table 7.3: Test-plan for the selected control strategies

Test-case	**Scenario**	**Use-case**
Single-feeder grid	■ High load at the end of the feeder ■ High generation at the end of the feeder	■ Conventional control ■ Advanced control
Double-feeder grid	Contemporary high load and high generation at the end of the feeders	Advanced control with BESS (Coordinated voltage control)

7.4.3 Test-case 1: Single-feeder grid

A single-feeder grid topology is implemented to test the OLTC operation once with the conventional control and once with the advanced control, as depicted in Fig. 7.22. The setup includes 4 cable segments of type NAYY 4x150 mm^2 series-connected with a total length of 750 m that connect the OLTC to the BUS 1. The PHIL system together with variable resistors are connected at the end of the feeder and are used to emulate the required scenarios. Particularly, the PA is mainly used for the emulation of generation

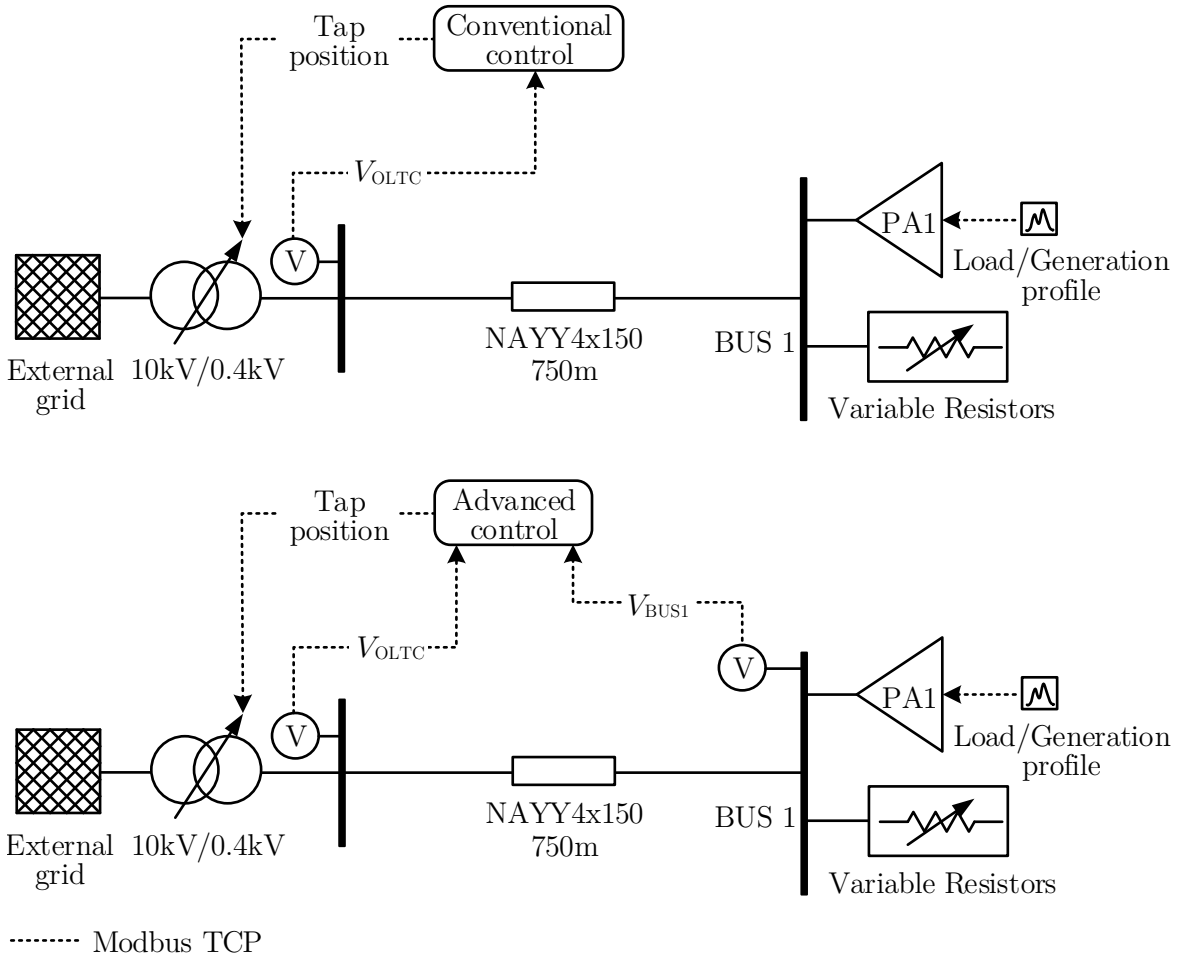

Fig. 7.22: Single-feeder grid setup with conventional OLTC control (top) and advanced OLTC control (bottom)

profiles. Within the conventional control a single voltage measurement (V_{OLTC}) is needed while the advanced control requires an additional voltage measurement at BUS 1. The voltage measurements are acquired by the controller via Modbus TCP/IP and within a time interval of 1 s. Similarly, the trigger signals to move the tap position of the OLTC are sent via Modbus TCP/IP. As described in Table 7.3, two extreme scenarios consisting of high load and high generation are emulated at BUS 1 in order to compare the performance of the two control methods. The test results are shown in Fig. 7.23. In both scenarios the conventional control is not able to detect the voltage violations at the end of the feeder. In fact, for all the test duration $\mathrm{V_{OLTC}}$ is confined within the tolerance band, thus no control actions are performed. The conventional control results more effective for

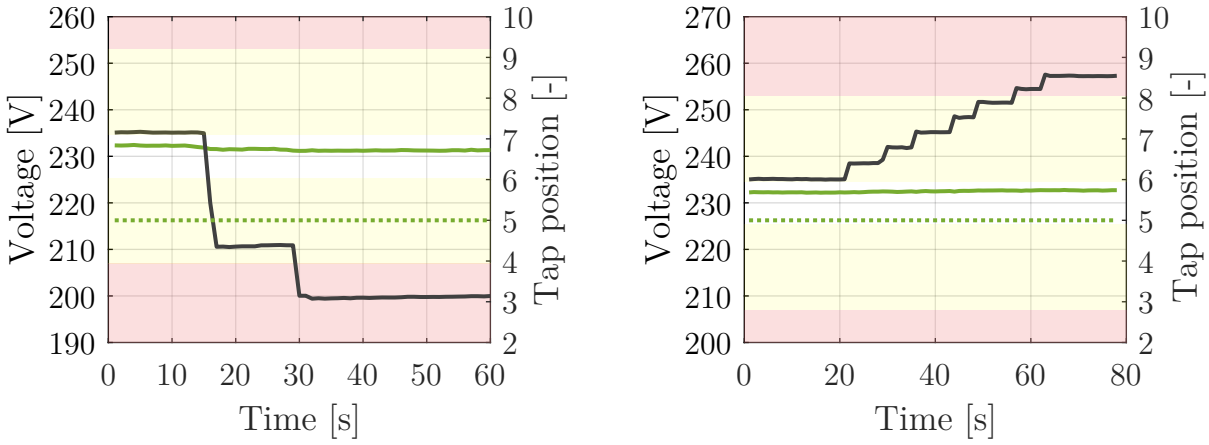

(a) Conventional voltage control: high-load scenario (left), high-generation scenario (right)

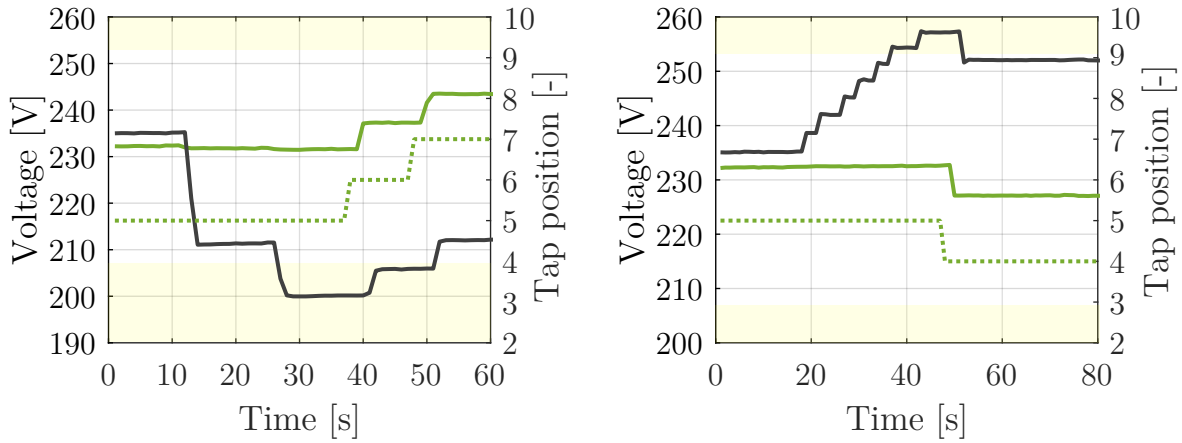

(b) Advanced voltage control: high-load scenario (left), high-generation scenario (right)

Fig. 7.23: Comparison between conventional and advanced voltage control with OLTC in case of single-feeder grid configuration

compensating possible voltage variations from the upper voltage level that are directly detected from the voltage measurement at the secondary side of the OLTC. Similar test scenarios are reproduced to prove the advanced control. In this case, the voltage violation can be detected and the OLTC is operated in order to restore voltage magnitude within the defined tolerance. Particularly, as soon as the voltage magnitude exceeds the slow-action threshold the internal control timer is activated. Therefore, a tap trigger of the OLTC is performed within the time interval of 10 s and the voltage violations in both the considered scenarios are successfully restored.

7.4.4 Test-case 2: Double-feeder grid

The network emulator is configured to implement a double-feeder grid topology with cable type NAYY 4x150 mm^2. A schematics of the implemented setup is given in Fig. 7.24. One feeder with a total length of 400 m connects the OLTC to BUS 1 in which high load absorption is emulated by PA 1 and variable resistors. A second feeder with a total length of 350 m connects the OLTC to BUS 2 where PA 2 emulates high generation profiles. The Redox flow BESS is also connected to BUS 2 to support the OLTC for voltage control within the coordinated voltage control algorithm to be proven. For this test purpose, the BESS is initially set in standby mode with a SoC of 50 %. Test results are shown in Fig. 8.2. The load at BUS 1 is increased

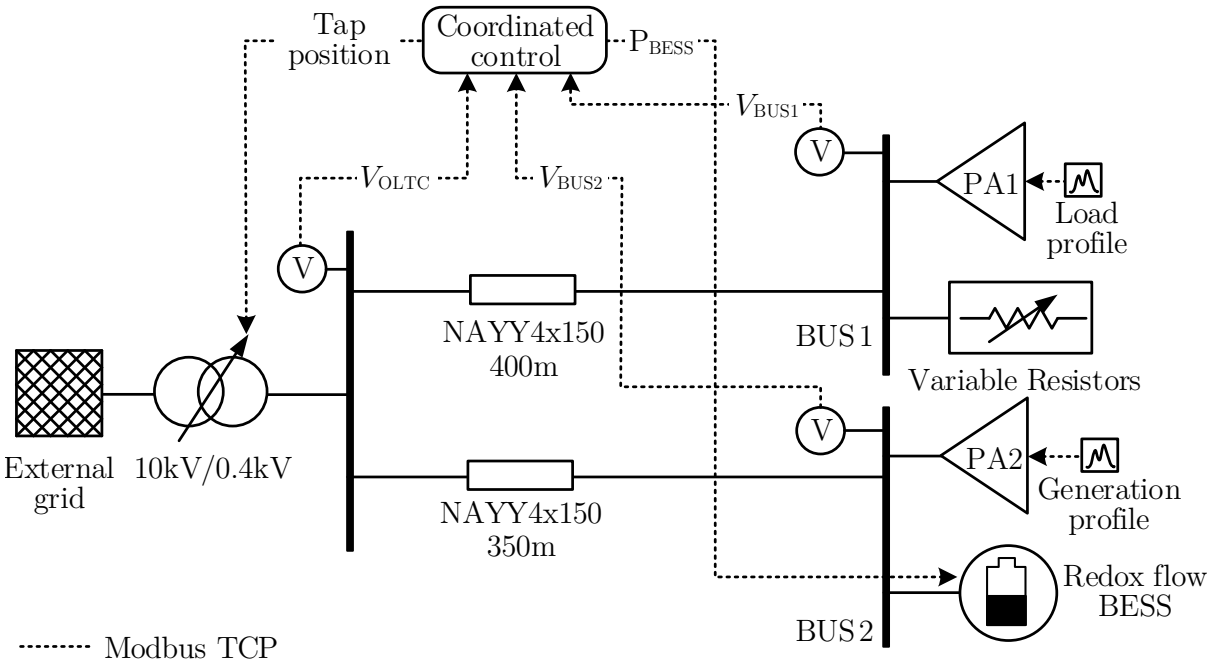

Fig. 7.24: Double-feeder grid setup with OLTC–BESS coordinated voltage control

until the voltage magnitude exceeds the selected threshold. Differently, the power generation at BUS 2 is increased until the voltage magnitude increases to a value close to the limit. This situation emulates a critical condition in which the OLTC alone is not able to restore voltages. In fact, a tap increase would restore the undervoltage at BUS 1 but would lead to an overvoltage on BUS 2. The coordinated control algorithm is able

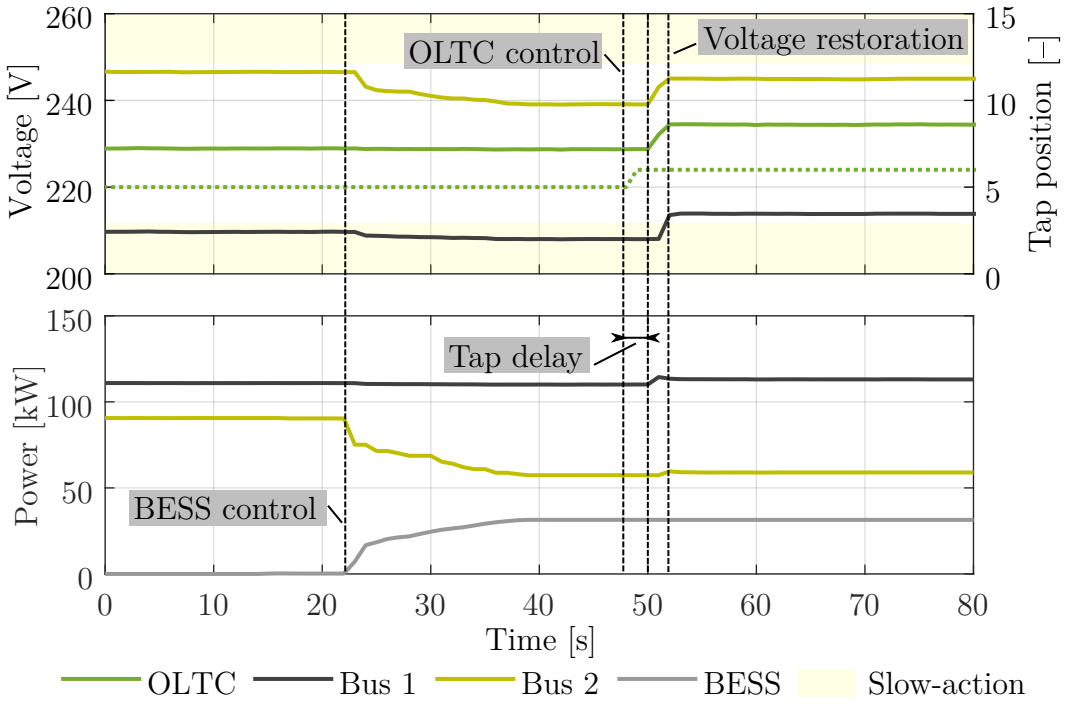

Fig. 7.25: Coordinated voltage control with OLTC-BESS for double-feeder grid with contemporary high load and high generation at the end of the feeders

to detect this situation and perform a support request to the BESS. The BESS control acquires the support request and evaluates possible charging operations according to the actual SoC. As the actual SoC is 50 %, charging operations can be performed without restrictions. At 22 s the BESS starts charging operations by increasing its power until the maximum of 30 kW. Therefore, the total power flow at BUS 2 is reduced and voltage magnitude decreases. Once the voltage at BUS 2 decreases to a suitable value, the coordinated control algorithm recognizes that a tap change can take place without further restrictions. Therefore, a tap change of the OLTC is finally performed, thus solving the voltage drop at BUS 1. According to the logic of the control algorithm, the BESS will maintain the reference charging power for the following 20 min after the support request. In case of real-world implementations, if network conditions evolve resulting in to secure voltage values, the support request is disabled and the OLTC returns to operate as the principal voltage controller.

7.4.5 Remarks

Coordinated voltage control is considered as an exemplary application to prove the laboratory capability to perform tests at the system level. Devices for different purpose and from different manufacturers such as the OLTC, the Redox flow BESS and the KoCoS meters are integrated and operated as type II components for a common control purpose. The PHIL system is operated as a major flexible type I component to reproduce suitable load and generation scenarios. This confirms the valuable contribution of the PHIL system to enhance laboratory capability not only for conventional PHIL simulation but also for full hardware testing.

The benefits of an adequate laboratory design that follows the non-functional requirements defined within Chapter 4 can be recognized. Among others, the modular design of the major laboratory components enhanced the practical and effective interconnection of the various component within the similar setup. The reconfiguration capability provided by both the design of the network emulator as well as the developed configuration cabinets allows rapid and straightforward setup commutation for the different test-cases. The implementation of the ICT infrastructure that allows the deployment of standard communication protocols provided a proper interoperability of the various components.

Similar setups can be implemented by including additional components for voltage control. For instance, the developed PV system emulator can be used as inverter–based generation source. This allows for more advanced tests in which the interactions between internal voltage support functionalities of the PV inverter and the operation of the presented coordinated voltage control can be further analyzed. Moreover, additional components such as the existing line voltage regulator prototype can be included in the coordinated voltage control algorithm, thus extending control capability. Additional grid topology can be implemented by operating the re-configurable network emulator. However, the limited number of cable segments together with the

limited amount of type I components restrict the total topology configuration options. Therefore, for further studies on voltage control the extension of the laboratory test network can be considered.

Chapter 8

Summary, discussion and outlook

Practical issues in design and operation of advanced smart grid test infrastructures are assessed within this work. Both aspects are analyzed with particular emphasis on enhancing the test capability of smart grid laboratories based on PHIL technique. Finally, the assessed design and operational concerns are evaluated on an existing smart grid laboratory infrastructure in which a PHIL system is deployed to extend the overall test capability. The principal contributions along with the major outcomes for each considered aspect are summarized in the follows.

- Requirements analysis is performed to determine the key design and quality attributes that advanced smart grid test facilities should provide. Particularly, a number of minimal non-functional requirements are stated as essential attributes to enhance the operation and the performance of smart grid test infrastructures. Among others, modularity and reconfiguration are identified as crucial requirements especially for PHIL applications. These ensure practical and flexible setup configuration for different test purposes. Further non-functional requirements such as

integration and interoperability are stated as fundamental features to meet typical test requirements for smart grid applications.

- An architectural classification of testing equipment is suggested. Particularly, the minimal laboratory equipment is classified into specific typologies according to their function while performing a tests. The suggested classification aims to provide a structural and modular approach to identify the fundamental type of components and their role within an advanced test facility. On the one hand, this can favourite the design process of an overall complex test infrastructure. On the other hand, this approach provides a method to describe the applied devices and their functions within a given test setup. The latter aspect is of particular importance when operating complex setups including multiple components for system-level testing.

- Specific design concepts for PHIL systems are also assessed. These include design aspects for both RTSs and PAs as stand-alone devices as well as for a comprehensive use of the two components as a whole PHIL system. Therefore, besides dynamic requirements that are typically considered for PHIL simulation, complementary aspects such as power and safety concerns are also taken into account.

- A set of fundamental operational use-cases for advanced testing is proposed. These use-cases are suggested as the most practice-relevant applications for testing and validation at both the component and the system level. Particularly, practical setup configurations for CHIL as well as PHIL testing are provided for different applications. Besides the conventional understanding of these testing approaches, the defined operational use-cases provide complementary functionalities for a more extensive applicability. Practical setup solutions are also suggested for particular applications such as PHIL experiments including series-connected components.

- Evaluation of the assessed design and operational aspects is carried out on the existing SGTL infrastructure at TU Dortmund University. This includes a PHIL system that is deployed within this work to further assess design and operational aspects on a physical system. First, the proposed architectural classification is applied to describe the actual design of SGTL, thus proving the feasibility of this approach. Later, practical aspects and challenges in the design and integration of the PHIL system into the SGTL facility are assessed. Particularly, gained integration concerns led to a limitation of the PA system operation in favor of a more cost-effective and task-oriented design. This remarks that the proper PA system integration plays a key role for its straightforward operation as stand-alone device as well as for PHIL applications. Practical solutions as the employment of dedicated configuration cabinets are also discussed as possible options to enhance the overall laboratory systems integration.
- Preliminary tests are performed with the existing PHIL system to prove some of the operational use-cases stated within this work. First, basic tests are performed to examine the elemental functionalities of the deployed PHIL system. Tests of PA dynamic response together with basic PHIL experiments with the most popular IAs are performed to assess different behaviors between their theoretical and practical implementation. Further tests are carried out to verify the additional features as well as the limitations of applying PHIL systems rather than conventional ones for the given test purpose. Particularly, the PHIL system is first open-loop operated to reproduce reference signals modelled within the RTS into the physical laboratory test environment. Later, a closed-loop setup for the emulation of active and reactive power profiles is implemented. Dedicated software interfaces based on the API of the RTS are implemented to provide additional functionalities and to integrate different systems within a common setup. Finally, a practical application of the proposed setup is presented, thus proving its major functionalities.

- A number of collected experiences based on the use of the deployed PHIL system for practical research needs are provided. These include experimental setups for testing at the component and at the system level according to the operational use-cases defined within this work. As results of these tests, the major advantages and limitations of applying PHIL technique are proven. Moreover, the benefits of a proper facility design are consolidated during the various test executions. PHIL capability for emulating power components is verified in the case of PV-system emulation. Among others, practical challenges on coupling simulated components with commercial hardware devices are found when interfacing a commercial PV inverter. The flexibility of adapting the deployed PHIL system for special research needs is verified by developing a testbed for DSRs. Unless minor setup limitations, commercial DSRs are properly operated at rating currents for HV systems within a LV test infrastructure. A testbed for decentralized frequency control with DER is implemented to prove the valuable contribution of applying PHIL for testing under worst-case scenarios otherwise unfeasible within field tests. Suitable frequency deviations are successfully emulated in a safe and controlled manner and applied to the looped physical components. Moreover, further laboratory features such as the ICT framework enhanced controller testing including standard communication protocols. Finally, a coordinated voltage control algorithm is proven within a system-level setup. This proved the benefits of a proper facility design together with the complementary use of PHIL system to test multiple components also from different domains within various scenarios.

Conclusive remarks and recommendations

Advanced testing procedures based on HIL are promising options to improve testing and validation capability especially for innovative smart grid applications. Particularly, the PHIL approach results in a viable solution for testing full-scale power components within a multi-domain setup. However, the combined use of software and power hardware parts within a common setup increases the overall complexity. Based on the experience gained with experimental trials on the existing SGTL infrastructure the following remarks and recommendations can be deducted.

- The proper design of advanced testing infrastructures is essential for the effective application of such innovative testing procedures. Particularly, the definition and the implementation of non-functional requirements is a fundamental aspect to improve the capability of a test facility. The modular architecture together with practical reconfiguration means are highly recommended to guarantee flexible setup implementation and straightforward systems integration especially for PHIL applications.
- The combined use of RTSs and PAs provides complementary operational use-cases that in addition to conventional PHIL simulation can extend the overall PHIL system applicability. Therefore, PHIL systems result advanced and flexible components that are essential to reproduce the required scenarios within a physical test environment. A fast and reliable communication link between RTS and PA system is the core element to enable such functionalities. Optical fiber link based on SFP modules results of high performance and therefore strongly recommended for the connection between RTS and PA system.
- PHIL testing requires sophisticated setups that need to be properly assessed. Particularly, conventional PHIL simulation arises a number of challenges otherwise not considered in theory. Although many IAs are proposed in the literature, a few only result of practical feasibility. Moreover, for practical applications, PHIL accuracy remains particularly

difficult to be evaluated especially for complex setups that include auxiliary elements within the test loop. Further issues might arise when interfacing commercial power components. These are designed for field applications and their deployment within a PHIL setup might require slight adaptions. However, component manufacturers often do not share detailed device information or do not allow specific parameters tuning. This might make such hardware interfacing more challenging.

- Regarding RTSs, the use of a modelling tool based on existing commercial software for power system simulation is recommended. This allows for project exchange between different users and facilitates model development from existing projects. However, specific model adjustments needed to make the model compatible for the real-time execution, often result challenging especially for inexperienced users. Particularly, in contrast to offline simulators, operating RTSs requires additional expertise to avoid possible modelling issues between the RTS platform and the third party modelling tool. In case of large power system models, additional skills are required to recognize and implement suitable model simplifications to avoid simulation overruns. Although different solutions can be applied to simplify complex models, the selection of small-size network models often results the most effective one. In this case, network model size is reduced in favour of a more detailed simulation. This is particularly suitable for PHIL applications as the principal objective of the test is typically the hardware part rather than the simulated one.

- PA systems are central elements for PHIL testing. Besides typical requirements for conventional PHIL simulation, the selection of a PA system should take into account complementary aspects for the proper system integration within the overall test facility. The deployment of switched-mode PAs requires additional considerations. Due to the output filters, suitable protection devices are necessary to guarantee safety system operation and to avoid undesired trips. Moreover, proper filters design should limit leakage currents to prevent improper operations when interfacing

hardware components. To further extend system capability, a modular design with multiple PA groups rather than a single and more powerful unit is also recommended. Among others, this provides more flexibility when interfacing series-connected power components. Moreover, multiple PA groups can be independently operated and connected at different buses of a physical test network, thus improve scenarios emulation.

- Data visualization and control tools are essential for a straightforward test execution. For this purpose, the deployment of APIs based on common scripting tools is highly recommended. Among others, these are particular valuable for providing a central platform for the practical management of complex setups including multiple components. With this regard, the node-red software that was often deployed within this work is suggested as suitable option for fast and straightforward implementation of laboratory control and monitoring platforms.

Future work

Although experimental trials performed within this work show encouraging results, further studies are required to improve performances of the presented testbeds and to evaluate the applicability of the defined design and operational concepts for further research needs. Particularly, the following considerations for future work are suggested.

- As not all of the defined operational use-cases are applied within this work, further setups should be implemented to evaluate the potential of the leftover ones in practical applications. Particularly, the assessment of use-cases related to CHIL simulation and co-simulation are recommended. Due to their special design and their potential capabilities, trials with PHIL setups in co-simulation with a different test facilities are particularly suggested in future work.

- Minor issues detected during the experimental tests need to be further investigated. Particularly, unexpected behaviors detected with the presented testbed for PV-system emulation require to be properly assessed. Additional tests with physical inverters from different manufacturers can be performed to verify similarities or improvements with respect to the results obtained with the presented hardware setup.

  Concerning the suggested testbed for DSR, further improvements for the setup impedance compensation are required to enhance the overall simulation accuracy. Moreover, extensive tests can be performed to assess the functionality limitations observed within Configuration II. Further grid topologies should be implemented to prove setup stability and accuracy also within diverse grid conditions.

  The proposed testbed for decentralized frequency control with DER included a simplified power system model based on the single area network. More detailed models can be implemented to provide more accurate outcomes. For instance, the deployed RMS models can be replaced with more precise EMT type ones for a more accurate frequency response. According to the test purpose, additional functionalities such as secondary frequency control can also be included within the simulated model.

  Further trials with the presented testbed for coordinated voltage control are required to proper assess the control functionalities of the deployed algorithm. For this purpose, emulation of more exhaustive scenarios including different network topologies together with further control components can be considered.

- As the scope of this work is to identify the potential applications for advanced testing procedures, less rigorous scientific case-studies are considered in favour to more representative applications. Although this is effective to prove the principal setups functionalities and restrictions, future work should focus on the deployment of the presented testbeds for more detailed and scientific-relevant applications.

Regarding future work explicitly related to the SGTL facility, it is clearly understandable that there are several possibilities for further laboratory improvements. Although these are mostly dictated by specific research projects needs, some general suggestions can be deduced as consequence of this work. Test capability of the deployed PHIL system results adequate to the current development state of SGTL. However, as essential components for advanced testing, the installation of additional PHIL systems optionally based on different commercial solutions can be considered to extend test capability and to evaluate performance between different products. Moreover, further upgrades of the test network by additional cable segments or cable emulation systems is also recommended. This in combination with additional PHIL systems will provide a wider range of scenarios emulation especially suitable for testing in the area voltage control.

Future work should also consider the development of suitable frameworks to integrate existing resources and tools for power system simulation available at ie^3 within SGTL. Particularly, advanced simulation tools as the existing agent–based distribution network planning and operation tool (SIMONA) can be combined with PHIL setups at SGTL within a comprehensive co-simulation. Moreover, further co-simulation setups can be developed by linking SGTL to the existing Protection and Automation Lab at ie^3. The latter is equipped with RTSs together with specific hardware components for testing innovative protection and automation systems for smart grid applications. Merging the potential of these two facilities will provide additional test capability for more comprehensive studies on smart distribution grids.

Finally, more extensive research activities carried out in a close cooperation with industrial partners and network operators are also highly encouraged. Among others, these are essential to make sure that the research activities are relevant from the practical viewpoint, thus reducing the gap between purely academic research and commercialized industrial products or services.

Appendix

PV-emulation parameters

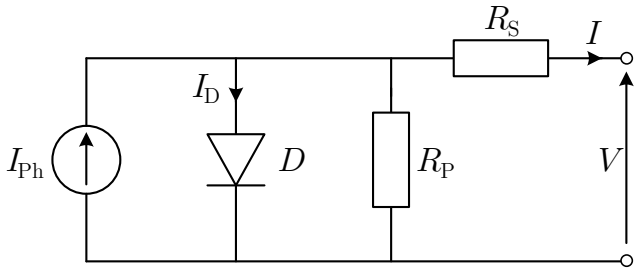

Fig. 8.1: Single diode PV-cell equivalent model

The module current I can be expressed as function of the module voltage V as shown in the following equations:

$$I_D = I_0 \left[exp\left(\frac{qV}{nKT}\right) - 1 \right] \tag{8.1}$$

$$I_0 = I_{0,STC} \left(\frac{T_{STC}}{T}\right)^3 exp\left[\frac{qE_g}{nK}\left(\frac{1}{T_{STC}} - \frac{1}{T}\right)\right] \tag{8.2}$$

$$I_{sc} = I_{sc,STC}\left[1 + \alpha\left(T - T_{STC}\right)\right] \tag{8.3}$$

$$V_{oc} = V_{oc,STC}\left[1 + \beta\left(T - T_{STC}\right)\right] \tag{8.4}$$

$$I = I_{Ph} - I_D \left[exp\left(\frac{q\left(V + R_s I\right)}{nKT}\right) - 1 \right] - \frac{\left(V - R_s I\right)}{R_p} \tag{8.5}$$

$$I_{Ph} = \frac{E}{E_{STC}} I_{sc} \tag{8.6}$$

where:

I_{Ph} Current generated by absorption of photons

I_0 Diode saturation current

The main constants and parameters applied to the simulated PV-system are listed in Table 8.1.

Table 8.1: Constants and parameters for the simulated PV-system

Standard Test Conditions (STC)		
E_{STC}	1000 W/m^2	Irradiance
T_{STC}	298.15 K	Temperature
AM	1.5	Air Mass
Reference PV-module: Galaxy Energy GS260m-60*		
P_{MPP}	260 W	Nominal Power
V_{MPP}	30.8 V	Nominal Voltage
I_{MPP}	8.44 A	Nominal current
V_{oc}	38.1 V	Open circuit voltage
I_{sc}	8.93 A	Short-circuit current
N	60	Number of cells
Technology	Si-monocrystalline	
α	0.055 %/K	Current temperature factor
β	-0.35 %/K	Voltage temperature factor
Further constants and model parameters		
K	1.381×10^{-23} J/K	Boltzmann's constant
Q	1.602×10^{-19} C	Electron charge
E_{g}	1.107 eV	Wide-bandgap Si semiconductors
n	1.2	Diode ideality factor
R_{s}	0.2267 Ω	Series resistance
R_{p}	4960 Ω	Parallel resistance
PV-system configuration		
N_{s}	20	Series connected modules (string)
N_{p}	11	Number of parallel strings

* All values refer to STC

OLTC Control Algorithm

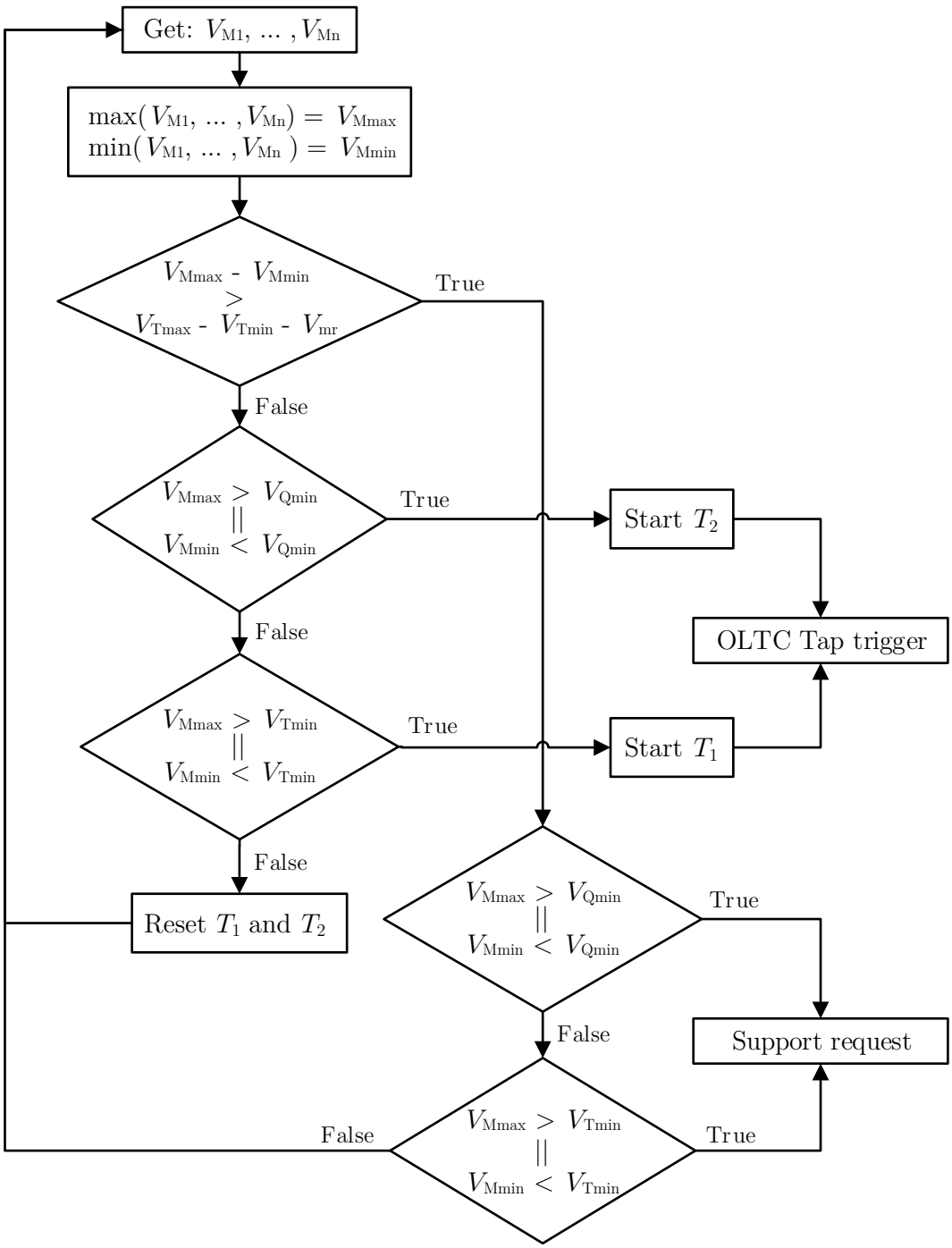

Fig. 8.2: Coordinated voltage control algorithm [151]

where:

$V_{M1}, ..., V_{Mn}$ Voltage from n measurement points

V_{Tmax}, V_{Tmin} Slow-action voltage limits

V_{Qmax}, V_{Qmin} Quick-return voltage limits

T_1 Timer for slow-action activation

T_2 Timer for quick-return activation

V_{mr} Voltage margin

BESS control algorithm for voltage support

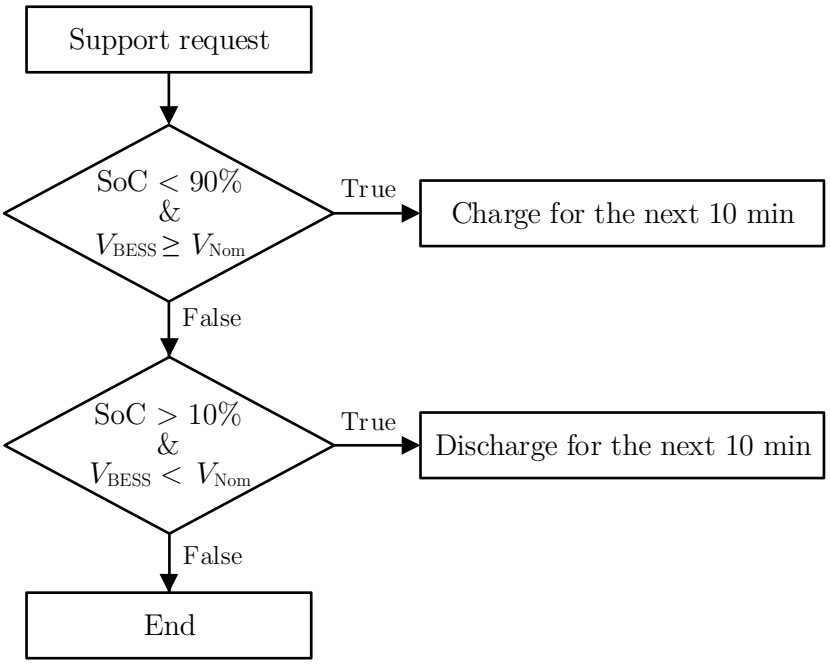

Fig. 8.3: BESS algorithm for voltage support [151]

where:

V_{Nom} Nominal voltage

V_{BESS} Actual BESS voltage

BESS algorithm for frequency control

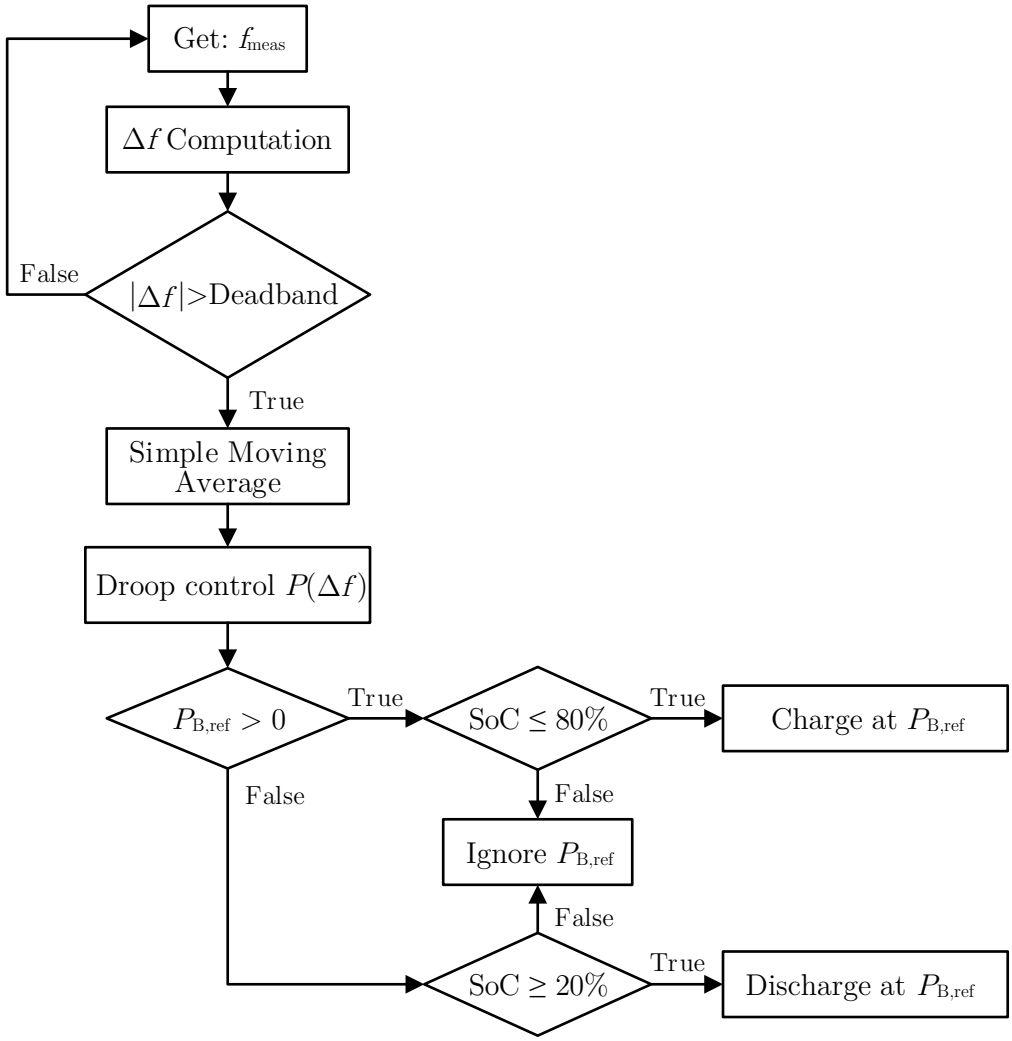

Fig. 8.4: BESS algorithm for frequency control

Droop control:

$$P_{\text{B,ref}} = \frac{\Delta f_{\text{min}} - \Delta f}{\Delta f_{\text{min}} - \Delta f_{\text{max}}} P_{\text{B,max}} \tag{8.7}$$

where:

$P_{\text{B,ref}}$ BESS power setpoint

$P_{\text{B,max}}$ BESS max power

$\Delta f_{\text{min}}, \Delta f_{\text{max}}$ min and max frequency deviation

Single area network model

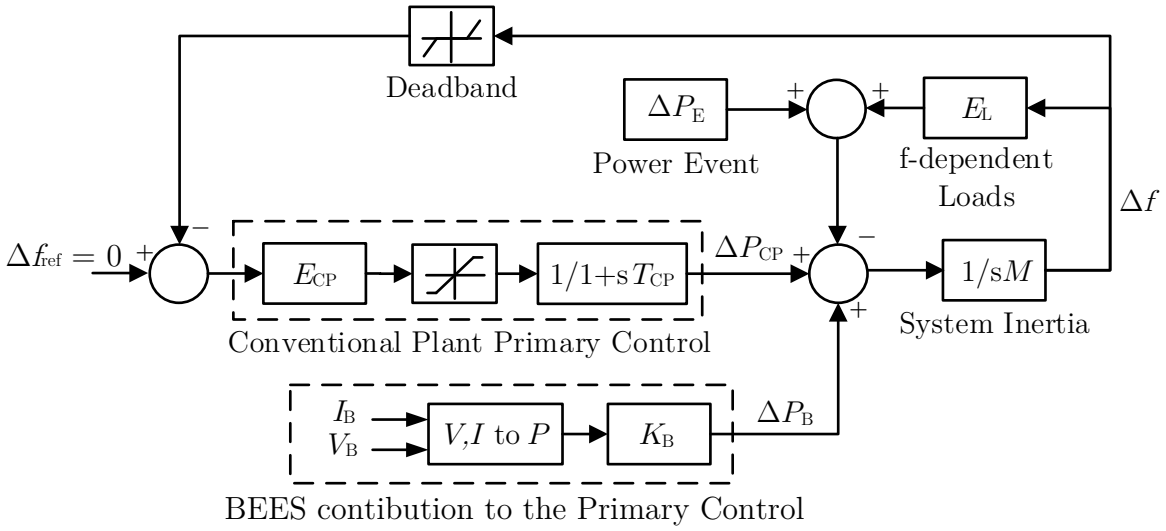

Fig. 8.5: Single area network model

where[1]:

ΔP_{CP} Conv. plant power variation

E_{CP} Power-frequency characteristic of conv. plant (15000 MW/Hz)

T_{CP} Time constant of the conv. plant (20 s)

E_L Self-regulation of loads (1500 MW/Hz)

M Power system inertia (30000 MW s/Hz)

I_B, V_B BESS current and voltage, respectively

ΔP_B BESS power variation

K_B BESS gain factor (varying for each scenario)

ΔP_E Power event (varying for each test-case)

Δf_{ref} Reference frequency deviation

Δf frequency deviation

Primary control reserve conv. plant 3000 MW

Frequency deadband ± 20 mHz

[1]The model of the power system along with the primary control parameters are selected according to the recommended values by ENTSO-E [147], [148]

References

[1] Federal Ministery for the Environment Nature Conservation Building and Nuclear Safety (BMUB), "Climate Action Plan 2050," 2016. Accessed: Feb. 1, 2021. [Online]. Available: https://www.bmu.de/fileadmin/Daten_BMU/Pools/Broschueren/klimaschutzplan_2050_en_bf.pdf.

[2] United Nations Framework Convention on Climate Change, "Paris Agreement," 2015. Accessed: Feb. 1, 2021. [Online]. Available: http://unfccc.int/resource/docs/2015/cop21/eng/l09r01.pdf.

[3] International Energy Agency (IEA), "Global EV Outlook 2020," Tech. Rep., 2020. Accessed: Feb. 1, 2021. [Online]. Available: https://www.iea.org/reports/global-ev-outlook-2020.

[4] G. Chicco, S. Riaz, A. Mazza, and P. Mancarella, "Flexibility from distributed multienergy systems," *Proceedings of the IEEE*, vol. 108, no. 9, pp. 1496–1517, 2020.

[5] A. Ciocia, V. A. Boicea, G. Chicco, P. Di Leo, A. Mazza, E. Pons, F. Spertino, and N. Hadj-Said, "Voltage control in low-voltage grids using distributed photovoltaic converters and centralized devices," *IEEE Transactions on Industry Applications*, vol. 55, no. 1, pp. 225–237, 2019.

[6] A. Ciocia, G. Chicco, and F. Spertino, "Benefits of on-load tap changers coordinated operation for voltage control in low voltage grids with high photovoltaic penetration," in *2020 International Conference on Smart Energy Systems and Technologies (SEST)*, Sep. 2020, pp. 1–6.

[7] M. Carlen, R. Jakobs, A. Slupinski, F. Cornelius, M. Schneider, I. Buschmann, J. Tepper, and H. Wiesler, "Line Voltage Regulator for Voltage Adjustment in MV-Grids," in *CIRED 23rd International Conference on Electricity Distribution*, Jun. 2015, pp. 1–5.

[8] M. Holt, J. Maasmann, and C. Rehtanz, "Line voltage regulator based on magnetic-controlled inductors for low-voltage grids," in

CIRED 24th International Conference and Exhibition on Electricity Distribution, Jun. 2017, pp. 1–4.

[9] M. Holt, G. Grosse-Holz, and C. Rehtanz, "Line voltage regulation in low voltage grids," in *CIRED Workshop*, Jun. 2018, pp. 1–4.

[10] M. Holt and C. Rehtanz, "Optimizing line-voltage-regulators with regard to power quality," *Electric Power Systems Research*, vol. 190, p. 106654, 2021.

[11] O. Pohl, F. Rewald, S. Dalhues, P. Jörke, C. Rehtanz, C. Wietfeld, A. Kubis, R. K. Tamgue, and D. Kirsten, "Advancements in Distributed Power Flow Control," in *2018 53rd International Universities Power Engineering Conference (UPEC)*, Sep. 2018, pp. 1–6.

[12] A. Kossiakoff, W. N. Sweet, S. J. Seymour, and S. M. Biemer, *Systems Engineering Principles and Practice*, 2nd ed. John Wiley & Sons, Inc., 2011, pp. 3–40.

[13] A. Dennis, B. H. Wixom, and R. M. Roth, *System Analysis and Design*, 5th ed. John Wiley & Sons, Inc., 2012, pp. 5–97.

[14] I. Graessler, J. Hentze, and T. Bruckmann, "V-models for interdisciplinary systems engineering," in *15th International Design Conference (DESIGN)*, May 2018, pp. 747–756.

[15] A. Engel, *Verification, Validation, and Testing of Engineered Systems*. John Wiley & Sons, Inc., 2010, pp. 3–59.

[16] IEEE, "The Authoritative Dictionary of IEEE Standards Terms," *IEEE Std 100-2000*, pp. 1–1362, 2000.

[17] M. Paolone, C. Gaunt, X. Guillaud, M. Liserre, A. Meliopoulos, A. Monti, T. Van Cutsem, V. Vittal, and C. Vournas, "Fundamentals of power systems modelling in the presence of converter-interfaced generation," in *21st Power Systems Computation Conference (PSCC)*, Jun. 2020, pp. 1–35.

[18] K. Yamashita, H. Renner, S. Martinez Villanueva, K. Vennemann, J. Martins, P. Aristidou, T. Van Cutsem, Z. Song, G. Lammert, L. Pabon, L. Zhu, I. Green, G. Irwin, D. Geibel, S. Jankovic, C. Zhan, F. Ciausiu, K. Karoui, K. Chan, and M. Steurer, "Modelling of inverter-based generation for power system dynamic studies," 2018. Accessed: Mar. 10, 2021. [Online]. Available: http://cired.net/uploads/default/files/727-web.pdf.

[19] P. Kundur, *Power system stability and control*. McGraw-Hill, 1994, pp. 0045–1099.

[20] G. Lammert, K. Yamashita, L. D. P. Ospina, H. Renner, S. M. Villanueva, P. Pourbeik, F. E. Ciausiu, and M. Braun, "International Industry practice on modelling and dynamic performance of inverter based generation in power system studies," *CIGRE Science and Engineering Journal*, vol. 8, no. 1, pp. 25–37, 2017.

[21] N. Watson and J. Arrillaga, *Power Systems Electromagnetic Transients Simulation.* London: The Institution of Engineering and Technology, 2003, pp. 1–98.

[22] J. A. Martinez-Velasco, *Transient Analysis of Power Systems.* Wiley-IEEE Press, 2020, pp. 9–99.

[23] H. W. Dommel, "Digital Computer Solution of Electromagnetic Transients in Single-and Multiphase Networks," *IEEE Transactions on Power Apparatus and Systems (PAS)*, vol. 88, no. 4, pp. 388–399, 1969.

[24] V. Venkatasubramanian, H. Schättler, and J. Zaborszky, "Fast Time-Varyng Phasor Analysis in the Balanced Three-Phase Large Electric Power System," vol. 40, no. 11, pp. 1975–1982, 1995.

[25] T. Demiray, G. Andersson, and L. Busarello, "Evaluation study for the simulation of power system transients using dynamic phasor models," in *2008 IEEE/PES Transmission and Distribution Conference and Exposition: Latin America*, Aug. 2008, pp. 1–6.

[26] S. M. Kotian and K. N. Shubhanga, "Dynamic phasor modelling and simulation," in *2015 Annual IEEE India Conference (INDICON)*, Dec. 2015, pp. 1–6.

[27] A. A. Van Der Meer, M. Gibescu, M. A. Van Der Meijden, W. L. Kling, and J. A. Ferreira, "Advanced hybrid transient stability and EMT simulation for VSC-HVDC systems," *IEEE Transactions on Power Delivery*, vol. 30, no. 3, pp. 1057–1066, 2015.

[28] Q. Huang and V. Vittal, "Advanced emt and phasor-domain hybrid simulation with simulation mode switching capability for transmission and distribution systems," *IEEE Transactions on Power Systems*, vol. 33, no. 6, pp. 6298–6308, 2018.

[29] L. Bam and W. Jewell, "Review: power system analysis software tools," in *IEEE Power Engineering Society General Meeting, 2005*, vol. 1, Jun. 2005, pp. 139–144.

[30] H. Al-Sheikh and N. Moubayed, "An overview of simulation tools for renewable applications in power systems," in *2012 2nd International Conference on Advances in Computational Tools for Engineering Applications (ACTEA)*, 2012, pp. 257–261.

[31] J. Mahseredjian, V. Dinavahi, and J. A. Martinez, "Simulation tools for electromagnetic transients in power systems: Overview and challenges," *IEEE Transactions on Power Delivery*, vol. 24, no. 3, pp. 1657–1669, 2009.

[32] F. Milano, *Power System Modelling and Scripting*. Springer-Verlag Berlin Heidelberg, 2010, pp. 31–58.

[33] A. Shapovalov, C. Kittl, C. Rehtanz, L. Jendernalik, A. C. Schneider, and D. Giavarra, "Application of time-resolved input data for smart grid simulation," *CIRED - Open Access Proceedings Journal*, vol. 2017, no. 1, pp. 2106–2109, 2017.

[34] L. Jendernalik, D. Giavarra, C. Engels, J. Hiry, C. Kittl, and C. Rehtanz, "Holistic network planning approach: Enhancement of the grid expansion using the flexibility of network participants," *CIRED - Open Access Proceedings Journal*, vol. 2017, no. 1, pp. 2312–2315, 2017.

[35] L. Robitzky, S. C. Müller, S. Dalhues, U. Häger, and C. Rehtanz, "Agent-based redispatch for real-time overload relief in electrical transmission systems," in *2015 IEEE Power Energy Society General Meeting*, Jul. 2015, pp. 1–5.

[36] L. Robitzky, S. Dalhues, M. Albrecht, S. C. Müller, U. Häger, and C. Rehtanz, "Agent-based prevention of voltage collapse in electrical transmission systems," in *2016 Power Systems Computation Conference (PSCC)*, Jun. 2016, pp. 1–7.

[37] U. Häger, K. Görner, and C. Rehtanz, "Hardware model of a Dynamic Power Flow Controller," in *2011 IEEE Trondheim PowerTech*, Jun. 2011, pp. 1–6.

[38] R. O. Nelson, D. C. Flegel, B. K. Johnson, and H. L. Hess, "Undergraduate research and teaching opportunities from a transient network analyzer," in *Annual Conference American Society for Engineering Education (ASEE)*, Jun. 2002, pp. 7.1222.1–7.1222.10.

[39] S. J. Frobin, C. Freye, L. Vogelsang, D. Wienold, A. Cimino, J. Huppertz, and M. Gamlin, "Large Scale Synthetic Laboratory Imitation of Transient Voltage Stresses of MMC-HVDC Links: Design Aspects on "Very Slow Front Overvoltages"," in *VDE High Voltage Technology 2020; ETG-Symposium*, Nov. 2020, pp. 1–6.

[40] M. La Scala, S. Bruno, S. Lamonaca, U. Stecchi, L. Tapfer, G. Contento, R. Amirante, M. Dassisti, M. Piccioni, A. Fraddosio, and P. Stefanizzi, "Labzero, an interdisciplinary living laboratory for

the promotion of renewables and energy efficiency," in *2016 AEIT International Annual Conference (AEIT)*, Oct. 2016, pp. 1–6.

[41] A. Flammini, M. Pasetti, S. Rinaldi, P. Bellagente, A. C. Ciribini, L. C. Tagliabue, L. E. Zavanella, S. Zanoni, G. Oggioni, and G. Pedrazzi, "A Living Lab and Testing Infrastructure for the Development of Innovative Smart Energy Solutions: The eLUX Laboratory of the University of Brescia," in *2018 110th AEIT International Annual Conference (AEIT)*, Dec. 2018, pp. 1–6.

[42] L. F. Ugarte, D. N. Sarmiento, F. T. Mariotto, E. Lacusta, and M. C. de Almeida, "Living Lab for Electric Mobility in the Public Transportation System of the University of Campinas," in *2019 IEEE PES Innovative Smart Grid Technologies Conference - Latin America (ISGT Latin America)*, Sep. 2019, pp. 1–6.

[43] F. Delfino, "Living Labs and Partnerships for Progress: How Universities can Drive the Process towards the Sustainable City," *International Journal of Environmental Sciences & Natural Resources*, vol. 18, no. 2, pp. 071–073, 2019.

[44] M. O. Faruque, T. Strasser, G. Lauss, V. Jalili-Marandi, P. Forsyth, C. Dufour, V. Dinavahi, A. Monti, P. Kotsampopoulos, J. A. Martinez, K. Strunz, M. Saeedifard, X. Wang, D. Shearer, M. Paolone, R. Brandl, M. Matar, A. Davoudi, and R. Iravani, "Real-Time Simulation Technologies for Power Systems Design, Testing, and Analysis," *IEEE Power and Energy Technology Systems Journal*, vol. 2, no. 2, pp. 63–73, 2015.

[45] C. Dufour, J. Mahseredjian, and J. Belanger, "A Combined State-Space Nodal Method for the Simulation of Power System Transients," *IEEE Transactions on Power Delivery*, vol. 26, no. 2, pp. 928–935, 2011.

[46] C. Dufour, S. Alma, S. Cuni, G. Scrosati, G. Valvo, and G. Sapienza, "Renewable Integration and Protection Studies on a 750-Node Distribution Grid Using a Real-Time Simulator and a Delay-Free Parallel Solver," in *CIRED 23rd International Conference on Electricity Distribution*, Jun. 2015, pp. 1–5.

[47] H. Hooshyar, L. Vanfretti, and C. Dufour, "Delay-free parallelization for real-time simulation of a large active distribution grid model," in *IECON 2016 - 42nd Annual Conference of the IEEE Industrial Electronics Society*, Oct. 2016, pp. 6278–6284.

[48] C. Dufour, S. Cense, V. Jalili-Marandi, and J. Bélanger, "Review of state-of-the-art solver solutions for HIL simulation of power systems,

power electronic and motor drives," in *2013 15th European Conference on Power Electronics and Applications (EPE)*, Sep. 2013, pp. 1–12.

[49] H. Saad, T. Ould-Bachir, J. Mahseredjian, C. Dufour, S. Dennetiere, and S. Nguefeu, "Real-time simulation of MMCs using CPU and FPGA," *IEEE Transactions on Power Electronics*, vol. 30, no. 1, pp. 259–267, 2015.

[50] G. F. Lauss, M. O. Faruque, K. Schoder, C. Dufour, A. Viehweider, and J. Langston, "Characteristics and design of power hardware-in-The-loop simulations for electrical power systems," *IEEE Transactions on Industrial Electronics*, vol. 63, no. 1, pp. 406–417, 2016.

[51] C. Rehtanz and X. Guillaud, "Real-time and co-simulations for the development of power system monitoring, control and protection," in *2016 Power Systems Computation Conference (PSCC)*, Jun. 2016, pp. 1–20.

[52] T. Simolin, K. Rauma, P. Järventausta, and A. Rautiainen, "Optimised controlled charging of electric vehicles under peak power-based electricity pricing," *IET Smart Grid*, pp. 1–9, 2020.

[53] A. Avalos, A. Zamora, O. Escamilla, and M. R. Paternina, "Real-Time Hardware-in-The-loop Implementation for Power Systems Protection," *2018 IEEE PES Transmission and Distribution Conference and Exhibition - Latin America (T and D-LA)*, pp. 1–5, Sep. 2018.

[54] J. A. Montoya-Arias, O. A. Tobar-Rosero, and G. D. Zapata-Madrigal, "Automatic Configuration of Distance Relays with Process Bus under a Hardware in the Loop Scheme," in *2019 FISE-IEEE/CIGRE Conference - Living the energy Transition (FISE/CIGRE)*, Dec. 2019, pp. 1–6.

[55] D. Hilbrich, S. W. A. Shah, and C. Rehtanz, "Automated Application Oriented Testing using Real Power Network Models for Combined Protection and Control Systems," in *2019 IEEE PES Innovative Smart Grid Technologies Europe (ISGT-Europe)*, Sep. 2019, pp. 1–5.

[56] R. Majumder, B. C. Pal, C. Dufour, and P. Korba, "Design and real-time implementation of robust FACTS controller for damping inter-area oscillation," *IEEE Transactions on Power Systems*, vol. 21, no. 2, pp. 809–816, 2006.

[57] B. Poudel, E. Amiri, J. R. Ramamurthy, I. Leevongwat, T. E. Field, R. Rastgoufard, and P. Rastgoufard, "Hardware-in-the-Loop Testing of Dynamic Grid Voltages for Static Var Compensator Controllers with Single-Phase Induction Motor Loads," *IEEE Open Access Journal of Power and Energy*, vol. 7, pp. 307–319, 2020.

[58] X. Wang, D. W. Gao, J. Wang, W. Yan, W. Gao, E. Muljadi, and V. Gevorgian, "Implementations and evaluations of wind turbine inertial controls with FAST and digital real-time simulations," *IEEE Transactions on Energy Conversion*, vol. 33, no. 4, pp. 1805–1814, 2018.

[59] I. Munteanu, A. I. Bratcu, S. Bacha, D. Roye, and J. Guiraud, "Hardware-in-the-loop-based simulator for a class of variable-speed wind energy conversion systems: Design and performance assessment," *IEEE Transactions on Energy Conversion*, vol. 25, no. 2, pp. 564–576, 2010.

[60] H. Hooshyar, F. Mahmood, L. Vanfretti, and M. Baudette, "Specification, implementation, and hardware-in-the-loop real-time simulation of an active distribution grid," *Sustainable Energy, Grids and Networks*, vol. 3, pp. 36–51, Sep. 2015.

[61] S. Sarri, M. Pignati, P. Romano, L. Zanni, and M. Paolone, "A hardware-in-the-loop test platform for the performance assessment of a pmu-based real-time state estimator for active distribution networks," in *2015 IEEE Eindhoven PowerTech*, Jun. 2015, pp. 1–6.

[62] G. Lauss, F. P. Andrén, F. Leimgruber, and T. I. Strasser, "Analyzing standardization needs for CHIL-based testing of power systems and components," in *2018 IEEE International Conference on Industrial Electronics for Sustainable Energy Systems (IESES)*, Feb. 2018, pp. 523–528.

[63] A. Newaz, J. Ospina, and M. O. Faruque, "Controller Hardware-in-The-Loop Validation of a Graph Search Based Energy Management Strategy for Grid-Connected Distributed Energy Resources," *IEEE Transactions on Energy Conversion*, vol. 35, no. 1, pp. 520–528, 2020.

[64] R. Palaniappan, B. Bauernschmitt, D. Hilbrich, and C. Rehtanz, "An intelligent measurement and control device for active distribution grids," in *2020 IEEE PES Innovative Smart Grid Technologies Europe (ISGT-Europe)*, Oct. 2020, pp. 975–979.

[65] J. V. Barreras, C. Fleischer, A. E. Christensen, M. Swierczynski, E. Schaltz, S. J. Andreasen, and D. U. Sauer, "An Advanced HIL Simulation Battery Model for Battery Management System Testing," *IEEE Transactions on Industry Applications*, vol. 52, no. 6, pp. 5086–5099, 2016.

[66] R. Mo, M. Steurer, and H. Li, "Controller hardware-in-the-loop (CHIL) simulation of a multi-functional energy storage system based on modular multilevel DC/DC converter (M2DC) for MVDC grid," in

2016 IEEE 8th International Power Electronics and Motion Control Conference (IPEMC-ECCE Asia), May 2016, pp. 1980–1984.

[67] D. Kler, A. Zabetian Hosseini, S. Varghese, C. Sun, and G. Joos, "A Rule Based EMS for Fast Charging Station with CHIL Implementation," in *2020 IEEE Energy Conversion Congress and Exposition (ECCE)*, Oct. 2020, pp. 1319–1324.

[68] J. Noon, H. Song, B. Wen, R. Burgos, I. Cvetkovic, D. Boroyevich, S. Srdic, and G. Pammer, "A power hardware-in-the-loop testbench for aerospace applications," in *2020 IEEE Applied Power Electronics Conference and Exposition (APEC)*, Mar. 2020, pp. 2884–2891.

[69] J. Langston, F. Bogdan, J. Hauer, K. Schoder, M. Steurer, D. Dalessandro, T. Fikse, J. Cherry, and S. Gonstead, "Megawatt-scale power hardware-in-the-loop simulation testing of a power conversion module for naval applications," in *2015 IEEE Electric Ship Technologies Symposium (ESTS)*, Jun. 2015, pp. 268–275.

[70] K. S. Amitkumar, R. S. Kaarthik, and P. Pillay, "A Versatile Power-Hardware-in-the-Loop-Based Emulator for Rapid Testing of Transportation Electric Drives," *IEEE Transactions on Transportation Electrification*, vol. 4, no. 4, pp. 901–911, 2018.

[71] Z. Zhang and L. Fickert, "Power hardware-in-the-loop test of the energy feedback device in urban rail transportation system," in *2018 19th International Scientific Conference on Electric Power Engineering (EPE)*, May 2018, pp. 1–4.

[72] C. Depature, T. Jokela, W. Lhomme, A. Bouscayrol, L. Boulon, P. Sicard, and A. Belahcen, "Full-Scale Power Hardware-In-the-Loop Simulation of an Electric Vehicle Using Energetic Macroscopic Representation," in *2015 IEEE Vehicle Power and Propulsion Conference (VPPC)*, Oct. 2015, pp. 1–6.

[73] B. A. Mather, M. A. Kromer, and L. Casey, "Advanced photovoltaic inverter functionality verification using 500 kW power hardware-in-loop (PHIL) complete system laboratory testing," in *2013 IEEE PES Innovative Smart Grid Technologies Conference (ISGT)*, Feb. 2013, pp. 1–6.

[74] T. Reinikka, H. Alenius, T. Roinila, and T. Messo, "Power Hardware-in-the-Loop Setup for Stability Studies of Grid-Connected Power Converters," in *2018 International Power Electronics Conference (IPEC-Niigata 2018 -ECCE Asia)*, May 2018, pp. 1704–1710.

[75] H. Kikusato, T. S. Ustun, J. Hashimoto, K. Otani, T. Nagakura, Y. Yoshioka, R. Maeda, and K. Mori, "Developing Power Hardware-in-the-Loop Based Testing Environment for Volt-Var and Frequency-Watt Functions of 500 kW Photovoltaic Smart Inverter," *IEEE Access*, vol. 8, pp. 224 135–224 144, 2020.

[76] A. Varais, X. Roboam, F. Lacressonniere, E. Bru, and N. Roux, "Reduced Scale PHIL Emulation Concepts Applied to Power Conversion Systems with Battery Storage," *IEEE Transactions on Industrial Electronics*, vol. 68, no. 5, pp. 3973–3981, 2021.

[77] M. Steurer, C. S. Edrington, M. Sloderbeck, W. Ren, and J. Langston, "A megawatt-scale power hardware-in-the-loop simulation setup for motor drives," *IEEE Transactions on Industrial Electronics*, vol. 57, no. 4, pp. 1254–1260, 2010.

[78] A. Schmitt, J. Richter, M. Gommeringer, T. Wersal, and M. Braun, "A novel 100 kw power hardware-in-the-loop emulation test bench for permanent magnet synchronous machines with nonlinear magnetics," in *8th IET International Conference on Power Electronics, Machines and Drives (PEMD 2016)*, Apr. 2016, pp. 1–6.

[79] A. Helmedag, T. Isermann, and A. Monti, "Fault ride through certification of wind turbines based on a hardware in the loop setup," *IEEE Transactions on Instrumentation and Measurement*, vol. 63, no. 10, pp. 2312–2321, 2014.

[80] A. Mejia-Barron, M. Valtierra-Rodriguez, J. P. Amezquita-Sanchez, D. Granados-Lieberman, and G. Tapia-Tinoco, "A Power Hardware-In-the-Loop Scheme for Load Emulation Applications," in *2018 IEEE International Autumn Meeting on Power, Electronics and Computing (ROPEC)*, Nov. 2018, pp. 1–6.

[81] S. Sanchez, S. D'Arco, A. Holdyk, and E. Tedeschi, "An approach for small scale power hardware in the loop emulation of HVDC cables," in *2018 Thirteenth International Conference on Ecological Vehicles and Renewable Energies (EVER)*, Apr. 2018, pp. 1–8.

[82] F. J. Viglus and M. Lobo Heldwein, "Hybrid Subsea Power Cable Emulator," in *2019 IEEE Applied Power Electronics Conference and Exposition (APEC)*, Mar. 2019, pp. 3373–3379.

[83] M. Boby and P. Pillay, "A power hardware-in-the-loop emulation of a faulted inverter," in *2019 IEEE International Electric Machines and Drives Conference (IEMDC)*, May 2019, pp. 1641–1646.

[84] G. Tanuku and P. Pillay, "Induction Machine Emulation under Asymmetric Grid Faults," in *2020 IEEE Energy Conversion Congress and Exposition (ECCE)*, Oct. 2020, pp. 2351–2356.

[85] Y. Cao, Y. Li, X. Liu, and C. Rehtanz, *Cyber-Physical Energy and Power Systems*. Springer Singapore, 2020, pp. 1–216.

[86] B. Lundstrom, B. Palmintier, D. Rowe, J. Ward, and T. Moore, "Trans-oceanic remote power hardware-in-the-loop: Multi-site hardware, integrated controller, and electric network co-simulation," *IET Generation, Transmission and Distribution*, vol. 11, no. 18, pp. 4688–4701, 2017.

[87] E. Bompard, S. Bruno, S. Frittoli, G. Giannoccaro, M. La Scala, A. Mazza, E. Pons, and C. Rodio, "Remote PHIL Distributed Co-Simulation Lab for TSO-DSO-Customer Coordination Studies," in *2020 AEIT International Annual Conference (AEIT)*, Sep. 2020, pp. 1–6.

[88] L. L. Jansen, N. Andreadou, I. Papaioannou, and A. Marinopoulos, "Smart grid lab research in Europe and beyond," *International Journal of Energy Research*, vol. 44, no. 3, pp. 1307–1336, 2020.

[89] N. Andreadou, L. L. Jansen, A. Marinopoulos, and I. Papaioannou, "Smart Grid Laboratories Inventory 2018," Tech. Rep., 2018. Accessed: Aug. 3, 2020. [Online]. Available: https://ec.europa.eu/jrc.

[90] D. Grubbs, "gridPULSE: Catalog of National Laboratory Testing Resources for Grid Devices," 2018. Accessed: Aug. 3, 2020. [Online]. Available: https://www.osti.gov/biblio/1528814.

[91] R. Bründlinger, T. Strasser, G. Lauss, A. Hoke, S. Chakraborty, G. Martin, B. Kroposki, J. Johnson, and E. De Jong, "Lab Tests: Verifying That Smart Grid Power Converters Are Truly Smart," *IEEE Power and Energy Magazine*, vol. 13, no. 2, pp. 30–42, 2015.

[92] T. Strasser, F. Pröstl Andrén, G. Lauss, R. Bründlinger, H. Brunner, C. Moyo, C. Seitl, S. Rohjans, S. Lehnhoff, P. Palensky, P. Kotsampopoulos, N. Hatziargyriou, G. Arnold, W. Heckmann, E. Jong, M. Verga, G. Franchioni, L. Martini, A. Kosek, O. Gehrke, H. Bindner, F. Coffele, G. Burt, M. Calin, and E. Rodriguez-Seco, "Towards holistic power distribution system validation and testing—an overview and discussion of different possibilities," *Elektrotechnik und Informationstechnik*, vol. 134, no. 1, pp. 71–77, 2017.

[93] K. Heussen, C. Steinbrink, I. F. Abdulhadi, V. H. Nguyen, M. Z. Degefa, J. Merino, T. V. Jensen, H. Guo, O. Gehrke, D. E. Morales Bondy, D. Babazadeh, F. P. Andrén, and T. I. Strasser, "ERIGrid Holistic Test Description for Validating Cyber-Physical Energy Systems," *Energies*, vol. 12, no. 14, pp. 1–31, 2019.

[94] M. Ginocchi, A. Ahmadifar, F. Ponci, and A. Monti, "Application of a smart grid interoperability testing methodology in a real-time hardware-in-the-loop testing environment," *Energies*, vol. 13, no. 7, pp. 1–25, 2020.

[95] E. De Jong, R. Graaff, P. Vaessen, P. Crolla, A. Roscoe, F. Lehfuss, G. Lauss, P. Kotsampopoulos, and F. Gafaro, *European White Book on Real-Time Power Hardware-in-the-loop testing*, pp. 1–48, 2012. Accessed: Jan. 6, 2020. [Online]. Available: https://strathprints.strath.ac.uk/43450/1/noe_005_phil.pdf.

[96] A. J. Roscoe, A. MacKay, G. M. Burt, and J. R. McDonald, "Architecture of a network-in-the-loop environment for characterizing AC power-system behavior," *IEEE Transactions on Industrial Electronics*, vol. 57, no. 4, pp. 1245–1253, 2010.

[97] Q. Hong, I. Abdulhadi, D. Tzelepis, A. Roscoe, B. Marshall, and C. Booth, "Realization of High Fidelity Power-Hardware-in-the-Loop Capability Using a MW-Scale Motor-Generator Set," *IEEE Transactions on Industrial Electronics*, vol. 67, no. 8, pp. 6835–6844, 2020.

[98] V. Prodanov and M. Banu, "Power amplifier principles and modern design techniques," *Wireless Technologies: Circuits, Systems, and Devices*, pp. 349–381, 2017.

[99] T. F. Schubert and E. M. Kim, *Fundamentals of Electronics*. Morgan & Claypoo, 2015, vol. 2, pp. 543–558.

[100] D. Self, *Audio Power Amplifier Design Handbook*, 5th ed. Focal Press, 2009, pp. 26–379.

[101] M. Orr, "Selecting a linear or PWM power source," *EE: Evaluation Engineering*, vol. 47, no. 11, pp. 46–51, 2008. Accessed: Feb. 21, 2020. [Online]. Available: https://www.evaluationengineering.com.

[102] F. Lehfuss, G. Lauss, P. Kotsampopoulos, N. Hatziargyriou, P. Crolla, and A. Roscoe, "Comparison of multiple power amplification types for power Hardware-in-the-Loop applications," in *2012 Complexity in Engineering (COMPENG). Proceedings*, Jun. 2012, pp. 1–6.

[103] E. García-Martínez, J. Ballestín, J. Muñoz-Cruzado, and J. F. Sanz, "Analysis of a switched and linear power amplifier for power hardware-in-the-loop testing of smartgrid systems," in *2019 24th IEEE International Conference on Emerging Technologies and Factory Automation (ETFA)*, Sep. 2019, pp. 747–753.

[104] W. Ren, "Accuracy Evaluation of Power Hardware-in-the- Loop (PHIL) Simulation," Ph.D. dissertation, 2007. Accessed: Jan. 6, 2020.

[Online]. Available: http://diginole.lib.fsu.edu/islandora/object/fsu:176356/datastream/PDF/view.

[105] S. Paran, C. Edrington, and B. Vural, "Investigation of HIL interfaces in nonlinear load studies," in *2012 North American Power Symposium (NAPS)*, Sep. 2012, pp. 1–6.

[106] R. Brandl, "Operational range of several interface algorithms for different power hardware-in-the-loop setups," *Energies*, vol. 10, no. 12, pp. 1–21, 2017.

[107] F. Lehfuß and G. F. Lauss, "Power Hardware-in-the-Loop Simulations for Distributed Generation," in *CIRED 21st International Conference on Electricity Distribution*, Jun. 2011, pp. 1–4.

[108] T. Hatakeyama, A. Riccobono, and A. Monti, "Stability and accuracy analysis of power hardware in the loop system with different interface algorithms," in *2016 IEEE 17th Workshop on Control and Modeling for Power Electronics (COMPEL)*, Jun. 2016, pp. 1–8.

[109] S. Ruhe, M. Fechner, S. Nicolai, and P. Bretschneider, "Simulation of coupled components within power-hardware-in-the-loop (phil) test bench," in *2020 55th International Universities Power Engineering Conference (UPEC)*, Sep. 2020, pp. 1–6.

[110] J. Wang, B. Lundstrom, I. Mendoza, and A. Pratt, "Systematic Characterization of Power Hardware-in-the-Loop Evaluation Platform Stability," *2019 IEEE Energy Conversion Congress and Exposition (ECCE)*, pp. 1068–1075, Sep. 2019.

[111] E. Guillo-Sansano, M. H. Syed, A. J. Roscoe, G. M. Burt, and F. Coffele, "Characterization of Time Delay in Power Hardware in the Loop Setups," *IEEE Transactions on Industrial Electronics*, vol. 68, no. 3, pp. 2703–2713, 2020.

[112] N. D. Marks, W. Y. Kong, and D. S. Birt, "Stability of a switched mode power amplifier interface for power hardware-in-the-loop," *IEEE Transactions on Industrial Electronics*, vol. 65, no. 11, pp. 8445–8454, 2018.

[113] M. G. Kashani, H. Pulakhandam, S. Bhattacharya, F. Katiraei, and D. Kaiser, "Design considerations and test setup assessment for power hardware in the loop testing," in *2017 IEEE Industry Applications Society Annual Meeting*, Oct. 2017, pp. 1–8.

[114] O. Tremblay, H. Fortin-Blanchette, R. Gagnon, and Y. Brissette, "Contribution to stability analysis of power hardware-in-the-loop simulators," *IET Generation, Transmission and Distribution*, vol. 11, no. 12, pp. 3073–3079, 2017.

[115] P. C. Kotsampopoulos, F. Lehfuss, G. F. Lauss, B. Bletterie, and N. D. Hatziargyriou, "The limitations of digital simulation and the advantages of PHIL testing in studying distributed generation provision of ancillary services," *IEEE Transactions on Industrial Electronics*, vol. 62, no. 9, pp. 5502–5515, 2015.

[116] E. Guillo-Sansano, M. H. Syed, A. J. Roscoe, and G. M. Burt, "Assessment and development of stability enhancing methods for dynamically changing power hardware-in-the-loop simulations," in *CIRED 25th International Conference and Exhibition on Electricity Distribution*, Jun. 2019, pp. 1–5.

[117] G. Lauss and K. Strunz, "Accurate and Stable Hardware-in-the-Loop (HIL) Real-time Simulation of Integrated Power Electronics and Power Systems," *IEEE Transactions on Power Electronics*, vol. 36, no. 9, pp. 10 920–10 932, 2021.

[118] W. Ren, M. Sloderbeck, M. Steurer, V. Dinavahi, T. Noda, S. Filizadeh, A. R. Chevrefils, M. Matar, R. Iravani, C. Dufour, J. Belanger, M. O. Faruque, K. Strunz, and J. A. Martinez, "Interfacing issues in real-time digital simulators," *IEEE Transactions on Power Delivery*, vol. 26, no. 2, pp. 1221–1230, 2011.

[119] G. F. Lauss, "Interfacing challenges in PHIL simulations for investigations on P-Q controls of grid connected generation units in electric power systems," *IFAC-PapersOnLine*, vol. 50, no. 1, pp. 10 964–10 970, 2017.

[120] B. Lundstrom and M. V. Salapaka, "Optimal power hardware-in-the-loop interfacing: Applying modern control for design and verification of high-accuracy interfaces," *IEEE Transactions on Industrial Electronics*, vol. 68, no. 11, pp. 10 388–10 399, 2021.

[121] S. Paran and C. S. Edrington, "Improved power hardware in the loop interface methods via impedance matching," in *2013 IEEE Electric Ship Technologies Symposium (ESTS)*, Apr. 2013, pp. 342–346.

[122] A. Aguirre, M. Davila, P. Zuniga, F. Uribe, and E. Barocio, "Improvement of damping impedance method for power hardware in the loop simulations," in *2016 IEEE International Autumn Meeting on Power, Electronics and Computing (ROPEC)*, Nov. 2016, pp. 1–6.

[123] J. Siegers and E. Santi, "Improved power hardware-in-the-loop interface algorithm using wideband system identification," in *2014 IEEE Applied Power Electronics Conference and Exposition - APEC 2014*, Mar. 2014, pp. 1198–1204.

[124] A. Riccobono, A. Helmedag, A. Berthold, N. R. Averous, R. W. De Doncker, and A. Monti, "Stability and Accuracy Considerations of Power Hardware- in-the-Loop Test Benches for Wind Turbines," *IFAC-PapersOnLine*, vol. 50, no. 1, pp. 10 977–10 984, 2017.

[125] D. Barakos, P. Kotsampopoulos, A. Vassilakis, V. Kleftakis, and N. Hatziargyriou, "Methods for stability and accuracy evaluation of Power Hardware In the Loop simulations," in *MedPower 2014*, Nov. 2014, pp. 1–5.

[126] IEEE SA, "P2004 - Hardware-in-the-Loop (HIL) Simulation Based Testing of Electric Power Apparatus and Controls." [Online]. Available: https://standards.ieee.org/project/2004.html

[127] P. Kotsampopoulos, D. Lagos, N. Hatziargyriou, M. O. Faruque, G. Lauss, O. Nzimako, P. Forsyth, M. Steurer, F. Ponci, A. Monti, V. Dinavahi, and K. Strunz, "A Benchmark System for Hardware-in-the-Loop Testing of Distributed Energy Resources," *IEEE Power and Energy Technology Systems Journal*, vol. 5, no. 3, pp. 94–103, 2018.

[128] W. Ren, M. Steurer, and S. Woodruff, "Applying Controller and Power Hardware-in-the-Loop Simulation in Designing and Prototyping Apparatuses for Future All Electric Ship," in *2007 IEEE Electric Ship Technologies Symposium*, 2007, pp. 443–448.

[129] E. Guillo-Sansano, M. H. Syed, A. J. Roscoe, and G. M. Burt, "Initialization and Synchronization of Power Hardware-In-The-Loop Simulations: A Great Britain Network Case Study," *Energies*, vol. 11, no. 5, pp. 1–14, 2018.

[130] M. Lemaire, G. Pammer, and B. Black, "Smarter drives need smarter development," *2016 IEEE Transportation Electrification Conference and Expo (ITEC)*, pp. 1–63, Jun. 2016.

[131] J. Bélanger, L. A. Snider, J.-N. Paquin, C. Pirolli, and W. Li, "A Modern and Open Real-Time Digital Simulator of Contemporary Power Systems," in *International Conference on Power Systems Transients (IPST)*, Jun. 2009, pp. 1–10.

[132] S. Abourida, C. Dufour, J. Bélanger, and V. Lapointe, "Real-Time, PC-Based Simulator of Electric Systems and Drives," in *International Conference on Power Systems Transients 2003 (IPST 2003)*, Sep. 2003, pp. 1–6.

[133] S. Abourida, C. Dufour, and J. Bélanger, "Real-Time and Hardware-In-The-Loop Simulation of Electric Drives and Power Electronics: Process , problems and solutions," in *The 2005 International Power Electrinics Conference*, Apr. 2005, pp. 1908–1913.

[134] S. Mikkili and A. K. Panda, "Review of RT-LAB and steps involved for implementation of a simulink model from MATLAB to REAL-TIME," *International Journal of Emerging Electric Power Systems*, vol. 14, no. 6, pp. 641–658, 2013.

[135] OPAL-RT, "Electrical simulation software Electrical engineering test," Accessed: Jan. 10, 2021. [Online]. Available: https://www.opal-rt.com/simulation-systems-overview-2/.

[136] EGSTON Power Electronics, "CSU200-2GAMP4," Accessed: Feb. 16, 2021. [Online]. Available: https://www.egstonpower.com/portfolio/csu200/.

[137] Doepke, "AC-DC sensitive residual current devices (Type B RCDs) - Instructions for use and technical information," Tech. Rep., 2017. Accessed: Mar. 1, 2021. [Online]. Available:https://www.doepke.de/uploads/media/doepke_5900194_allstromfibel_inf_web_en.pdf.

[138] T. Gruhn, J. Glenney, and M. Savostianik, "Type B Ground-Fault Protection on Adjustable Frequency Drives," *IEEE Transactions on Industry Applications*, vol. 54, no. 1, pp. 934–939, 2018.

[139] KoCoS Technology Group, "EPPE CX - Technical specifications," Accessed: Mar. 25, 2021. [Online]. Available: https://www.kocos.com/fileadmin/download/EPPE/Specsheet/ENG/DB_EPPECX_022018_ENG.pdf.

[140] IEEE, "IEEE Recommended Practice for Monitoring Electric Power Quality," *IEEE Std 1159-2019 (Revision of IEEE Std 1159-2009)*, pp. 1–98, 2019.

[141] ——, "IEEE Recommended Practice for Voltage Sag and Short Interruption Ride-Through Testing for End-Use Electrical Equipment Rated Less than 1000 V," *IEEE Std 1668-2017 (Revision of IEEE Std 1668-2014)*, pp. 1–85, 2017.

[142] VENIOS GmbH, "Venios Energy Platform," accessed: Apr. 10, 2021. [Online]. Available: https://venios.de/en/venios-energy-platform/.

[143] D. Divan and H. Johal, "Distributed facts - a new concept for realizing grid power flow control," *IEEE Transactions on Industrial Electronics*, vol. 22, no. 6, pp. 2253–2260, Nov. 2007.

[144] Smart Wires Inc., "PowerLine Guardian," Accessed: Feb. 16, 2021. [Online]. Available: https://www.smartwires.com/.

[145] D. Das, F. Kreikebaum, D. Divan, and F. Lambert, "Reducing transmission investment to meet renewable portfolio standards using smart

wires," in *Proc. IEEE PES Transm. Distrib. Conf.*, Apr. 2010, pp. 1–7.

[146] M. Albrecht, C. Strunck, and C. Rehtanz, "Hardware-in-the-loop Simulation of a Battery Energy Storage System and External Storage Controller to provide Primary Control," in *2019 IEEE Milan PowerTech*, Jun. 2019, pp. 1–4.

[147] ENTSO-E, "P1-Policy 1: Load-Frequency Control and Performance," Tech. Rep., 2009. Accessed: Sep. 6, 2019. [Online]. Available: https://eepublicdownloads.entsoe.eu/clean-documents/pre2015/publications/ce/oh/Policy1_final.pdf.

[148] ——, "A1-Appendix 1: Load-Frequency Control and Performance," Tech. Rep., 2004. Accessed: Sep. 6, 2019. [Online]. Available: https://eepublicdownloads.entsoe.eu/clean-documents/pre2015/publications/entsoe/Operation_Handbook/Policy_1_Appendix%20_final.pdf.

[149] M. Albrecht, W. Horenkamp, M. Eichhorn, and C. Rehtanz, "Development of a novel Underfrequency Relay and Energy Storage Controller for Underfrequency Protection," in *Internationaler ETG-Kongress 2019; ETG Symposium*, May 2019, pp. 1–6.

[150] C. Strunck, M. Albrecht, and C. Rehtanz, "Provision of ancillary services by different decentralized energy resources," in *2019 IEEE Milan PowerTech*, Jun. 2019, pp. 1–6.

[151] S. Martinmäki, S. Repo, K. Rauma, A. Spina, and C. Rehtanz, "Robust coordinated voltage control in low-voltage networks validated through an experimental study – collaboration of an on-load tap changer and a battery energy storage," in *CIRED Workshop*, Sep. 2020, pp. 1–3.

Evidence of scientific activity

Supervised Bachelor and Master thesis

- F. Kuhn, “Implementation and validation of control strategies for the flexible operation of distribution networks with energy sector coupling approach”, Master thesis, Apr. 2021.
- M. Alkayali, “Implementation and comparisons of Interface algorithms for Power hardware-in-the-loop setups”, Master thesis, Jan. 2021.
- I. Lezaun, “Design and implementation of a MQTT–based communication interface for a hardware controller of a stationary Battery Energy Storage System”, Bachelor thesis, Jul. 2019.
- D. Kröger, “Development and Implementation of a Smart Charging Strategy for Electric Vehicles Considering Voltage and Thermal Constraints”, Master thesis, Jan. 2019.
- J. Spinneken, “Modellierung eines Photovoltaikmoduls auf einem Echtzeitsimulator für netztechnische Untersuchungen von PV-Anlage mittels PHIL Verfahren”, Bachelor thesis, Jul. 2018.
- S. Eichhoff, “Modellierung und Simulation eines Hochspannungsnetzes mit Impedanzreglern zur Leistungsflussregelung in einer Echtzeitsimulation”, Master thesis, Jul. 2018.
- D. Schmid, “Konzeptionierung und agentnbasierte Modellierung eines innovativen Netzbetriebs-Agenten unter Berücksichtigung eines regionalen Flexibilitätsmarktes”, Bachelor thesis, Oct. 2017.

Publications

Book contributions

- A. Spina, C. Aldejohann, U. Häger and C. Rehtanz "Smart Grid Technology Lab: die erweiterte Testumgebung für das zukünftige Verteilnetz," *Anlagentechnik 2021*, VDE Verlag, 2021, Berlin.

Journal Articles

- J. Min, F. Ma, Q. Xu, Z. He, A. Luo and A. Spina, "Analysis, Design and Implementation of Passivity Based Control for Multilevel Railway Power Conditioner," *IEEE Transactions on Industrial Informatics*, vol. PP, no. 99, 2017, pp. 415–425.

Conference Proceedings

- O. Pohl, A. Spina and U. Häger, "Demonstration of Automated Curative Power Flow Control with a Multi-Agent System Using Distributed Series Reactors in a PHIL Simulation," *XXII Power System Computation Conference (PSCC)*, Porto, 2022, pp. 1–6. (Accepted)
- A. Spina, O. Pohl, U. Häger and C. Rehtanz, "A Power-hardware-in-the-loop Setup for Testing Distributed Series Reactors," *AEIT International Annual Conference*, virtual conference, 2020, pp. 1–6.
- S. Martinmäki, S. Repo, K. Rauma, A. Spina and C. Rehtanz, "Robust coordinated voltage control in low-voltage networks validated through an experimental study – collaboration of an on-load tap changer and a battery energy storage," *CIRED Workshop*, Berlin, 2020, pp. 1–3.
- L. Specht, K. Rauma, A. Spina and C. Rehtanz, "Autonomous and cost-efficient operation of a stationary battery energy storage in low voltage networks," *CIRED*, Madrid, 2019, pp. 1–4.

- D. Kröger, K. Rauma, A. Spina and C. Rehtanz, "Scheduled charging of electric vehicles and the increase of hosting capacity by a stationary energy storage," *CIRED*, Madrid, 2019, pp. 1–5.
- A. Spina, K. Rauma, C. Aldejohann, M. Holt, J. Maasmann, P. Berg, F. Rettberg and C. Rehtanz, "Smart Grid Technology Lab – A Full-Scale Low Voltage Research Facility at TU Dortmund University," *AEIT International Annual Conference*, Bari, 2018, pp. 1–6.
- A. Spina, R. Palaniappan, D. Hilbrich, U. Häger, C. Rehtanz, "Comparison between CHIL simulation and hardware test of a Dynamic Power Flow Controller," *12th IEEE PES PowerTech Conference*, Manchester, 2017, pp. 1–6.

Research Projects

- *IQ Dortmund* – Innovative district energy supply solutions in the city of Dortmund

  Contribution: Development of a laboratory setup to test grid management solutions for energy sector coupling applications

- *Smart Grid Technology Lab (SGTL)* – A development and test environment for smart grid technologies

  Contribution: Test and further development of the overall laboratory components with special focus on PHIL applications

- *IDEAL* – Distributed series reactors and coordination of decentralized autonomous power flow controllers

  Contribution: Implementation of a PHIL testbed for commercial distributed series reactors

- *Designetz* – Connected with creative energy solutions

  Contribution: Further development of an agent–based simulation tool for the management of flexibility in smart grids